Université d'Ottawa • University of Ottawa

STRUCTURAL AND MAGNETIC FABRIC STUDY OF THE LATE ARCHEAN SPARROW AND PROSPEROUS PLUTONS, PROSPEROUS SUITE, SLAVE PROVINCE, CANADA

by

Natalie M. Ham

A thesis submitted to the School of Graduate Studies and Research
in partial fulfillment of the requirements
for the degree of M. Sc. in Earth Sciences

OTTAWA-CARLETON GEOSCIENCE CENTRE

AND

UNIVERSITY OF OTTAWA

OTTAWA, CANADA

0-612-58459-3

ABSTRACT

The late Archean (~2595 Ma) Sparrow and Prosperous granite plutons near Yellowknife, NWT, intrude cordierite and andalusite bearing metagreywacke typical of the Slave Province. The objective of this thesis is to determine the structure of the plutons, mode of emplacement and timing in relation to regional deformation. Field and microstructural studies of the plutonic and host rocks are complemented by an analysis of the anisotropy of magnetic susceptibility (AMS) of the granites.

Minor recrystallization of quartz within the plutons, with most grains showing subgrain development, suggests that the fabrics in the granites formed before the granites had completely cooled, probably during emplacement. Paramagnetic Fe-phyllosilicates (biotite and chlorite) and very fine-grained magnetite contribute to the magnetic susceptibility and its anisotropy. Moderate to steeply dipping magnetic foliations strike predominantly NNW to NW parallel to the elongate dimensions of the plutons and to foliation in the country rock. Additionally, shallow-dipping E-W striking foliations are common in the Prosperous pluton. Magnetic lineations in both plutons are horizontal and trend parallel to the NNW to NW striking foliations.

Magmatic mica-rich and mica-poor layers lie parallel to a shallow-dipping basal contact of the Prosperous pluton. Magnetic susceptibility (K) maps of the plutons, which can be used as petrographic mapping tools, also show a zonation/layering, seen as reflecting varying amounts of biotite and of very fine-grained inclusions of magnetite within the biotite. It is interpreted that this

zonation/layering was initially horizontal to sub-horizontal and was subsequently folded.

The plutons are inferred to have been emplaced during a second phase of regional deformation (D_2), with ENE-WSW to NE-SW bulk shortening across the internal and external foliations, and NNW-SSE to NW-SE horizontal stretching marked by the magnetic lineations, a strain pattern that would be compatible with regional dextral transpression. Granitic dykes were injected into the country rocks and subsequently folded during progressive D_2 deformation with axial-surface traces parallel to the regional S_2 foliation. Continued D_2 shortening resulted in pinching and swelling of a second minor set of granite dykes that were emplaced along the S_2 foliation. Within the plutons, the foliations that parallel S_2 formed before the plutons had cooled, as indicated in thin section by the lack of significant subsolidus deformation. With further deformation the foliation and horizontal zonation/layering were folded about axes parallel to the magnetic lineations (in agreement with the preservation of shallow-dipping foliations in the Prosperous Pluton and the K map pattern in the Sparrow pluton). A continuation of deformation after the plutons had cooled is shown by greenschist facies shear zones in both plutons.

It is proposed that the Sparrow and Prosperous plutons are laccoliths that were emplaced horizontally during D_2 deformation, and subsequently were deformed as they crystallized during later stages of D_2. The exposed floor and roof contacts of the Prosperous Pluton dip shallowly to the east, suggesting a tabular shape approximately 2 km thick. Gravity modeling of profiles across the Prosperous and Sparrow plutons (Sheply, 2000) also supports the conclusions that the plutons are thin tabular sheets that have been subsequently folded. The magma may have ascended as dykes, exploiting a large-scale fracture system, and then followed sub-horizontal surfaces of anisotropy within the crust.

TABLE OF CONTENTS

LIST OF FIGURES

ACKNOWLEDGEMENTS

The work was financed by a research contract with Indian and Northern Affairs Canada, awarded to K. Benn, and a SNORCLE Lithoprobe University Supporting Geoscience Grant, awarded to K.Benn and W.R. Roest. Dr. Keith Benn is thanked for introducing the author to the thesis topic and the intricacies of the AMS technique as well as providing many useful comments that have greatly improved this thesis. The field work was made possible by logistical support from Indian and Northern Affairs Canada, and the Geological Survey of Canada. N. Ham was employed by the Geological Survey of Canada while doing field work in 1996 and 1997. W. Padgham, P. Corcoran, the Brophy's, M. Pollock, C. Relf, and V. Jackson are thanked for their hospitality and assistance during stays in Yellowknife. W. K. Fyson is also thanked for valuable discussions of the regional geology, and of structures in granites. W. Bleeker is greatly thanked for logistical support, informative field trips, invigorating discussions on the tectonic setting and structural evolution of the southern Slave Province, and constructive criticism on the thesis. G. J. Borradaile is gratefully acknowledged for access to the rock magnetics facilities at Lakehead University. E. Hearne is thanked for his help with various computer assisted drafting techniques. M. Jean is thanked for his cheerful field assistance in 1997. G. S. Pignotta participated in field work and data reduction in 1996.

There are many others to be thanked, you know who you are, and you have helped beyond belief. My thanks will be conveyed in person since they are too personal to put down on paper.

To all prospective graduate students: in undertaking graduate studies you are guaranteed to learn a lot either about your chosen field, life, or both.

Chapter 1: Introduction

The Slave Province is an Archean granite-greenstone terrain located in the northwestern part of the Canadian Shield, Northwest Territories and Nunavut, Canada. The geological province is ~190,000 km^2 in size and lies between 61^{0}N to 69^{0}N, and 105^{0}W to 117^{0}W (Fig. 1-1)

The southern and northwestern margins, as well as parts of the north-central region, are unconformably overlain by Paleoproterozoic rocks (Fig. 1-1). To the west of the province lies the Wopmay Orogen (1.9-1.8 Ga), and its eastern boundary is a tectonic front known as the Thelon Front (2.0-1.9 Ga; Hoffman, 1989).

Approximately 33% of the surface area of the Slave Province is composed of supracrustal rocks (Padgham, 1985). The Archean supracrustal rocks are dominated by greywacke-mudstone assemblages and volcanic sequences. The greywacke-mudstones (Fig. 1-1) compose about 73% of the supracrustal rocks while the remaining 27% are volcanic. Of the volcanic rocks, almost 45 % are felsic-intermediate in composition. Two types of greenstone belts occur. The basalt-dominated belts, typified by the Yellowknife greenstone belt (Fig. 1-1), are called Yellowknife-type volcanic belts. The felsic-dominated belts (Fig 1-1) are named Hackett-type belts and predominate in a northwesterly trending zone southwest of the Bathurst Fault. Henderson (1970) combined all

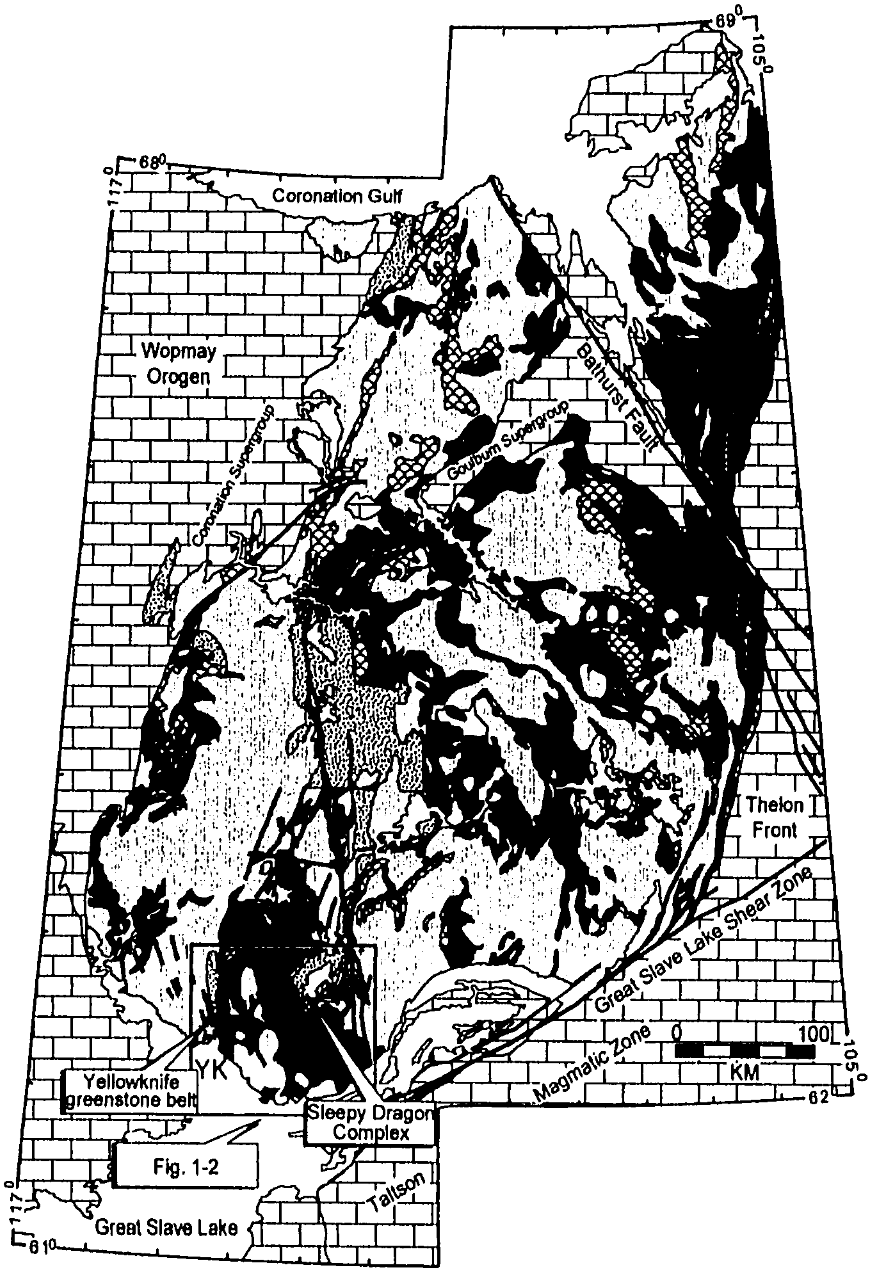

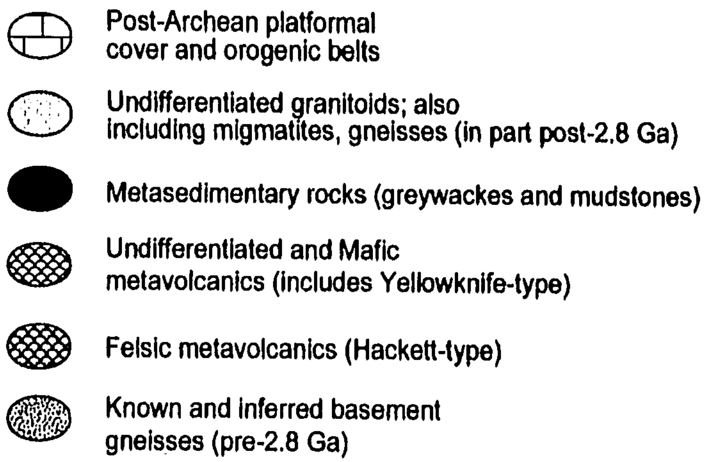

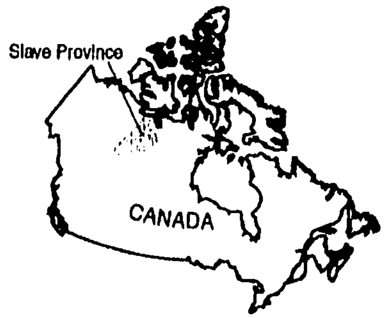

Fig. 1-1: Generalized geology of the Slave Province after Bleeker et al. (1999b), Henderson (1985) and references therein. YK stands for Yellowknife.

of the Archean supracrustal rocks in the Slave Province under the name Yellowknife Supergroup.

Approximately 65% of the Slave Province is composed of granitoid rocks and gneisses. Granodiorites, granites, gneisses, migmatites, tonalites and trondhjemites older than 2.8 Ga are considered part of an old sialic basement in the Slave Province (Fig. 1-1; Bleeker and Davis, 1999). The remainder of the granitoids are represented by different suites that intruded the basement and the Yellowknife Supergroup (Fig. 1-1).

Between 2.72 and 2.66 Ga felsic and mafic volcanics (part of the Yellowknife Supergroup) were erupted (Henderson et al., 1987). This was followed by the deposition of greywacke-mudstone turbidites (ca. 2661 Ma; Bleeker et al., 1999b). Near Yellowknife, these turbidites belong to the Burwash Formation (Fig. 1-2; Henderson, 1985). The turbidites are interbedded with and overlie the volcanic rocks. Between 2.63 to 2.59 Ga, granitoid plutons intruded the supracrustal domains and are associated with broad "thermal highs" indicated by the cordierite isograds in Fig. 1-2 (Davis and Bleeker, 1999).

Three types of tectonic models have been proposed to explain the formation of the Slave province: 1) intracratonic-extensional (Henderson, 1981; Easton, 1985; Thompson, 1989), 2) collisional-accretionary (such as island arc-continent collisions (Folinsbee et al, 1968; Hoffman, 1986; Kusky, 1989; King et al., 1990) and 3) Andean-type margin (Fyson and Helmsteadt, 1988). Bleeker et al. (1997) recognized that the overall tectonostratigraphy is more complex than

Fig. 1-2: Location of study area. Modified after Davis and Bleeker (1999).

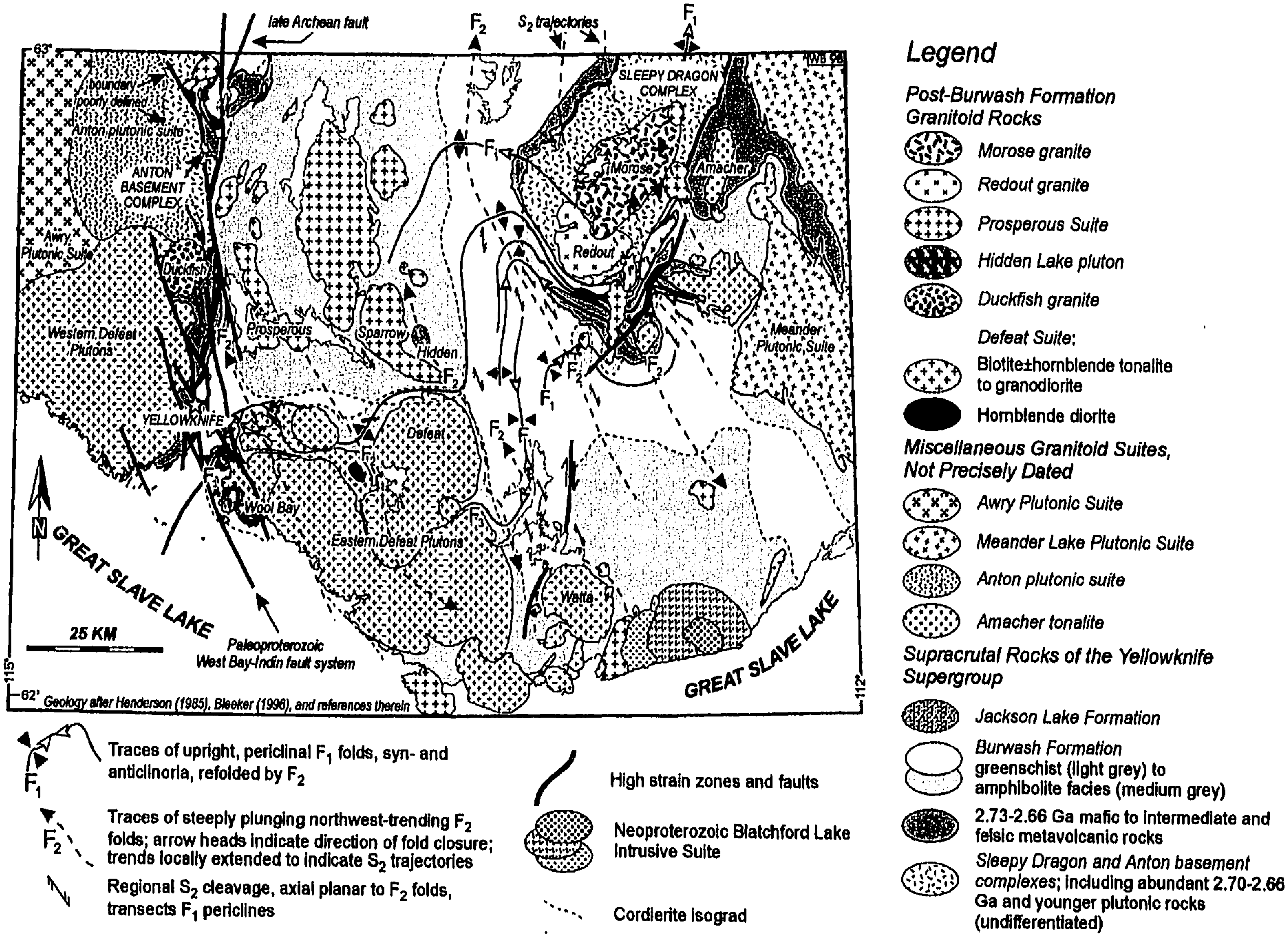

previously realized, with multiple unconformities, and proposed a multistage tectonic evolution which includes elements of the above three models. The tectonic models are discussed in detail in section 2.2 (Tectonic Interpretations). Recent work has focused on determining the ages of the various units, deformation events and timing of metamorphism, and incorporating these new data with field evidence to support a province wide tectonic model (Bleeker et al., 1999a, b; Bethune et al., 1999).

In regions with complex deformation histories, such as the southern Slave Province, the internal fabrics of syntectonic granite plutons can preserve a record of the strain field associated with synmagmatic tectonics. This thesis focuses on the Late Archean Sparrow and Prosperous plutons, two of the principal intrusions of the Prosperous Suite (Fig. 1-2). The peraluminous two-mica Prosperous Granite Suite is located 40 km northeast of Yellowknife and crops out within the cordierite and andalusite bearing metagreywackes of the Burwash Formation (Fig. 1-2). The Burwash Formation has undergone two main Archean deformation events: upright folding (D_1, bracketed between 2660-2628 Ma; Davis and Bleeker, 1999) and regional scale refolding about steeply plunging fold axes (D_2, ca. 2600 Ma; Bleeker et al., 1997). The Prosperous Suite plutons represent collisional-type granite magmatism associated with the D_2 event as defined by Bleeker and Beaumont-Smith (1995) and Bleeker et al. (1997).

In conjunction with the SNORCLE Lithoprobe seismic transect and the Slave Province NATMAP program, structural analyses of the granites and their host rocks and magnetic fabric analyses of the granites have been undertaken as part of a broader study of the relationships between plutonism and tectonics in the Yellowknife region. The studies are designed to establish the timing of granite plutonism with respect to the regional structural evolution, to help unravel the kinematics of the regional deformation and to provide a better understanding of the mechanisms of syntectonic pluton emplacement in the region. It is hoped this will lead to a clearer understanding of the D_2 deformation event in the southern Slave Province and provide insights into crustal dynamics in Late Archean terranes.

The specific objectives of this thesis are to determine the structure of the plutons, timing of pluton emplacement in relation to the D_2 deformation event, and the mode of pluton emplacement. To achieve those goals, field and microstructural studies of the granites and their host rocks are complemented by analysis of the anisotropy of magnetic susceptibility (AMS) of the granites.

The thesis is organized into seven chapters. Chapter 1 is the introduction. Chapter 2 discusses the regional geology of the southern Slave Province, tectonic interpretations, deformation events and metamorphism. Chapter 3 details the previous work performed on the Prosperous Suite in relation to mineralogy, trace element analysis, metamorphism and structure. Chapter 4 outlines the methodology used and gives background on the AMS technique. Chapter 5 presents and discusses the porphyroblast-fabric relationships in the Burwash Formation adjacent to the Prosperous and Sparrow plutons. Chapter 6 presents and discusses microstructure, magnetic mineralogy and AMS results for the plutons. Chapter 7 discusses the timing of pluton emplacement, the significance of the magnetic lineations, presents models for the emplacement of granitic magmas, proposes an emplacement model for the Prosperous Suite, and gives the conclusions of the study. Appendix I contains the compiled AMS data and stereonets of AMS fabric orientations for each site. Appendix II contains a map of all station locations, and a table listing sample numbers.

The information in this thesis has also been presented at the Yellowknife Geoscience Forum in 1996 and 1997 (Ham et al., 1996; Ham et al., 1997a), the Lithoprobe SNORCLE and Cordilleran Tectonics Workshop in 1997 and 1998 (Ham et al., 1997b; Ham et al., 1998a) and at the GAC/MAC Annual Meetings in 1997 and 1998 (Ham et al., 1997c; Ham et al., 1998b). The magnetic fabric results from the Sparrow pluton have been published in the Journal of Structural Geology (Benn et al., 1998a). A Department of Indian Affairs and Northern Development (DIAND) open file report has also been released on the Prosperous and Sparrow plutons (Ham and Benn, 1998).

Chapter 2: Geology and Tectonic Setting of the Southern Slave Province

This chapter discusses the regional geology of the Yellowknife Domain. The Yellowknife Domain was designated by Bleeker and Beaumont-Smith (1995) as the area between 62^0N-63^0N and 112^0W-116^0W that was covered by Henderson's (1985) compilation map. Descriptions of the basement rocks, the Yellowknife Supergroup and post-Yellowknife Supergroup plutonic suites are provided. The Prosperous Suite, which is the topic of this thesis, is introduced in this chapter and discussed in detail in Chapter 3. Also included in this chapter are tectonic interpretations for the southern Slave, descriptions of the deformation events and structures in the Burwash Formation turbidites, and a summary of the metamorphism.

2.1 LITHOTECTONIC ASSEMBLAGES

The supracrustal rocks of the Yellowknife Domain (Fig. 1-1, and Fig 1-2) are included in the Yellowknife Supergroup (Henderson, 1970), which is composed of mafic and felsic volcanic rocks at its base overlain by metasedimentary rocks of the Burwash Formation. The latter consists predominantly of turbiditic greywackes. The Sleepy Dragon Complex, a multiphase granitoid-gneiss complex that structurally and stratigraphically underlies the Yellowknife Supergroup (Davidson, 1972; Henderson, 1985; Kusky, 1990; Bleeker, 1996) outcrops in the eastern part of the region (Fig.1-2).

Metamorphosed granodiorites and quartz diorites of the Anton Complex (Henderson, 1985), which is also believed to underlie the Yellowknife Supergroup, outcrop to the west. Intruding the Yellowknife Supergroup are several plutonic suites (Henderson, 1985; Davis and Bleeker, 1999). The following discussions of the principal assemblages are based on Henderson (1985) unless otherwise noted.

2.1.1 Basement Rocks

Granodiorites, granites, gneisses, migmatites, tonalites and trondhjemites older than 2.8 Ga (Fig. 1-1) are considered basement in the Slave Province (Davis and Bleeker, 1999). The basement rocks shown in Fig. 1-2 consist of the Anton Complex and the Sleepy Dragon Complex. These complexes are discussed further below.

Anton Complex (AC)

The Anton Complex is located west of Yellowknife and is about 30 km long by 15 km wide (Fig. 1-2). It consists of metamorphosed and unmetamorphosed intrusions of granite, granodiorite and tonalite. The age of at least some of the basement granitoids and gneisses is ca. 2945 Ma (Isachsen and Bowring, 1997; Bleeker et al., 1999b). Henderson (1985) describes the complex as compositionally and texturally heterogeneous. The Anton Complex contains massive homogeneous units and units displaying centimeter- to meter-thick layering (structural). Plagioclase (occasionally as augen), quartz, biotite, microcline, hornblende and epidote are present. Overall, the gneisses are medium- to fine-grained and equigranular. A steeply dipping north to northeast trending foliation, with local irregularities, is defined by biotite and oblate quartz aggregates. The complex is older than the surrounding plutonic rocks, and most contacts with adjacent plutonic rocks have been noted to be irregular to gradational in nature.

Sleepy Dragon Complex (SDC)

The Sleepy Dragon Complex located east-northeast of Yellowknife (Fig. 1-2) is a multiphase granitoid-gneiss complex that forms the basement to the Yellowknife Supergroup (Bleeker et al., 1997a, Bleeker, 1999b). It is 45 by 25 km in size. The complex consists of tonalites, granodiorites and granites. Intrusive phases are both unmetamorphosed and metamorphosed. The most abundant rock type is a foliated granodiorite to quartz diorite, containing plagioclase, quartz, biotite and microcline phenocrysts (Kusky, 1990). Elongated folded metagabbro inclusions display fold axes parallel to the main foliation in the granodiorite (Kusky, 1990). Minor diorite and mafic tonalite, which are locally intruded by the granodiorite, are also part of the Sleepy Dragon Complex (Kusky, 1990). The center of the complex contains younger intrusive granitic phases (such as the Morose granite and Redout granite shown in fig. 1-2 which are not part of the complex). Recent U-Pb dating shows that most of the rocks forming the SDC are between 2.9-2.71 Ga with the core of the SDC containing 2.68 and 2.58 Ga plutons which are not part of the complex (Ketchum and Bleeker, 1999). Bleeker and Beaumont-Smith (1995) proposed that the overall geometry of the Sleepy Dragon Complex resulted from two phases of regional deformation resulting in a mushroom fold interference pattern.

The Central Slave Basement Complex

Bleeker and Ketchum (1998a) present evidence that the Anton Complex and the Sleepy Dragon Complex are both part of a single, larger basement domain that is believed to underlie the south-central Slave Province (Fig. 2-1). They have named this complex the Central Slave Basement Complex (Fig. 2-2).

Mapping by Bleeker et al. (1999b) has shown that there are similarities amongst the basement rocks within the south-central region of the Slave Province. There are two dominant rock types: gneisses and granitoids. The gneisses are dioritic to tonalitic in composition, heterogeneous, and contain an old migmatitic layering. The gneisses are cut by deformed mafic dykes and intruded by younger granitoids. The granitoids are non-migmatized tonalites, granodiorites and minor granite. These granitoids are foliated and intruded by three sets of mafic dykes (Bleeker et al., 1999a).

The basement rocks become more strained as the contact with the supracrustal rocks is approached. The basement is unconformably overlain by a thin, highly deformed cover sequence. Bleeker et al. (1999b) propose that this

Fig. 2-1: Topology map of the Central Slave Basement Complex (CSBC). AC: Anton Complex; SDC: Sleepy Dragon Complex; JLC: Jolly Lake Complex; BC: Beniah Complex; SC: Step'nduck Complex; BLC: Big Lake Complex. Taken from Bleeker et al. (1999b) p. 1087.

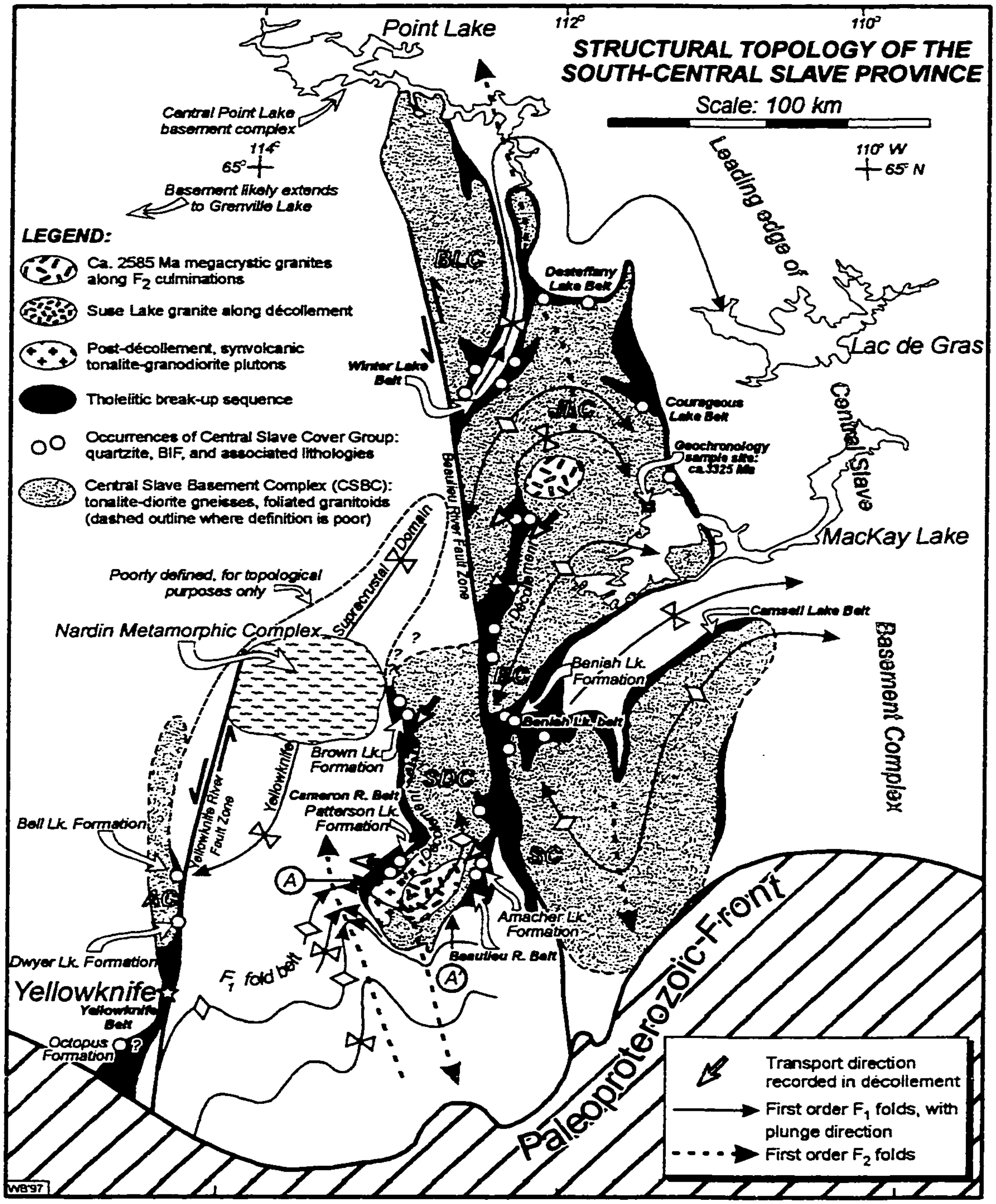

Fig. 2-2: Revised Formation Table for the Yellowknife Supergroup taken from Bleeker et al. (1999b). Lithologies from Bleeker et al. (1999b) and Henderson (1985).

	GROUP/SUITE	FORMATION	LITHOLOGY	INTERPRETATION
YELLOWKNIFE SUPERGROUP	UNNAMED GROUP	JACKSON LAKE FORMATION BEAULIEU RAPIDS FORMATION KESKARRAH FORMATION (and similar formations)	Conglomerates and sandstones	Post-F1 ca. 2600 Ma
	unconformity			
	Poorly defined assemblages in the northeast and southwest regions of the Slave Province			ca. 2630-2605
	DUNCAN LAKE GROUP AND EQUIVALENTS	BURWASH FORMATION	Greeschist grade metagreywackes, siltstones and mudstones; amphibolite grade psammitic to pelitic schists	Tubidites ca. 2661 Ma
		WALSH LAKE FORMATION	Similar to the Burwash Formation	Turbidites
	BANTING GROUP AND EQUIVALENTS	BANTING GROUP (and equivalents)	Felsic volcanics	Calc-alkaline successor arc sequence
		RAQUETTE LAKE FORMATION and DETOUR LAKE FORMATION	Quartzite sandstone and conglomerate	Basal conglomerate
	local unconformity			
	KAM GROUP AND EQUIVALENTS	Kam Group volcanic formations and equivalents	Mafic volcanics	Parautochthonous to allochthonous tholeiitic break-up sequence ca. 2.7 Ga. Affected by ca. 2687 Ma to ca. 2734 Ma high strain zone.
	CENTRAL SLAVE COVER GROUP	BELL FORMATION DWYER LAKE FORMATION PATTERSON LAKE FORMATION BROWN LAKE FORMATION AMACHER LAKE FORMATION BENIAH LAKE FORMATION (other unnamed formations)	Mafic to ultramafic volcanics, conglomerate, chromite bearing fuchsitic quartzites, silicate or oxide facies banded iron formation; local intrusions of ultramafic sills	Autochthonous to parautochthonous cover sequence. Affected by ca. 2687 Ma to ca. 2734 Ma high strain zone.
unconformity/ca. 2687 Ma to ca. 2734 Ma high strain zone				
	CENTRAL SLAVE BASEMENT COMPLEX	ANTON COMPLEX SLEEPY DRAGON COMPLEX STEP'NDUCK COMPLEX BENIAH COMPLEX JOLLY LAKE COMPLEX BIG LAKE COMPLEX POINT LAKE COMPLEX	Heterogeneous dioritic to tonalitic gneisses; tonalites, granodiorites, minor granite; mafic dykes	Old sialic basement ca. 2.9 Ga to 3.3 Ga

thin cover sequence be named the Central Slave Cover Group and be considered the base of the Yellowknife Supergroup.

2.1.2 Yellowknife Supergroup

The Yellowknife Supergroup was originally defined by Henderson (1970) to contain all the Archean supracrustal rocks in the Slave Province. Bleeker et al. (1999b) show that the Yellowknife Supergroup consists of a thin autochthonous volcanic and clastic cover sequence at its base (the Central Slave Cover Group) overlain by volcanic rocks and greywacke turbidites (Burwash Formation) (see Fig. 2-2 for stratigraphic summary). Younger Archean conglomerates occur at the top of the Yellowknife Supergroup.

Central Slave Cover Group (CSCG)

The contact of the Central Slave Cover Group (CSCG; Bleeker et al., 1999b) with the underlying Central Slave Basement Complex is a sheared unconformity (Fig. 2-1 for location of CSCG; Fig 2-3 for the tecotonostratigraphy). The CSCG is a highly deformed, thin (generally ≤200 m thick), discontinuous, and locally imbricated post 2.93 Ga succession. It contains minor volcanic rocks, clastic sedimentary rocks (including fuchsitic quartzites) and banded iron formation. Mafic and ultramafic volcanics occur locally at the base followed by conglomerates and/or immature quartz-rich grits. Overlying this are detrital chromite-bearing fuschitic quartzites, felsic volcanics (locally), and silicate or

Fig. 2-3: Tectonostratigraphy of the Central Slave Cover Group (CSCG). Taken from Bleeker et al. (1999a) p. 1115.

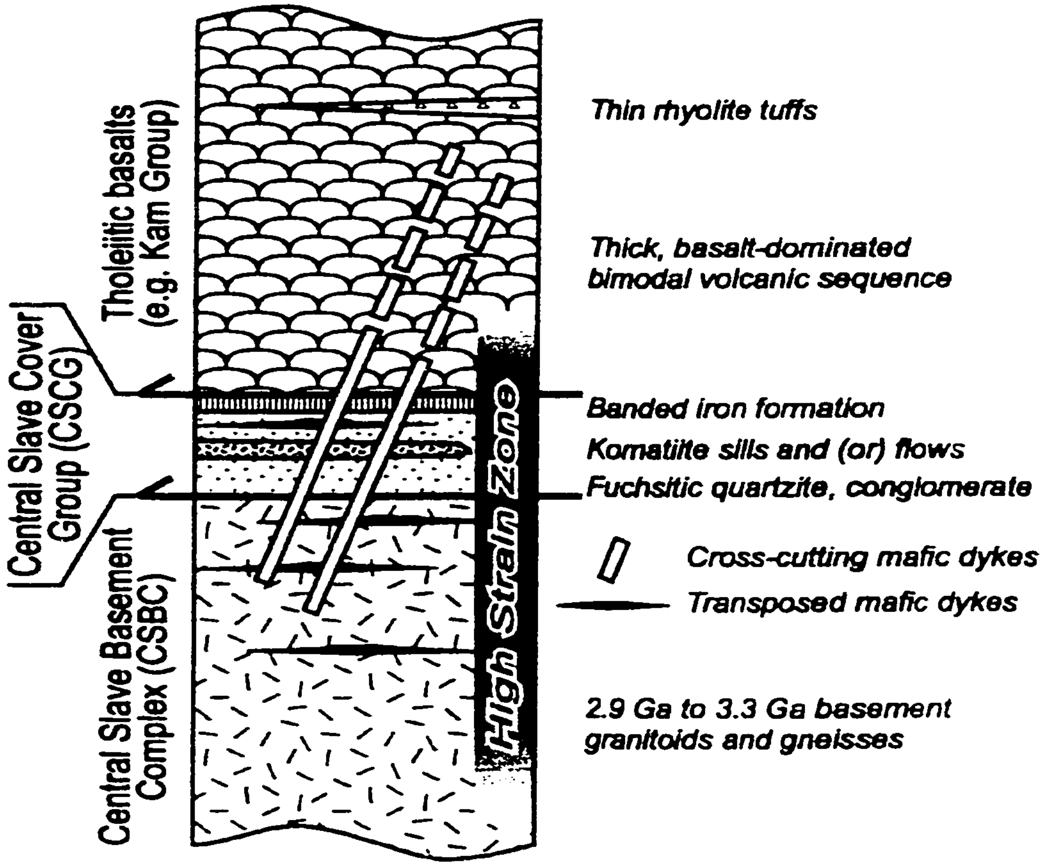

oxide facies banded iron formation. The sequence is locally intruded by ultramafic sills (Bleeker et al, 1999b).

Bleeker et al. (1999b) proposed that the ultramafic and mafic volcanics, as well as the conglomerates, are the result of active plume induced rifting of the Central Slave Basement Complex. Local shallow shelves, resulting from the subsidence, allowed for the accumulation of weathered basement material. Extensive weathering is proposed to have eliminated all minerals except for minor potassium feldspar, quartz and heavy minerals such as chromite, zircon, etc., resulting in chromite bearing fuchsitic quartzites. Bleeker et al. (1999b) further proposed that the transition to the banded iron formation occurred when the shallow shelves became sediment starved.

Volcanic Rocks

Between 2.72 and 2.66 Ga (Isachsen and Bowring, 1994) felsic and mafic volcanics were erupted. The volcanic rocks were later metamorphosed to lower greenschist to amphibolite grade. In the western region of the Slave Province, these bimodal tholeiitic mafic-felsic series volcanics (Hoffman, 1989; King and Helmstaedt, 1997) lie above the Central Slave Cover Group and Central Slave Basement complex. The contact between the volcanics and the underlying units is a regional décollement (Bleeker and Ketchum, 1998b). The volcanics near Yellowknife belong to the Yellowknife Greenstone Belt (Fig. 1-2) and consist of pillow lavas with abundant gabbroic bodies, dykes, minor cherts and felsic tuffs overlain by rhyodacite breccias, tuffs (welded in places) and pillowed dacites (Helmstaedt and Padgham, 1986). The volcanics near the Sleepy Dragon Complex belong to the Cameron River Belt (Fig. 1-2) and are composed of mafic volcanics with lenses of ultramafic rocks (locally near the base), followed by pillow lavas with intermediate to felsic rocks in the upper part of the succession (Fyson, 1990). Most of the greenstone belts overlying the Central Slave Basement Complex are similar in tectonostratigraphy with a tholeiitic breakup sequence unconformably overlain by a calc-alkaline sequence (Bleeker and Ketchum, 1998b).

Both Yellowknife and Cameron River belts display similar structural relationships. The Yellowknife Belt consists of steep to vertical northeast trending units that dip toward the east (away from the basement rocks) (Isachsen and Bowring, 1997). The units of the Cameron River Belt strike northwest to north, and northeast, and dip steeply to the west away from the basement rocks (Fyson, 1990).

Burwash Formation

The Burwash Formation conformably overlies the volcanic rocks. It consists of greenschist to amphibolite grade turbidite deposits (Henderson, 1985). The contact between the volcanics and the turbidites is locally sharp. In the absence of underlying volcanics, the Burwash Formation is separated from the

Central Slave Basement Complex by a regional unconformity (Bleeker and Ketchum, 1998b).

The Burwash Formation is 5-10 km thick and consists predominantly of greywacke-mudstone couplets with occasional thin (<2 cm thick) tuff layers. Beds are laterally continuous with constant thickness. Massive greywacke units can be in excess of 8 m thick, and as thin as mm-scaled laminations. Bouma sequences (Fig. 2-4) are evident in the Burwash Formation, supporting the interpretation that the sediments are turbidites. Usually, only the upper parts of the Bouma sequence are preserved, with occasional groups of thicker, coarse grained, grainflow beds. The bases of beds often show small scale scours, as well as load and flame structures. Dewatering features, such as ball and pillow structures, sandstone dykes and sills, are common. Concretions are also present.

Recent work by Waldron and Bleeker (1997) identified three possible facies associations in the Burwash Formation: 1) outer fan or inter-channel mid-fan deposits characterized by thin bedded, laterally continuous units with Bouma sequences; 2) levee systems contained thick bedded sandstones with scour and fill structures, dewatering sheets, and possible traction carpets; and 3) channel fill deposits characterized by massive sandstones with minor conglomerates. Waldron and Bleeker (1997) interpreted the Burwash Formation to be formed by turbidity currents and other sediment gravity flow mechanisms.

The sediments are texturally and chemically immature, with an average grain size of up to 1.5 mm (greywackes). For the greywackes, the matrix is

Fig. 2-4: Bouma Sequence. Modified from Walker (1992) and Bouma (1962).

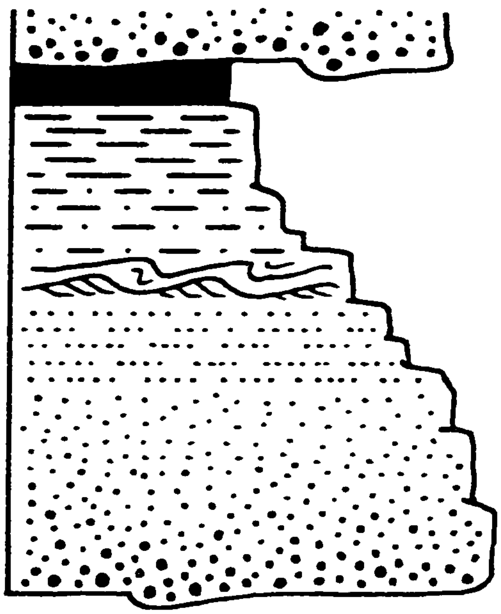

DIVISION	STRUCTURES
A	structureless
E(h)	pelitic interval (hemipalgic origin)
E(t)	pelitic interval (turbidite origin)
(D)	parallel laminated silt and mud
C	rippled and/or convoluted
B	parallel laminated sand
A	structureless

dominant followed by lesser amounts of quartz, feldspar and lithic rock fragments. The matrix consists of chlorite, muscovite, biotite and quartzofeldpathic material. The matrix is derived from original argillaceous material, and diagenetic breakdown of coarse components. Overall, sediments in the Burwash Formation are derived from both intermediate to felsic, granitic and volcanic sources (Henderson, 1985; King and Helmsteadt, 1997).

The amphibolite facies rocks of the Burwash Formation consist of schists, psammites to pelites, that are commonly porphyroblastic. These rocks contain various assemblages of quartz, plagioclase, biotite, muscovite, cordierite, andalusite, sillimanite, staurolite, and garnet. The primary structures and compositional characteristics of turbidites are locally preserved, despite the high metamorphic grade. See section 2.3 for the discussion of the deformation and metamorphism in the Burwash Formation.

2.1.3 Plutonic Rocks

Intruding the Yellowknife Supergroup are several plutonic suites (Fig. 1-2, Fig. 2-5). The Defeat, Prosperous and Morose suites are described below. Only a brief description of the Prosperous Suite is given, since it is discussed in detail in Chapter 3.

Defeat Suite

The Defeat Suite, which has been dated at 2624 Ma (U-Pb zircon, Davis and

Fig. 2-5: Lithologies of the plutonic suites which intrude the Yellowknife Supergroup. Lithologies from Henderson (1985) and Davis and Bleeker (1999).

EON	SUITE/PLUTON		AGE	LITHOLOGY
ARCHEAN	**Relative age of the Meander Lake Plutonic Suite not defined**			
	MOROSE GRANITE		2586±2 Ma [1] U-Pb monazite	White-pink-brown biotite-muscovite granite (not equigranular)
	STAGG PLUTONIC SUITE		2588±7 Ma [2] U-Pb zircon	Grey-dark pink, equigranular to coarsely porphyroblastic, biotite granite to tonalite with hornblende locally
	REDOUT GRANITE		2370-2550 Ma [3] K-Ar	Pink, heterogeneous, equigranular muscovite granite and pegmatite
	PROSPEROUS GRANITE		2596±2 Ma [1] U-Pb monazite	White-buff, homogeneous, equigranular, biotite muscovite granite and pegmatite
	DUCKFISH GRANITE		2608±3 Ma [2] U-Pb titanite	Mauve-pink, equigranular biotite granite
	MEANDER LAKE PLUTONIC SUITE		†	Heterogenous, biotite (with muscovite locally) granite to granodiorite
	AWRY PLUTONIC SUITE		2550-2630 Ma [4] U-Pb	Light pink, equigranular, heterogenous biotite granite to granodiorite, and pegmatite
	DEFEAT SUITE	DEFEAT PLUTONIC SUITE	2624 Ma [1] U-Pb zircon and titanite	White-pink, equigranular, homogeneous, biotite granodiorite to tonalite; rare hornblende
	DEFEAT SUITE	WOOL BAY QUARTZ DIORITE	2628±3 Ma [1] U-Pb zircon	Dark grey-black, equigranular quartz diorite
	DEFEAT SUITE	DETOUR GRANODIORITE	†	Grey, prophyritic granodiorite; metamorposed

† no age available
1 Davis and Bleeker (1999)
2 van Breemen et al. (1992)
3 Green and Baadsgaard (1971); age unreliable
4 Dudás et al. (1990)

Bleeker, 1999), intrudes the Yellowknife Supergroup and the SDC. The suite consists of biotite-bearing diorite, tonalite, granodiorite, and minor granite (Fig. 2-6). The large plutonic complexes and individual plutons are commonly circular or lobate in shape, though irregular shaped plutons also occur. Henderson (1985) also noted small (< 1 km) lens- or sill-shaped plutons. The Defeat plutons cut upright F_1 folds, and the S_2 foliation refracts around the plutons (Davis and Bleeker, 1999). The internal fabric of the plutons merges into the trajectories of the regional S_2 foliation (Davis and Bleeker, 1999). Porphyritic dykes containing plagioclase and quartz associated with the Defeat Suite, cut across F_1 folds and are folded by F_2 (Davis and Bleeker, 1999). Based on the above field relationships, Davis and Bleeker (1999) propose that the Defeat Suite is late to post-F_1 but pre-F_2, with plutonism starting by 2628 Ma and continuing to at least 2620 Ma, and possibly until ca. 2615 Ma (U-Pb zircon dates from Davis and Bleeker, 1999).

The Defeat Suite is described by Henderson (1985) as medium grained, homogeneous, and equigranular. Weathered surfaces are buff, white, and pink in colour. Fresh surfaces are white to dark red in colour. The plutons are dominantly composed of plagioclase, quartz and biotite. The plagioclase crystals, which are distinctive of the suite, are subhedral to euhedral, stubby, strongly zoned, equigranular, and occur as phenocrysts or aggregates. Potassium feldspar (normally microcline) is also present. Muscovite, where present, is believed to be of secondary origin. The Defeat Suite is locally hornblende bearing, with

Fig. 2-6: Modal analysis plot for the Defeat, Prosperous and Morose plutons. Modified from Henderson (1985). Plutonic rock classification after Streckeisen (1976).

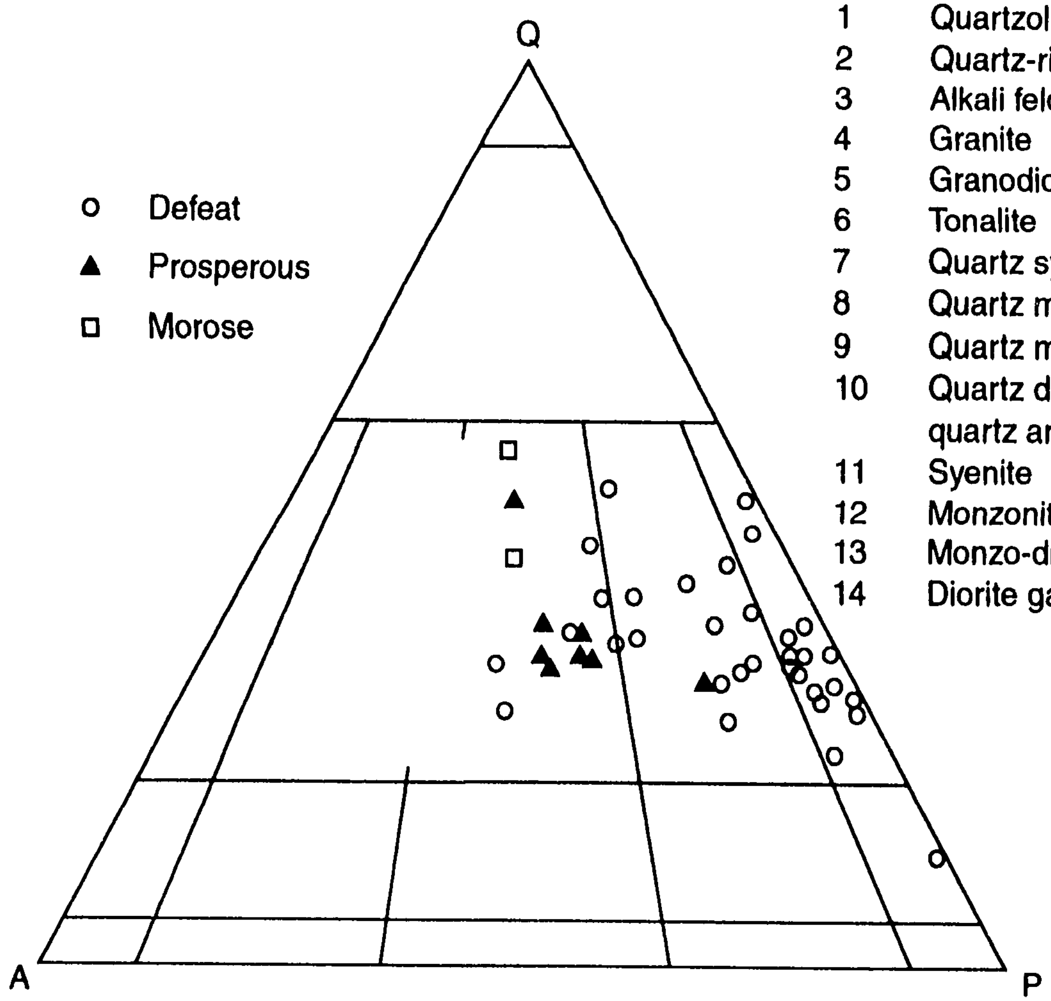

1 Quartzolite
2 Quartz-rich granitoids
3 Alkali feldspar granite
4 Granite
5 Granodiorite
6 Tonalite
7 Quartz syenite
8 Quartz monzonite
9 Quartz monzo-diorite/gabbro
10 Quartz diorite, quartz gabbro, quartz anorthosite
11 Syenite
12 Monzonite
13 Monzo-diorite/gabbro
14 Diorite gabbro anorthosite

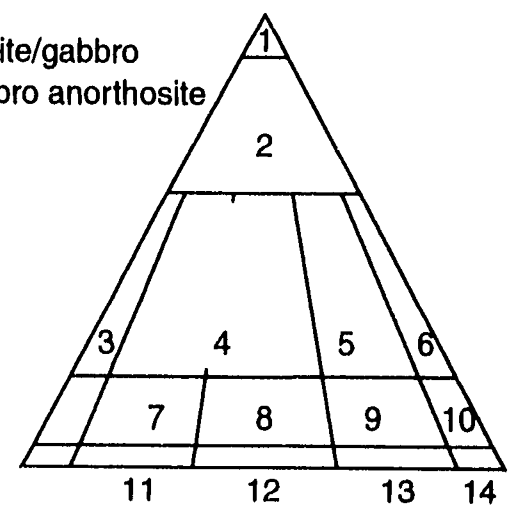

apatite, titanite and opaque minerals as the dominant accessory minerals (Henderson, 1985).

Henderson (1985) suggested that the Defeat Suite may have been formed in part from the remobilization of the pre-existing sialic crust. It has also been suggested that the Defeat Suite granitoids could represent subduction-related magmatism (eg. Fyson and Helmstaedt, 1988; Kusky, 1989; Kusky, 1990).

Prosperous Suite

The Prosperous Suite (2596±2 Ma, U-Pb monazite, Davis and Bleeker, 1999), intrudes metasedimentary rocks of the Yellowknife Supergroup and to a lesser extent rocks of the Sleepy Dragon Complex. It is predominantly composed of homogeneous, medium to coarse grained, foliated, muscovite-biotite granites (Fig. 2-6), with associated pegmatitic phases. The plutons are interpreted to be syn-D_2, and tabular in shape (Bleeker and Beaumont-Smith, 1995; Ham and Benn, 1998; Benn et al., 1998a). The Prosperous Suite is discussed in detail in Chapter 3.

Morose Granite

The Morose Suite is dated at 2586±2 Ma (U-Pb monazite, Davis and Bleeker, 1999), and intrudes the Yellowknife Supergroup and SDC. The suite consists of unmetamorphosed biotite granite (Fig. 2-6). The Morose Pluton, which intrudes the Sleepy Dragon Complex, is 25 km by 15 km in size and roughly elliptical in shape (Spark et al., 1999). The Morose Suite comprises coarse grained K-feldspar megacrystic granite with minor equigranular leucogranite pegmatite phases. Contacts with the host rocks are commonly sharp, although local narrow migmatitic zones occur in the Sleepy Dragon Complex (Henderson, 1985).

The plutons are white to pink to pale brown, or buff, in colour. The most obvious characteristic is the presence of elongate microcline megacrysts up to 5 cm long (Davis and Bleeker, 1999). The Morose Pluton contains large rafts or roof pendants (up to several kilometers in size) that are similar to the granitoid gneisses of the Sleepy Dragon Complex. Spark et al. (1999) defined two fabric domains in the Morose Pluton, based on field observations and magnetic fabric data. The center of the Morose Pluton displays a concentric/domal foliation pattern with shallow dips, defined by the potassium feldspar megacrysts. Weak magnetic lineations are parallel to the regional F_2 fold axes affecting the Sleepy Dragon Complex (Fig 1-2). The foliation at the margins of the pluton is steep. Davis and Bleeker (1999) observed local folding of the marginal foliation with attitudes that are similar to those of regional F_2 folds. Towards the northwest margin of the Morose Pluton, the magnetic lineation and mesoscopic foliation rotate to become almost parallel to the pluton contact (Spark et al., 1999). The magnetic lineations also rotate to near-parallelism with the pluton contact. Spark et al. (1999) propose that dextral shearing along the northwestern margin late during crystallization may account for the change in fabric orientation. They further suggest that the shallow dipping foliation in the center of the Morose Pluton represents a magma-emplacement fabric with the magnetic lineation recording tectonic reorientation of the fabric during crystallization.

2.2 TECTONIC INTERPRETATIONS

The three main types of models that have been proposed to explain the formation of the Slave province are: 1) intracratonic-extensional (e.g. Henderson, 1981; Easton, 1985; Thompson, 1989), 2) collisional-accretionary (Card and King, 1992; island arc-continent collisions are proposed by Folinsbee et al., 1968, Hoffman, 1986, Kusky, 1989, and King et al., 1990) and 3) Andean-type margin (Fyson and Helmsteadt, 1988). Bleeker et al. (1997a) proposed a multistage tectonic evolution which includes elements of the above three models. Each type is discussed further below.

Henderson (1981, 1985) interpreted the contact between the Sleepy Dragon Complex and the Yellowknife Supergroup as an unconformity, and proposed a tectonic model wherein the Yellowknife Supergroup represents the fill of an ensialic rift basin, bordered to the east by the Sleepy Dragon Complex, and by the Anton Complex to the west (Fig. 2-7). This model has been criticized for the following reasons: 1) the metavolcanic-turbidite belts in the Slave do not contain alkalic volcanics, evaporites, or alluvial fan deposits (Hoffman, 1989); and 2) the model does not account for the observed tectonic shortening, or the large volumes of plutonic rocks.

Fig. 2-7: Henderson's (1985) tectonic model for the southern Slave. Taken from Henderson (1985) p. 57.

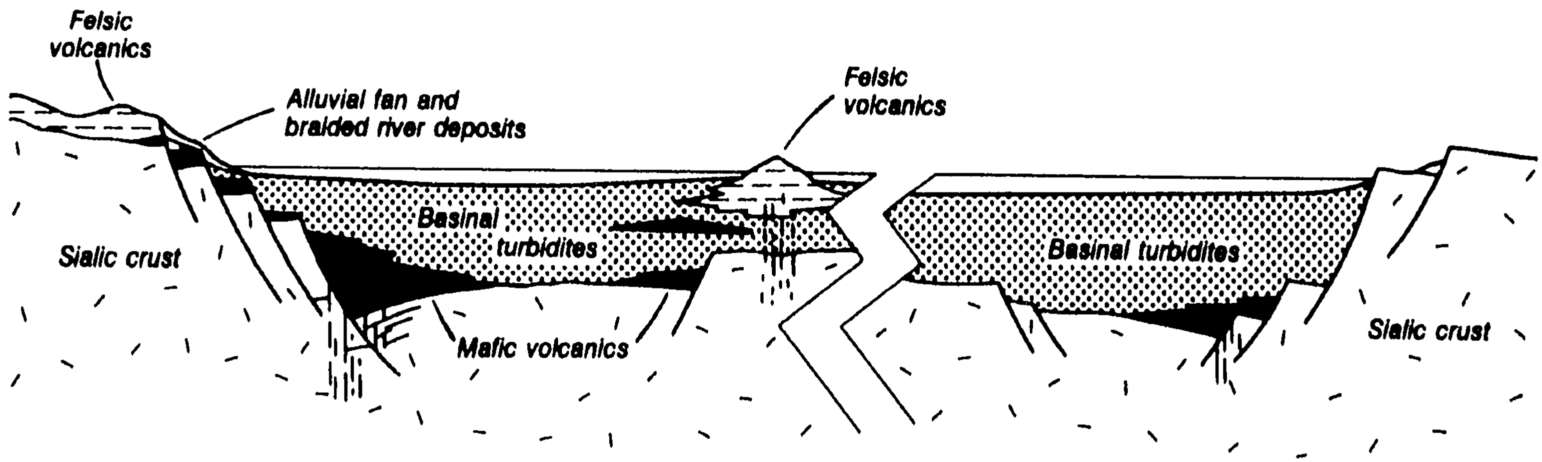

Subsequent workers proposed that the Yellowknife Supergroup represents the remnants of an oceanic basin (Fyson and Helmstaedt, 1988). Fyson and Helmstaedt (1988) proposed that the multiple mafic dykes and mafic pillow lavas suggest sea floor spreading, and that the mafic volcanics are megaxenolithic remnants of oceanic crust. As the ocean basin closed, plutonism and felsic volcanism occurred (Fig. 2-8). The felsic calc-alkaline magmas were due to a shallow dipping subduction zone. Once the basin was closed, underthrusting continued towards the east. This zone of underthrusting then shifted westward with time, causing calc-alkaline magmatism to migrate across the province. Fyson and Helmsteadt (1988) also state that the rectilinear zig-zag pattern of pluton-volcanic contacts is the result of plutons following crustal fracture systems.

Due to the lack of basement in the eastern portion of the Slave Province, Kusky (1989, 1990) proposed that obduction occurred during collision of a microcontinent (western Slave) with a west-facing magmatic arc (eastern Slave). Kusky (1989, 1990) divided the Slave Province into 4 terranes (Anton Terrane, Sleepy Dragon Terrane, Contwoyto Terrane, and the Hackett River Arc; Fig 2-9), separated by high strain zones, which would have been juxtaposed during collisional orogenesis. In Kusky's (1989, 1990) model, the Yellowknife Supergroup represents the remnants of a collage of arc assemblages, obducted oceanic crust and foredeep basin material thrust over the Sleepy Dragon Complex during a collisional event (Fig 2-9). In these models, calc-alkaline

Fig. 2-8: Fyson and Helmstaedt's (1988) model for the Slave Province.
A) Rifting of basement rocks. B) Basin closure and obduction of oceanic crust. C) Tectonic underplating and westward migrating magmatism. EL stands for present erosion level. Taken from Fyson and Helmstaedt (1988) p. 312

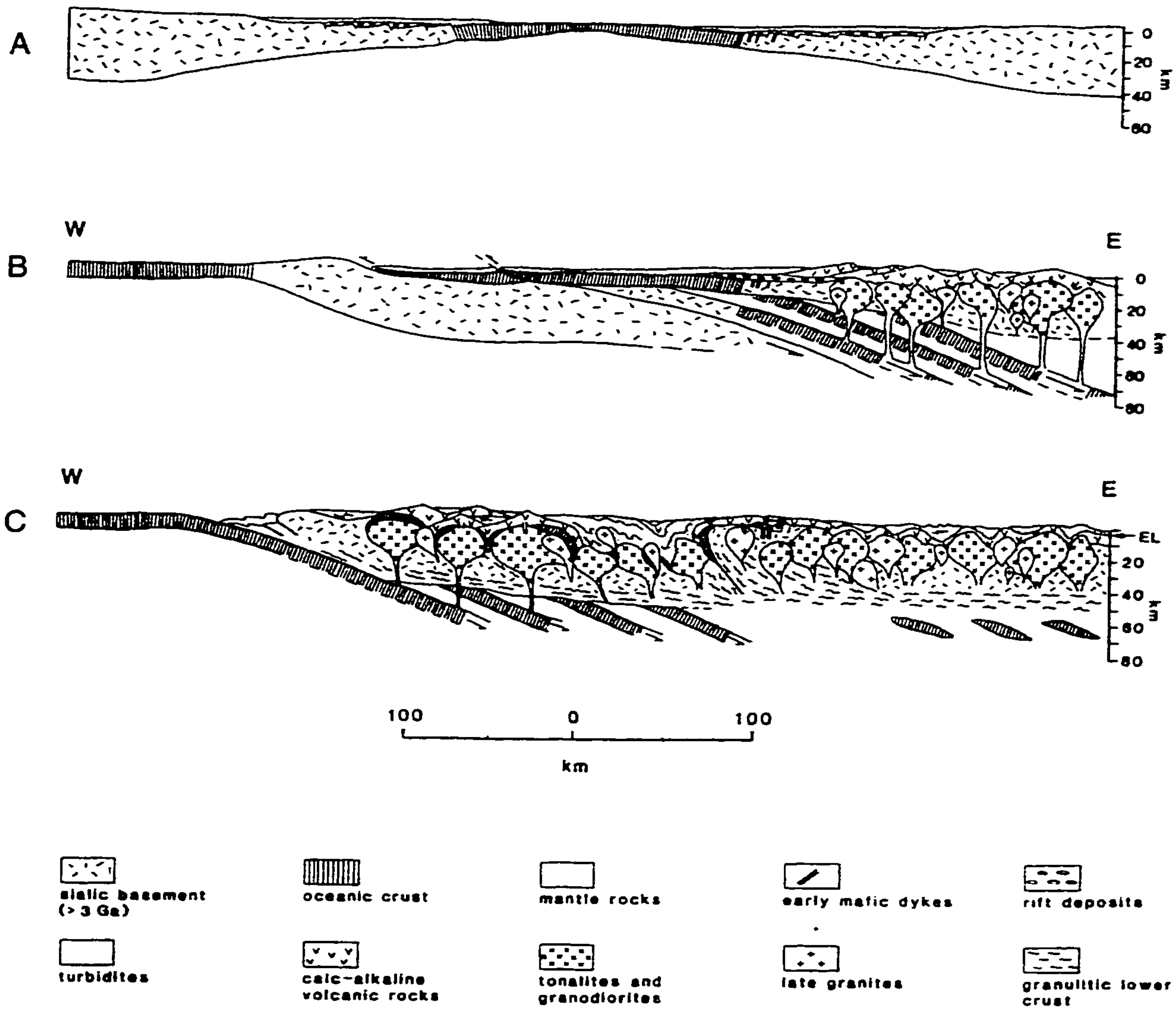

Fig. 2-9: Kusky's (1989) model for accretion of the Slave Province between 2.57 and 2.5 Ga. Taken from Hoffman (1989) p. 459, which was modified from Kusky (1989).

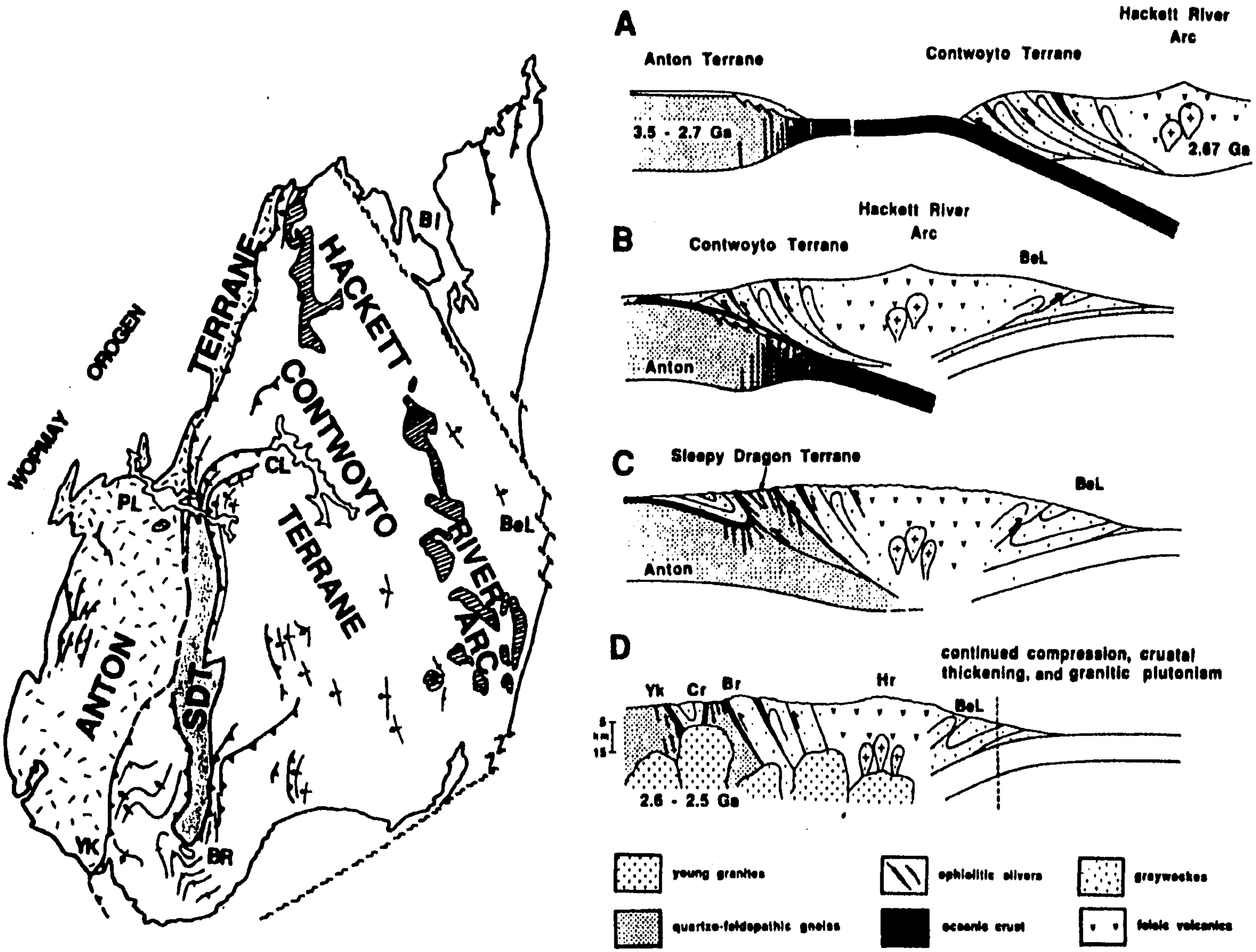

plutons such as the Defeat Suite granitoids would represent subduction-related magmatism.

There are several problems with Kusky's (1989, 1990) model. First, the Sleepy Dragon Terrane and the Anton Terrane are no longer believed to be distinct terranes; rather they are both interpreted to be part of the Central Slave Basement Complex (Bleeker et al., 1999b). Ultramafic rocks, that were proposed to be tectonic slices of obducted ophiolite, are actually sills and/or flows emplaced in the Central Slave Cover Group (Bleeker et al., 1999a). The observed stratigraphy of the greenstone belts does not support an origin within an ocean basin (Bleeker et al., 1999a, Bickle et al., 1994).

The most complete and comprehensive model to date is the one proposed by Bleeker et al. (1997a). Bleeker et al. (1997a) proposed a tectonic model for the Slave where, after initial rifting, juvenile arc terranes interacted with one or more microplates consisting of older sialic crust with their cover sequences (Fig. 2-10). In this model the Central Slave Basement Complex represents an old continental fragment with the Central Slave Cover Group as its characteristic cover sequence. Following an initial collision, a successor arc was built on the earlier collage, leading to a second phase of rifting and basin development (Bleeker et al., 1997a). The Burwash Formation was deposited as turbidites within this successor basin. Following this stage, the basin was closed and

Fig. 2-10: Bleeker et al.'s (1997) tectonic model for the Slave Province. SDC: Sleepy Dragon Complex; CSCG: Central Slave Cover Group. Diagram courtesy of W. Bleeker (unpublished data).

STAGE 1: 2730-2700 Ma
Microplate of old (2.85-3.35 Ga) sialic crust and cover sequence.

STAGE 2: 2710-2690 Ma
Back arc extension, drift and juvenile arc volcanism. Reversal in subduction direction.

STAGE 3: 2690 Ma
Docking of juvenile arc at ca. 2690 Ma. Volcanism in the Eastern Slave is interrupted. Thrusting, uplift, and erosion occur in the Western Slave. Development of a regional unconformity.

STAGE 4: 2686-2665 Ma
Construction of a continental, felsic, successor arc, and subduction steps back to the west. Shallow water clastic and carbonate rocks (e.g. Raquette Lake Formation) are deposited on the unconformity.

STAGE 5: 2670-2650 Ma
Rifting of the successor arc, back-arc extension and subsidence. Deposition of the Burwash Formation turbidites begins.

STAGE 6: Post-2658 Ma
Maximum opening of the back-arc basin and development of mafic magmatism.

LEGEND

- **Oceanic crust (not yet identified)**
- **Mafic to bimodal volcanic sequences: rift-drift transition**
- **Mafic dykes: breakup swarms**
- **Older supracrustal assemblages as part of basement**
- **2.85-3.35 Ga or older sialic crust, mostly tonalitic**
- **Juvenile mafic, intermediate, to felsic arc volcanics**
- **Syn-volcanic arc plutons: diorites, tonalites, to granodiorites**
- **Successor arc: calc-alkaline volcanics, abundant rhyolites**
- **Syn-volcanic arc plutons: diorites, tonalites, to granodiorites**
- **2665-2658 Ma Burwash Formation turbidites >5000m thick sequence**
- **Outboard terrane colliding during F1**

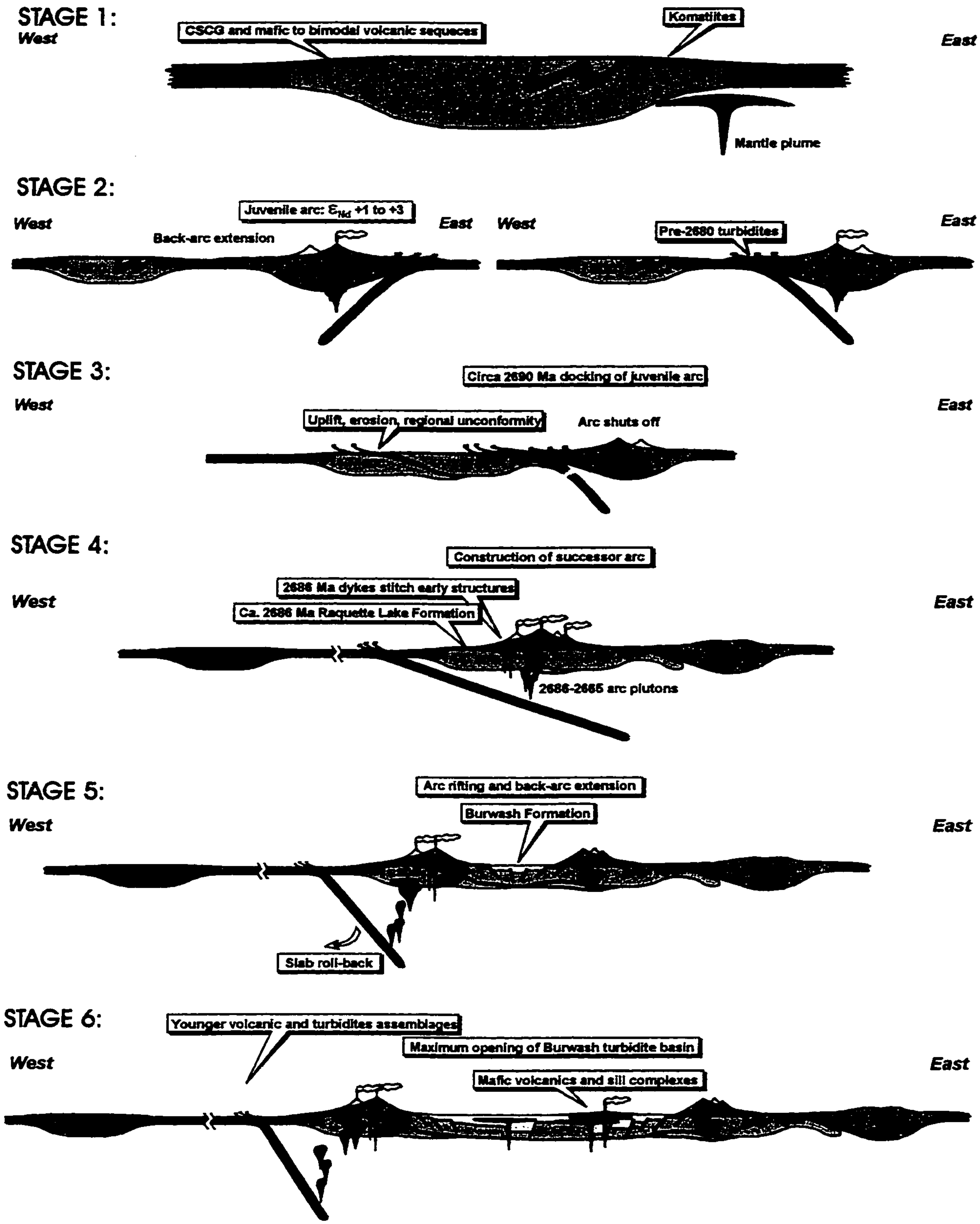
STAGE 1:
West
CSCG and mafic to bimodal volcanic sequeces
Komatiites
East
Mantle plume
STAGE 2:
Juvenile arc: ε_{Nd} +1 to +3
West
East
West
East
Back-arc extension
Pre-2680 turbidites
STAGE 3:
Circa 2690 Ma docking of juvenile arc
West
East
Uplift, erosion, regional unconformity
Arc shuts off
STAGE 4:
Construction of successor arc
2686 Ma dykes stitch early structures
Ca. 2686 Ma Raquette Lake Formation
West
East
2686-2665 arc plutons
STAGE 5:
Arc rifting and back-arc extension
Burwash Formation
West
East
Slab roll-back
STAGE 6:
Younger volcanic and turbidites assemblages
Maximum opening of Burwash turbidite basin
Mafic volcanics and sill complexes
West
East

shortened resulting in two deformation events that are attributed to successive distinct plate interactions (Bleeker et al., 1997a). The colliding terranes are as yet unidentified, although Bleeker et al. (1999a) suggests that the northeastern region of the Slave province may represent one such terrane. The Defeat Suite plutons are proposed to have developed in either a migrating subduction related arc system, or in a post-subduction, syn-collisional setting as a result of delamination (Davis and Bleeker, 1999). The two-mica and potassium feldspar granites (ca. 2.60-2.58 Ga) are proposed to be the result crustal shortening and lithospheric delamination (Davis et al., 1994) leading to melting in the crust. This would account for the wide distribution area of the granites.

2.3 STRUCTURE AND METAMORPHISM OF THE BURWASH FORMATION

Several phases of deformation, coupled with pluton emplacement, have resulted in locally complex structural geology of the Burwash Formation. The Formation is characterized by polyphase, tight to isoclinal folding, multiple cleavages, and layer parallel faulting (King and Helmsteadt, 1997).

Fyson (1980) recognized three principal regional scale fabrics. The oldest regional cleavage is a bedding parallel foliation (S_1) proposed to be the result of isoclinal folding. The bedding and S_1 have been subsequently deformed, resulting in variable orientation throughout the region. D_2 resulted in tight to isoclinal, upright, steeply plunging folds, with a NW trend, as well as dome-and-basin style F_1-F_2 fold interference patterns. Small upright, horizontal folds (F_3), that are slightly oblique to F_2, and formation of a regional NW-trending cleavage (S_3) are the result of a later D_3 event.

Bleeker and Beaumont-Smith (1995) also recognized three generations of structures through regional mapping of the Burwash Formation turbidites. The oldest regional foliation (S_1), a slaty cleavage, is axial planar to tight or isoclinal, upright, doubly-plunging folds (F_1). D_2 Deformation caused regional-scale refolding (F_2), about mostly steeply plunging axes, of the F_1 fold belt and resulted in the development of the principal regional foliation, S_2, a NW to N striking crenulation cleavage (i.e. Fyson's D_2 and D_3 events). This crenulation cleavage (S_2) is axial planar to F_2 folds which trend N-NW and are steeply plunging. The D_2 event resulted in fold interference that produced steeply plunging mushroom folds in the supracrustal cover and in the structurally lower basement complexes (Fig. 1-2; Bleeker, 1996). D_2 is interpreted to be the expression of regional dextral transpressive tectonics that was the far-field effect of a collisional event along the periphery of the proto-Slave craton as it existed at ca. 2600 Ma (Bleeker et al., 1997a). The dextral transpressive nature of D_2 deformation is inferred from the kinematics of discrete late-D_2 strike-slip shear zones and from the pattern of refolding of F_1 folds (Fig. 1-2). Regionally developed extension lineations associated with the main D_2 deformation phase are lacking in the Burwash Formation. Late during the D_2 event, deformation was localized within discrete shear zones, such as the Watta Lake and Yellowknife River Deformation Zones, which contain shallowly plunging extension lineations and associated dextral shear sense indicators (Bleeker and Beaumont-Smith, 1995). Locally, younger NE trending open F_3 folds and an associated coarsely spaced crenulation cleavage (S_3) overprint D_1 and D_2 structures. Retrograde chlorite is associated with S_3. Unless otherwise stated, all references to fabric generations, from this point forward, refer to those defined by Bleeker and Beaumont-Smith (1995).

The Burwash Formation has been affected by two main metamorphic events: M_1 regional low pressure metamorphism associated with the development of the F_1 fold belt, and M_2 pluton-enhanced regional and contact metamorphism occurring roughly during D_2 (Bleeker and Beaumont-Smith, 1995; Bethune and Carmichael, 1998; Bethune et al., 1999).

M_1 is only preserved in areas distant from plutonic rocks, and is defined by chlorite, biotite, and muscovite which occur aligned within an axial-planar slaty cleavage (Bethune and Carmichael, 1998; Bethune et al., 1999). Although M_1 is preserved at greenschist facies (Thompson, 1978; Davidson, 1967; Fyson, 1975), the maximum M_1 metamorphic grade is unknown (Bethune, 1999). Bethune and Carmichael (1998) further state that the transition between M_1 and M_2 was more or less a continuous progression that was punctuated by a change in deformation style. M_1 established a set of regional isotherms, that were later modified by burial and the thermal spikes associated with the intrusion of individual plutons (M_2). The combination of M_1 and M_2 resulted in thermal highs near plutons, with lows in the intervening areas (Fig 1-2). M_2 is characterized by amphibolite grade rocks containing cordierite, andalusite, staurolite and/or garnet, with sillimanite replacing the andalusite at pluton contacts (Bethune and Carmichael, 1998).

During D_2, Thompson (1978) proposed that high geothermal gradients were locally imposed on a 40-50 km thick sialic crust, resulting in low pressure metamorphism (M_2 according to Bethune and Carmichael, 1998) and partial melting. The partial melting is interpreted to be the source of the granitoids (Thompson, 1978). Work done by Bethune and Carmichael (1998) shows that M_2 was diachronous over approximately 50 Ma, with the metamorphic aureole around the Defeat Suite being the oldest, followed by the Prosperous Suite aureole, and the Morose-Redout aureole to the east being the youngest.

The Defeat aureole contains assemblages representative of Bathozone 2 (Bethune and Carmichael, 1998), where staurolite predominates and is regionally extensive and cordierite is rare. The isograds around the Defeat aureole are 20-30 Ma older than the Prosperous Suite isograds (Bethune et al., 1999). Where the Prosperous aureole overlaps the Defeat aureole, the staurolite, andalusite, and garnet are variably retrograded (Bethune et al., 1999).

The Prosperous aureole, which is wider than the Defeat aureole, contains andalusite, cordierite, staurolite, garnet, muscovite, biotite, plagioclase, and quartz assemblages that are also indicative of Bathozone 2 (Bethune and Carmichael, 1998). Bethune and Carmichael (1998) noted that staurolite formed first, followed by andalusite, and then cordierite in a clockwise P-T path (Fig 2-11), with staurolite forming at higher pressure but lower temperature. Bethune and Carmichael (1998) also observed cordierite rims on staurolite and andalusite, which have been interpreted to represent decompression.

There are a number of possible reasons for the Defeat aureole to be narrower than the Prosperous aureole. One reason for this may be due to the pluton shapes (Bethune et al., 1999). The Deafeat Suite may be made up of batholiths and stocks with steep sided contacts (Bethune et al., 1999), while the Prosperous Suite is proposed to be more "sheet-like" (Ham and Benn, 1998), with shallow contacts. The water content of the different magmas may also have played a role (Bethune et al., 1999). Tonalitic to granodioritic magmas of the Defeat Suite would have had a lower water content than the two-mica granite magma of the Prosperous Suite (Bethune et al., 1999). The increase in water content can contribute to higher advective heat transfer (Bethune et al., 1999). Another possibility is that the Prosperous Suite contains more radioactive elements (Bethune et al., 1999). Bethune et al. (1999) also suggested that heat may have accumulated in the orogen faster than it was being dissipated, therefore the Prosperous Suite may have intruded into a hotter crust.

The Defeat, Prosperous and Morose-Redout plutons are all interpreted to have been emplaced under pressures and temperatures corresponding to Bathozone 2 (2.5-3.7 kbar, 500-600^{0}C; Carmichael, 1978; Bethune et al., 1999), suggesting that emplacement depths were between 9 and 13 km. Quantitative

Fig. 2-11: P-T diagram for metamorphism in the Yellowknife Domain for D_2. Modified from Bethune and Carmichael (1998)

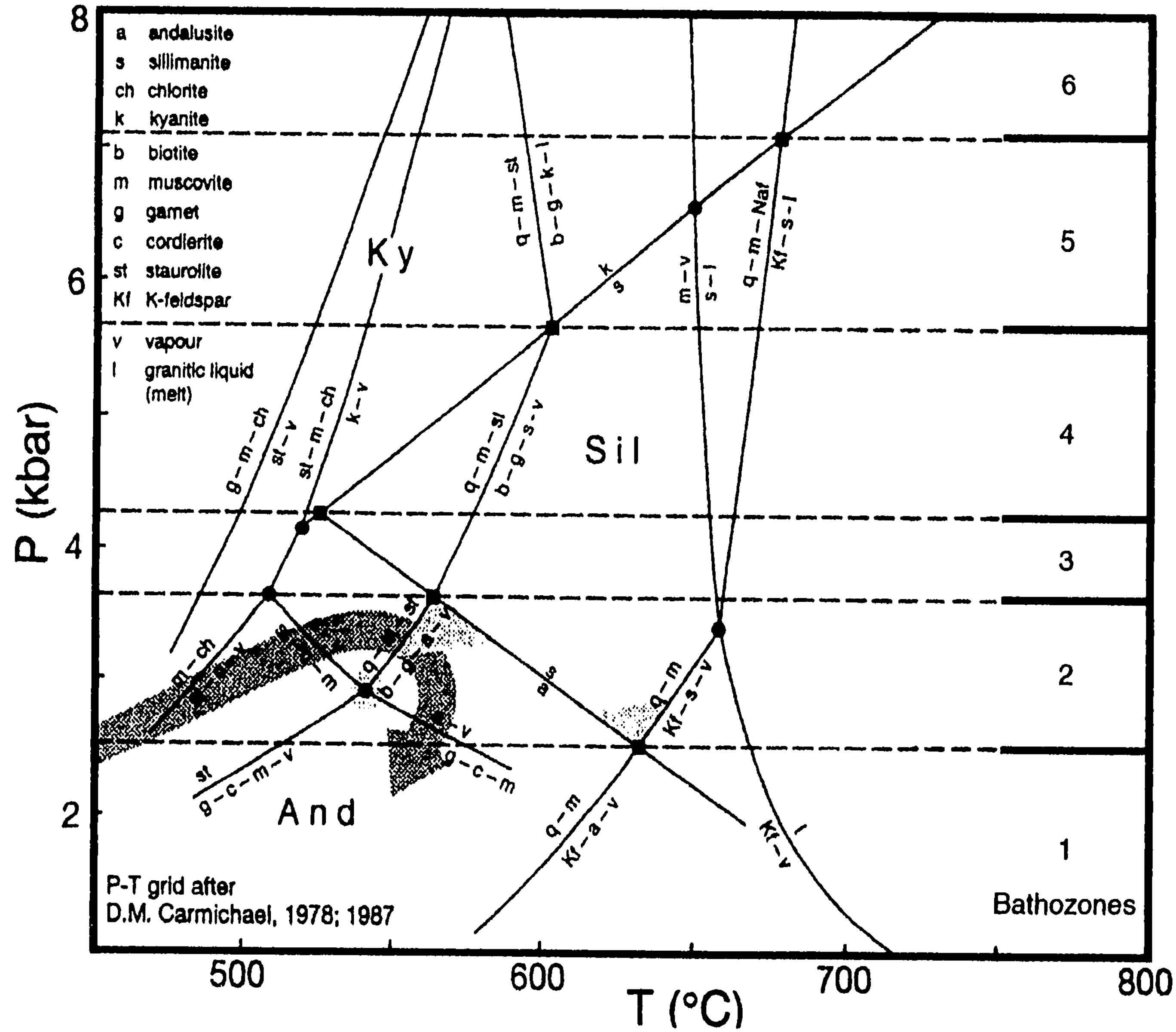

thermobarometry carried out by Bethune et al. (1999) has narrowed the range to 3.0-3.5 kbar and 550-600°C, for the Prosperous Suite. It is believed that the Defeat suite was intruded at slightly higher pressures (i. e. greater depth), than the Prosperous Suite, as suggested by the presence of abundant staurolite in its aureole (Bethune et al., 1999).

Bethune et al. (1999) believe that the Defeat Suite intruded early in the tectonic cycle, when the crust was still relatively cool. This resulted in a narrow aureole and faster cooling rates (Bethune et. al, 1999). Following this, more plutons were intruded (those of the Prosperous Suite) while the crust had become warmer (Bethune et al., 1999). Due to the lower temperature difference between the plutons and country rocks, slower cooling rates and broader metamorphic aureoles resulted (Bethune et al., 1999). Approximately 10 Ma after the Prosperous aureole formed, the cordierite isograd around the granites in the Sleepy Dragon Complex developed (Bethune et al., 1999) as a result of the intrusion of the Morose and Redout granites (Davis and Bleeker, 1999).

Chapter 3: The Prosperous Suite

This chapter summarizes previous research on the petrology and petrography of the Prosperous Suite. For results obtained as part of the present study the reader is referred to chapter 5.

The Prosperous Suite is composed of massive, predominantly homogeneous, medium to coarse grained (3-5 mm), cream to light pink (fresh and weathered surfaces), muscovite-biotite granites with associated pegmatitic phases (Henderson, 1985). The plutons occur as discrete lobes, averaging approximately 5 km in diameter, with little lithological variation between lobes (Henderson, 1985). The larger plutons of the suite are elongated in a NNW-SSE direction and, at the large scale, are discordant with the structural trend of the country rocks (the Burwash Formation; Fig. 3-1). W. Bleeker (unpublished data, 1998) noted that sheets of the Prosperous Granite Suite also occur as saddle reefs in regional F_2 fold hinges. The contacts between the granites and the Burwash Formation are sharp, with dykes and sills of granite and pegmatite locally occurring in the surrounding metasedimentary rocks (Henderson, 1985). Both the north and south ends of plutons are at high angles to the foliation in the metagreywackes and the granite.

The plutons exhibit a weak to strong foliation defined by micas, feldspar, oblate xenoliths and also slightly oblate quartz aggregates. The margins of the granites tend to display a stronger foliation than the central regions. The

Fig. 3-1: Map of the Prosperous Suite in relation to the cleavage and fold trends in the metasedimentary rocks of the Burwash Formation. YK stands for Yellowknife. After Henderson (1985) and Fyson (1998, pers. comm.).

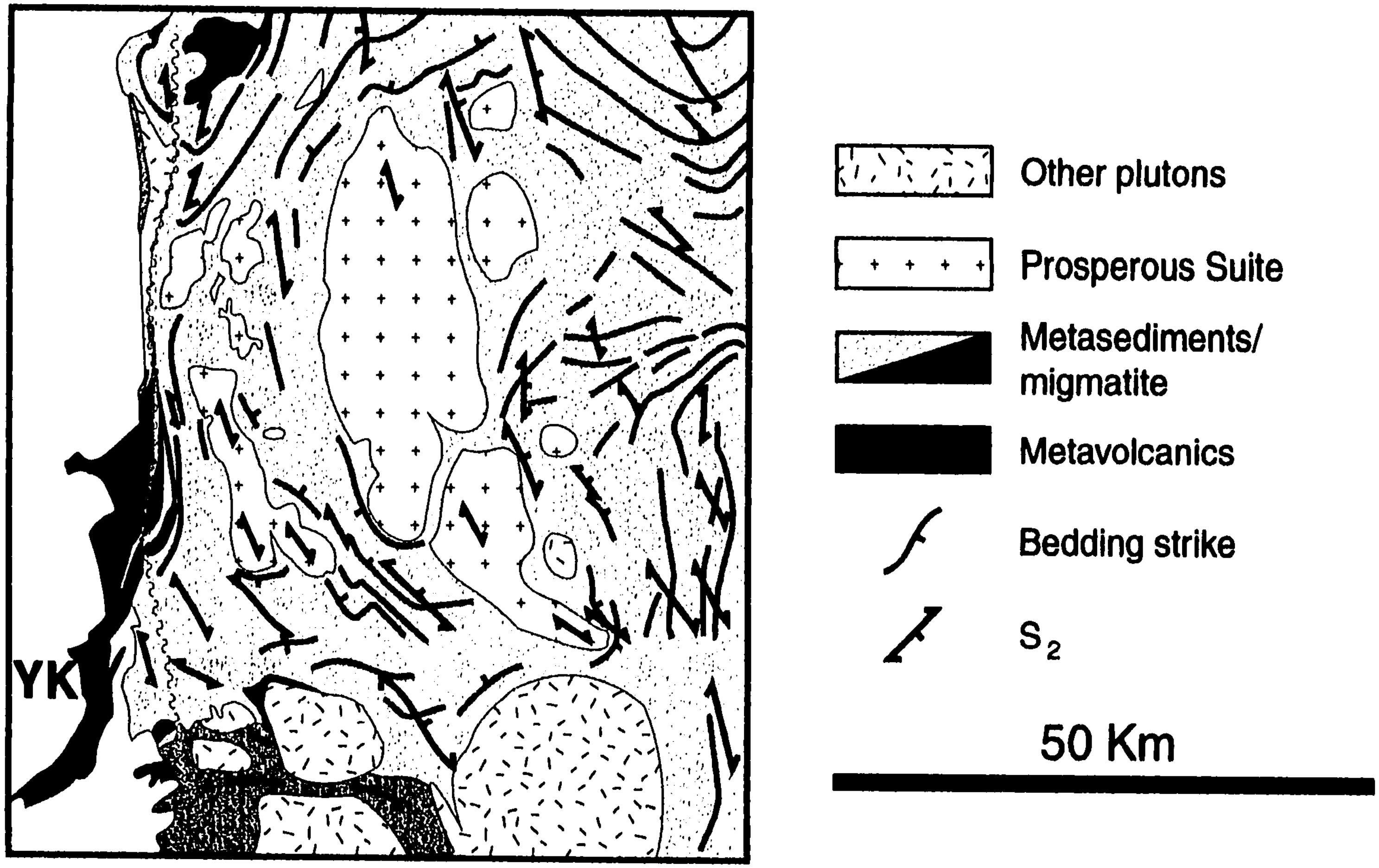

internal foliation, in both the Sparrow and Prosperous plutons, has a strike that is parallel to the S_2 foliation in the country rocks and merges smoothly with the external foliation (Ham and Benn, 1998; Benn et al., 1998a; Davis and Bleeker, 1999). Large xenoliths of the country rock within the Sparrow Pluton also appear to have their long axes oriented parallel to the S_2 foliation in the country rocks.

Typical Prosperous granite consists of 30% quartz, 35% plagioclase, 25% K-feldspar (microcline), 8% muscovite, and 2% biotite, with accessory apatite, and locally garnet (Fig. 2-6). The quartz grains are interstitial to equant in shape and strained, but not polygonized. Anhedral plagioclase crystals are usually fine grained and weakly zoned (Henderson, 1985). Plagioclase crystals contain inclusions of quartz and mica, and are more altered than the K-feldspar crystals (Henderson, 1985). K-feldspar crystals are anhedral to euhedral in shape and are the coarsest mineral in the granites. The microcline crystals display Carlsbad twinning and can be up to 8 mm long, locally giving the granites a porphyritic texture (Henderson, 1985). Quartz, plagioclase, and mica are common inclusions in the K-feldspar crystals (Henderson, 1985). The percentage of muscovite and biotite in the granite varies, with muscovite typically more abundant than the biotite (Davis and Bleeker, 1999). The muscovite forms coarse flakes that in many cases define the foliation, along with the biotite. The reddish-brown biotite crystals are usually 1-2 mm in size and partially altered to chlorite (Henderson, 1985; Davis and Bleeker, 1999). Aquamarine-coloured apatite crystals, which are a diagnostic accessory phase, are <1 mm in size, and may be associated with biotite (Davis and Bleeker, 1999; Henderson, 1985). Other accessory minerals include tourmaline and euhedral garnets. Iron oxides are rare (Henderson, 1985).

The associated pegmatite dykes occur within the region limited by the cordierite isograd (Kretz et al., 1989b). Pegmatites within the pluton contain quartz, plagioclase, K-feldspar, muscovite and tourmaline (Kretz, 1968). The composition of the dykes varies with distance from the Prosperous Suite plutons, and characteristic minerals were used to define the following zonation, from proximal to distal: tourmaline, beryl, spodumene, and columbite-tantalite (Kretz, 1989b).

Most of the work on the petrology and chemistry of the Prosperous Suite and its associated pegmatites was done by Kretz (1964, 1968, 1970, 1985) and Kretz et al. (1982, 1989a, 1989b). The following is a summary of their work. Kretz (1985) proposed that the pegmatite and the granite had a common source or that the pegmatites were derived from the granite. In the Sparrow Pluton, Kretz et al. (1989b) identified two chemically distinct phases corresponding to the central and marginal areas of the pluton, and compared these areas to the composition of the pegmatites. The central region of the granite contains slightly higher concentrations of Ti, Fe, Mg, Zr and Ba than do the pegmatites (Kretz, 1985). The pegmatites are poor in Ti, Fe, Mg, Mn, Li, Zr and Ba, and rich in Rb and P (Kretz, 1985; Kretz et al., 1989b). The marginal areas of the granite contain intermediate concentrations of Fe (compared to the central granite and pegmatites), and are low in Ti, Mg, Li, Sr, Zr, Ba (Kretz, 1985). The marginal areas are also high in P and Rb (Kretz, 1985). The similarity in the relative concentration and depletion of elements for the granites and pegmatites supports the idea of a common source.

The source of the granites is believed to be partial melting of the sediments belonging to the Burwash Formation (Boyle, 1961; Green et al., 1968; Drury, 1979; Thompson, 1978). The composition of the Prosperous granites is similar to the minimum melt composition at 3 kbar (3 kbar ≈ 10-11 km) in the Q-Ab-Or system (Drury, 1979). The Prosperous granites and a minimum melt composition at 3 kbar have similar rare-earth element patterns, low Sr and Eu contents and high K/Rb ratios (Drury, 1979). This is consistant with a high percentage of partial melt extracted from a plagioclase-rich residuum (Drury, 1979). The pegmatites and granite are from a common source and were separated prior to complete crystallization of the granite (Kretz, 1968). The pegmatite fluid then intruded along grain boundaries and fine fractures, accumulating in active dilatant zones in the country rock and granite (Kretz, 1968). P-T conditions of pluton emplacement, and descriptions of the Prosperous Suite aureole were discussed in section 2.3 (Structure and metamorphism of the Burwash Formation).

Chapter 4: Methods

Four techniques were used in the structural study of the Prosperous Suite: field mapping and sampling, microstructural analysis, the anisotropy of magnetic susceptibility (AMS), and magnetic mineralogy studies. Each is described in detail below.

4.1 FIELD WORK

Field work focused on the Sparrow and Prosperous plutons of the Prosperous Suite granites (Fig. 4-1). Mapping was completed between July 4 and August 20, 1996 (Sparrow Pluton) and from June 24 to August 18, 1997 (Prosperous Pluton). Data collection was concentrated primarily within the granites and to a lesser degree within the surrounding country rock of the Burwash Formation. Grain size, foliation, lineations, orientations and compositions of pegmatite dykes, shear zones, bedding, tops, folds and metamorphic minerals were recorded on mylar overlays, on a set of 1:22 000 black and white aerial photos dating from the 1940s. Oriented hand samples of the country rocks were collected along transects near the pluton contact. Particular attention was paid to mineral assemblages, and taking samples that demonstrated a potential for preserving good porphyroblast-fabric relationships. Fig. 4-2 (Sparrow Pluton) and 4-3 (Prosperous Pluton) show sample locations

Fig. 4-1: Location of Sparrow and Prosperous plutons. AC stands from Anton Complex. SDC stands for the Sleepy Dragon Complex. Yk stands for Yellowknife. The thick dashed line represents the SNORCLE seismic transect.

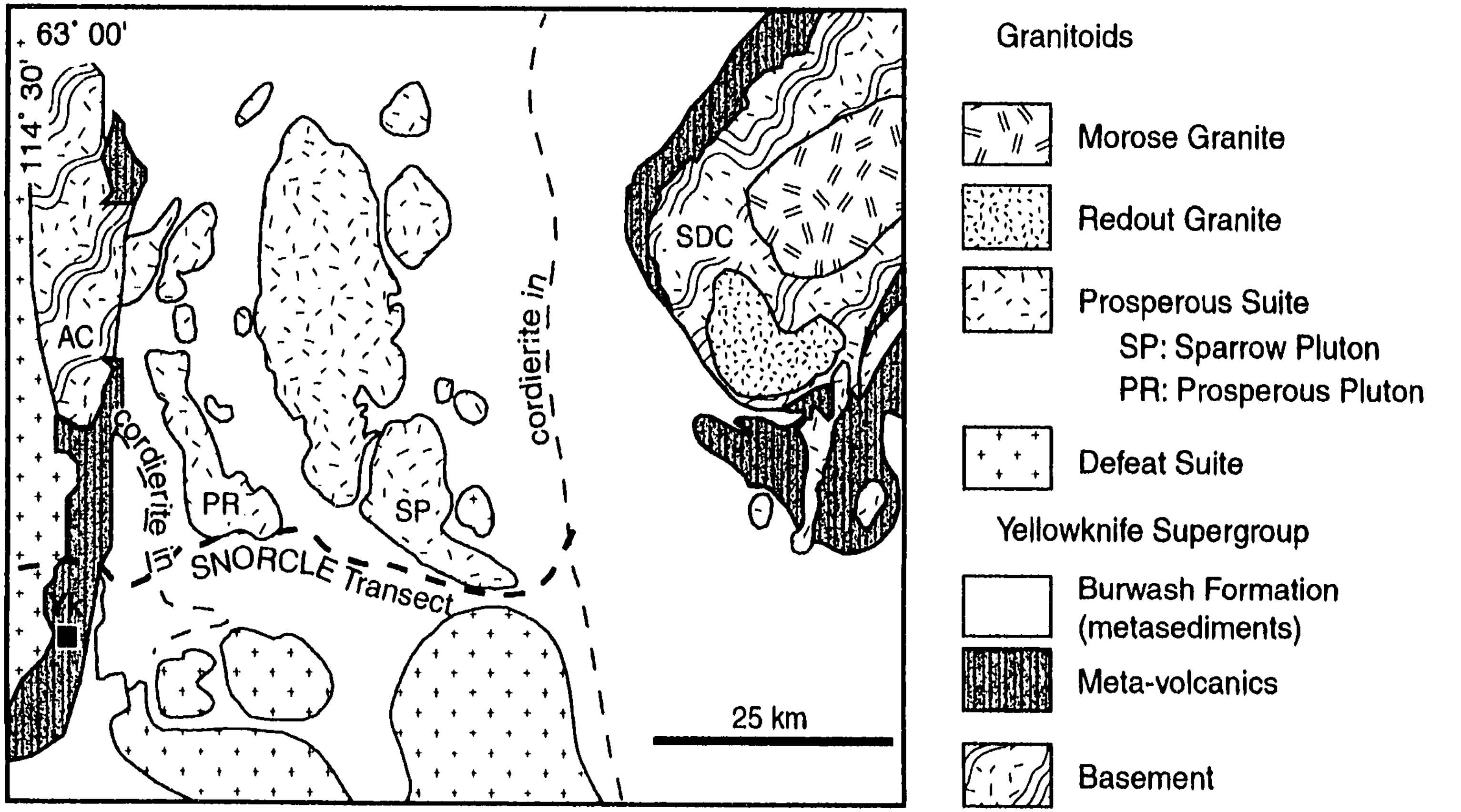

Fig. 4-2: Locations of outcrops, hand samples, drill cores, and thin sections for the Sparrow Pluton.

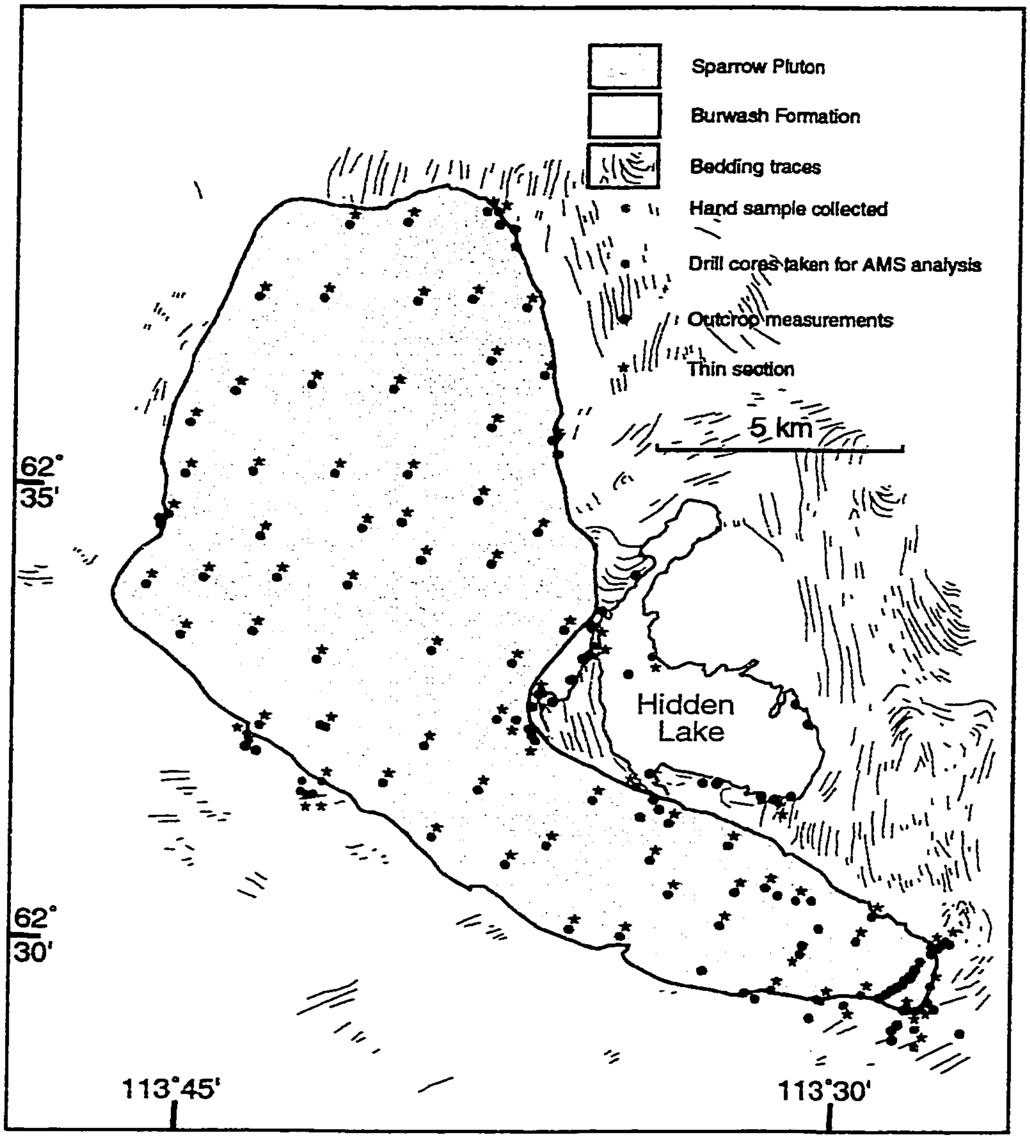

Fig. 4-3: Locations of outcrops, hand samples, drill cores, and thin sections for the Prosperous Pluton.

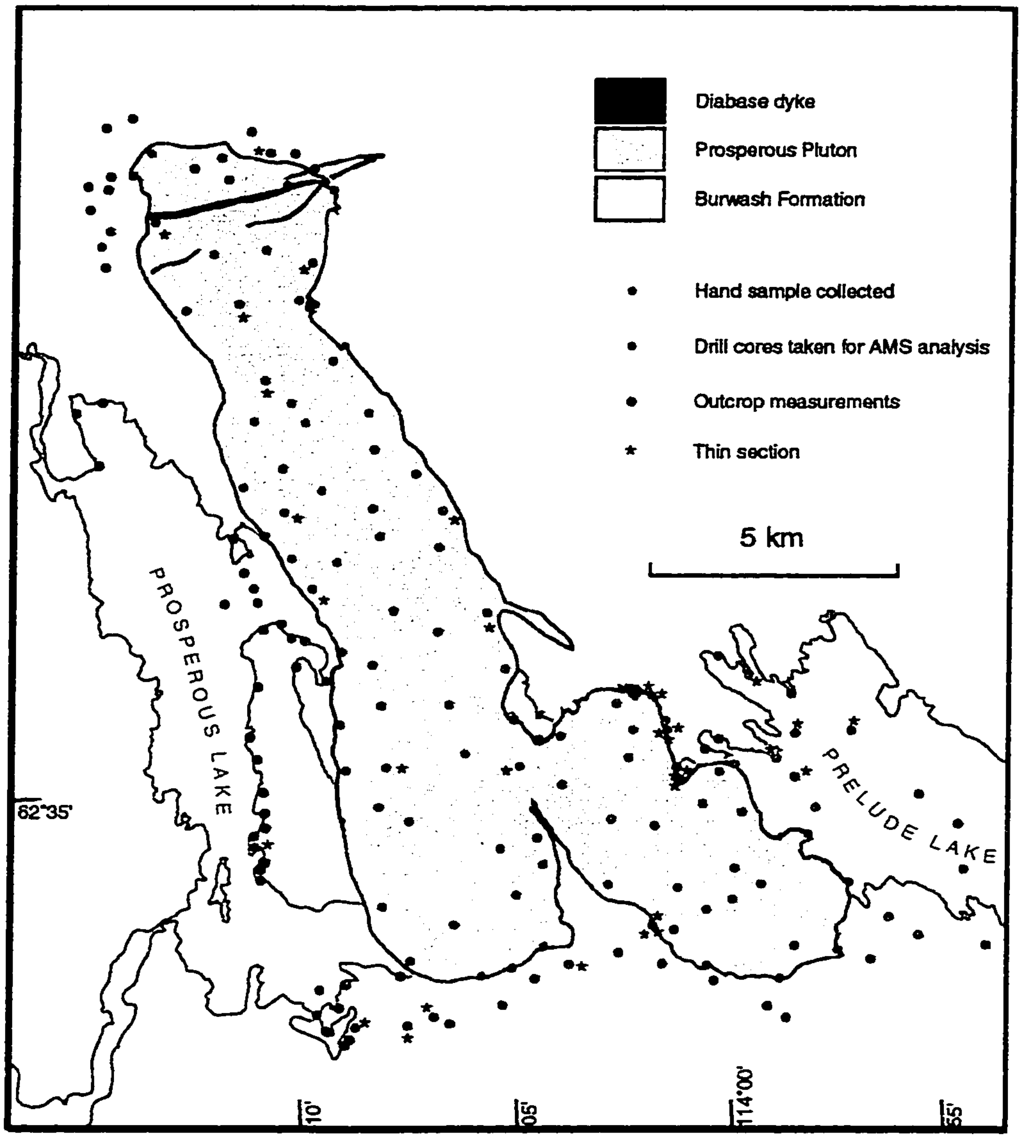

within the study area. See Appendix II for station numbers and sample numbers.

4.2 MICROSTRUCTURAL ANALYSIS

For the granites, a total of 78 thin sections were examined. One thin section per AMS drilling site was studied for the Sparrow Pluton. Each section was examined for igneous textures, mineralogy (which could influence AMS results) and evidence of solid state deformation. Results were fairly consistent among the samples. Because of this, only 10 representative samples were selected for examination from the Prosperous Suite (Fig. 4-2 and 4-3 for sample locations). These samples were selected so that they encompassed a range of mesoscopic fabric intensities.

Forty pairs of oriented thin sections were made from the country rocks (Fig. 4-2 and 4-3 for sample locations). Selections were made based on metamorphic mineralogy, and transects away from the plutons were sampled. The aim was to obtain sections that would show porphyroblast-fabric relationships, which would help determine the timing of contact metamorphic mineral growth in relation to regional deformation and fabric development. All section pairs were cut with one section parallel to the mineral lineation (or intersection lineation) and perpendicular to the foliation plane, and the other section perpendicular to both the lineation and foliation plane. This means that, in cases where the lineation is a mineral lineation, the first section was cut in the XZ fabric plane, and the second section in the YZ plane (see Fig. 4-4).

4.3 ANISOTROPY OF MAGNETIC SUSCEPTIBILITY (AMS)

Anisotropy of magnetic susceptibility (AMS) is a technique where an oriented sample is subjected to a weak applied magnetic field (ca. 0.1 mT, Borradaile and Henry, 1997) at different orientations with respect to sample coordinates. Differences in the strength of the acquired magnetization can reflect the degree of crystal alignment and the net shape of the grains (Tarling and Hrouda, 1993).

This technique is useful in granite fabric studies because it can show information on fabric orientations, fabric strengths, and subtle mineralogical zonation. It is especially useful in situations where the fabric or zonation is not obvious in the field. The following discussion of the fundamental principles of AMS (section 4.3.1) is based on Tarling and Hrouda (1993), unless otherwise stated.

4.3.1 Fundamental Principles

Above absolute zero, all materials have some magnetic properties, and can be characterized into three general types: diamagnetic, paramagnetic and ferromagnetic. Fig. 4-5 illustrates some magnetic properties for the three groups. Diamagnetic minerals have complete electron shells and when a magnetic field

Fig. 4-4: Thin sections were cut perpendicular to the foliation and parallel to the lineation (shown by the grey arrow on the sample) in the XZ plane, and perpendicular to the foliation and lineation in the YZ plane.

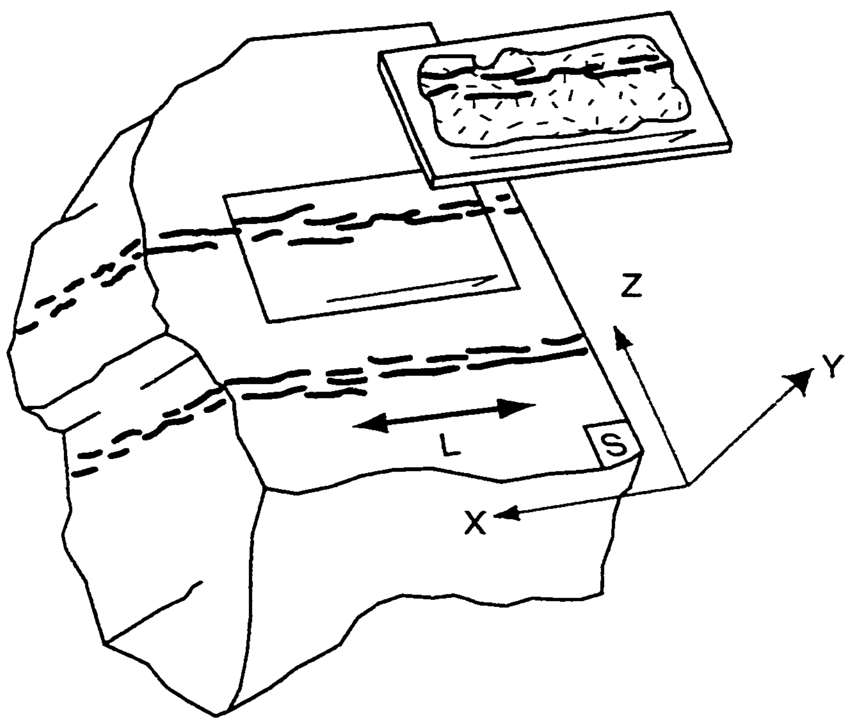

Fig. 4-5: The three general types of magnetic minerals: diamagnetic, paramagnetic, and ferromagnetic (sensu lato). Large solid arrows represent the applied field. Hollow arrows show the induced field. Smaller solid arrows represent electron spin directions. Modified from Tarling and Hrouda (1993).

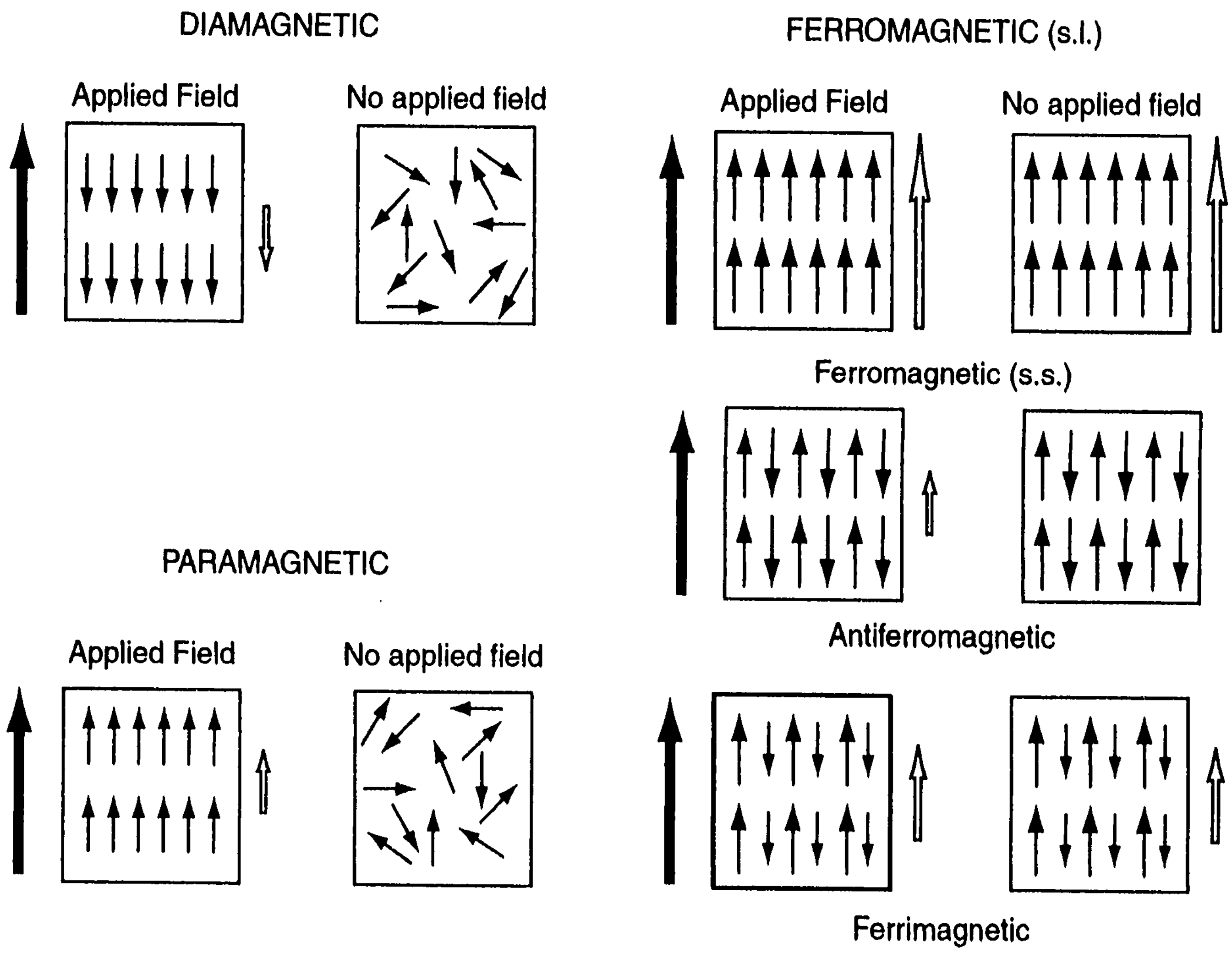

is applied, it induces a magnetization opposite to the applied field. Paramagnetic minerals have incomplete electron shells and a weak magnetization is in the same direction as the applied field. In both paramagnetic and diamagnetic minerals, the magnetization disappears as soon as the applied field is removed. Minerals which retain magnetic alignment after an external field has been removed (i.e. display remanence) are termed ferromagnetic (sensu lato or s. l.). Ferromagnetic (s. l.) refers to a group of minerals including ferromagnetic (sensu stricto or s. s.), antiferromagnetic, and ferrimagnetic properties. Ferromagnetic (s. s.) minerals have all the electron spins aligned and aquire, and retain, a very strong magnetization (Fig. 4-5). Antiferromagnetic minerals have no external magnetic fields (in the absence of an applied field) due to electron spin alignments being exactly paired in opposite directions (Fig. 4-5). Ferrimagnetic minerals have magnetic alignments in opposite directions but not of the same magnitude (Fig. 4-5), resulting in a weaker external magnetization compared to ferromagnetic (s. s.) minerals. Fig. 4-6 lists some common minerals that belong to the diamagnetic, paramagnetic and ferromagnetic (s. l.) groups.

The action of lattice forces on the electron spin configuration causes crystalline anisotropy in certain minerals (e.g. all Fe-silicates). For a given crystal, there will be specific crystallographic directions along which the electron spins align more readily. Shape anisotropy is the result of north and south magnetic poles forming at opposite ends of an elongate grain on the surface of a grain

Fig. 4-6: Susceptibilities (K_m), anisotropies (P), and shape factors (T) for some common diamagnetic, paramagnetic, and ferromagnetic (s. l.) minerals. For diamagnetic and paramagnetic minerals: modified from Borradaile and Henry (1997) and references therein. Data for ferromagnetic minerals is from Rochette et al. (1992), and Tarling and Hrouda (1993).

Mineral	K_m ($\times 10^{-6}$ SI)	P	T	Fabric Type
Diamagnetic				
Calcite	-13.60	1.11	1.00	Inverse
Feldspars	-14.00	+	+	Normal
Quartz	-13.40	1.01	1.00	Normal
Paramagnetic				
Amphiboles	903.00	1.14	0.53	Normal
Biotite	1042.00	4.38	0.62	Normal
Chlorite	552.00	1.19	0.28	Normal
Dolomite	40.00	+	+	Normal
Epidote	639.00	1.33	0.11	Normal
Muscovite	140.00	1.27	0.56	Normal
Phlogopite	273.00	1.54	0.78	Normal
Pyroxenes	500-5000	≥1.30	+	Normal
Siderite	3980.00	1.56	-0.90	Normal
Tourmaline	1690.00	1.01	1.00	Inverse
Ferromagnetic (s. l.)				
Goethite	≈3500	2?	+	Inverse
Hematite	≤6000	2.5-100	1.00	Normal
Magnetite (MD)	2800000	<5	+	Normal
Magnetite (SD)	2000000	∞?	+	Inverse
Pyrrhotite	≈1500000	>100	0.80	Normal

+ Undefined or variable parameter

when electron spins are aligned by an external field. Magnetite is the only common mineral with shape anisotropy.

The strength of the induced magnetization can be described as follows:

$$M = KH$$

Where M is the magnetic dipole moment, H is the strength of the applied field, and K is a proportionality constant known as the magnetic susceptibility. If the measurements were made using a sample of known volume (m^3), M and H have the units A/m and K (dimensionless in SI) is known as the bulk susceptibility or volumetric susceptibility. If a sample of known mass (kg) is used, then the mass susceptibility is obtained. Unless otherwise stated, in this work K will always refer to the volumetric or bulk susceptibility. Diamagnetic minerals have very weak (ca. 10^{-6} SI) negative susceptibilities and paramagnetic minerals have weak positive susceptibilities, ca. 10^{-4} SI. Ferromagnetic (s. l.) minerals have a positive susceptibility that is stronger than the paramagnetic minerals, and generally greater than 10^{-2} SI (Fig. 4-6).

The measured bulk susceptibility and the anisotropy of the rock sample are the geometric sum of all the individual susceptibilities and anisotropies of the constituent crystals. In order to correctly interpret AMS data, one must know what minerals are present in the sample and how they contribute to the magnetic signal. For example, the bulk susceptibility (K) may be dominated by ferromagnetic minerals (s. l.) if these minerals represent more than 0.1% of the total volume of the sample. In the absence of ferromagnetic minerals, paramagnetic minerals may dominate the susceptibility, assuming they represent ≥ 1% of the sample volume. Diamagnetic minerals may dominate if the rock contains <0.0001% of ferromagnetic minerals, and <1% of paramagnetic minerals. It should be noted that the susceptibility may be dominated by one mineral species, and the anisotropy may be dominated by another.

For a given sample, the magnetization strength depends on the orientation of the sample in the applied field. This variation in susceptibility with sample orientation can be represented as a second rank tensor, K_{ij}. The eigenvectors for this tensor are the principal axes orientations and the eigenvalues are termed the principal susceptibilities (K_1, K_2, K_3, where $K_1 \geq K_2 \geq K_3$) and can be graphically represented as the AMS ellipsoid (Fig. 4-7).

The magnitude of the anisotropy will depend on the intrinsic AMS of the individual mineral grains and the degree of alignment of the grains. AMS data is represented with scalar parameters and directional components.

Scalar Parameters

The average susceptibility (K), the degree of anisotropy (P′), and the shape factor (T) are scalar parameters used to describe the AMS ellipsoid. The average susceptibility is expressed as:

$$K_{mean} = (K_1 + K_2 + K_3)/3$$

Fig. 4-8 shows the resulting susceptibility for concentrations of specific minerals. Some ferromagnetic (s. l.) minerals, such as magnetite, have an intrinsic

Fig. 4-7: The AMS ellipsoid. K3 is the pole to the magnetic foliation and K1 is the magnetic lineation. K1, K2, and K3 are the semi-axial lengths of the ellipsoid, representing the principal susceptibilities.

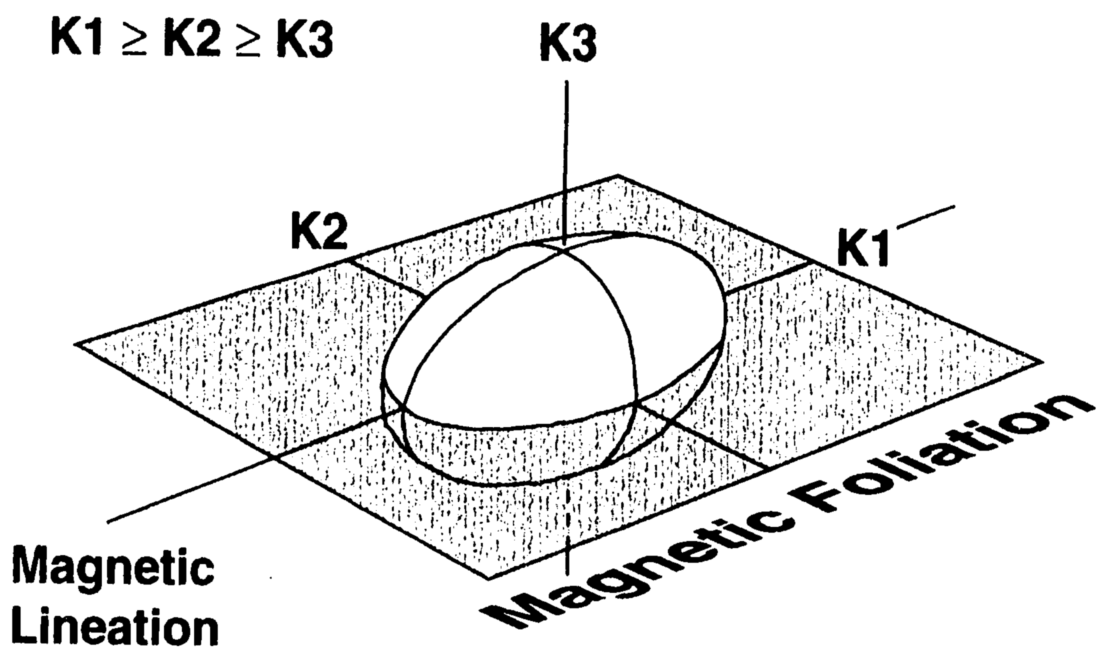

Fig. 4-8: Mineral concentration in a sample vs. sample susceptibility for magnetite, hematite, ilmenite, biotite, hornblende, pyroxene, and muscovite. Modified from Tarling and Hrouda (1993).

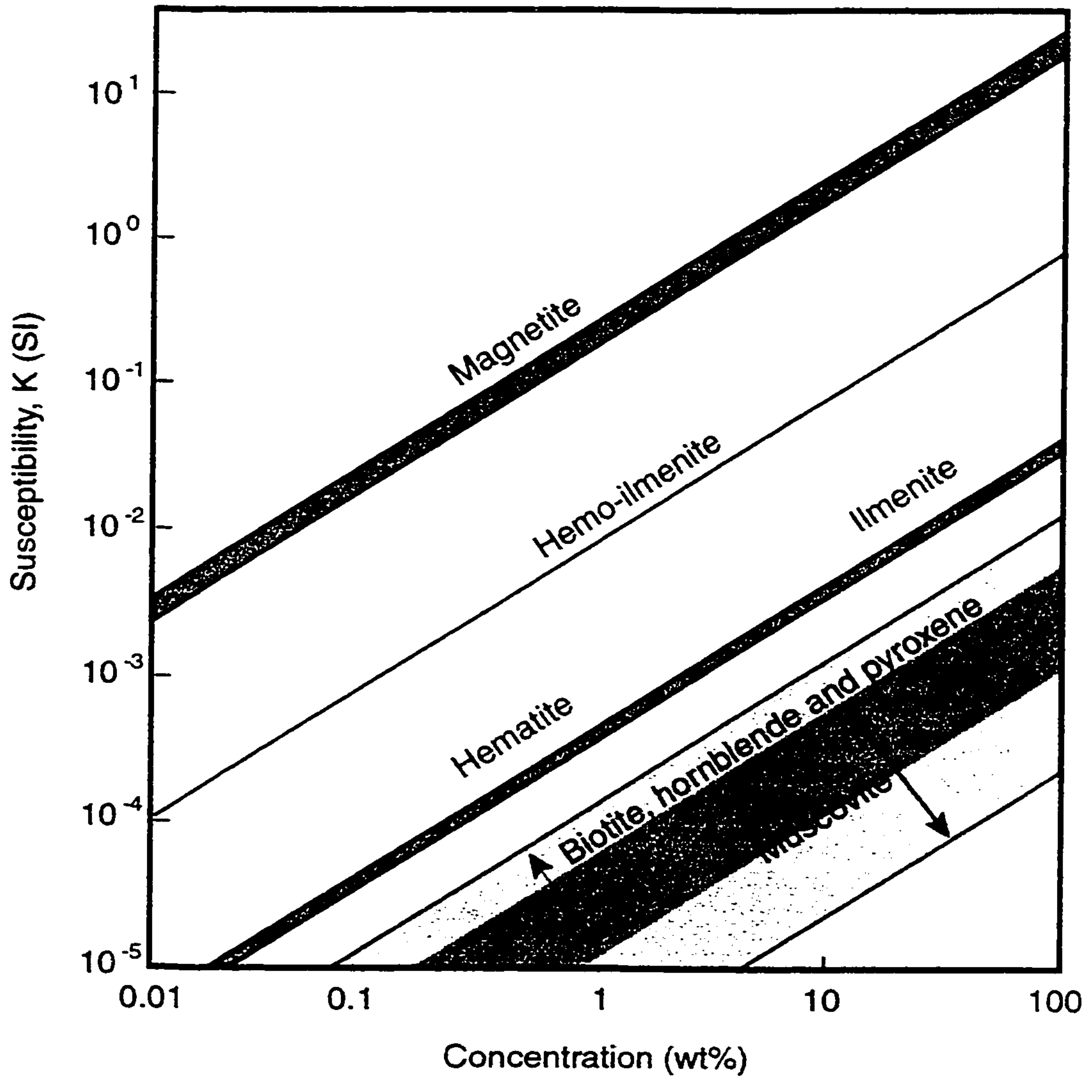

susceptibility much higher than paramagnetic minerals such as muscovite or biotite. The plot (Fig. 4-8) shows that even concentrations of magnetite as low as 0.1% (wt) will result in a mean susceptibility higher than that resulting from even 100% biotite or muscovite. Hence, the 0.1% of magnetite would dominate the bulk susceptibility (K). In rocks where the susceptibility is dominated by paramagnetic minerals, the magnetic susceptibility (K) can be used as a petrographic mapping tool. This is possible since K values are a linear function of the iron content in the paramagnetic minerals (Gleizes et al., 1993).

The degree of anisotropy can be expressed as P'% = (P'-1)*100, where P' (Jelinek, 1981) is calculated by:

$$P' = \exp\sqrt{2\left[(\eta_1 - \eta_m)^2 + (\eta_2 - \eta_m)^2 + (\eta_3 - \eta_m)^2\right]}$$

where $\eta_i = \ln(K_i)$ (i = 1 to 3) and $\eta_m = \sqrt[3]{\eta_1 \cdot \eta_2 \cdot \eta_3}$. For weakly magnetic rocks, K_i can be corrected by addition of an isotropic diamagnetic component (K_{dia}) carried by all minerals (Rochette, 1994). In rocks with very low susceptibilities, the correction for K_{dia} is meant to render values of P'% that are more representative of the contributions from paramagnetic and ferromagnetic minerals (Rochette, 1994). For the granitic rocks in this study, where 85% of the rock is composed of quartz and feldspar, $K_{dia} = -6 \times 10^{-6}$ was chosen to correspond to the susceptibility of the diamagnetic quartz-feldspar matrix (Rochette, 1994; Benn et al., 1998a). The magnetic anisotropy has a maximum level that is achieved when the crystal alignment is perfect. The maximum P' value for biotite is 1.35 and the maximum P′ value for other phyllosilicates is 1.2 to 1.35 (Rochette et al., 1992). If the degree of anisotropy is proportional to the degree of preferred orientation of the Fe-rich minerals, then P′% can be used to map relative finite strains, inasmuch as petrofabric intensity may be used as a strain gauge. It should be noted that this may not be the case in rocks that have undergone a complex strain history (Benn, 1994), or that have a complex magnetic mineralogy (Rochette et al., 1992).

The shape factor of the AMS ellipsoid is expressed as:

$$T = \left[2 \frac{\ln K_2 - \ln K_3}{\ln K_1 - \ln K_3} \right] - 1$$

T is calculated after the correction of K_i, as discussed in the previous paragraph. The ellipsoid is oblate for $0 < T \leq 1$, prolate for $-1 \leq T < 0$, and neutral for $T=0$.

In cases where the magnetic fabric is dominated by a single mineral, minerals that are not monoclinic or triclinic, or by minerals with similar intrinsic AMS and coaxial petrofabrics, T and P′% can be very useful if they infer variations in the anisotropies and shapes of petrofabric ellipsoids (Hrouda and Schulmann, 1990). In these cases, the shape of the AMS ellipsoid can reflect the symmetry of the fabric, and the degree of anisotropy will depend on the degree of preferred orientation (Benn et al., 1998a). However, one must be careful when interpreting AMS in terms of petrofabric intensities and symmetries since traces of secondary ferromagnetic minerals (such as magnetite) may significantly affect

T and P'% without noticeably modifying the orientation of the magnetic fabric (Borradaile and Werner, 1994; Borradaile and Henry, 1997).

Directional Parameters

The orientation of the principal axes of the AMS ellipsoid are controlled by the lattice preferred orientations of the various minerals (or grain shape preferred orientations in the case of magnetite) making up the rock sample. The magnetic lineation is represented by the K_1 direction, and the K_3 direction is the pole to the magnetic foliation (Fig. 4-7). In order to use AMS data to map foliations and lineations in the field, one must know how the AMS axes correspond to the mineral preferred orientations. Example relationships for biotite, tourmaline, and magnetite are described below.

Biotite is a paramagnetic phyllosilicate mineral. Single crystals of biotite, and also other phyllosilicates such as muscovite and chlorite, have the K_3 axis nearly perpendicular to the basal cleavage of the crystal (Fig. 4-9). In cases where the magnetic fabric is dominated by phyllosilicates such as biotite, chlorite, or muscovite the magnetic foliation will approximate the mineral foliation. The magnetic lineation of a population of biotite crystals will be parallel to the zone axis of the population (Fig. 4-10) (Bouchez, 1997).

For a tourmaline crystal, the minimum susceptibility (K_3) corresponds to the c-axis of the crystal. Therefore, the minimum susceptibility axis for tourmaline corresponds to the long dimensional axis of the crystal (Rochette et

Fig. 4-9: Orientation of AMS and crystallographic axes for a biotite crystal. Modified from Borradaile and Werner (1994).

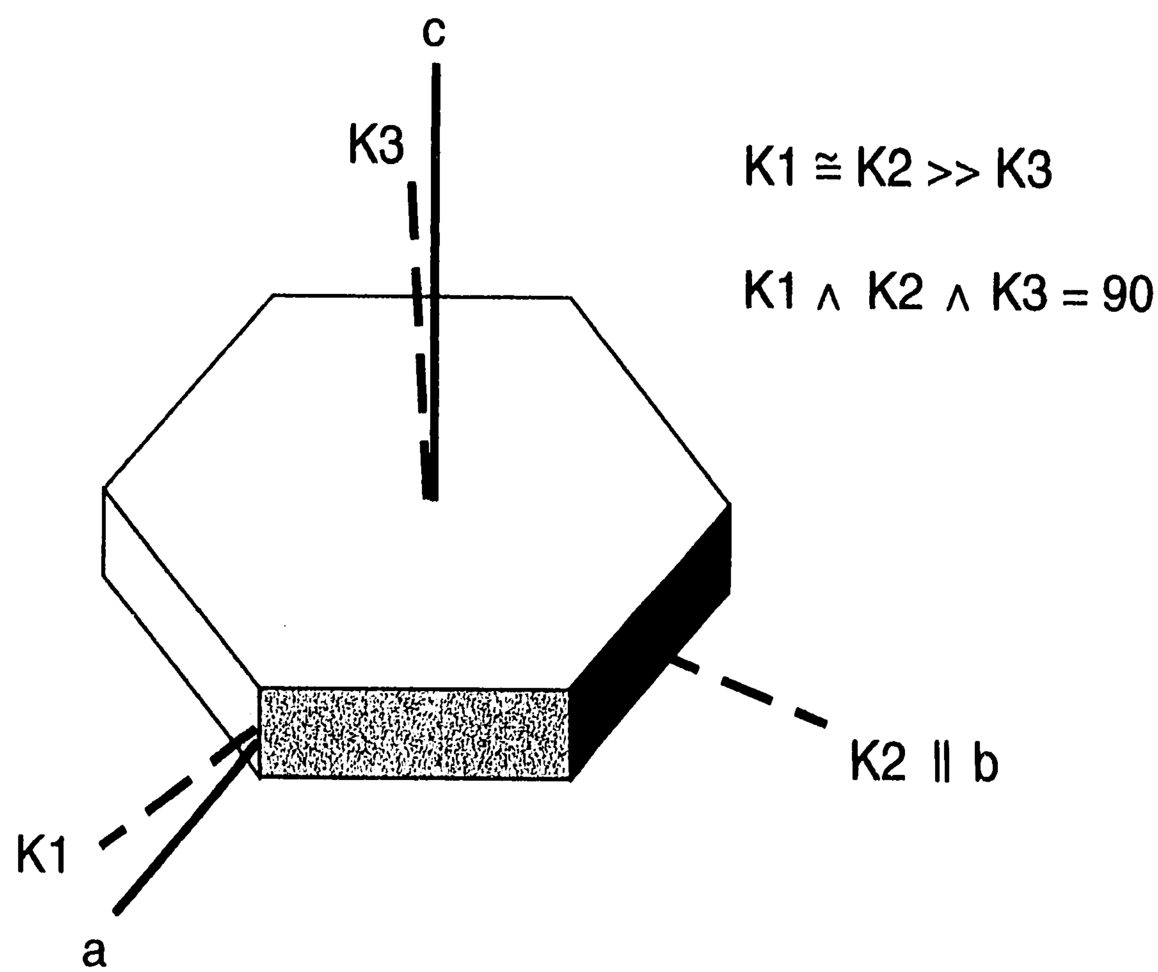

Fig. 4-10: Orientation of AMS axes for a sample containing biotite crystals. K3 is the pole to the foliation and K1 represents the zone axis. Modified from diagram by K. Benn (unpublished data).

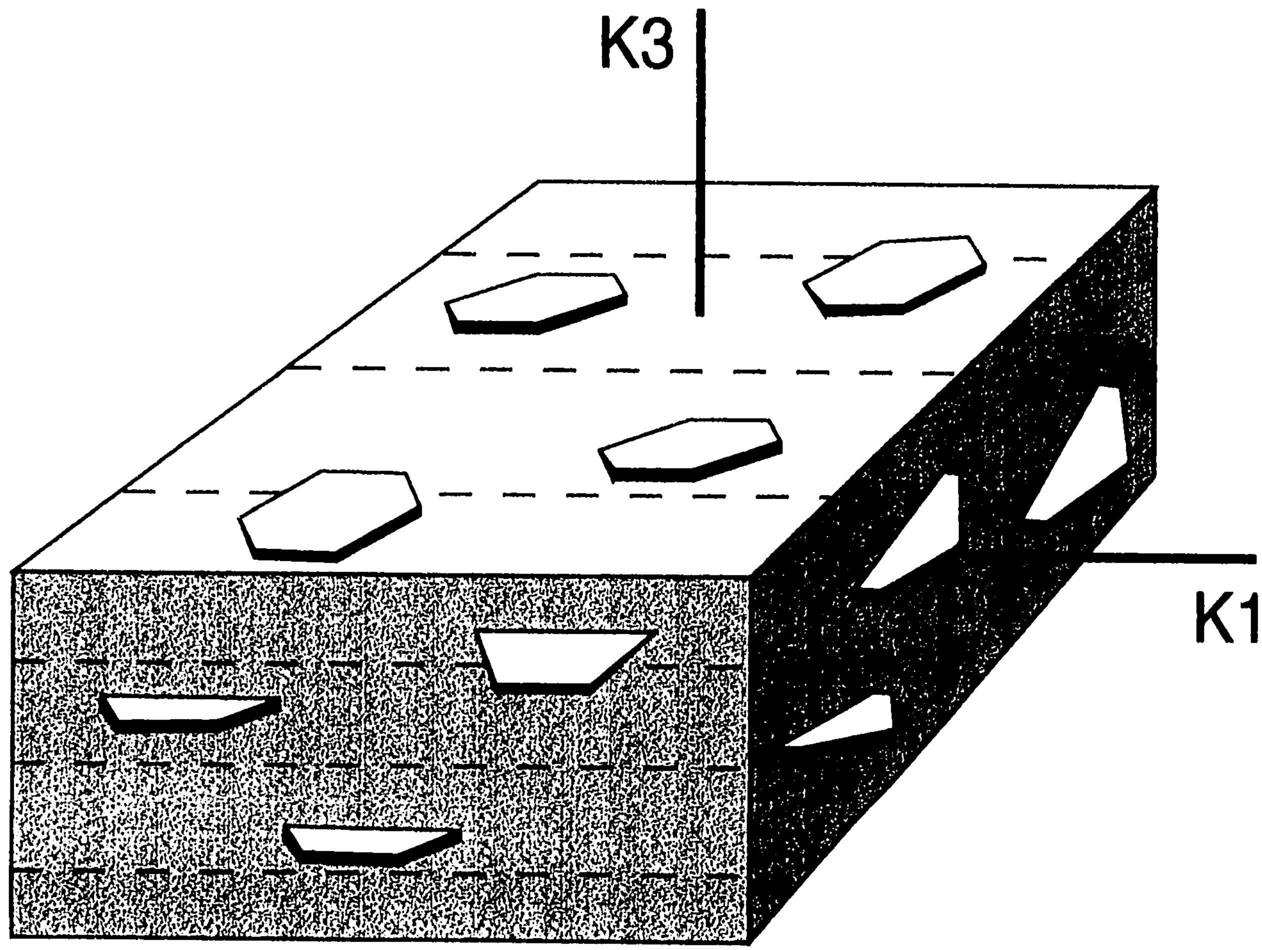

al., 1992). So, for a tourmaline crystal an inverse fabric occurs resulting in K_3 defining the magnetic lineation (see Normal vs. inverse AMS-petrofabric relationships on p. 66 for more information; Rochette et al., 1992). If there is enough tourmaline in the sample so that it dominates the magnetic fabric, the K_1 may be perpendicular to the mineral lineation.

In the case of magnetite, the magnetic susceptibility anisotropy is controlled by grain shape. The grain size is predominant in determining whether the grains are superparamagnetic, single domain, pseudo-single domain or multidomain (Fig. 4-11). Fig. 4-11b shows the effect of changing length/width ratios on the domain state of magnetite. Fig. 4-11a shows the domain type for equidimensional magnetite grains and their corresponding susceptibility. Superparamagnetic grains lose their acquired magnetization due to a direct strong field (i.e. >10 mT) immediately after the field has been removed. Single-, pseudo-single, and multidomain grains are named for the number of magnetic domains they contain and how the domains interact.

Domains are volume elements, or regions, within a crystal that contain their own magnetization direction. In one domain all the electrons will be aligned in one direction, and in the next domain, the electron spins will be aligned in a different direction. Pseudo-single domain grains contain more than one domain, but due to crystal lattice imperfections, the different domains cannot interact, and so the grain behaves as though it were single domain.

Fig. 4-11: (A) shows the domain type for equidimensional magnetite grains and their corresponding susceptibility. (B) shows the grain length and axial ratios for superparamagnetic (SP) grains, single domain grains (SD), pseudosingle domain grains (PSD), and multidomain grains (MD). Modified from Tarling and Hrouda (1993).

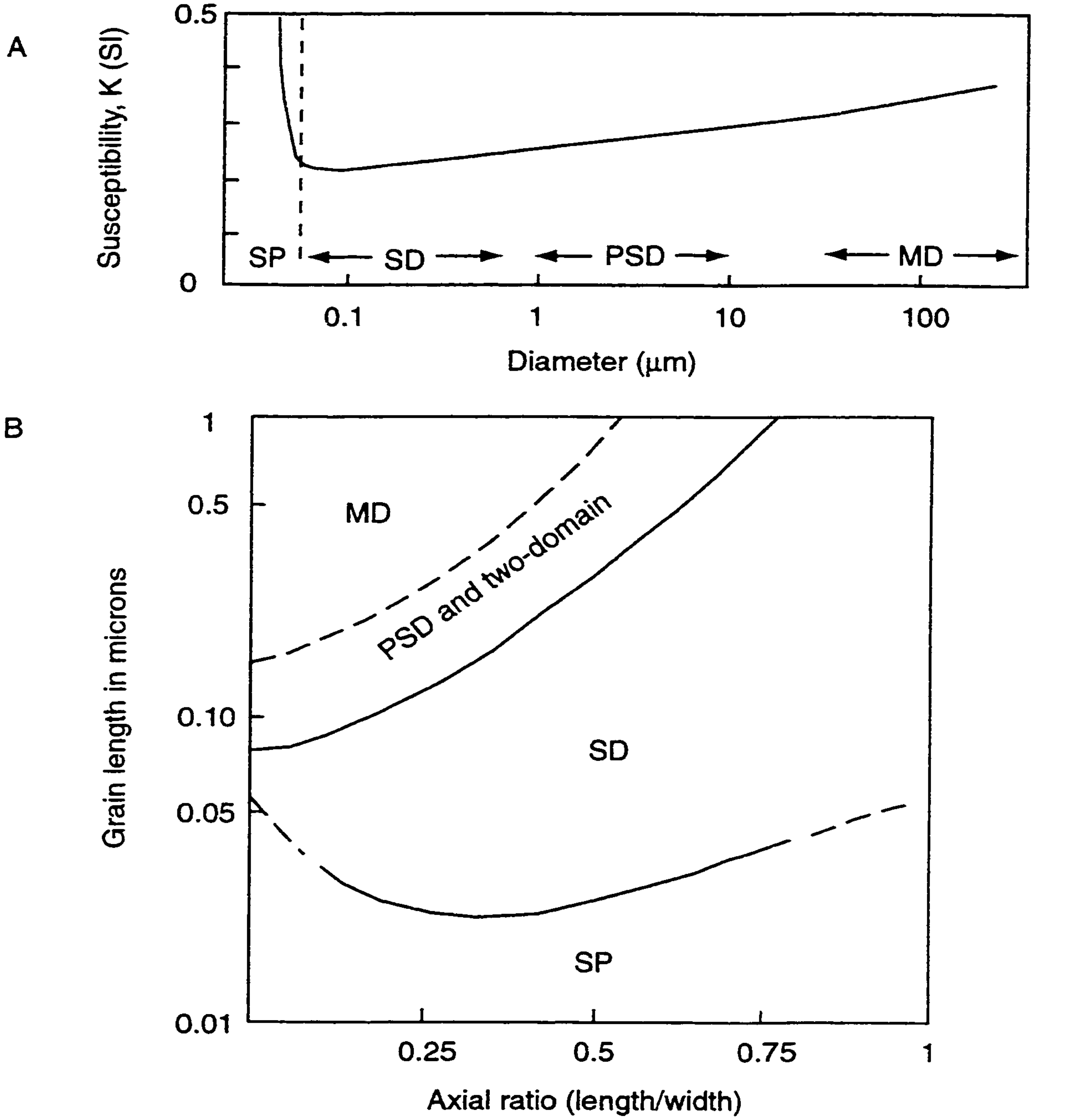

Small grains behave superparamagnetically, larger grains are pseudo-single domain or multidomain. In strongly elongate grains, or when magnetite is present as exsolution lamellae, it is more likely to show single-domain behaviour. Superparamagnetic and single domain magnetite result in K_1 being parallel to the short axis and K_3 coincident with the long axis. In the case of multi-domain magnetite, K_1 corresponds with the long axis of the grain, and K_3 parallels the short axis. Pseudo-single domain grains, behave as single domain grains, with K_1 being parallel to the short axis and K_3 is coincident with the long axis. It should also be noted that if magnetite represents more than 10% of the rock, then individual grains may interact with one another, giving the impression of one large grain (Tarling and Hrouda, 1993).

Normal vs. inverse AMS-petrofabric relationships

A normal AMS-petrofabric relationship is one where the K_1 direction is parallel to the mineral lineation, and the K_3 direction is perpendicular to the mineral foliation plane. When the K_1 direction is not parallel to the mineral lineation, and/or the K_3 direction is not perpendicular to the mineral foliation plane it is termed an anomalous magnetic fabric (Rochette et al., 1992). The different types of inverse fabrics are: false normal (K_1 and K_2 switched), intermediate fabric (K_2 switched with K_3), false inverse (K_1 switched with K_2 and K_2 switched with K_3), and inverse fabric (K_2 and K_3 switched). Fig. 4-12 shows the various anomalous fabrics that can result for a sample containing a mixture of

Fig. 4-12:
Model of normalized principal susceptibilities for samples containing a mixture of two minerals with coaxial petrofabrics, but with normal (multidomain, MD, magnetite) and inverse (single domain, SD, magnetite) magnetic fabrics. P is the proportion of the inverse component in the mean susceptibility. For (A) the shapes of the end member ellipsoids are exactly inverse; 1 represents a normal AMS fabric, and 2 represents an inverse fabric. For (B) the normal component is less oblate than the inverse component; 1 represents a normal fabric, 2 represents an intermediate fabric, 3 represents a false inverse fabric, 4 represents an inverse fabric. For (C) the normal component is more oblate than the inverse component; 1 is a normal fabric, 2 is a false normal fabric, 3 is a false inverse fabric, and 4 is an inverse fabric. Modified from Rochette et al. (1992).

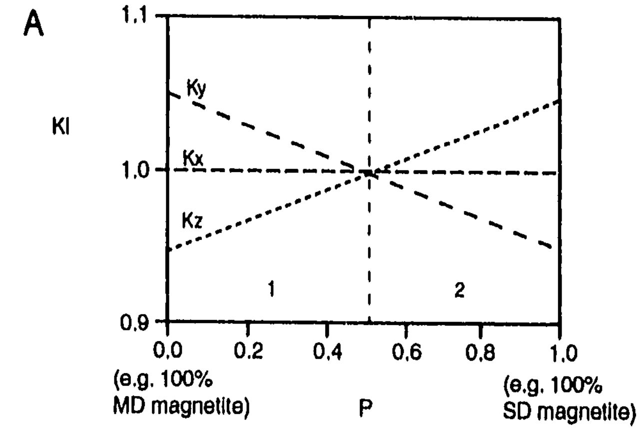

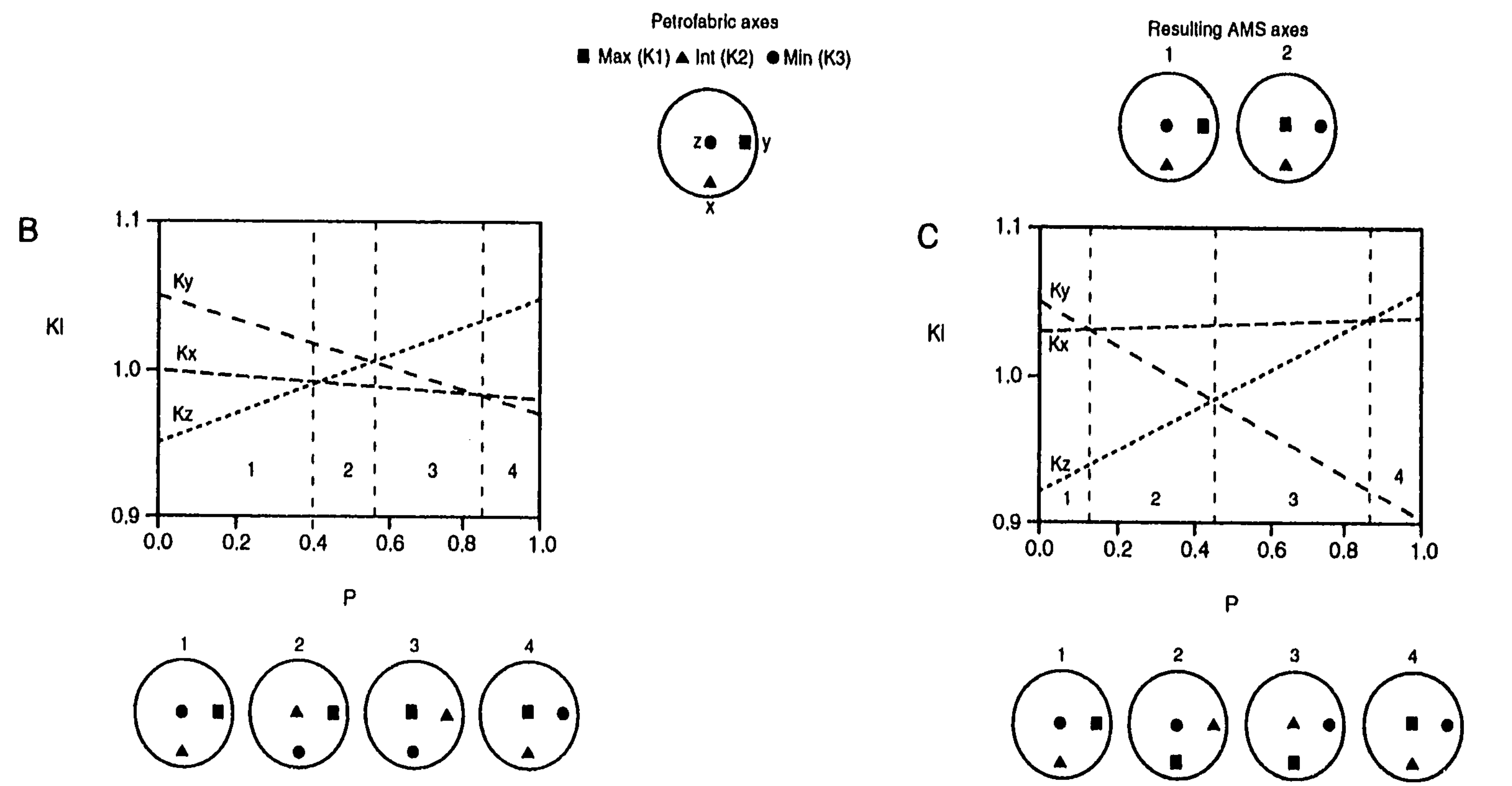

two minerals with coaxial petrofabrics, but normal and inverse intrinsic magnetic fabrics (i.e. inverse for single crystals). Fig. 4-12 shows the extreme cases than can result when minerals that display inverse fabrics are present in a sample. Potter and Stephenson (1988) and Rochette et al. (1992) suggest that a more common effect on samples containing minerals with inverse fabrics is a decrease in the degree of anisotropy (P).

Inverse fabrics may be caused by the presence of single or pseudo-single domain magnetite, tourmaline, certain carbonates, and goethite. For single or pseudo-single domain magnetite, the magnetization is saturated in the long axis and cannot be increased by an applied field. To an induced field, the susceptibility is zero in the long axis and greater than zero in a perpendicular direction, hence resulting in an inverse intrinsic AMS. In the case of tourmaline, certain carbonates, and goethite, the short dimensional axis direction, acquires a magnetization easier than the long axis, resulting in K_1 being perpendicular to the mineral lineation (Rochette et al., 1992).

In some cases, identification of a potential inverse fabric can be as simple as noting that the magnetic foliation/lineation is approximately perpendicular to that of the surrounding samples or to measurements taken in the field. The susceptibility values will also give an indication of what type of minerals dominate a sample (i.e. for diamagnetic minerals $K \approx -1 \times 10^{-5}$ SI; for paramagnetic minerals $K \approx 5 \times 10^{-4}$; for ferromagnetic minerals $K > 5 \times 10^{-3}$ SI). Thin sections should be made for suspect samples and examined for the presence of magnetite, tourmaline, goethite, and other minerals known to produce inverse fabrics. If no minerals with inverse fabrics are found, it is possible that the inverse fabric is due to single domain magnetite that is not visible under the microscope. To determine the orientation of the ferromagnetic minerals, anisotropy of anhysteretic remanent magnetization (AARM) can be used. This technique uses successive permanent magnetizations applied at different directions. The variation in magnetization corresponds to the grain shape of the remanence bearing minerals (i. e. magnetite; Borradaile and Henry, 1997). Other methods, such as analysis of hysteresis loops (see section 4.4) may also be used.

It should be noted that inverse fabrics are rare in AMS dominated by phyllosilicates. When they do occur, they are commonly the result of pseudo-single domain magnetite that is present as tiny inclusions (Borradaile and Werner, 1994). Magnetite may be present as impurities in chlorite, muscovite, or biotite, or as the result of alteration. Ferromagnetic minerals, such as hematite, maghematite, magnetite or goethite, may form under diagenetic to low grade metamorphic conditions. The breakdown of iron-bearing paramagnetic minerals under natural conditions will often result in crystalline orientations that mimic the fabric of the host paramagnetic mineral.

In all AMS-petrofabric studies, the mineralogy of the sample must be known. This can be done through field observation, thin section analysis, anisotropy of remanence, or high field AMS measurements and analysis of the resulting hysteresis loops (see section 4.4).

Composite Fabrics

If there is more than one mineral preferred orientation or fabric in a rock, and both fabrics are defined by Fe-rich minerals, the resulting AMS will be influenced by both mineral species (Housen et al., 1993). This is known as a composite fabric.

Composite magnetic fabrics will not directly reflect the shapes and orientations of the individual mineral fabrics in a sample. For example, one has a sample composed of minerals with equal susceptibilities and the susceptibility axes shown in Fig. 4-13a, and within the sample these minerals define two perpendicular planar fabrics. In this case the maximum susceptibility axis will be located at the intersection of the two planar fabrics (Fig. 4-13b) (Housen et al., 1993). Even if the mineral susceptibilities are not equal the maximum susceptibility will still be at the intersection of the fabrics. However, as the individual susceptibilities approach equality, P will decrease (Housen et al., 1993). Assuming the individual fabrics are oblate, as the susceptibilities of the two fabrics approach each other, or as the angle between the fabrics increases, the shape of the composite ellipsoid will go from oblate to prolate (Housen et al., 1993). If K and P are very similar for the two fabrics then the intermediate and minimum susceptibility axes will occur between the two fabrics as shown in Fig. 4-13b (Housen et al., 1993). If one fabric carries less than approximately 40% of the susceptibility then the AMS will reflect the stronger fabric (Housen et al.,

Fig. 4-13: Orientation of AMS axes for a hypothetical planar fabric (A). Orientation of AMS axes for two perpendicular planar fabrics (B). Modified from Housen et al. (1993).

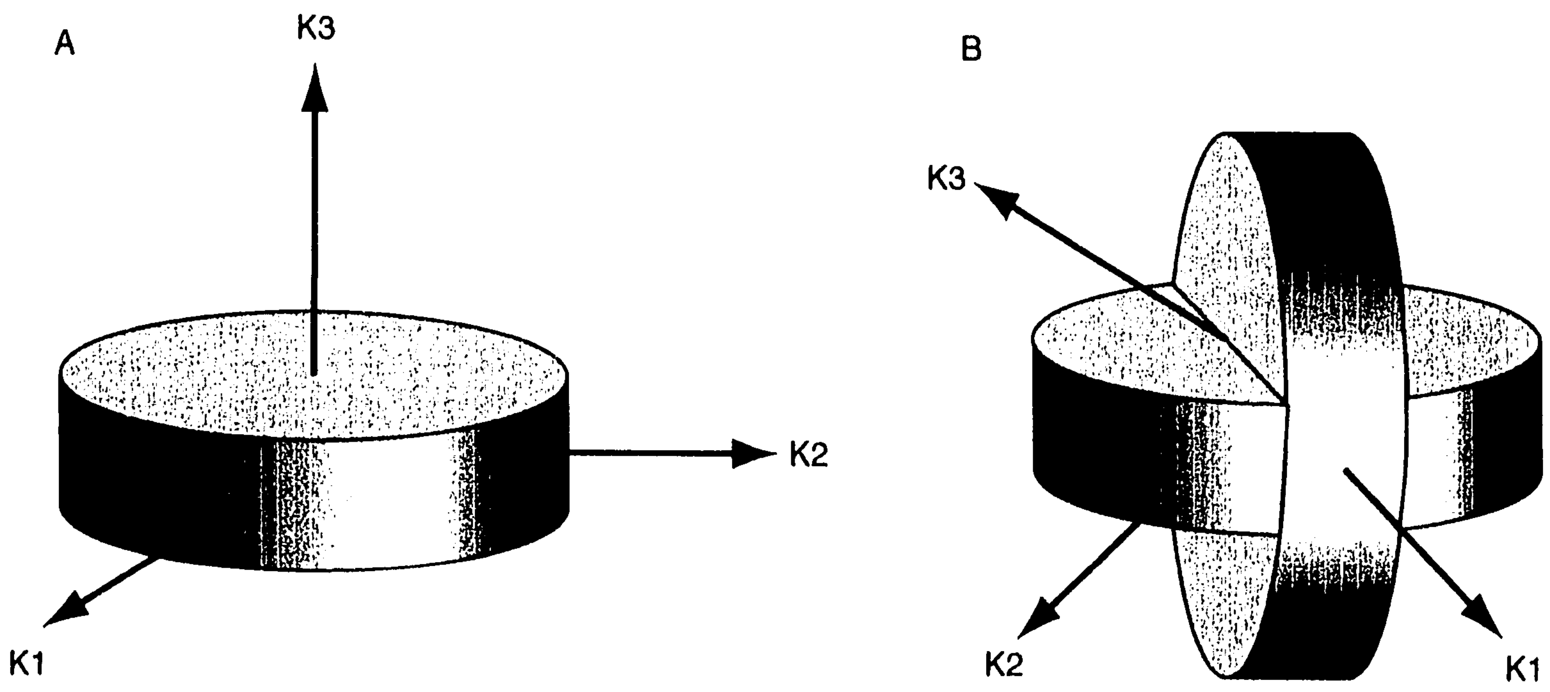

1993). The presence of composite fabrics makes structural interpretation through AMS difficult if not impossible.

Composite fabrics due to the same kinematic event such as the development of S-C fabric in mylonites (Aranguren et al., 1996) may have a different kinematic interpretation from the fabrics described in the previous paragraph. The magnetic foliation will occur between the C- and S-planes. The intermediate susceptibility axis, as opposed to the maximum susceptibility axis, will now lie along the intersection of the two fabrics, and maximum susceptibility will almost parallel the stretching lineation. The reason for this is the fact that both fabrics are the result of one deformation event—simple shear. As deformation occurs the minerals in both planes will align themselves to the maximum stretch direction. Since it is the same event, the maximum stretch directions are equivalent, resulting in a maximum susceptibility axis that almost parallels the stretch direction (Aranguren et al., 1996).

Considering the possible presence of composite fabrics is important when interpreting AMS results. It should be remembered that mineralogy will have the strongest influence on the shape of magnetic fabrics. The mineralogy will define a range of P values for the sample, however this range will be influenced by the presence of composite fabrics, and to a much lesser extent, the degree of mineral alignment (Housen et al., 1993). Studies by Housen et al. (1993) have also shown that composite magnetic fabrics can result in the maximum susceptibility axis being oriented parallel to the bedding cleavage intersection in sedimentary rocks.

4.3.2 Prosperous Suite Data Acquisition

The Sparrow and Prosperous plutons (belonging to the Prosperous Suite) rarely display strong mesoscopic foliations or lineations. Foliations are stronger near pluton margins, where they can be easily measured. This is often not the case in the central regions of the plutons. Measurable lineations are rare anywhere in the plutons. Obtaining orientations of foliations and lineations everywhere in the plutons gives a clearer picture of their structure. This information can then be used to help interpret how the plutons were emplaced, their timing of emplacement, and how they are related to regional deformation.

In the Prosperous and Sparrow plutons, foliations that were measured in the field were fairly consistent. Since this was the case, a one to two kilometer grid for AMS sampling stations was set up. This resulted in 68 sites for the Sparrow Pluton, and 81 sites for the Prosperous Pluton (Fig 4-2 and 4-3). Drilling locations at the sampling sites were placed where there were no visible tourmaline crystals, joints, or shears, and where the fresh rock was representative of the outcrop. Two or three 25 mm diameter cores, a minimum of 55 mm long, were collected at each site, using a portable drill. Cores were then oriented, with the trend and plunge direction marked on each core (Fig. 4-14).

Fig. 4-14: How core samples are marked before they are removed. Lower figure shows the trend and plunge markings on a core sample.

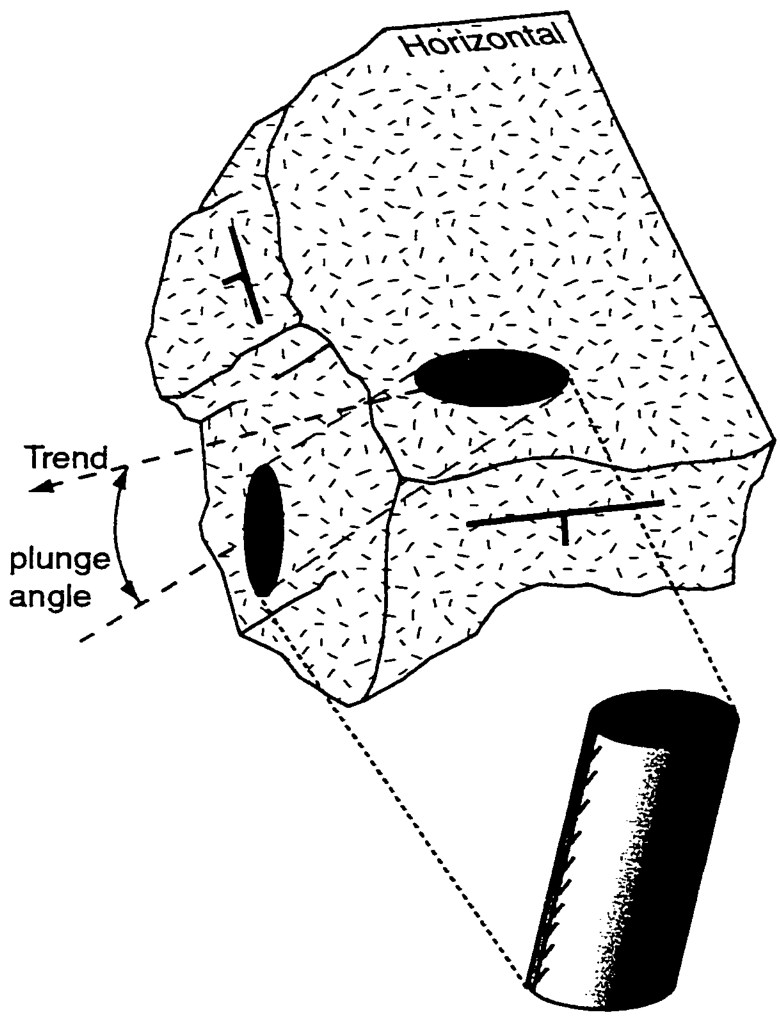

Any broken cores were glued using diamagnetic epoxy (which did not effect the AMS result). Each core was then cut into two samples 22 mm long with the top 5 mm or each core discarded to eliminate the effects of weathering. The ends of each sample were polished using 240 grit silicon carbide to remove any residual metal from the saw blade. All samples were then put in an ultrasonic bath to remove polishing materials.

Samples were measured on a Kappabridge KLY-2 instrument at the University of Ottawa, which measures axial susceptibility with an alternating current (4 X 10^{-4} T, 920Hz). The machine was calibrated using a dry weight standard (ETALON No. 134, measured in range 5, with a value of 1164), and the sample holder was measured. The ANI20 computer program (Geofyzika) was used to treat the magnetic signal. The program subtracts the susceptibility of the sample holder from all measurements preformed on a sample, and transforms the data into geographic coordinates. Each sample was measured in fifteen orientations, and the data were displayed on the computer screen, with statistical errors. If residual errors exceeded a value of 5 X 10^{-6} SI, the measurements were redone. The results were then printed out for each specimen, and data were saved to disk. Once all specimens for a site were measured, the programs ASTA and ASTAOK (Geofyzika) were used to calculate site averages using the Jelinek (1978) tensorial mean method.

4.4 MAGNETIC MINERALOGY STUDIES

To determine the ferromagnetic and paramagnetic contributions to the bulk susceptibility of the studied samples, and to help determine the magnetic mineralogy, the magnetic properties of two samples from the Sparrow pluton were measured by G. S. Pignotta on the Micromag alternating gradient force magnetometer (AGFM) at Lakehead University. One sample represented a normal AMS-petrofabric relationship, and the other sample displayed a potentially inverse fabric. Measurements were made on four fragments (10 to 20 mg) from each sample. The Micromag also measures the acquisition of isothermal remanent magnetization (IRM) and the progressive demagnetization of saturation remanence by direct field (Borradaile and Werner, 1994).

An example plot of the strength of the applied magnetic field vs. the sample magnetization is known as a hysteresis diagram (Tarling and Hrouda, 1993). If the sample contains ferromagnetic minerals, then a sigmoidal loop will result in the diagram (Fig. 4-15a). This sigmoidal loop represents the effects of applying a magnetic field, H, to a sample containing ferromagnetic minerals, slowly increasing it in strength to a high value, and then reversing the direction of the field. The slope of the line, outside the area of hysteresis, will give the susceptibility due to the paramagnetic and diamagnetic minerals (K_{para} + K_{dia}) (Fig. 4-15a). The plot is then rotated so the areas outside the region of hysteresis are horizontal (Fig. 4-15b). The rotated plot allows the determination of susceptibility of the ferromagnetic component (K_{ferro}), saturation magnetization

Fig. 4-15: Hysteresis loops. (A) shows an unrotated loop where the slope of the linear part is Kpara + Kdia. (B) shows the rotated loop with the saturation magnetization (Ms). Mr (remanent magnetization) is the magnetization when the applied field is zero. Hc (coercivity) is the value of the magnetic field when the magnetization is zero. Modified form Borradaile and Werner (1994).

A

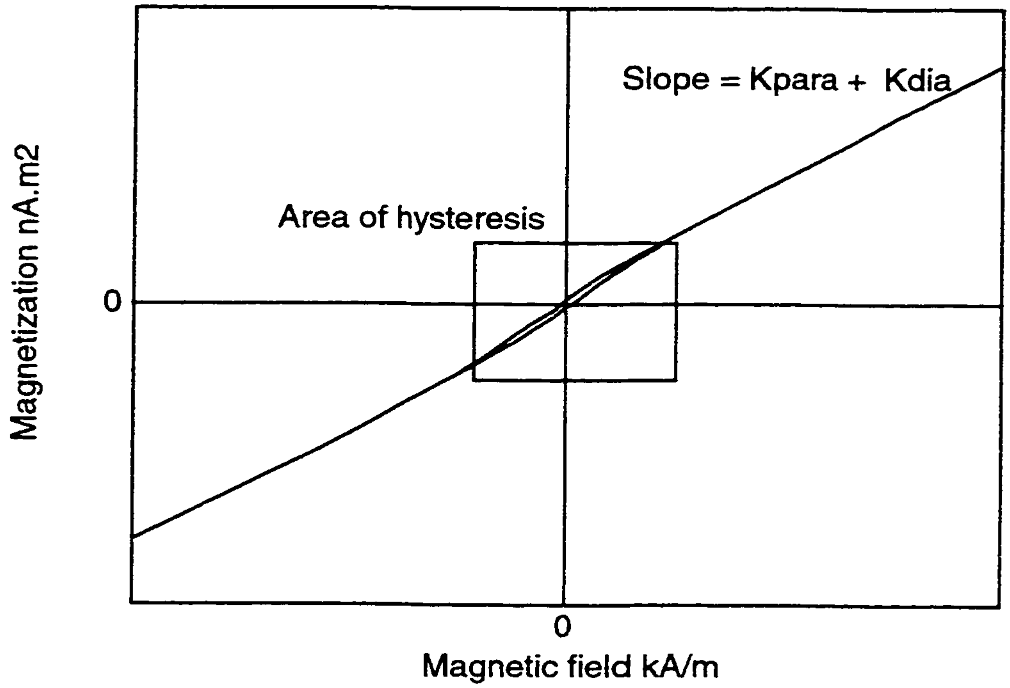

B

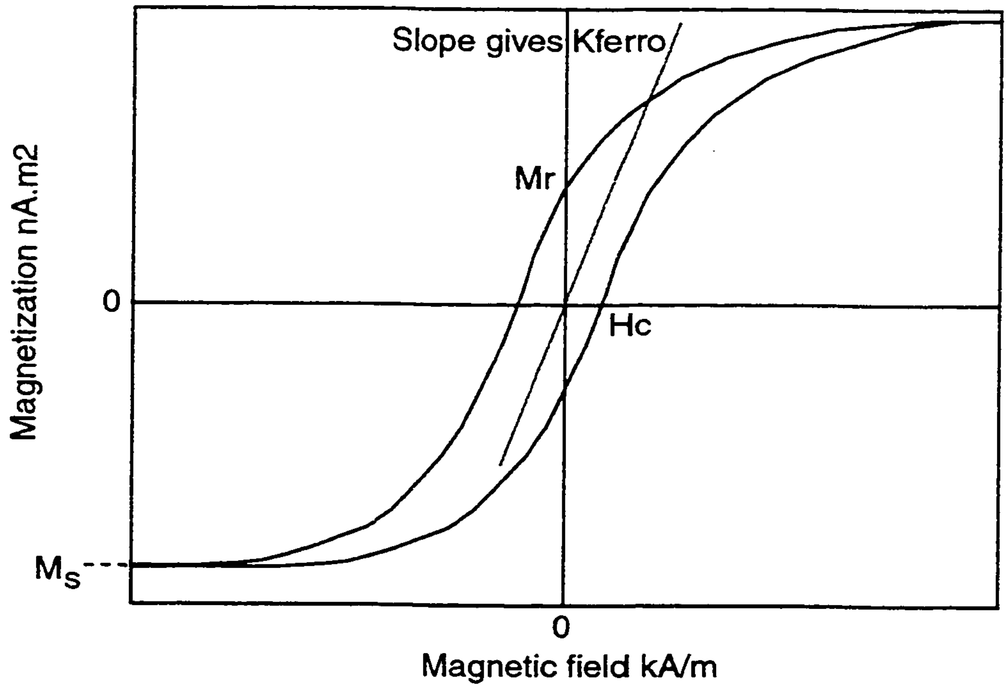

(M_s), maximum remanent magnetization (M_r), and coercivity (H_c) (Fig. 4-14b) (Borradaile and Werner, 1994). The coercivities of remanence (H_{cr}) were determined using the Micromag, through demagnetization of saturation remanence. H_c and H_{cr} estimated from the demagnetization curve, during direct field magnetization, will characterize the carriers of the ferromagnetic susceptibility (Borradaile and Werner, 1994). The percent of the susceptibility carried by the ferromagnetic component (%K_{ferro}) is calculated by:

$$\%K_{ferro} = 100\left[\frac{K-\left(K_{para}+K_{dia}\right)}{K}\right]$$

where K is the total susceptibility, K_{para} is the paramagnetic component of the susceptibility, and K_{dia} is the diamagnetic component of susceptibility.

The ratios of H_{cr}/H_c and M_r/M_s may be used to characterize the grain size and domain structure of fine-grained magnetite in the samples (Day et al., 1977; Borradaile and Werner, 1994).

Chapter 5: Porphyroblast-Fabric Relationships

This chapter presents and discusses the results from the porphyroblast-fabric studies on the Burwash Formation surrounding the Prosperous Suite. Section 5.1 presents the summary of petrographic observations, which are then discussed in section 5.2. Section 5.3 discusses the observations made on traverses starting within the plutons and extending out into the country rocks.

5.1 PETROGRAPHIC OBSERVATIONS

Examination of thin sections of the Burwash Formation near the Prosperous and Sparrow plutons showed that porphyroblasts of biotite, chlorite, staurolite, cordierite, muscovite, tourmaline, and garnet are commonly present. The occurrence of each mineral is discussed further below. Fig. 5-1 shows sample locations and occurrence of selected metamorphic minerals. In addition to the above minerals, minor plagioclase was also observed.

Two generations of biotite are present in the country rocks. The older generation typically contains quartz inclusions and is irregular in shape (Fig. 5-2). The younger generation is composed of subhedral biotite laths (Fig. 5-2), which cross-cut the earlier generation and define the main foliation (Fig. 5-3). In horizontal sections, the quartz inclusions mentioned above are either parallel or slightly oblique to the external foliation (S_e, which is defined by the biotite laths; Fig. 5-4). Biotite is commonly retrograded to chlorite (Fig. 5-5).

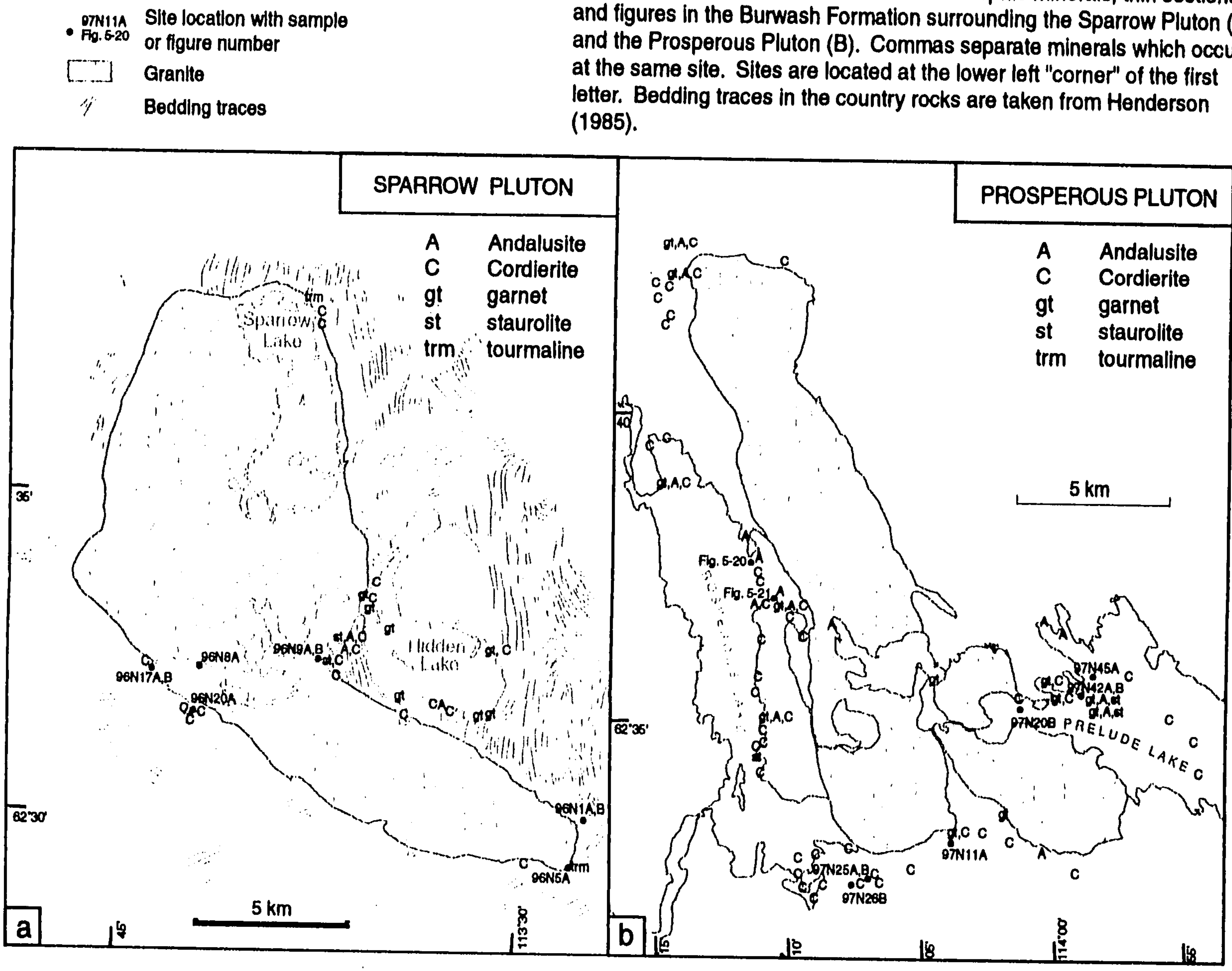

Fig. 5-1: Maps of the occurrence of selected metamorphic minerals, thin sections and figures in the Burwash Formation surrounding the Sparrow Pluton (A) and the Prosperous Pluton (B). Commas separate minerals which occur at the same site. Sites are located at the lower left "corner" of the first letter. Bedding traces in the country rocks are taken from Henderson (1985).

Fig. 5-2: Two generations (lath shaped and irregularly shaped) of biotite crystals present in the country rocks. Sample number 96N1A, horizontal section, plane polarized light, Burwash Formation.

Fig. 5-3: Arrow shows where a biotite lath cross-cuts an older biotite crystal. Sample number 96N1B, vertical section, plane polarized light, Burwash Formation.

Fig. 5-4: Inclusions of quartz (qtz) in older biotite crystals. Quartz inclusions are parallel to oblique to the external foliation. Sample number 97N25A, horizontal section, plane polarized light, Burwash Formation.

Fig. 5-5: Arrow shows where biotite is retrograded to chlorite (chl). Sample number 96N8A, horizontal section, plane polarized light, Burwash Formation.

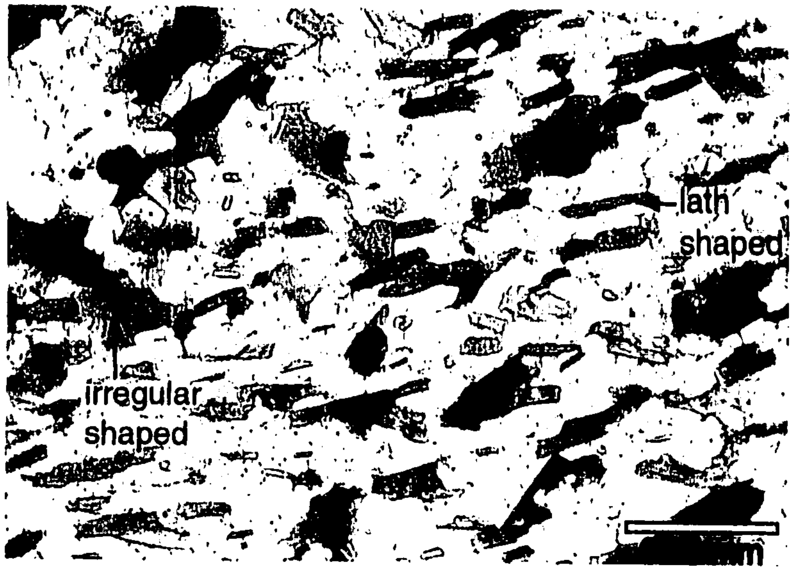

Fig. 5-2

Fig. 5-3

Fig. 5-4

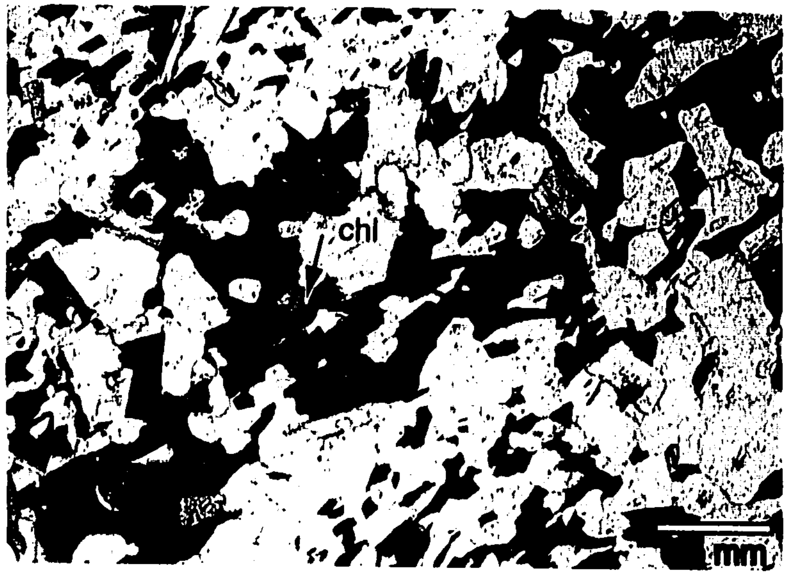

Fig. 5-5

Chlorite is also present in the form of small blades that cross-cut the biotite (lath) S_e foliation at a high angle in both horizontal and vertical planes (Fig. 5-6). Chlorite is locally concentrated in darker lamellae with crystal orientations being parallel and oblique to the lamellae boundaries (horizontal plane; Fig. 5-7).

Staurolite, pseudomorphed by sericite, was observed in many thin sections and often appears as a yellow "stain" in plain polarized light (Fig. 5-8). Staurolite crystals usually contain both quartz and biotite; the biotite crystals are too small to assign to a generation. Inclusion trails, where present, are straight and parallel to the external foliation (S_2, defined by micas) in horizontal sections. In some sections (in both vertical and horizontal planes) the staurolite crystals have their long axes parallel to the biotite foliation. Some sections also display partial muscovite coronas around the staurolite crystals (Fig. 5-9). Only one section (97N25B) displayed a crenulation visible both in the staurolite porphyroblast as well as outside of it (vertical plane; Fig. 5-10).

Cordierite is also common in the country rocks surrounding the plutons. The porphyroblasts, which are often elongate parallel to the S_2 biotite foliation (in horizontal sections), commonly contain inclusions of quartz and biotite (Fig. 5-11) and very rarely of tourmaline (sample 96N8A). Inclusion trails are frequently straight and tend to be parallel to S_e in horizontal and vertical sections, but inclusions also occur at an angle to the biotite foliation. Inclusion trails were observed both clockwise and counter-clockwise to S_e (defined by micas) in a horizontal plane (Fig. 5-12). In vertical sections the inclusion trails

Fig. 5-6: Small blades of chlorite cross-cutting the biotite foliation. Sample number 97N42A, horizontal section, plane polarized light, Burwash Formation.

Fig. 5-7: Chlorite concentrated in the darker lamellae of the Burwash Formation. Sample number 97N45A, horizontal section, plane polarized light, Burwash Formation.

Fig. 5-8: Staurolite pseudomorphed by sericite. Sample number 96N9B, vertical section, crossed polars, Burwash Formation.

Fig. 5-9: Muscovite corona around staurolite. Sample number 97N26B, vertical section, plane polarized light, Burwash Formation.

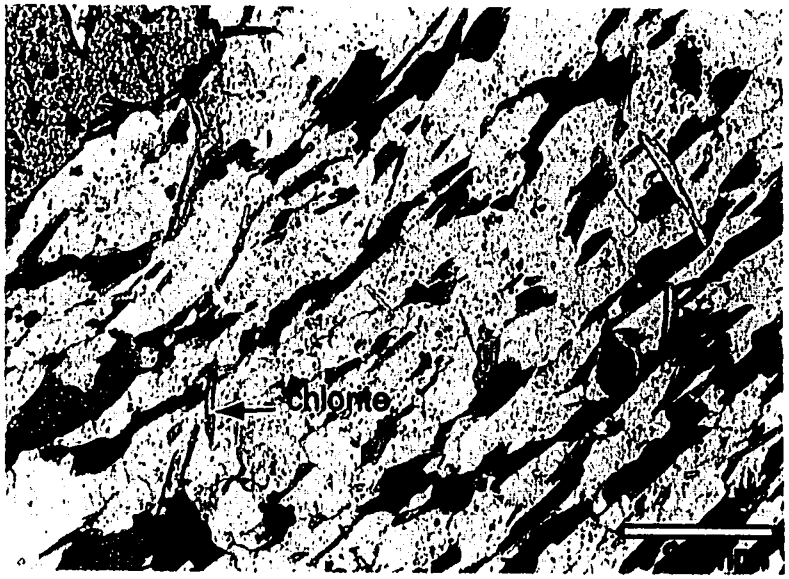

Fig. 5-6

Fig. 5-7

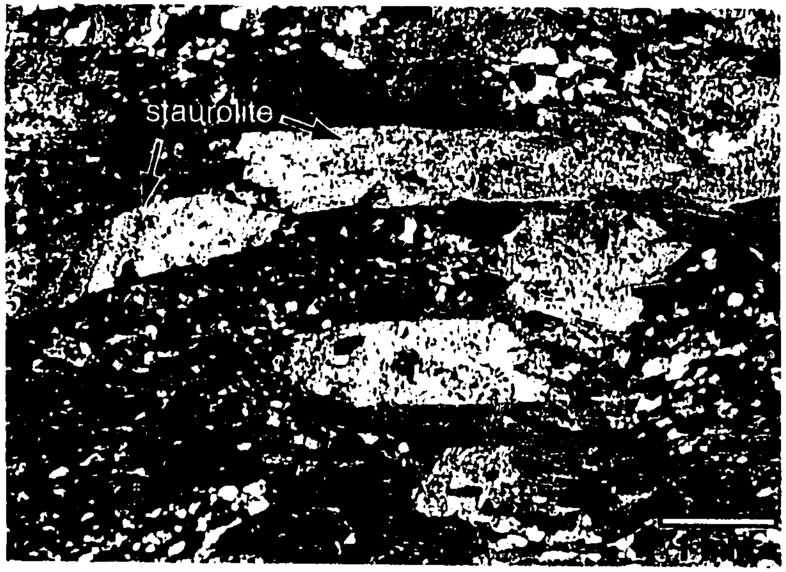

Fig. 5-8

Fig. 5-9

Fig. 5-10: Crenulation in the Burwash Formation. Sample number 97N25B, vertical section, plane polarized light, Burwash Formation.

Fig. 5-11: Cordierite (crd) porphyroblast with inclusions of biotite and quartz. Sample number 96N9A, horizontal section, plane polarized light, Burwash Formation.

Fig. 5-12: Cordierite (crd) porphyroblasts with quartz inclusion trails both clockwise and counterclockwise from the matrix foliation. Black dashed lines parallel inclusion trails. Sample number 96N17A, horizontal section, plane polarized light, Burwash Formation.

Fig. 5-13: Vertical section of cordierite (crd) porphyroblasts with quartz inclusion trails which are parallel/sub-parallel to the external foliation. White dashed lines parallel inclusion trails. Muscovite (musc) and biotite (bio) wrap around the cordierite. Sample number 96N17B, vertical section, plane polarized light, Burwash Formation.

Fig. 5-10

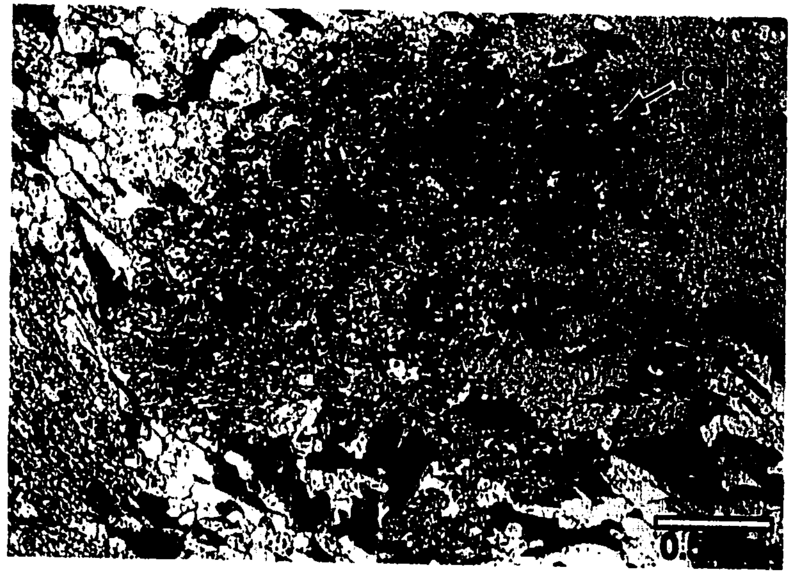

Fig. 5-11

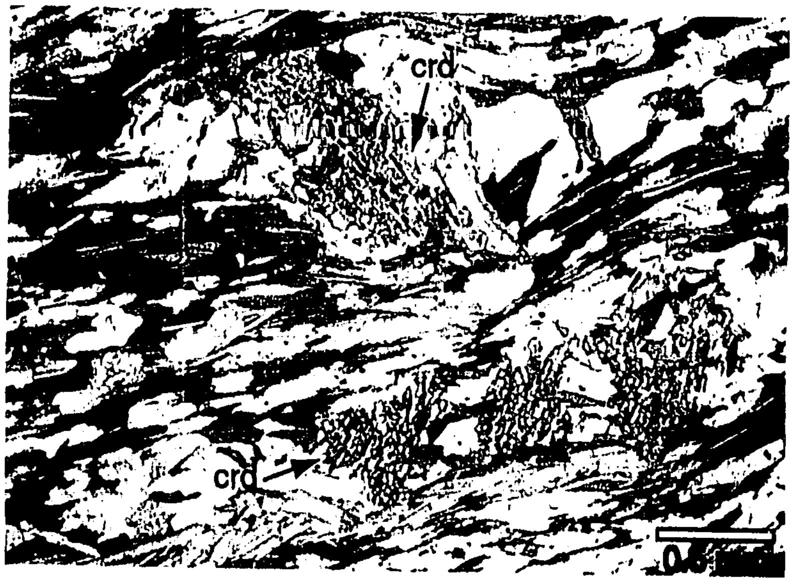

Fig. 5-12

Fig. 5-13

tend to be nearly parallel/parallel to the biotite foliation (Fig. 5-13). Cordierite also seems to partially envelop staurolite crystals (sample 96N9).

Muscovite is present in many sections. It is often associated with biotite and wraps around staurolite and cordierite (Fig. 5-13). Muscovite also occurs as straight inclusions in cordierite, which are at a high angle to the external foliation (in horizontal sections; Fig. 5-14). Laths of muscovite occasionally surround cordierite porphyroblasts, forming a spherical feature with chlorite and biotite commonly at the outermost edge (Fig. 5-15).

Tourmaline is most common near pluton contacts. Tourmaline appears to cross-cut some of the biotite crystals (cannot determine which biotite generation; Fig. 5-16) and also occurs roughly parallel to the S_2 biotite foliation in horizontal sections (Fig. 5-17). Inclusions in tourmaline are frequently randomly oriented and in some cases are parallel to the external biotite foliation (in the horizontal plane). The inclusions are occasionally parallel to the opaques (horizontal sections; Fig. 5-17), which in sample 96N5A are also parallel to S_2.

Study of the porphyroblast-fabric relationships in the country rocks to the east of the Prosperous pluton revealed garnets that contain straight inclusion trails that are at a high angle to the predominant mica foliation in a horizontal plane (Fig. 5-18). Vertical sections often show inclusions that are less elongate and that are parallel to the biotite foliation (Fig. 5-19). The biotite wraps around the garnets and pressure shadows are occasionally present (Fig. 5-18). The

Fig. 5-14: Muscovite (musc) inclusions in cordierite (crd). White dashed lines parallel inclusion trails. Sample number 96N20A, horizontal section, crossed polars, Burwash Formation.

Fig. 5-15: Cordierite (crd) surrounded by muscovite (musc), biotite (bio) and chlorite (chl). Sample number 97N11A, horizontal section, plane polarized light, Burwash Formation.

Fig. 5-16: Arrow shows where a tourmaline (trm) crystal cross-cuts a biotite (bio) crystal. Sample number 97N20B, vertical section, plane polarized light, Burwash Formation.

Fig. 5-17: Quartz (qtz) inclusions in tourmaline (trm) parallel to the external foliation defined by opaque crystals (op). Sample number 96N5A, horizontal section, plane polarized light, Burwash Formation.

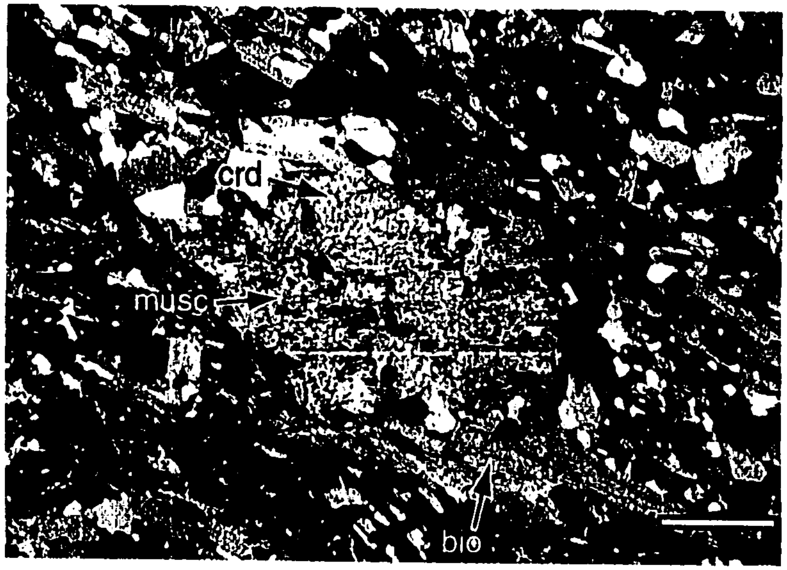

Fig. 5-14

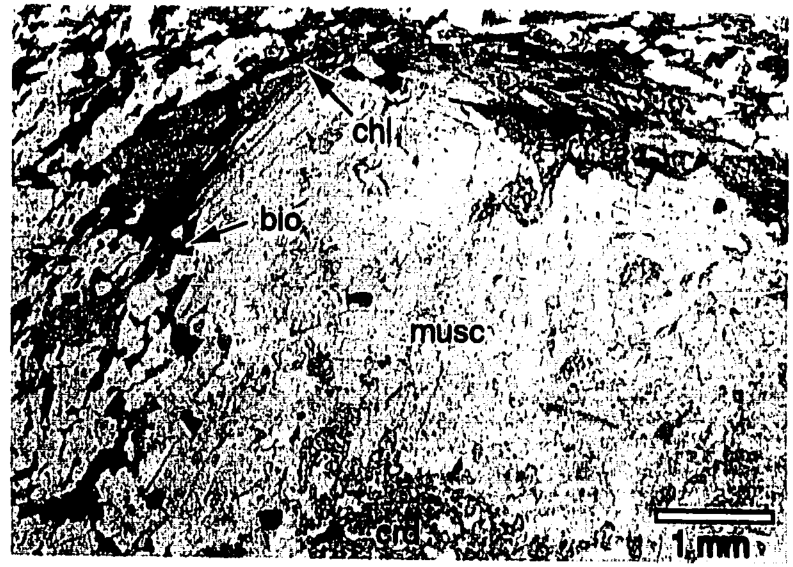

Fig. 5-15

Fig. 5-16

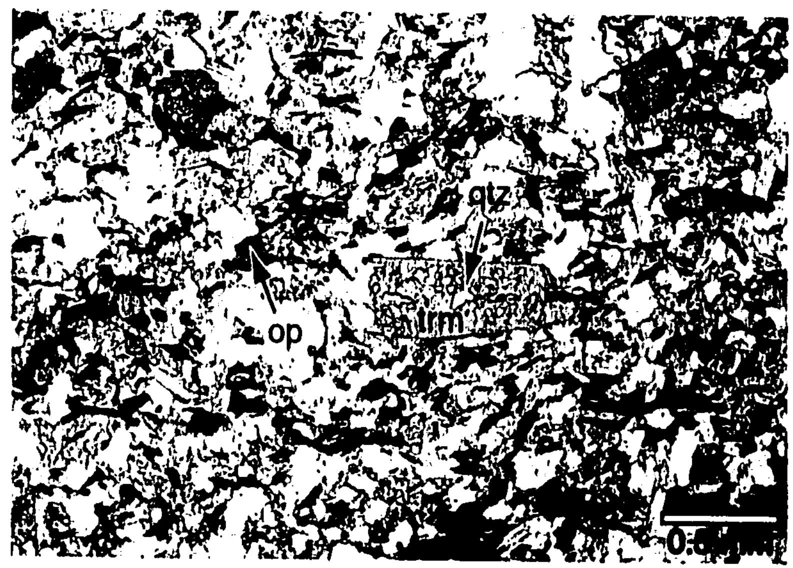

Fig. 5-17

Fig. 5-18: Garnet (gt) with quartz (qtz) inclusions at a high angle to the external foliation. Arrow points to a quartz pressure shadow. Biotite (bio) defines the matrix foliation and wraps around the garnet. Sample number 97N42A, horizontal section, plane polarized light, Burwash Formation.

Fig. 5-19: Garnet (gt) with quartz (qtz) inclusions parallel to the biotite (bio) foliation in a vertical section. Sample number 97N42B, vertical section, plane polarized light, Burwash Formation.

Fig. 5-20: Biotite (S_2) wrapping around andalusite crystals in outcrop. Burwash Formation west of Prosperous Pluton.

Fig. 5-21: Large andalusite crystals defining S_2 on an inclined surface. Silva compass for scale. Compass edge oriented north-south, with north to the left. Burwash Formation west of Prosperous Pluton.

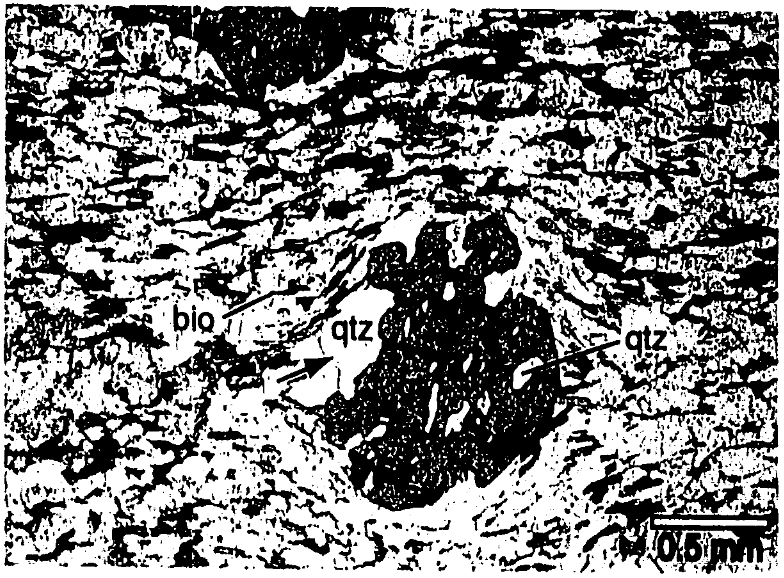

Fig. 5-18

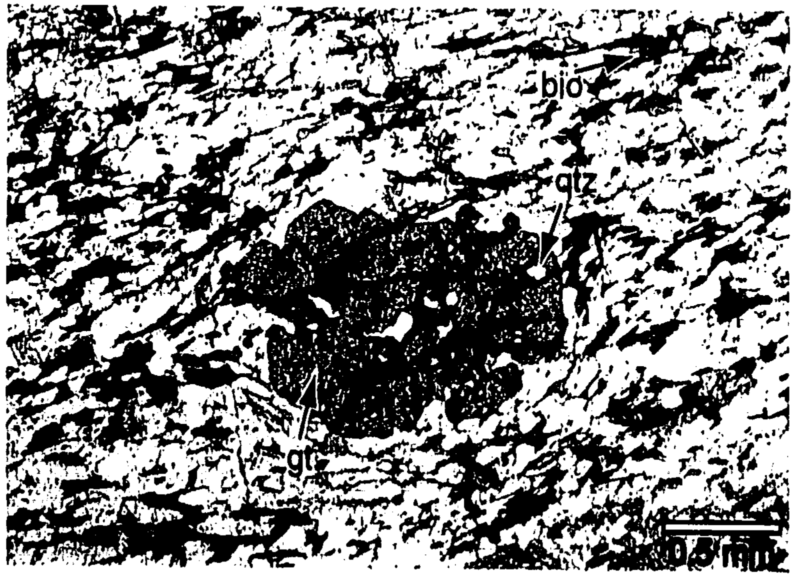

Fig. 5-19

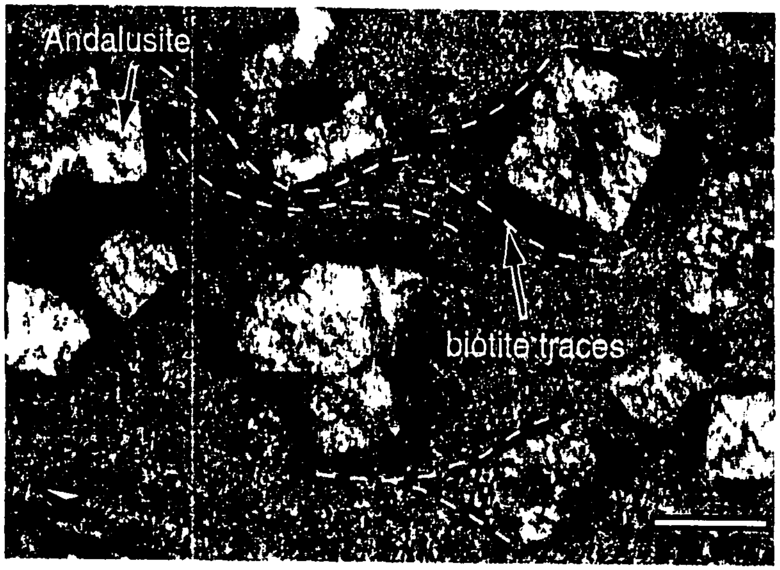

Fig. 5-20

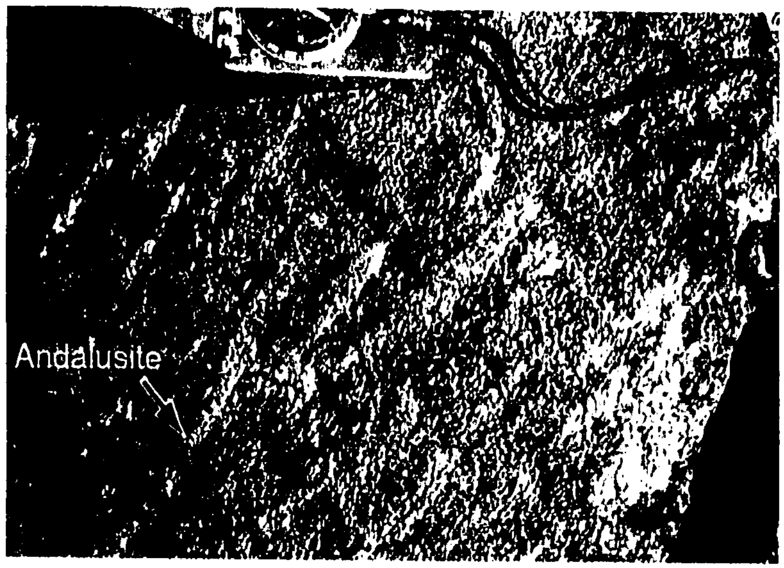

Fig. 5-21

pressure shadows are small and both symmetrical and asymmetrical with one high and the other low in horizontal sections.

5.2 PORPHYROBLAST-FABRIC RELATIONSHIPS

Biotite was one of the first metamorphic minerals to form. The irregular shaped generation mentioned above is the one that commonly contains quartz inclusions. These inclusions define a preserved, older foliation (S_i) which is not present in the matrix. Work by Fyson (1982) also shows that quartz inclusion trails in biotite crystals are at a high angle to the dominant regional foliation. In the vicinity of the Prosperous Pluton (west of the pluton and east of Yellowknife), the quartz inclusion trails strike roughly E-W (Fyson, 1982; Fyson and Helmstaedt, 1988). Fyson (1982) concluded that these inclusion trails represented a preserved cleavage (S_2A of Fyson, 1982, and S_1 of Bleeker and Beaumont-Smith, 1995) that formed preceding the emplacement of the Prosperous Pluton. Based on the above evidence, the inclusions are very probably preserved S_1. This generation of biotite is cross cut by a younger generation that is lath-like in shape and typically inclusion free. The "lath" foliation defines the regional S_2 foliation and is believed to have formed during D_2. Kretz (1968) also identified the two generations of biotite described above.

The next metamorphic mineral to form would have been staurolite. Staurolite crystals commonly contain straight inclusion trails and crystals have their long axes parallel to the S_2 biotite foliation (in the horizontal and vertical planes). Bethune and Carmichael (1998) also noted that the staurolite crystals contain inclusions at a high angle to the external foliation (in the horizontal plane). As with the inclusions in the biotite crystals, these inclusions are interpreted to probably represent S_1 (S_{i1}) which corresponds with the interpretation of Bethune and Carmichael (1998). The crenulation seen in sample 97N25B (vertical thin section) is interpreted to be the preservation of S_1 deformed during early D_2, since the matrix and the inclusion traces in the staurolite porphyroblast are both crenulated.

Andalusite formed next (Bethune and Carmichael, 1998). Athough none of the thin sections gathered in this study showed andalusite, field observations showed large andalusite crystals in outcrop with biotite wrapping around them (Fig. 5-20). Work done by Bethune and Carmichael (1998) showed that andalusite generally contained curved inclusion traces suggesting andalusite crystallization was synchronous with D_2, and possibly grew during the early stages of D_2.

Cordierite formed after staurolite, since there are cases where it partially envelops staurolite crystals. Rims of staurolite also occur on andalusite (Bethune and Carmichael, 1998). Inclusion trails in the cordierite are straight and parallel to the external foliation (horizontal and vertical sections), although cases occur where S_i is at an angle to S_e. This could be explained if more than one generation of cordierite is present. In the case of S_i being parallel to S_e in horizontal and vertical sections, the cordierite may have formed later, once S_2 had entirely overprinted S_1. This corresponds with Bethune and Carmichael's

(1998) observation of cordierite statically overgrowing S_2, which was most obvious in cases where cordierite rimmed staurolite and andalusite (Bethune and Carmichael, 1998). In cases where S_i is at an angle to S_e in the horizontal plane, vertical sections show S_i inclusions roughly parallel to S_e. In this case S_i could possibly represent preserved S_1. The fact that S_i is both counter-clockwise and clockwise to S_e in horizontal sections could suggest that the cordierite overgrew S_1 after it was folded by early D_2. More than one generation of cordierite, one forming early during D_2 and one forming after S_2 had already been established, would explain Bethune and Carmichael's (1998) observations as well as those seen in this study.

Tourmaline is most common at the pluton contact where it can occur in great abundance. The tourmaline is believed to be a result of metasomatism associated with pluton emplacement (this has also been suggested by Kretz, 1968). Tourmaline formed at some time after initial S_2 fabric development since it occasionally is seen to cross-cut biotite (which generation of biotite is cross-cut cannot be determined). D_2 continued during tourmaline formation resulting in tourmaline crystals being roughly aligned parallel to S_2 (best seen in horizontal sections).

Both biotite and muscovite formed throughout most of D_2. More than one generation of muscovite may be present. Straight inclusion trails of muscovite in cordierite being at high angles to the external S_2 foliation (in horizontal sections) would suggest that this muscovite might have been associated with D_1. A second generation of muscovite visible in thin section formed during D_2. Both biotite and muscovite were seen to wrap around staurolite and cordierite.

Garnet formed some time after D_1 and before D_2 was complete. The straight inclusions in the garnets are probably a preservation of S_1. The garnets display slightly asymmetric pressure shadows and straight inclusion trails at an angle to the external foliation in the horizontal plane. In the vertical plane these inclusions, when they are elongated at all, are parallel to S_2. This may be explained by the garnets forming early during D_2, when S_1 had been folded but not overprinted by S_2. The slightly asymmetric pressure shadows (seen in horizontal sections) were possibly the result of minor rotation of the garnets as D_2 continued.

Chlorite formed last. It is mainly a product of retrograde metamorphism, as shown by the partial alteration of biotite to chlorite in many samples. Where the chlorite forms as individual crystals, they are small and cross cut S_2 at a high angle (seen in both horizontal and vertical sections) defining S_3.

5.3 CHANGES IN MINERALOGY AND FABRIC AWAY FROM THE PLUTON CONTACTS

Several traverses were done starting in the plutons and extending out into the Burwash Formation. The purpose was to note variations in metamorphic mineralogy and fabrics in the country rocks.

Fig. 5-1 shows where cordierite, staurolite, garnet and tourmaline were observed. Cordierite is present in most outcrops and is the dominant porphyroblast (excluding micas). Crystals are 1-2 cm in size and define the mesoscopic regional (D_2) foliation along with micas near the plutons. Within 100 m of the contact, cordierite is wrapped by micas and displays a knotted schist texture. Traverses did not extend out of the cordierite isograd.

Staurolite, andalusite, and garnet were only observed within 2-3 km of the pluton contact. Staurolite is rarely visible in outcrop with crystals typically less than 0.5 cm in size. Andalusite occurs within 2 km of the contact. More andalusite was observed near the Prosperous Pluton than near the Sparrow Pluton (Fig. 5-1) possibly due to the better exposure. Andalusite crystals (chiastolite) are up to 20 cm in length (Fig. 5-21) with the larger crystals occurring near the western contact of the Prosperous Pluton.

Garnet was also observed within 2.5 km of the pluton contact. Crystals are generally <0.5 cm in diameter. The occurrence of garnet is strongly controlled by the rock composition. Garnets are usually concentrated in the Fe-rich beds.

Tourmaline is very common near the pluton contacts. Crystals are often small, < 1mm in size, and are difficult to see on the outcrop scale. The abundance and size of tourmaline diminishes rapidly away from the contacts.

The mesoscopic fabric at most sites was defined by micas and/or cordierite and defines the regional D_2 fabric. The observed porphyroblast-fabric relationships are consistent around the plutons and away from the plutons with the exception of minor crenulation visible in the rocks to the south of the Prosperous Pluton (i. e. sample 97N25A,B). This crenulation is possibly a preservation of S_1 being folded during early D_2. Where aureoles of the Defeat Suite and the Hidden Lake Pluton overlapped by the Prosperous Suite aureole, two fabrics are occasionally visible: the S_2 fabric described above, and a weak biotite fabric (probably due to D_1).

The relative intrusion of the plutons with respect to the structures in the Burwash Formation is discussed in section 7.1.2 .

Chapter 6: Structure and Magnetic Fabrics in the Granites

This chapter details the structure (section 6.1), microstructure (section 6.2), magnetic mineralogy (section 6.3), and the AMS results (section 6.4) for the Sparrow and Prosperous plutons. The data and interpretations have been presented at various conferences (Ham et al., 1996, 1997a, b, c, 1998a, b), and in an open file report (Ham and Benn, 1998). The data and interpretation of the field observations, magnetic fabrics and magnetic mineralogy for the Sparrow Pluton have also been published in Benn et al. (1998a).

6.1 STRUCTURAL GEOLOGY OF THE GRANITES

This section discusses the structural field mapping results from the Sparrow and Prosperous plutons, as well as the associated pegmatites.

6.1.1 Sparrow Pluton

The northern region of the Sparrow Pluton has a roughly rectangular shape whereas the southern region is an elongate "tail" that appears to be deflected sinistrally. The sinistral deflection could be a local effect due to the presence of an earlier pluton to the south (part of the Defeat Suite; Fig. 1-2) which acted as a rigid buttress during regional D_2 dextral transpression. Contacts of the Sparrow Pluton are sharp and locally discordant to the predominant regional D_2

fabrics in the country rocks, and to the foliation in the pluton which strikes parallel to the S_2 fabric in the country rocks (Fig. 6-1a).

The pluton is well foliated near its margins. Away from the margins, the foliation is often difficult to observe. The foliation, which is defined by biotite and slightly oblate quartz aggregates, is usually homogeneous at the outcrop scale. Close inspection of clean outcrop surfaces reveals that euhedral plagioclase crystals are also aligned parallel to the foliation. In the northern portion of the pluton the foliation strikes NNW-SSE and has mostly steep dips (Fig. 6-1a). In the "tail" of the pluton the foliation strikes NW-SE (Fig. 6-1a).

Decimeter- to meter-scale protomylonitic greenschist facies strike-slip shear zones (Fig. 6-2) are present mainly in the southern part of the pluton (Fig. 6-3). These shear structures are the result of deformation continuing as the granites cooled below the solidus at approximately 550^{0}C (Gapais, 1989). Gapais (1989) has noted a correlation between cooling of granites and an increase in strain localization and the development of shear bands. NW to N striking shear zones are dextral, which is consistent with bulk regional dextral D_2 shearing as described by Bleeker and Beaumont-Smith (1995). A second family of predominantly NW to E-W striking shear zones occurs in the southern "tail" of the pluton. Near the southern contact of the pluton the shears are sinistral (Fig. 6-3). Just to the north of these, dextral shears occur (Fig. 6-3). Granitic and pegmatitic dykes of the Prosperous Suite observed near the Sparrow pluton are folded with axial surfaces parallel to S_2 (Fig. 6-4), whereas dykes emplaced along

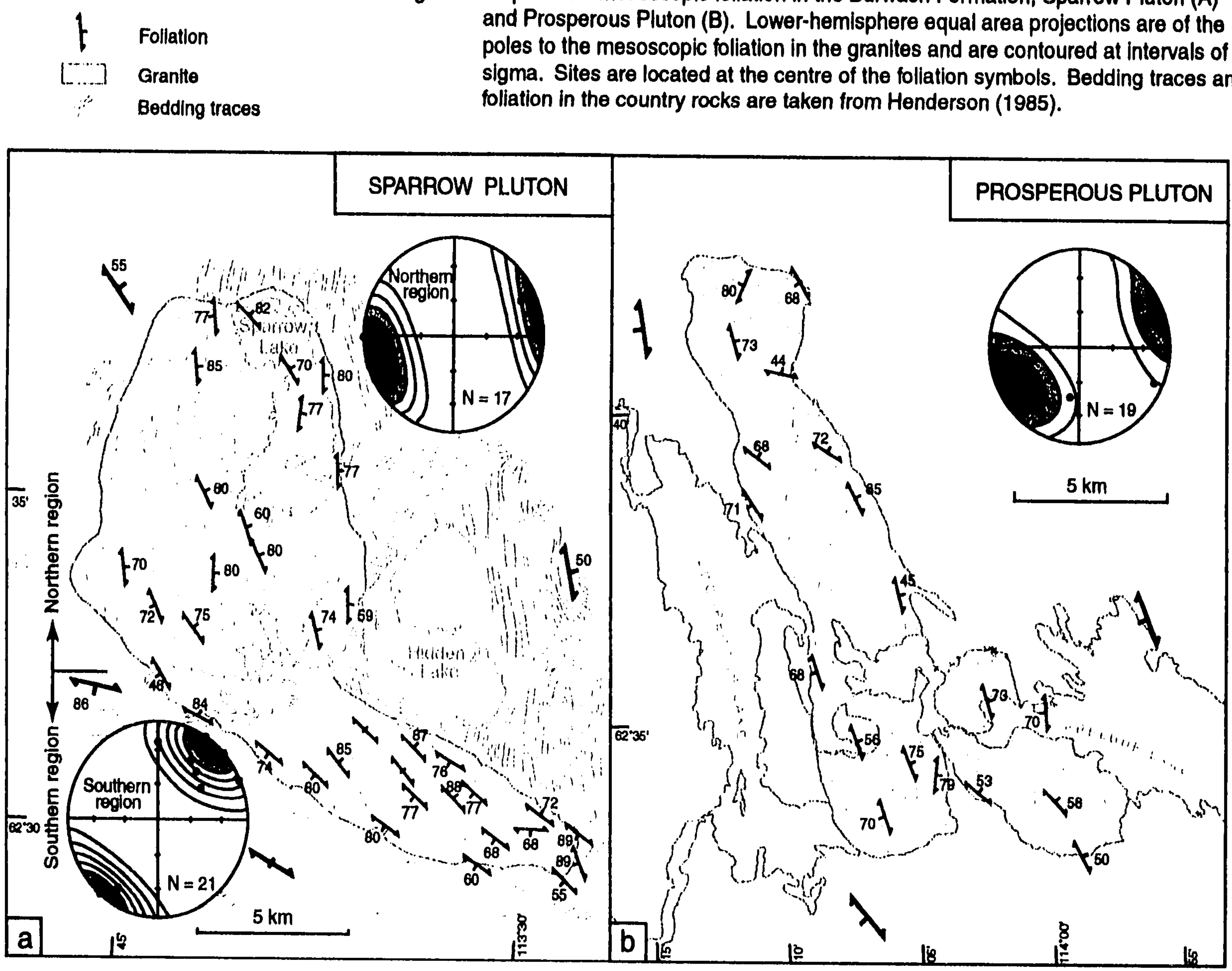

Fig. 6-1: Maps of the mesoscopic foliation in the Burwash Formation, Sparrow Pluton (A) and Prosperous Pluton (B). Lower-hemisphere equal area projections are of the poles to the mesoscopic foliation in the granites and are contoured at intervals of 3 sigma. Sites are located at the centre of the foliation symbols. Bedding traces and foliation in the country rocks are taken from Henderson (1985).

Fig. 6-2: Shear zone in the Sparrow Pluton displaying C-S fabric. Compass for scale.

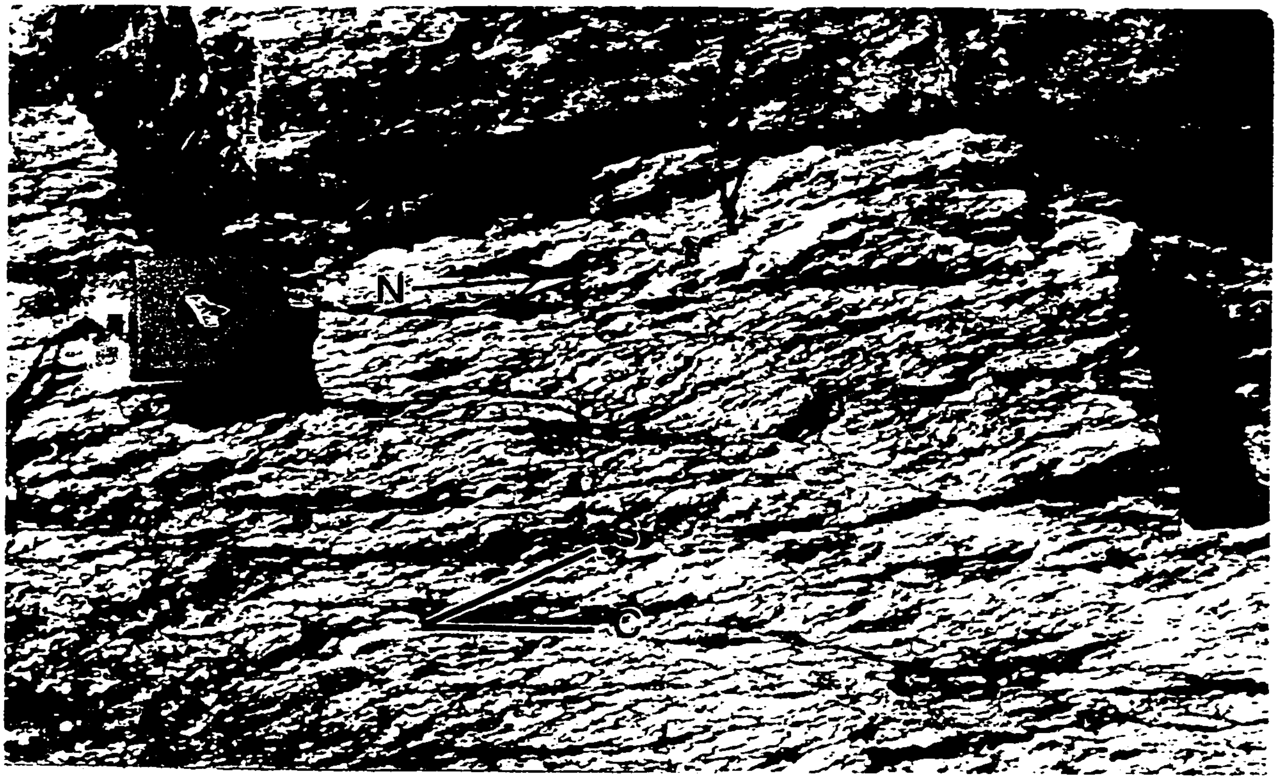

Fig. 6-3: Map of shear zones in the Sparrow Pluton. Bedding traces in the country rocks are taken from Henderson (1985).

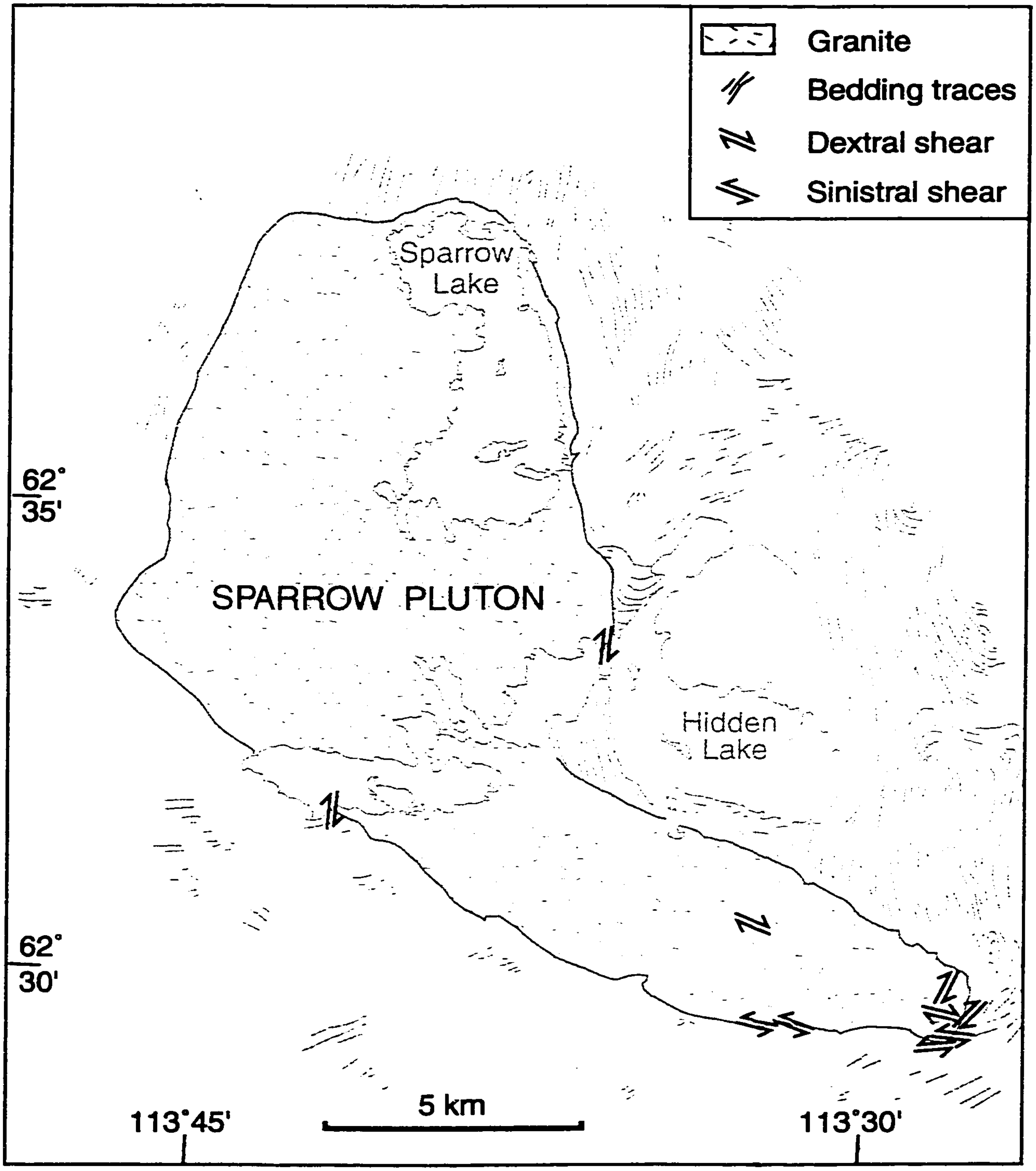

Fig. 6-4: Folded granite dyke in the Burwash Formation to the East of the Sparrow Pluton near Hidden Lake. Axial-planar cleavage in the Granite is parallel to the regional S_2 foliation in the Burwash Formation.

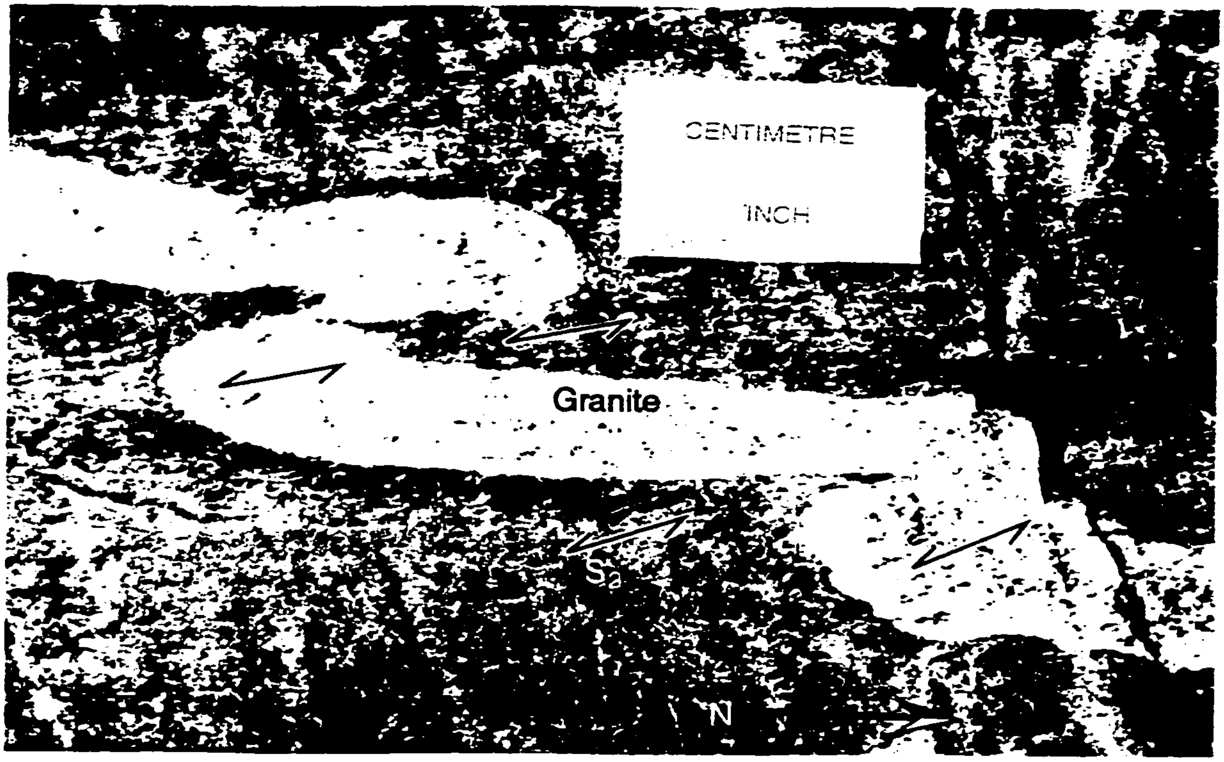

the foliation plane show pinching and swelling (Fig. 6-5). This further suggests D_2 deformation during granitic magmatism.

Numerous pegmatite dykes and quartz veins cross-cut the Sparrow Pluton and surrounding country rocks. The pegmatites contain quartz, potassium feldspar, plagioclase, muscovite, and often tourmaline (pers. obs.; Kretz, 1968). Two sets of pegmatite dykes cross-cut the Sparrow Pluton. In the northern region, dykes strike ENE-WSW and NNE-SSW (Fig. 6-6a). In the southern region the dykes strike NW-SE and NE-SW (Fig. 6-6a). This is consistent with the dykes in the southern "tail" having been rotated counter-clockwise during sinistral deflection of the "tail". The quartz veins are steep to vertical and dominantly strike N-S.

6.1.2 Prosperous Pluton

The Prosperous Pluton has an elongate NNW-SSE rectangular shape with a smaller lobe at its SE corner (Fig. 6-1b). As with the Sparrow Pluton, the contacts are sharp and locally discordant to the predominant regional D_2 fabric in the host rocks (Fig. 6-1b). The strike of the foliation within the pluton is parallel to the strike of the S_2 fabric in the country rocks, and approximately perpendicular to the contacts at the northern and southern ends of the pluton (Fig. 6-1b).

The Prosperous Pluton displays a moderately developed mesoscopic foliation near its margin and the foliation becomes more difficult to observe

Fig. 6-5: Granite dyke injected along S_2 cleavage in the Burwash Formation east of the Sparrow Pluton, near Hidden Lake. Note pinching and swelling of granite dyke.

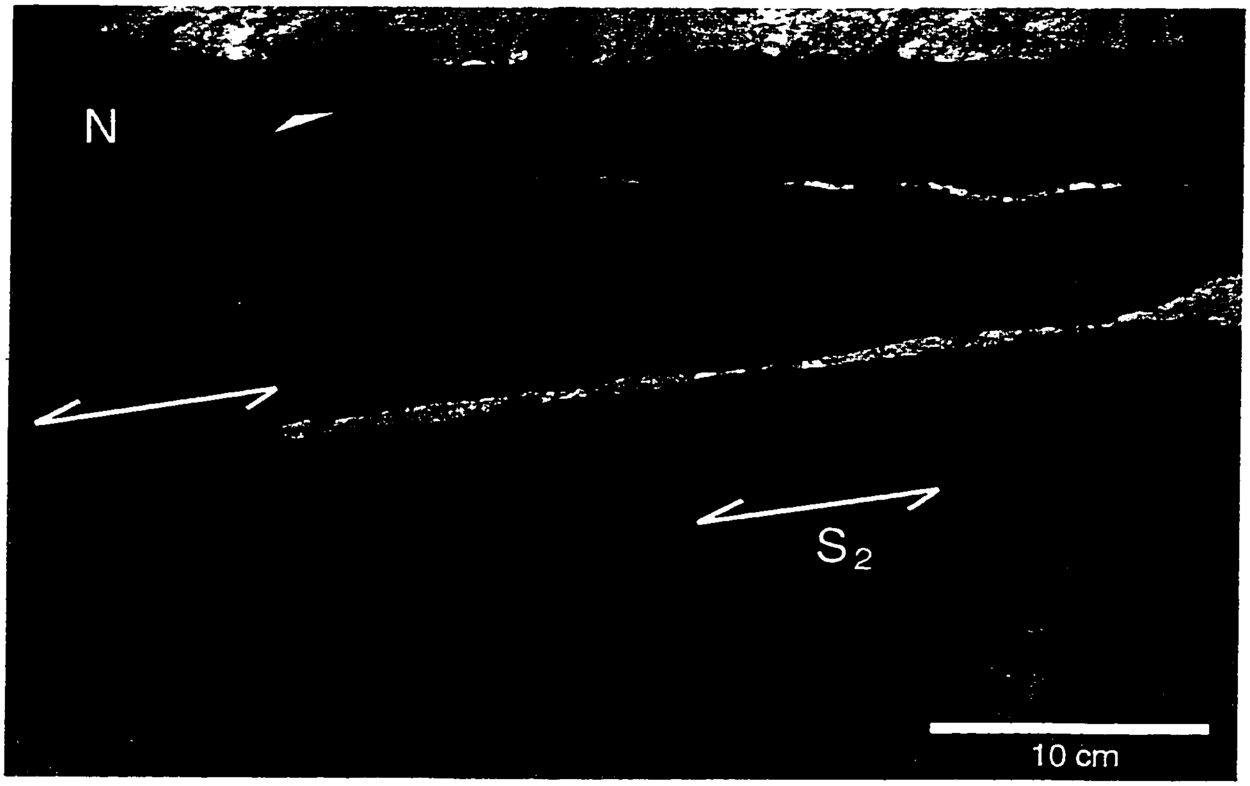

Fig. 6-6: Maps of the pegmatite dykes in the vicinity of the Sparrow Pluton (A) and Prosperous Pluton (B). Lower-hemisphere equal area projections are of the poles to the pegmatite dykes and are contoured at intervals of 3 sigma. Bedding traces in the country rocks are taken from Henderson (1985).

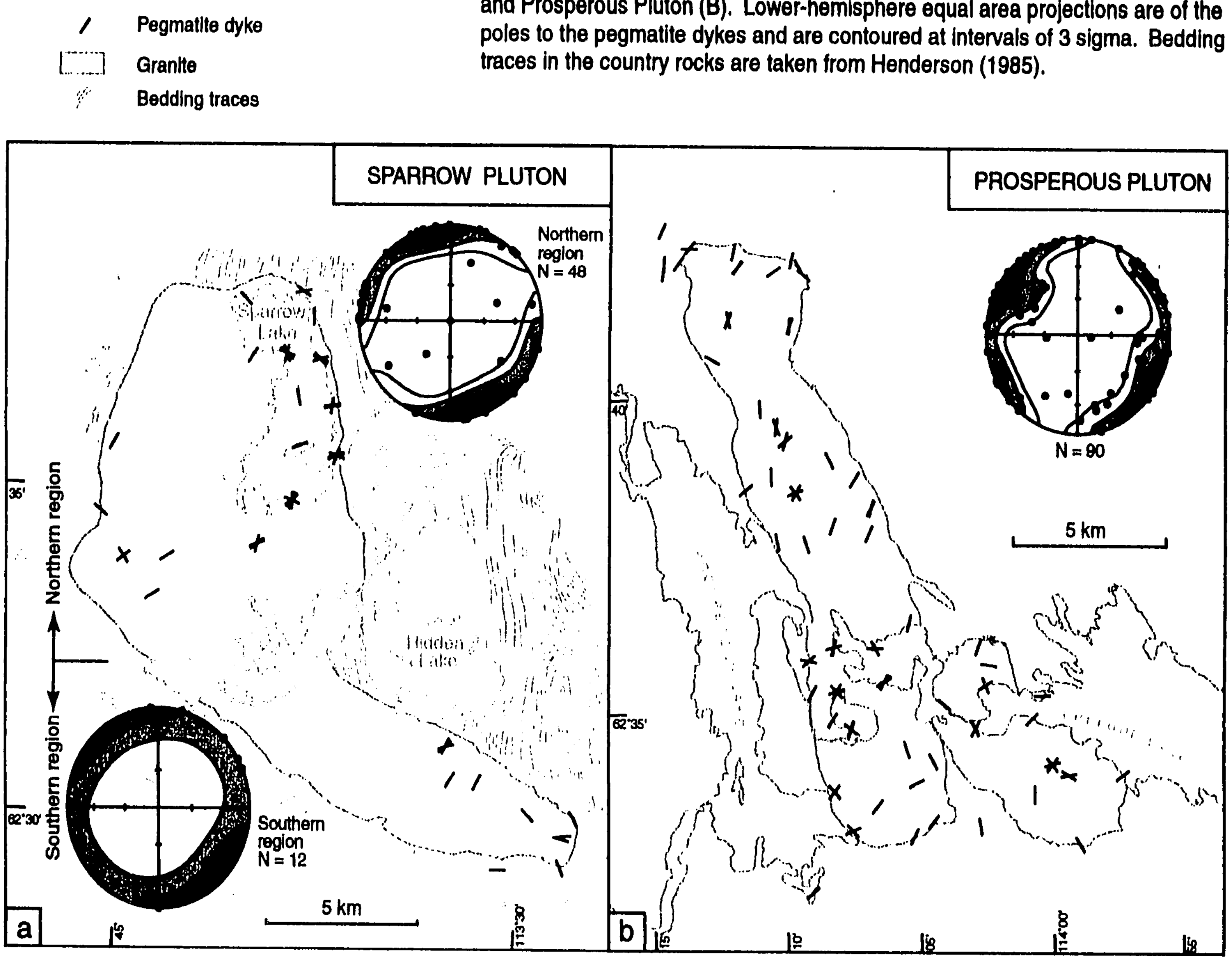

towards the center of the pluton. As with the Sparrow Pluton, the foliation is defined by biotite and slightly oblate quartz aggregates. The foliation strikes NNW-SSE, with moderate to steep dips, and is homogeneous at the outcrop scale (Fig. 6-1b). These orientations are concordant with the S_2 trajectories in the host rock.

Numerous pegmatite dykes cross-cut the granite and the surrounding country rocks. The dykes contain quartz, potassium feldspar, plagioclase, muscovite, with accessory tourmaline, and garnet. NE-SW orientations are dominant with a second set of dykes oriented approximately NW-SE (Fig. 6-6b). All dykes observed were steeply dipping. As near the Sparrow Pluton, folded pegmatite and granite dykes with fold axial surfaces parallel to the regional foliation where observed. In a few areas, such as to the east of the pluton, bedding parallel granite bodies were observed (Fig. 6-7).

Field observation of the exposed roof (Fig. 6-8a) and floor contacts (Fig. 6-8b) suggest that the pluton is tabular in shape. The floor of the pluton is exposed along the Ingraham Trail near Pontoon Lake, and dips 15^0 to the east (Fig. 6-8b). A magmatic layering and foliation parallel to the floor contact was also observed at this outcrop (Fig. 6-9). The roof, which is exposed on the north shore of Prelude Lake, 1.5 km east of the entrance to River Lake, dips to the east at 45^0 (Fig. 6-8a). By using trigonometry, the apparent thickness of the pluton (distance between the exposed floor and roof contacts) and the dip of the contacts, an approximate true thickness of 2 km for the pluton was obtained.

Fig. 6-7: Bedding parallel granite body (sill) in the Burwash Formation east of the Prosperous Pluton. Granite sill is 60 cm wide and dips to the east. Picture shows vertical section.

Fig. 6-8: Field photos showing the roof (A) and floor (B) contacts of the Prosperous Pluton.

A

B

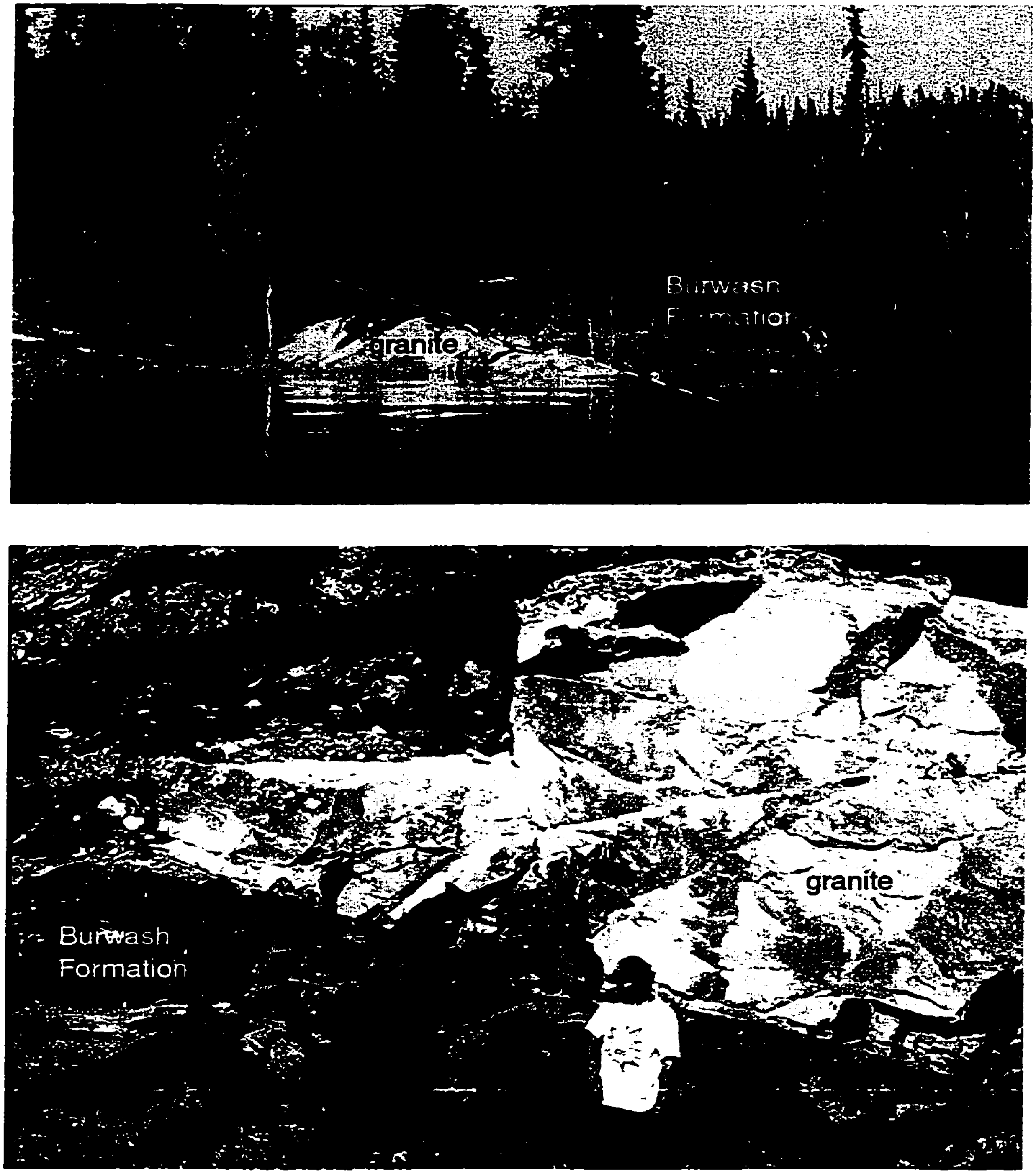

Fig. 6-9: Magmatic layering observed at the contact of the Prosperous Pluton near Pontoon Lake. A) Cartoon of layering observed. B) numbers refer to granite layers described in A. Both A and B are vertical sections looking north.

A

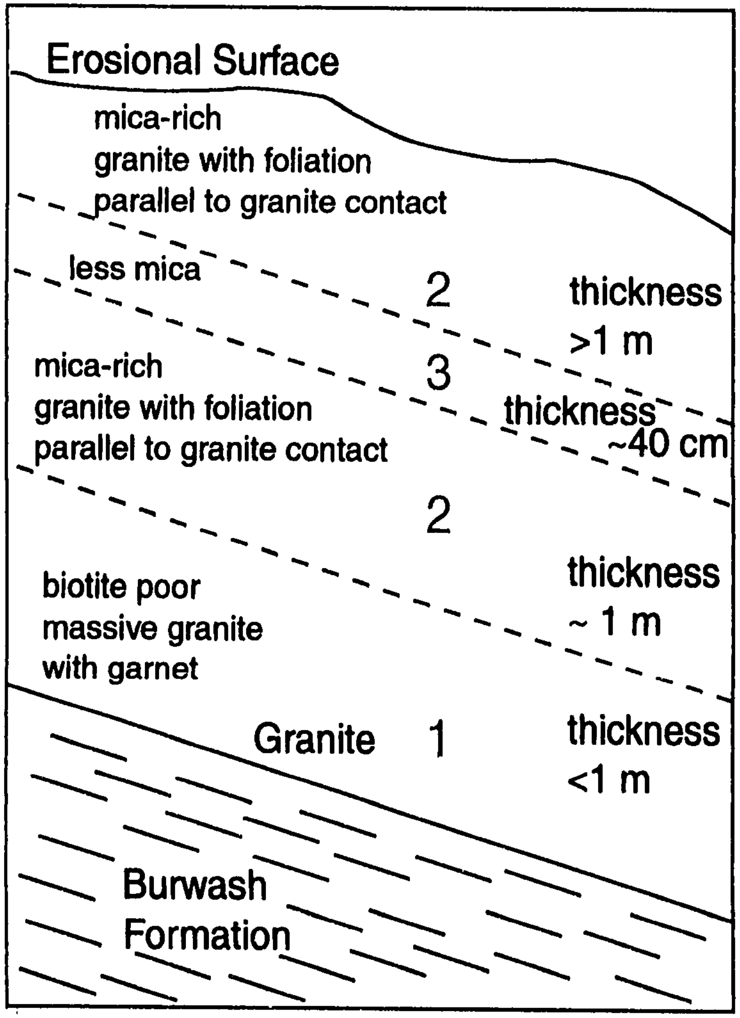

6.2 MICROSTRUCTURE

Thin sections of the granites were examined for minerals that would influence the AMS and for the degree of solid-state post-full crystallization (subsolidus) deformation. The microstructure results are given below (Fig. 6-10 shows the locations of the examples discussed below). The magnetic mineralogy is discussed in section 6.3.

Examination of thin sections made from the Prosperous and Sparrow plutons show that quartz, plagioclase, potassium feldspar, biotite, chlorite, and muscovite are common with apatite, garnet and tourmaline locally present. Quartz grains are anhedral with undulose extinction. Most quartz grains show subgrain development (Fig. 6-11) and minor recrystallization. In the southern "tail" of the Sparrow Pluton the quartz is largely recrystallized, especially near the pluton margins. Both plagioclase and potassium feldspar are dominantly anhedral to subhedral. The feldspars are locally altered to sericite (Fig. 6-12). Fractured and partially recrystallized feldspars are very rare (Fig. 6-13). Biotite commonly occurs as ragged laths (Fig. 6-14) and occasionally anhedral crystals that are partially altered to chlorite. Darker red-brown biotite crystals containing pleochroic halos, probably occurring around radioactive inclusions such as zircon, were also observed (Fig. 6-15). Muscovite is more common than biotite and appears as larger laths. Locally the phyllosilicates are bent and display undulose extinction (Fig. 6-16). Bent phyllosilicates are more common in the southern "tail" region of the Sparrow Pluton than in other areas of the Sparrow

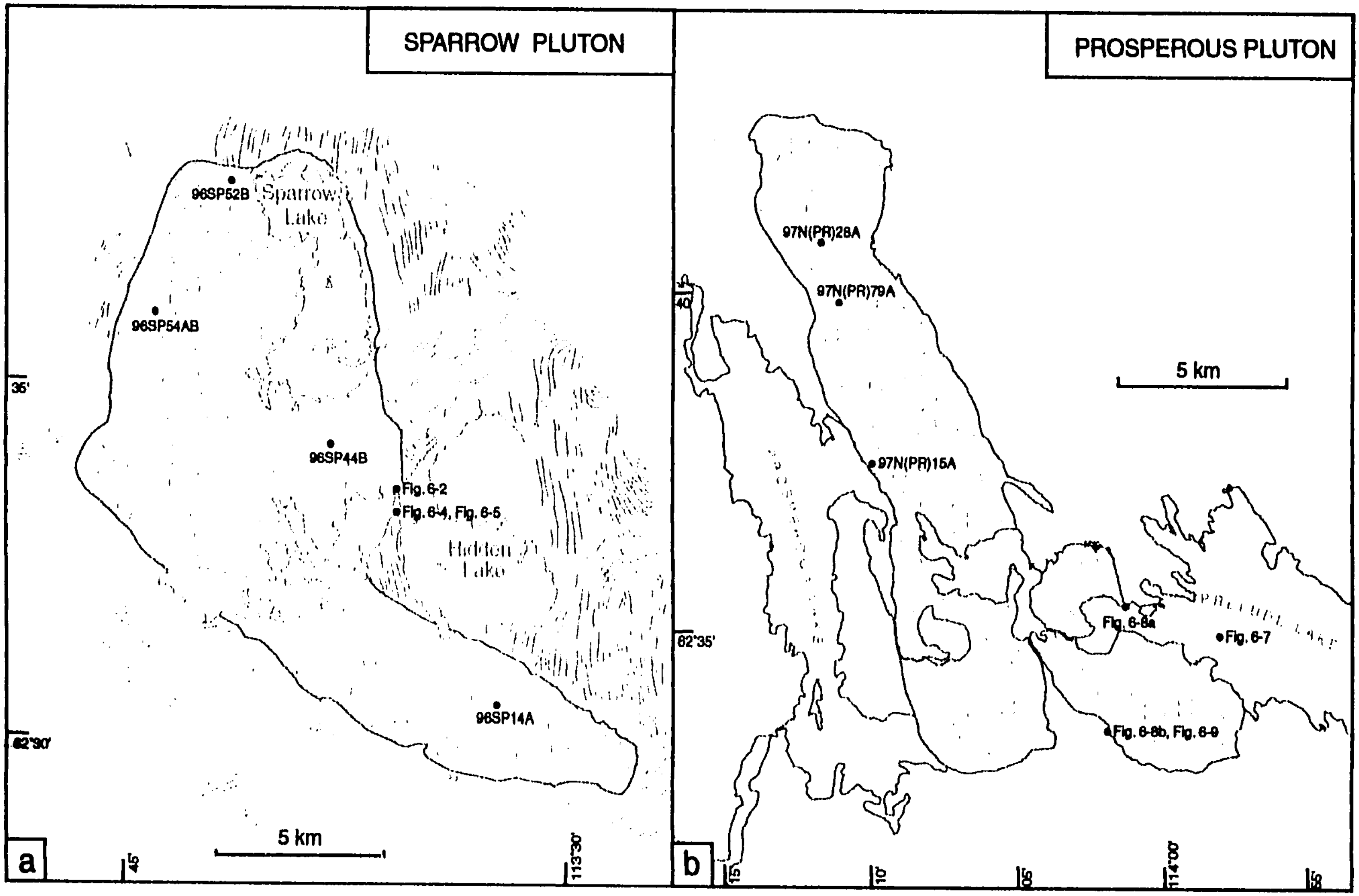

Fig. 6-10: Location maps for example thin sections and figures for the Sparrow Pluton (A) and the Prosperous Pluton (B). Bedding traces in the country rocks are taken from Henderson (1985). See Appendix II for all sample numbers and locations.

Fig. 6-11: Subgrain development in quartz (qtz). Sample number 96SP44B, crossed polars, Sparrow Pluton.

Fig. 6-12: Plagioclase (plag) crystal with sericite alteration. Sample number 97N(PR)28A, crossed polars, Prosperous Pluton.

Fig. 6-13: Arrow points to minor fracture in a plagioclase (plag) crystal. Potassium feldspar is indicated by kspar. Sample number 97N(PR)15A, crossed polars, Prosperous Pluton.

Fig. 6-14: Biotite (bio) partially altered to chlorite (chl). Sample number 96SP54AB, plane polarized light, Sparrow Pluton.

Fig. 6-11

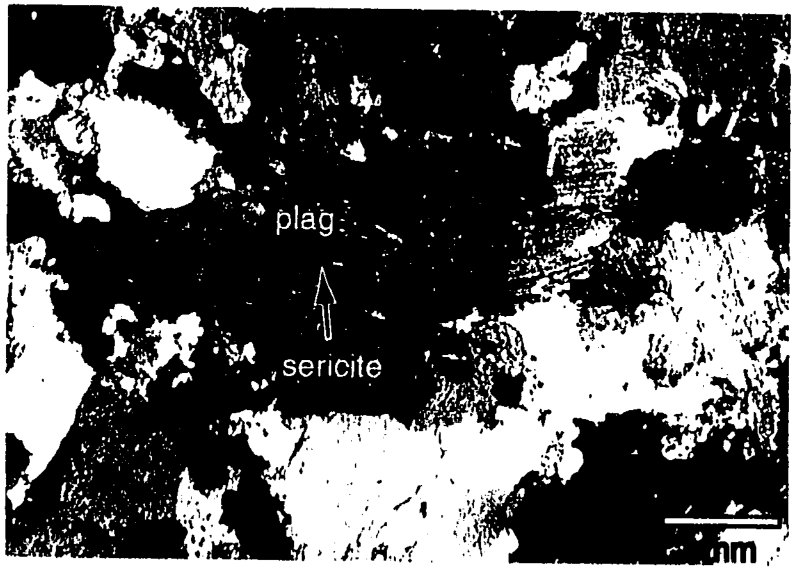

Fig. 6-12

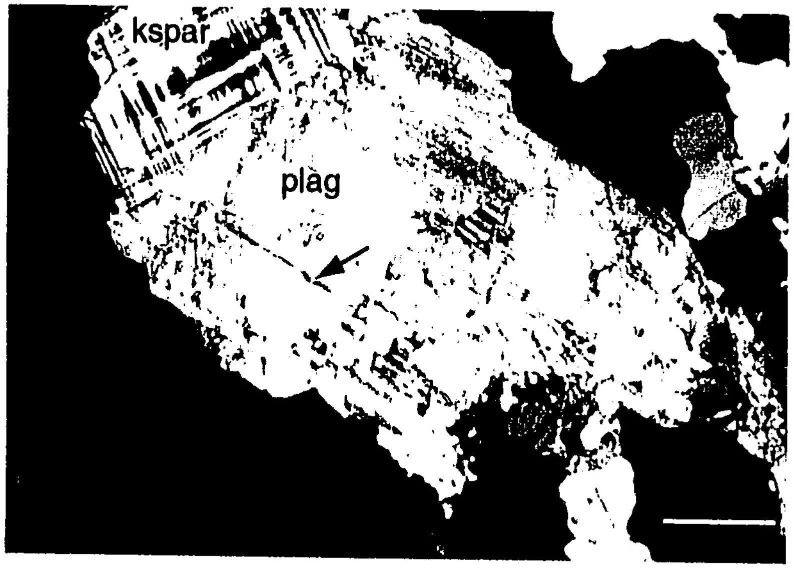

Fig. 6-13

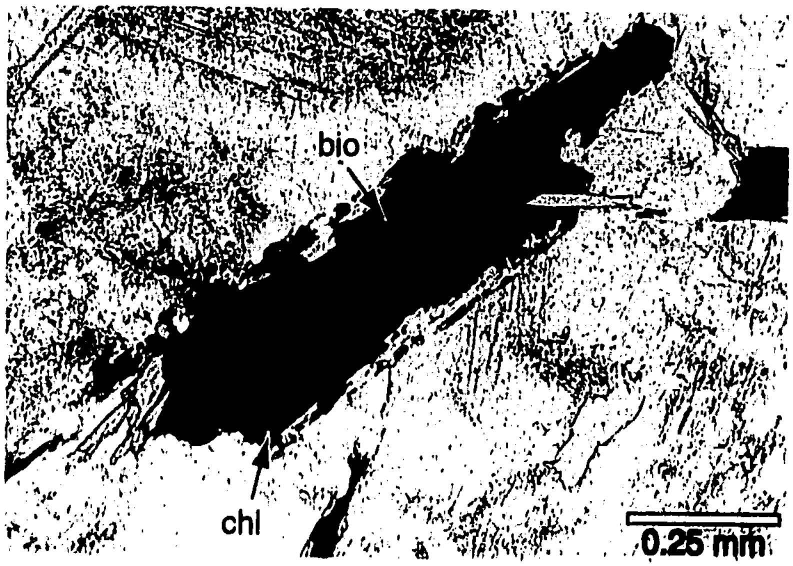

Fig. 6-14

Fig. 6-15: Biotite (bio) crystal with arrow pointing to a pleochroic halo possibly around zircon or allanite. Sample number 96SP14A, plane polarized light, Sparrow Pluton.

Fig. 6-16: Weakly bent muscovite (musc) crystal displaying undulose extinction. Sample number 96SP52B, crossed polars, Sparrow Pluton.

Fig. 6-17: Fractured garnet (gt) crystal. Sample number 97N(PR)79A, plane polarized light, Prosperous Pluton.

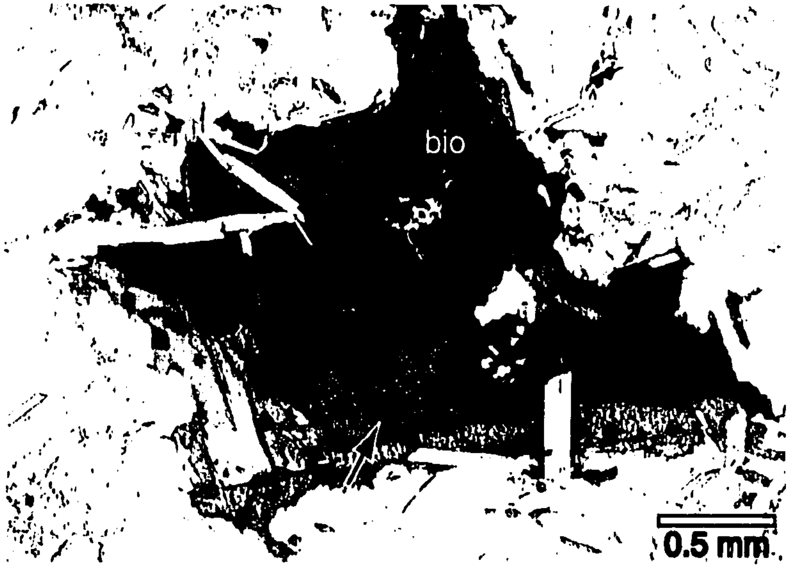

Fig. 6-15

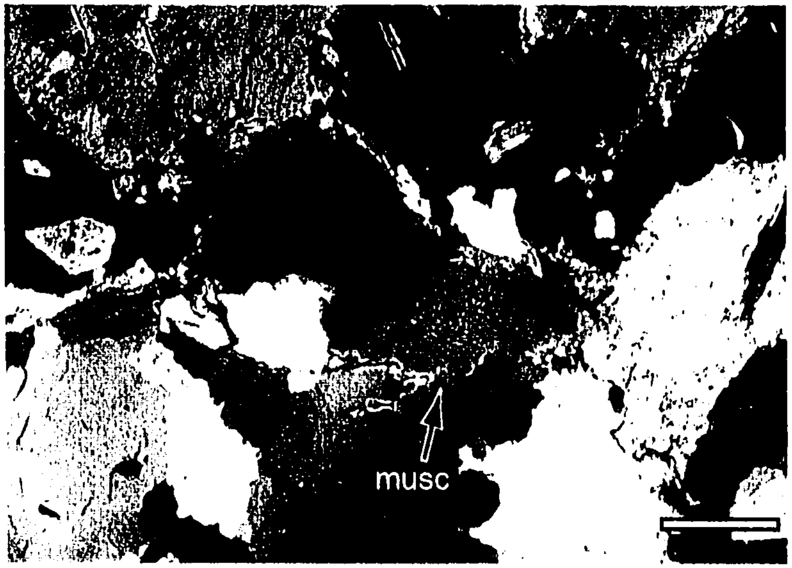

Fig. 6-16

Fig. 6-17

Pluton or Prosperous Pluton. Tourmaline and garnet are common near the pluton margins, with the rare garnet displaying fractures (Fig. 6-17).

It is interpreted that, outside of the small-scale greenschist facies shear zones, the granites have undergone only a minor but penetrative, high-temperature subsolidus deformation recorded by subgrain development in quartz. This suggests that the granites were still a crystal-mush when deformation was occurring. Grains were reoriented to parallel the S_2 foliation. As the granites cooled, deformation continued resulting in the recrystallized quartz and then strain was localized into the shear zones. Therefore, the foliation records a continuum in deformation from the magmatic state to high-temperature subsolidus conditions. In the northern, roughly rectangular region of the Sparrow Pluton and for the Prosperous Pluton the evidence of subsolidus deformation is restricted to subgrain development and minor recrystallization of quartz. In the southern "tail" of the Sparrow Pluton the quartz is largely recrystallized, especially near the pluton margins, and the homogeneous foliation is easily visible. Since the Sparrow and Prosperous plutons have undergone only minor subsolidus deformation, the fabrics mapped in the field and with the AMS technique are interpreted to represent magmatic to high temperature solid-state fabrics.

6.3 MAGNETIC MINERALOGY

As stated above, the granites contain biotite, chlorite, and muscovite, all of which contribute to the paramagnetic susceptibility. In the Sparrow Pluton, however, muscovite contains <2% FeO as opposed to biotite which contains > 22% FeO (Kretz et al., 1989b), so its contribution to the paramagnetic susceptibility is likely to be minor. Tourmaline is also present locally in the plutons forming polycrystalline clusters a few centimeters in diameter. Care was taken not to collect tourmaline-bearing samples since this mineral has an inverse intrinsic AMS (see section 4.3.1; Rochette et al., 1992). Examination of thin sections showed no coarse grained opaque minerals such as magnetite. This does not mean that very fine grained magnetite is not present as impurities in the iron-rich phyllosilicates (see below).

To determine the relative contributions to the bulk susceptibility (K) from the paramagnetic component and the ferromagnetic component, and to identify the magnetic mineralogy, a study of the hysteresis properties and coercivities of the granites was carried out (see section 4.4 for methodology). Measurements were performed by G. S. Pignotta (measurements done at the Rock Magnetics laboratory at Lakehead University with the permission of Dr. G. J. Borradaile) on samples from the Sparrow Pluton, and data reduction was done by K. Benn and G. S. Pignotta. Fields of up to 500 mT were used to saturate the ferromagnetic minerals. Coercivities (H_c) between 17.2 and 72.2 mT and coercivities of remanence (H_{cr}) between 34.1 and 71.1 mT were obtained. These values are comparable to those published for very fine-grained magnetite (Heider et al., 1987; Heider et al., 1996). To determine what type of magnetite is present the ratios of magnetization were plotted against the coercivity ratios in a plot modified from Day et al. (1977) with boundaries taken from Borradaile and Werner (1994) (Fig. 6-18a). The coercivities and the plot in Fig. 6-18a suggest that very fine-grained magnetite with possible pseudo-single domain behaviour is the predominant carrier of the K_{ferro} component in the measured samples. Comparison of the data in Fig. 6-18a with data published by O'Reilly (1984) suggests magnetite grain sizes of 1-10 μm. Results for all samples showed ferromagnetic contributions greater than 20% of their paramagnetic susceptibilities (Fig. 6-18b). Due to the similarities between the average susceptibilities for all specimens in the Sparrow (Fig. 6-18c) and the Prosperous (Fig. 6-18d) plutons, it is believed the above conclusions also apply to the Prosperous Pluton.

6.4 AMS

The magnetic foliation, magnetic lineation, magnetic susceptibility, anisotropy, and shapes of the AMS ellipsoids are discussed for both the Sparrow and Prosperous plutons.

6.4.1 Magnetic foliation and lineation

Sparrow Pluton

The magnetic foliation and lineation are plotted on maps in Figs 6-19a and 6-20a. Field measurements of the mesoscopic foliation in the pluton are plotted

Fig. 6-18: **A)** Ratios of magnetization plotted against coercivities. Mr is the maximum remanent magnetization; Ms stands for saturation magnetization; Hc and Hcr are the coercivity and the coercivities of remanence respectively. SD stands for single domain, PSD represents pseudo-single domain, MD corresponds to multi-domain. Diagram modified after Day et al. (1977) and Borradaile and Werner (1994). **B)** Plot of the ferro-magnetic and paramagnetic contributions to the susceptibilities. In A and B, filled circles correspond to sample 96SP60, and open circles are for sample 96SP49. **C)** K histograms for all specimens of the Sparrow Pluton. **D)** K histogram for all specimens of the Prosperous Pluton.

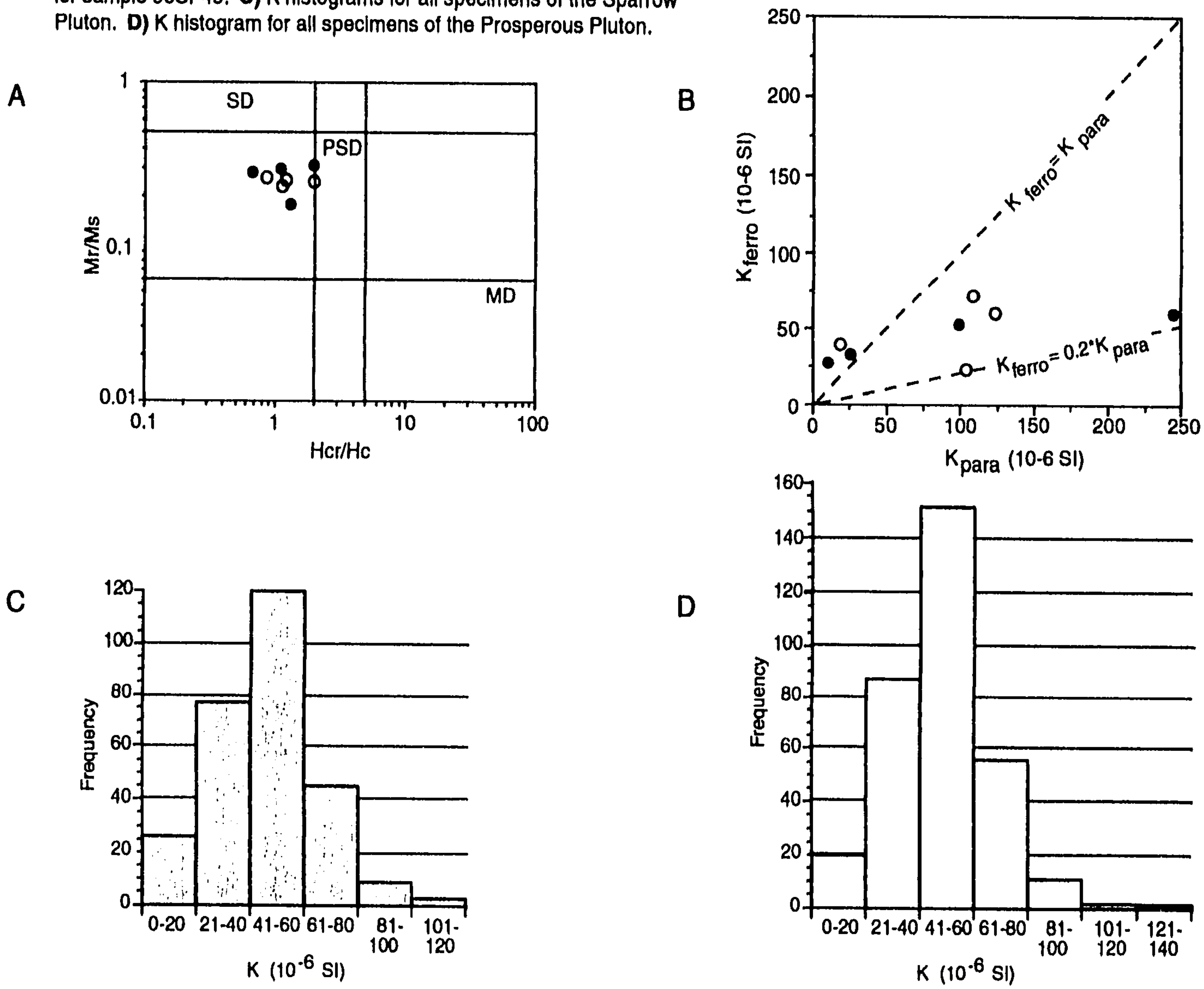

in Fig. 6-19b for comparison with the magnetic foliation. The orientation data for magnetic fabrics and field measurements are also plotted on lower-hemisphere Schmidt projections in Fig. 6-21a-f where the data are shown separately for the northern region and the southern tail region of the pluton. The magnetic fabric orientations (Figs 6-19a, 6-20a, and 6-21b, c, e, f) define very consistent patterns in both the northern and southern regions which can be directly compared to the orientations of the mesoscopic foliation measured in the granites and to the orientations of the D_2 in the country rocks.

In the northern region, the magnetic foliation strikes NNW-SSE and has variable but mostly steep dips (Figs 6-19a, 6-21b). In the southern region, the magnetic foliation is rotated in a counter-clockwise sense with respect to the fabrics in the northern region, striking NW-SE and dipping steeply at most outcrops (Figs 6-19a, 6-21e). The counter-clockwise rotation of the magnetic foliation in the southern region is coincident with the apparent sinistral deflection of the pluton's tail. The poles to the magnetic foliations in both the northern and southern regions (Fig. 6-21b, e) approximately lie on a great circle (great circle orientations are 253/83 for the northern region and 216/85 for the southern region; see Appendix III), suggesting that the foliation has been folded. The folds are near-cylindrical, close to open, and have sub-horizontal fold axes trending SE to SSE (fold axis for the northern region is 163/07 and 126/05 for the southern region; see Appendix III).

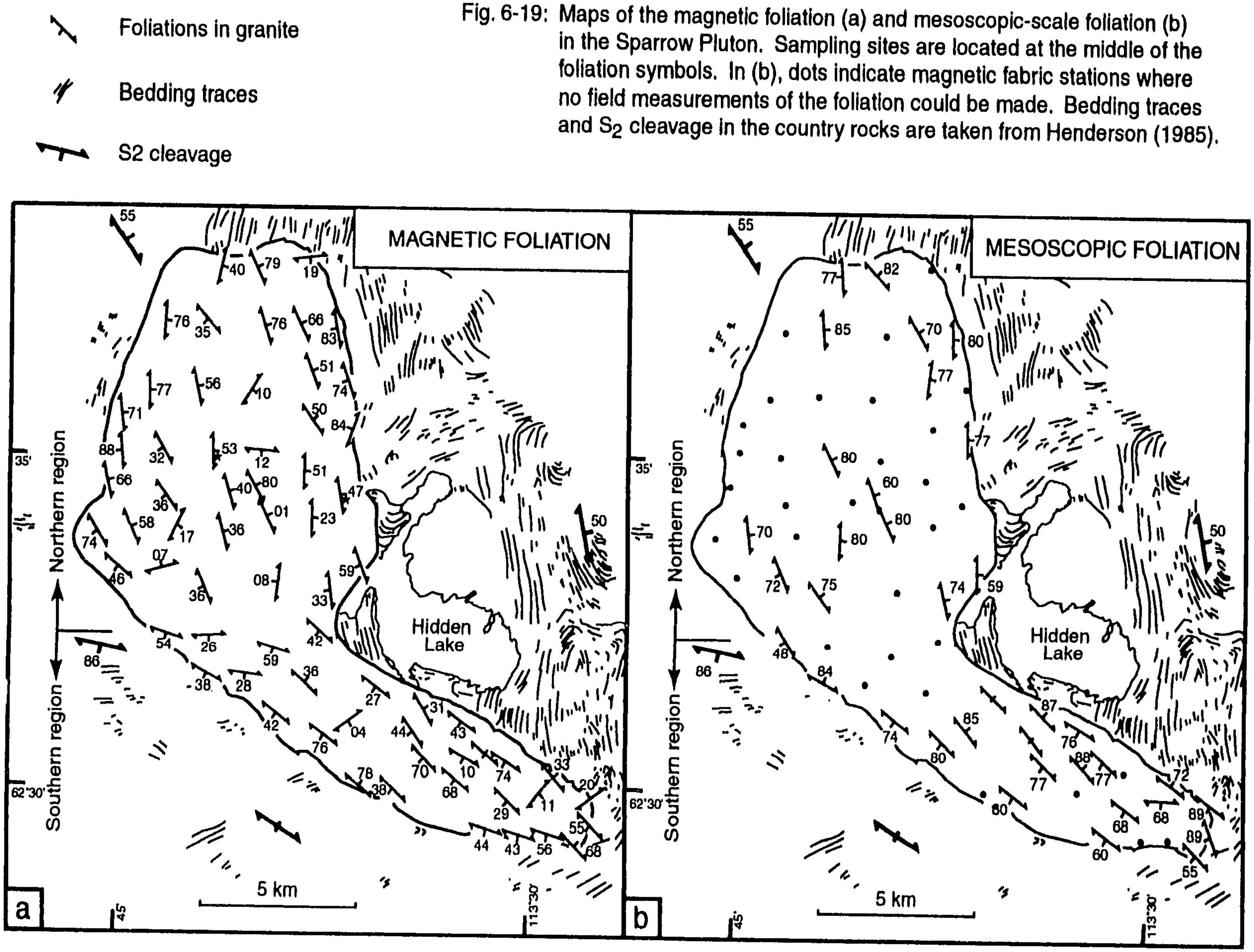

Fig. 6-19: Maps of the magnetic foliation (a) and mesoscopic-scale foliation (b) in the Sparrow Pluton. Sampling sites are located at the middle of the foliation symbols. In (b), dots indicate magnetic fabric stations where no field measurements of the foliation could be made. Bedding traces and S_2 cleavage in the country rocks are taken from Henderson (1985).

Lineations in granite

Bedding traces

Fig. 6-20: Maps of the magnetic lineation for the Sparrow Pluton (a) and for the Prosperous Pluton (b). Sampling sites are located at the base of the lineation symbols. Stars indicate probable anomalous magnetic lineations (see text). Bedding traces in the country rocks are taken from Henderson (1985).

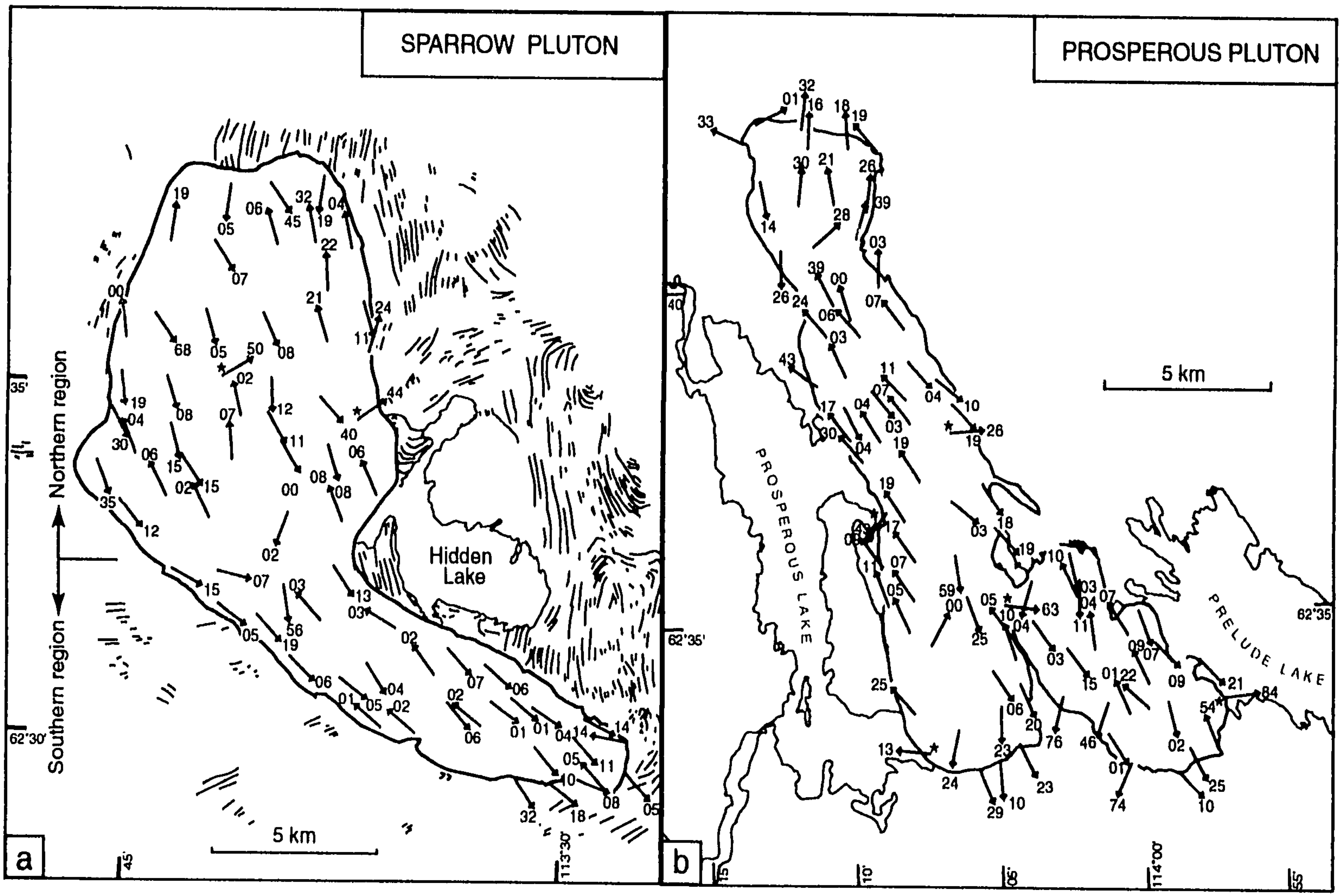

Fig. 6-21: Lower-hemisphere Schmidt projections for the Sparrow Pluton (a-f) and the Prosperous Pluton (g-i). Poles to field foliation are plotted in a, d, g. Poles to the magnetic foliation are plotted in b, e, h. Lineations are plotted in c, f, i. Contour intervals are 3 sigma.

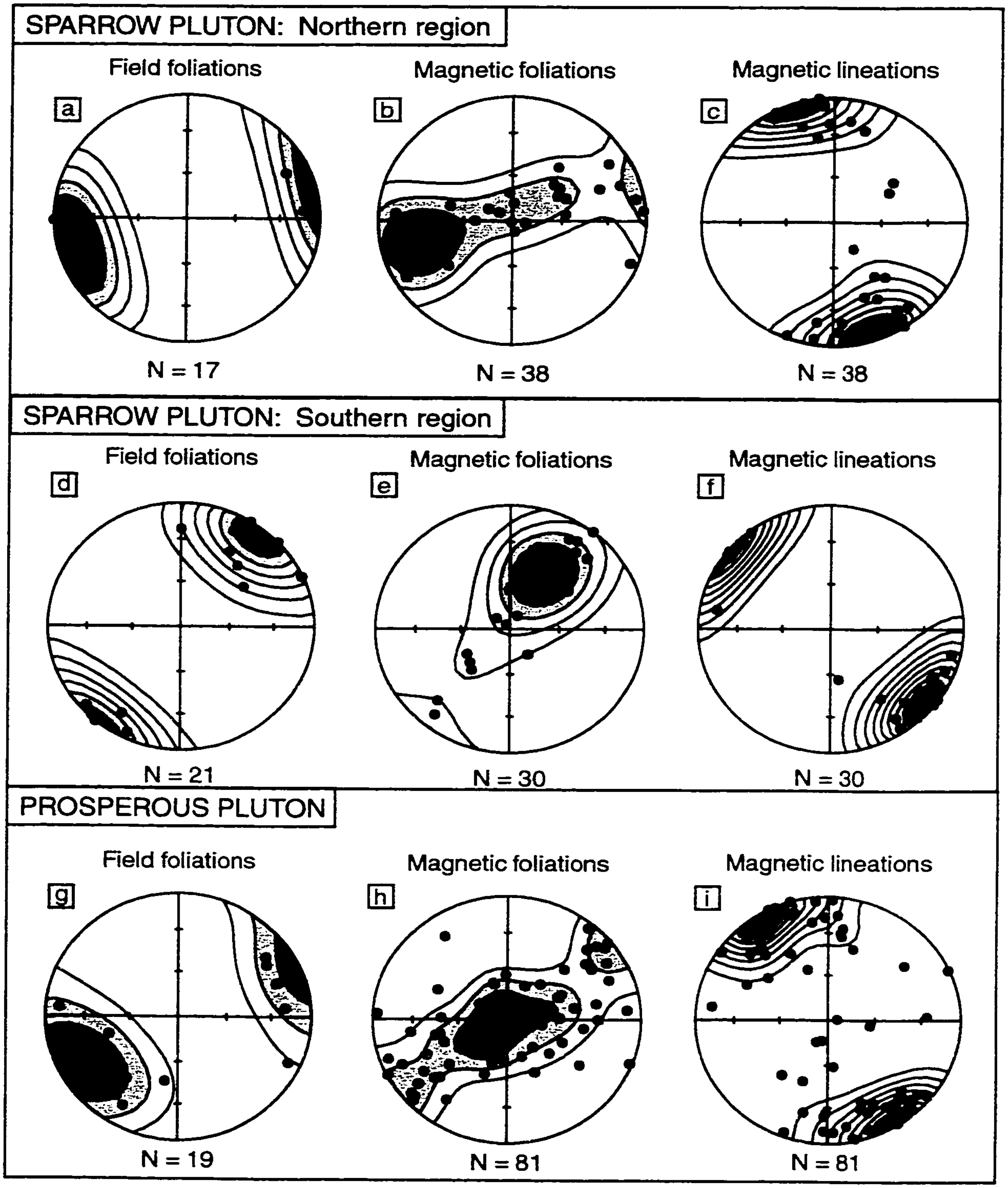

Comparison of the maps in Fig. 6-19 and the Schmidt projections in Figs 6-21a, b, d, and e, reveals that the magnetic foliation and the mesoscopic (biotite) foliation have very similar strikes at almost all of the sampled outcrops. This argues for a strong control of the biotite preferred orientation on the magnetic fabric. The dips of the magnetic and mesoscopic foliations differ significantly at some outcrops, and in a few cases shallowly dipping NE-SW striking magnetic foliations were measured at sites where field measurements indicate a more steeply dipping NW-SE striking mesoscale foliation. The more variable dips displayed by the magnetic foliations may result from the influence of fine-grained magnetite crystals on the AMS, causing the orientation of the magnetic fabric to deviate from the mesoscopic foliation. Alternatively, at some sampling sites the magnetic fabrics may provide a more precise determination of the fabric orientation than the field measurements, especially away from the pluton margins where the mesoscopic foliation is difficult to see, or very shallow dipping. Shallow to sub-horizontal foliations are more difficult to accurately measure in the field than steep foliations, so in this case the magnetic foliation may be more accurate.

In the northern and southern regions, the magnetic lineations have strong NNW-SSE and NW-SE trending and shallowly plunging preferred orientations. Since mesoscopic linear fabrics were not observed in the granites, it is not possible to make a direct comparison between the magnetic lineations and field measurements. In light of the influence of the biotite foliation on the magnetic fabric, the strongly oriented magnetic lineation is interpreted to be predominantly controlled by the biotite fabric at most sampling sites. Neither the presence of fine-grained magnetite, nor the local replacement of biotite by chlorite, seem to have a strong effect on the lineation orientations which are quite consistent (Figs 6-20a and 6-21c, f). Major contributions to the AMS from pseudo-single domain magnetite crystals would most likely cause an increased scatter in the lineation orientations and possibly flipping of the magnetic fabric axes (see section 4.3.1; Rochette et al., 1992). This is believed to be the case at the stations in Fig. 6-20 marked with stars, where magnetic lineations perpendicular to the dominant trend were measured.

Prosperous Pluton

The magnetic foliation and lineation are plotted on maps in Figs 6-22a and 6-20b. Field measurements of the mesoscopic foliation in the Prosperous Pluton are plotted in Fig. 6-22b for comparison with the magnetic foliation. The orientation data for magnetic fabrics and field measurements are also plotted on lower-hemisphere Schmidt projections in Fig. 6-21g, h. The magnetic fabric orientations (Figs 6-22a, 6-20b, and 6-21h, i) define very consistent patterns throughout the pluton and can be directly compared to the orientations of the mesoscopic foliation measured in the granites and to the orientations of D_2 in the country rocks.

Fig. 6-22: Maps of the magnetic foliation (a) and mesoscopic-scale foliation (b) in the Prosperous Pluton. Sampling sites are located at the middle of the foliation symbols. In (b), dots indicate magnetic fabric stations where no field measurements of the foliation could be made. S_2 cleavage in the country rocks are taken from Henderson (1985).

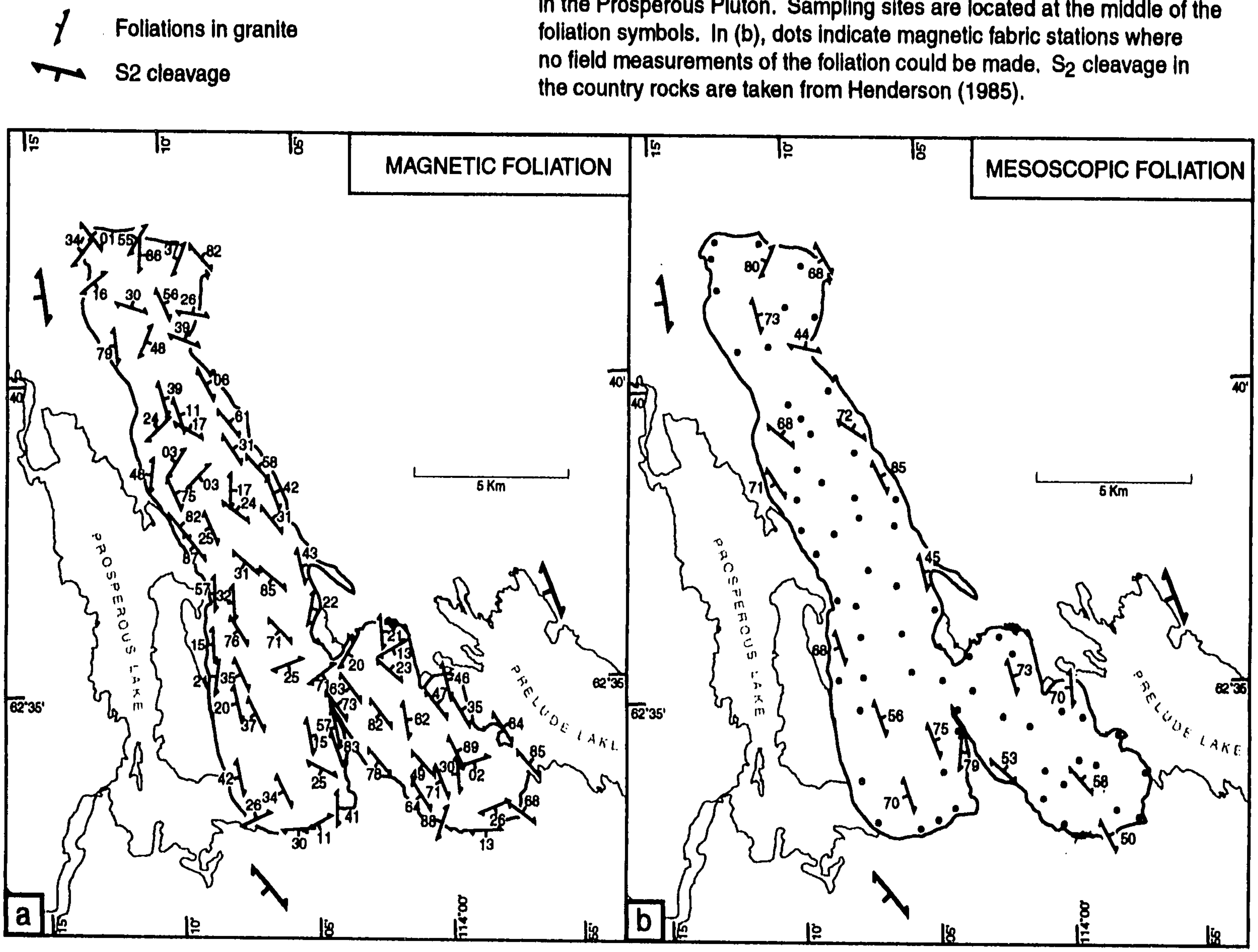

The magnetic foliation predominantly strikes NNW-SSE, though shallowly dipping foliations are common and strike more E-W. The map pattern of the magnetic foliations suggests D_2 deformation reworked an initially sub-horizontal magmatic foliation into steeper orientations. The poles to the magnetic foliations (Fig. 6-21h) approximately lie on a great circle (great circle orientation is 063/87; see Appendix III), suggesting that the foliation has been folded. The folds are near-cylindrical, open to close (with occasional gentle folds), and have sub-horizontal fold axes trending 333/03 (see Appendix III).

As in the Sparrow Pluton, comparison of the maps in Fig. 6-22 and the Schmidt projections in Fig. 6-21g, h, reveals that the magnetic foliation and the mesoscopic (biotite) foliation have very similar strikes at almost all of the sampled outcrops. This once again supports the interpretation that the biotite preferred orientation strongly controls the orientation of the magnetic fabrics.

The magnetic lineations have a consistent NNW-SSE trend and are shallowly plunging. It was not possible to measure the mesoscopic linear fabrics in the Prosperous Pluton, so a direct comparison between the magnetic lineations and field measurements is not possible. As in the Sparrow Pluton, the magnetic lineation is interpreted to be predominantly controlled by the biotite fabric at most sampling sites, and represents the zone axis of the biotite crystals. Stars beside lineations in Fig. 6-20b indicate sites where the presence of pseudo-single domain magnetite crystals may have resulted in a flipping of the magnetic fabric axes.

Fig. 6-23: K maps for the Sparrow Pluton (a) and for the Prosperous Pluton (b). Dots indicate sampling site locations. Bedding traces and S_2 cleavage in the country rocks are taken from Henderson (1985).

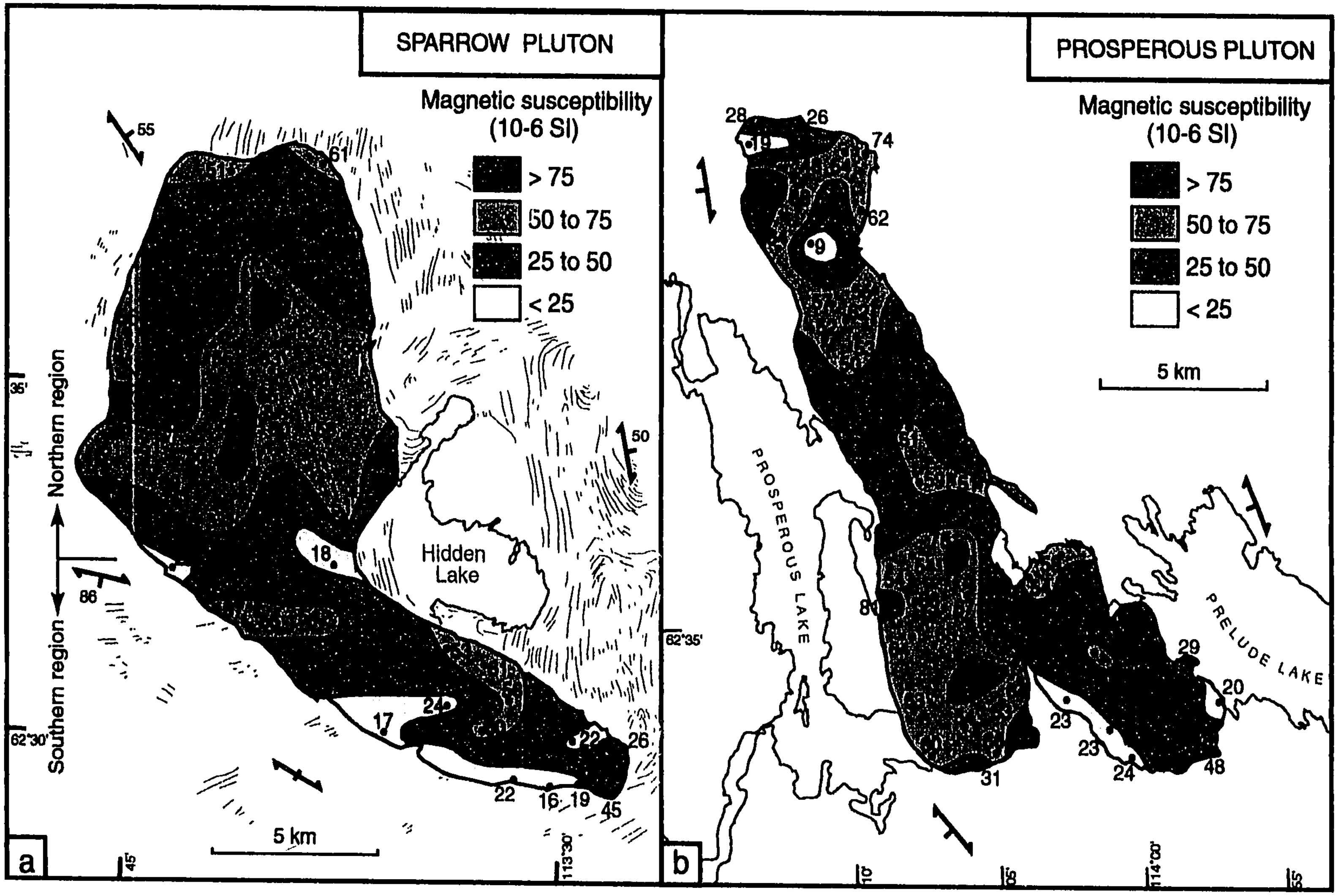

6.4.2 Magnetic susceptibility (K)

Sparrow Pluton

A contoured map of the site average magnetic susceptibilities is presented in Fig 6-23a. The values of K are low (< 120 X 10^{-6} SI, Fig 6-18c) and show only a small variation, with 87% of the samples having K values between 20 and 80 X 10^{-6} SI. Even with the small variations in K values a zonation pattern is recognized that suggests the presence of NNW to NW trending folds (Fig. 6-23a). This is most evident in the northern region, where the broad zone defined by 50 < K < 75 X 10^{-6} SI crosses the entire pluton and is highly discordant to the magnetic fabrics, defining an apparently doubly-plunging fold pattern. This interpretation is supported by the fact that the fold trends are parallel to the average foliation strikes, the magnetic lineation in the pluton, and to the regional D_2 structural trends in the host rocks. The interpretation implies that the K values in the northern part of the pluton define a thin and possibly initially horizontal zonation which may be of magmatic or deuteric origin (see below for a discussion on the possible origins of zonation), which was folded as D_2 deformation continued. In the southern region, several narrower zones are discordant to the magnetic fabric trajectories and may also be folded with an axial surface trace that is parallel to the NW trending magnetic fabrics.

Prosperous Pluton

The K values are low (< 140 X 10^{-6} SI, Fig. 6-18d), showing minimal variation, with 90% of the samples having K values between 20 and 80 X 10^{-6} SI. The K map of the Prosperous Pluton is shown in Fig. 6-23b. Comparison of the magnetic foliation patterns in the two plutons also suggests that the Prosperous Pluton has undergone less folding than the Sparrow Pluton. Both plutons contain NW-SE (approximate) magnetic foliations with moderate to steep dips. In the Prosperous Pluton there are also foliations striking E-W that have shallow dips. It is this change in the attitude of the magnetic foliation in the Prosperous Pluton that suggests a folded geometry. The continuation of deformation would result in steeper dips and the obliteration of the shallow E-W foliations resulting in a pattern similar to that seen in the Sparrow Pluton. Based on the interpretation that the Prosperous Pluton is less folded than the Sparrow Pluton, it is proposed that the pattern seen in Fig. 6-23b is probably the result of a gently folded zonation (similar to the Sparrow Pluton) intersecting a surface that has minimal relief and is approximately parallel to the zonation.

Possible Origins of Zonation

In rocks where the susceptibility is dominated by paramagnetic minerals, the magnetic susceptibility (K) can be used as a petrographic mapping tool. This is possible since K values are a linear function of the iron content in the paramagnetic minerals (Gleizes et al., 1993). The presence of magnetite has the effect of greatly increasing the susceptibility. The magnetite present in the

Prosperous and Sparrow plutons is interpreted to be pseudo-single domain magnetite 1-10 μm in size.

Magnetite may be present as impurities in chlorite, muscovite, or biotite, or as the result of alteration (Tarling and Hrouda, 1993). Ferromagnetic minerals, such as hematite, maghematite, magnetite or goethite, may form under diagenetic to low grade metamorphic conditions (Tarling and Hrouda, 1993). The breakdown of iron-bearing paramagnetic minerals under natural conditions will often result in crystalline orientations that mimic the fabric of the host paramagnetic mineral (Tarling and Hrouda, 1993).

It is proposed that the zonation seen in Fig. 6-23 is the result of varying amounts of biotite present in the granite and very fine grained inclusions of magnetite present in the biotite. Whether the magnetite is of magmatic or deuteric origin is unknown, but the preceding paragraph suggests that the magnetite is associated with the biotite. Fig. 6-9 shows mica rich and mica poor magmatic layers visible in the Prosperous Pluton. This layering is parallel to the basal contact of the pluton. These observations support the interpretation that the zonation visible in Fig. 6-23 is the result of thin horizontal layers, formed during pluton emplacement, that have been subsequently folded.

6.4.3 Anisotropies and shapes of the AMS ellipsoids

Sparrow Pluton

The contoured map of P'% is shown in Fig. 6-24a, where it can be seen that

Fig. 6-24: P'% maps for the Sparrow Pluton (a) and for the Prosperous Pluton (b). Dots indicate sampling site locations. Bedding traces and S_2 cleavage in the country rocks are taken from Henderson (1985).

S2 cleavage

Bedding traces

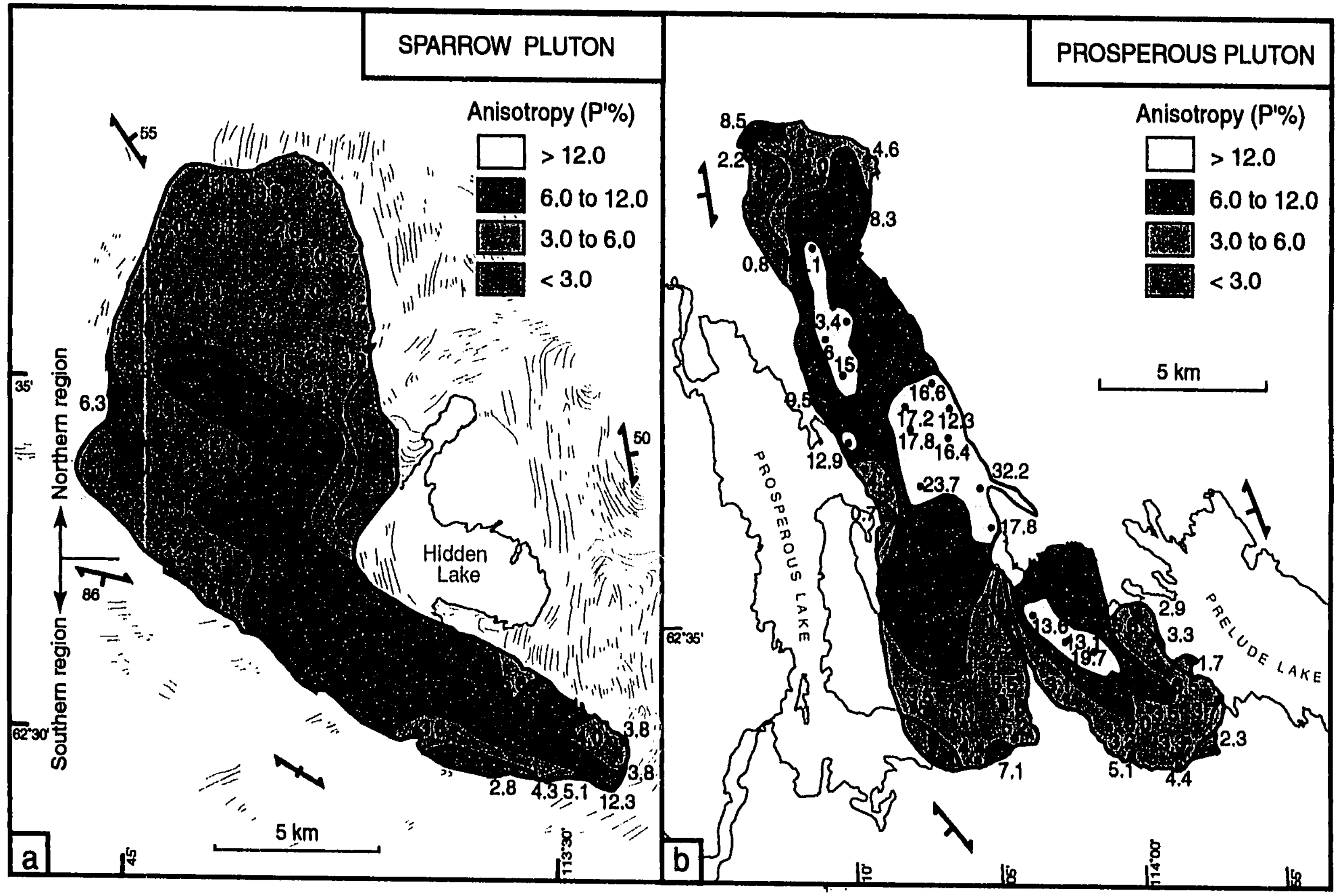

values range from 1.7 to 12.3. The southern tail of the pluton is characterized by P'% values mostly > 6, which extend into the core of the northern region (Fig. 6-24a). The concentration of stronger anisotropies, suggesting a higher degree of crystal alignment, along the pluton axis in the northern region and in part of the southern tail, is opposite to the fabric patterns documented for plutons emplaced by in-situ expansion, where degree of crystal alignment increase towards the pluton margins (e.g. Ramsay, 1989). The higher degree of crystal alignment may be due to deformation having been concentrated within the lower-viscosity, and still largely magmatic central parts of the pluton, as solidification of the granites proceeded inwards from the margins. Such a pattern of apparent strain concentration is in agreement with predictions based on thermal models of syntectonic intrusive sheets and their wall rocks (Pavlis, 1996) and is interpreted to be further evidence for syntectonic emplacement of the Sparrow Pluton.

The shapes of the AMS ellipsoids also show a wide variation from very oblate to very prolate. The T values define a recognizable map pattern (Fig. 6-25a) with oblate ellipsoids (T>0) concentrated in roughly northwest-southeast trending corridors (the horseshoe shaped zone of oblate fabrics in the northern region closes at a site where T = 0.08, i.e. where the AMS has a nearly neutral shape). This orientation is nearly parallel to the magnetic fabric in the pluton and to the S_2 trajectories in the country rocks, suggesting that the shape of the AMS ellipsoid in the Sparrow Pluton is related to D_2 tectonic strain field. The significance of the distribution of T values cannot be easily interpreted in terms

Fig. 6-25: T maps for the Sparrow Pluton (a) and for the Prosperous Pluton (b). Dots indicate sampling site locations. Bedding traces and S_2 cleavage in the country rocks are taken from Henderson (1985).

S2 cleavage

Bedding traces

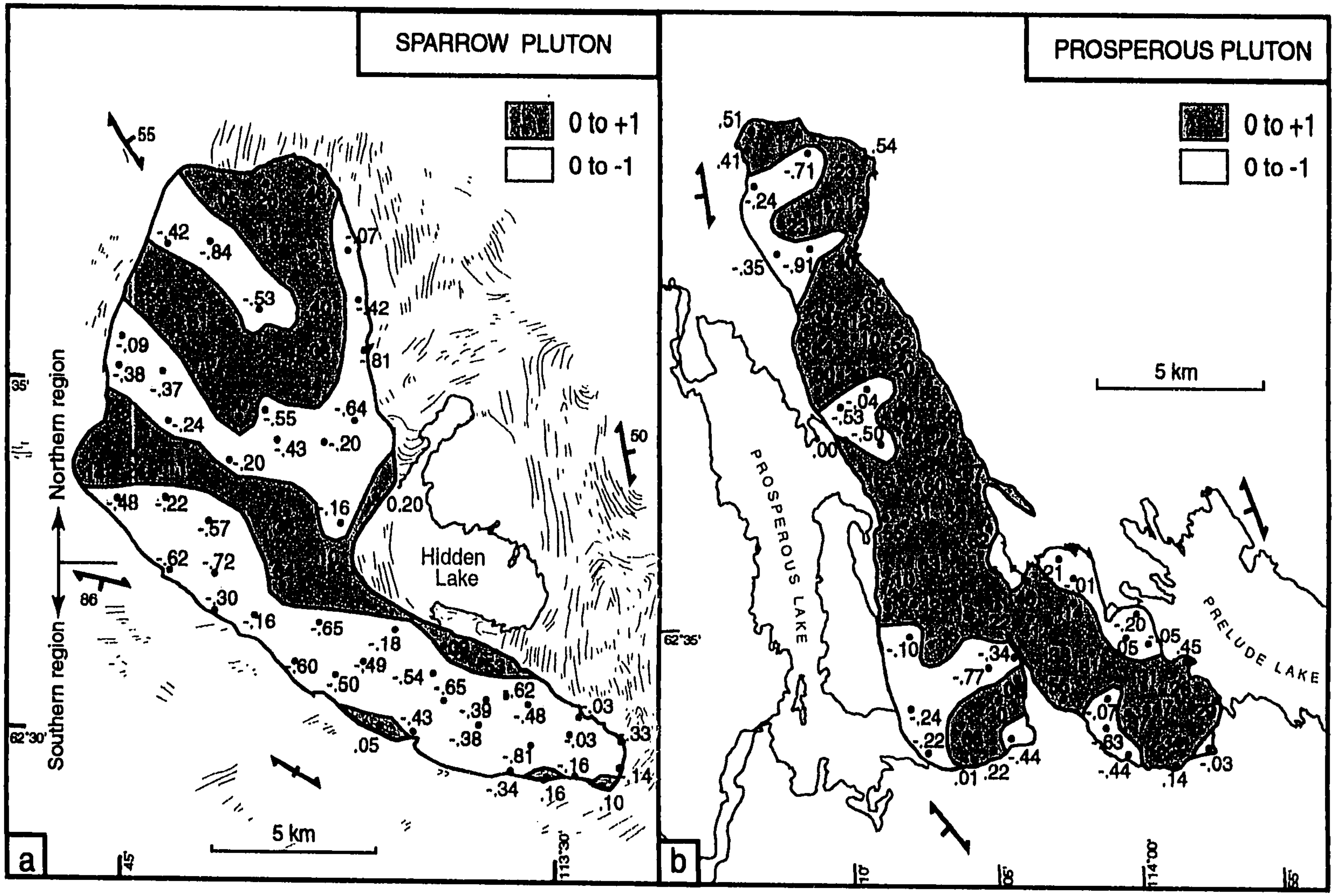

of relative magnitudes of finite strain since the magnetic fabric shapes may follow complicated paths during emplacement and crystallization of syntectonic plutons (Benn, 1994). It should also be noted that traces of secondary ferromagnetic minerals (such as magnetite) may significantly affect T and P'% without noticeably modifying the orientation of the magnetic fabric (Borradaile and Werner, 1994; Borradaile and Henry, 1997). However, the map pattern of T values provides further evidence for D_2 tectonic deformation of the Sparrow Pluton.

Prosperous Pluton

P'% and T maps are shown in Fig. 6-24b and 6-25b. The P'% map shows the strongest anisotropies tend to be localized along the center of the pluton, as in the Sparrow Pluton, although the P'% values tend to be higher in the Prosperous Pluton. The T map is contoured to show the different regions corresponding to oblate and prolate AMS ellipsoids, and unlike in the Sparrow Pluton, no pattern is evident.

Chapter 7: Discussion and Conclusions

Chapter 7 discusses the timing of pluton emplacement (section 7.1), comments briefly on the significance of the magnetic lineations in relation to the regional strain field (section 7.2), discusses emplacement models and presents a probable mode of emplacement for the Prosperous Suite (section 7.3). This chapter also suggests areas for further study (section 7.4), and gives the conclusions of this study (section 7.5)

7.1 TIMING OF PLUTON EMPLACEMENT

Field and microstructural observations, as well as AMS results support the conclusions that the plutons are syn-D_2 and were possibly emplaced during early D_2. A summary of the evidence in each category, followed by interpretation is given below.

7.1.1 Field Evidence

1) A locally developed foliation in the pluton, defined by biotite and by slightly oblate quartz aggregates, is homogeneous at the outcrop scale and is interpreted to records magmatic to subsolidus deformation of the pluton. The strike of the foliation is similar to that of the S_2 cleavage in the country rocks. Later, D_2 deformation of the pluton was concentrated into decimeter-scale shear zones interpreted to have formed as the pluton cooled to greenschist facies conditions.

2) Folded granitic and pegmatitic dykes within the country rocks have axial surfaces parallel to the regional foliation, whereas dykes emplaced along the S_2 foliation plane show pinching and swelling. Therefore, emplacement was still occurring after S_2 formed so that dykes could be emplaced along the S_2 foliation plane. Pinching and swelling of the dykes suggests that D_2 continued after these dykes were emplaced. This is further supported by the presence of the folded dykes with axial surfaces parallel to the regional S_2 foliation.

7.1.2 Microstructural Evidence

1) Probable S_1 fabrics are preserved as inclusion trails in porphyroblasts that are likely the result of contact metamorphism of the Prosperous and Sparrow Plutons since cordierite, staurolite, andalusite, and garnet are concentrated near the plutons (Fig, 5-1).

2) In the thin sections examined, the inclusion trails were rarely crenulated. It is therefore possible that pluton emplacement and porphyroblast formation occurs early during D_2 before the S_2 fabric had time to develop. Deformation continued during emplacement since granite is also injected along S_2 (see above).

3) There is no correlation between the apparent degree of subsolidus strain of the granites (as determined qualitatively by microstructural study) and the strength or the orientation of the AMS. The AMS values correspond to features that are presently preserved in the rock. If for example thin sections display

subsolidus strain, and increasing degrees of subsolidus strain corresponds to higher P values (which are an estimate of the degree of crystal alignment), so the AMS value is reflecting a feature formed after the granite cooled. Since there is no correlation in this study, the AMS results are reflecting features, such as the alignment of crystals, before the granite cooled. Therefore the AMS data represents fabrics which were present when the pluton was emplaced. This indicates that much of the D_2 tectonic deformation of the Sparrow and Prosperous plutons, as revealed by the magnetic data, occurred during crystallization.

7.1.3 AMS Evidence

1) The zonation of the Sparrow Pluton, revealed by mapping of the magnetic susceptibility, suggests the presence of a horizontal zonation that was folded. The fold axis is parallel to S_2.

2) The similarity of the structural patterns defined by the zonation in the Sparrow Pluton and by the magnetic fabrics in both plutons indicates fabric development occurred during D_2 deformation.

3) In the Sparrow Pluton the magnetic lineations are parallel to the axis of folding of the zonation, and the lineations are therefore a purely D_2 tectonic fabric element. They cannot unequivocally indicate the direction of magma flow during emplacement, but they are excellent indicators that emplacement and fabric development occurred during D_2.

7.2 COMMENTS ON THE REGIONAL STRAIN FIELD

In regions with complex deformation histories, such as the southern Slave Province, the internal fabrics of granite plutons can preserve a record of the strain field, and kinematics associated with the synmagmatic tectonic event. Benn (1994) has shown that magnetic lineations in granites that are associated with flow during emplacement can be overprinted by as little as 10% strain. Judging by the fold pattern in the Sparrow Pluton, and by the strength of the magnetic fabrics in both plutons, it is likely that the tectonic deformation of the magmas was strong enough to result in a predominantly tectonic fabric signature. In this case, the magnetic lineation should be close to the maximum principal finite stretch in the plutons (Benn, 1994). The magnetic lineations are sub-horizontal and trend NNW-SSE to NW-SE, suggesting NNW-SSE to NW-SE extension of the magma. In the absence of regional extension lineations in the Burwash Formation, the magnetic lineations in the plutons provide good indicators of the strong component of horizontal stretching associated with D_2 transpression, as called for by Bleeker et al.'s (1997a) tectonic model. Other peraluminous granite plutons emplaced within Phanerozoic transpressional belts have also revealed magnetic lineations that are parallel to extensively developed extension lineations in the country rocks (e.g. the Hercynian Trois-Seigneurs granodiorite in the French Pyrenees (Leblanc et al., 1996), and the Devonian South Mountain Batholith in the Meguma Terrane, Nova Scotia, (Benn et al., 1997). The stretching nature of the magnetic lineation is further supported by the fact that the lineations are perpendicular to the dominant set of pegmatite dykes (Bouillin et al. (1993) also noted this relationship), which are perpendicular to the long axes of the plutons, and interpreted to be emplaced in mode I factures. The second set of pegmatite dykes which parallel the pluton long axes are interpreted to be small scale fractures associated with more extensive fracture systems (such as those proposed by Fyson (1990) to explain the rectilinear map pattern of volcanic belts in the Slave Province). These fractures may have formed during D_2, or they may represent preexisting fractures that were reactivated during D_2. It is proposed that ENE-WSW to NE-SW bulk shortening occurred and resulted in the observed folding of both the zonation in the Sparrow Pluton and the foliation in the Prosperous Pluton.

7.3 ASCENT AND EMPLACEMENT MODELS

7.3.1. Ascent mechanisms

The ascent of magmas is primarily controlled by density and viscosity contrasts between the magma and its surrounding rocks. Usually a low-density, low-viscosity partially melted zone is overlain by cooler, high-density, high-viscosity crustal rock. This gravitationally unstable situation results in the mechanical rise of the magma. The upward force acting on the magma due to the density contrast is known as buoyancy. The magma will continue to rise until neutral buoyancy is achieved. As the magma is rising, viscous drag induces internal circulation (Schmeling et al., 1988).

Although density-contrast driven buoyancy is probably the main force behind rising magma, it is not the only proposed force. Confining pressure, or hydrostatic pressure, of the weight of a column of the melt reaching from the source up to the Earth's surface is also likely to play a role (Hutton, 1997). Volume change caused by melting can also generate a small overpressure which may be important in initiating fractures around the source (Petford, 1996).

Currently, there are two main competing end-member models for the ascent of magma between its generation level and its emplacement level. The first is diapirism and the second is ascent through dykes by fracture exploitation.

Diapiric ascent occurs when the country rocks and the pluton exchange places by flowage in opposite directions. The term diapir is often used when referring to a circular or ovoid-shaped pluton in plan view for which the ascent process was diapirism. During diapiric ascent, the surrounding rocks are deformed by viscous flow and may be forcibly shouldered aside or upward. Evidence in the field may be seen as deflection of structures (bedding, foliation, lineation) and varying styles of deformation in the host rocks (Schmeling et al., 1988). Upward movement of a diapir would also result in a strain history of heterogeneous simple shear (Bateman, 1985). However, due to the nature of this model, diapiric ascent is limited to the lower part of the crust because of the exponential increase in viscosity with decreasing depth (Clemens, 1998).

In contrast, fracture exploitation occurs when the magma flows through fractures in elastic/brittle rock. This mechanism is also often referred to as dyking. Bateman (1985) concluded that granitoid magmas commonly ascend as low-strength crystal mushes, probably along fracture and dyke systems. Modelling shows that dyke ascent is both rapid and thermally efficient (Clemens, 1998). Also, although this model accepts the possibility of flowing through pre-existing fractures, kinematic analysis of the model also show that fracture propagation is commonly catastrophic. This suggests that dykes will be self-propagating as long as they contain buoyant magma (Clemens and Mawer, 1992).

Although there is still controversy over which model is more generally applicable, an increasing number of authors seem to believe that the dominant mechanism is through fractures exploitation (Petford et al, 1994; Emerman and Marrett, 1990; Clemens and Mawer, 1992). Clemens (1998) states that there is an absence of field evidence supporting diapiric ascent and suggests that dyking is a more probable model. Alternatively, some authors believe that diapiric ascent occurs in the lower to middle crust, but the mechanism eventually transforms into fracture exploitation by the time the upper crust is reached (Brun et al., 1990; Weinberg, 1996). Magma ascent might therefore be a complex combination of the two models (Brun et al., 1990; W einberg, 1996).

The ascent rate of the melt can be approximated using Stoke's Law. The exact formula will vary according to the ascent model used. For a diapiric ascent model,

$$V = 2\Delta pgr^2 / 9\eta_{wr}$$

where V is the terminal velocity, Δp is the difference between the wall-rock density and the melt density, g is the acceleration due to gravity, r is the radius of the magmatic sphere and η_{wr} is the wall-rock viscosity. The critical parameter for the diapiric ascent model is the wall-rock viscosity (Brown and Solar, 1998).

The formula to calculate the ascent rate in a dyke is expressed as

$$V = \Delta pgw^2 / 12\eta_m$$

where w is the width of the dyke and η_m is the viscosity of the magma. In the case of a fracture exploitation ascent, the limiting factor is the viscosity of the magma (Clemens, 1998). Due to the difference in limiting factors, rates of magma ascent by dyking are 10^4 to 10^8 times faster than by any diapirism model.

Other factors that influence the ascent rate of the magma include the stresses existing in the lithosphere, the temperature of surrounding rocks, the thickness of the unstable buoyant layer, the volume of magma ascending, the degree of crystallization of the magma (affecting its viscosity), and the composition of the granitic magma (Clarke, 1992). Finally, different ascent methods will also transfer the melt through the crust at different rates (Clemens and Mawer, 1992; Clemens et al., 1997, Rutter, 1997)

A third model, proposed by Brown and Solar (1998), is applicable to convergent orogens. In their model magma is focused into crustal-scale shear zones and then transported upward. Below the brittle-ductile transition, magma flow is coupled with plastic deformation associated with contractional deformation.

The ascending magma stops when the upward forces of buoyancy are balanced by external forces (Clarke, 1992). This usually occurs when the strength of the overlying rocks is greater than what the magma can fracture or soften by heating. Another possibility of arresting ascent is the presence of an "easier" path for the magma. Melt rising through a fracture can be arrested if it encounters a sub-horizontal plane of weakness, such as a freely slipping horizontal joint (Weeterman, 1980) or a sub-horizontal strength anisotropy (Hogan and Gilbert, 1995). In these instances, the magma will spread laterally or accumulate instead of continuing its ascent. The final geometry of the pluton is dependant on the: emplacement mechanism and depth, supply rate of the magma, and state of stress in the lithosphere (Pollard and Johnson, 1973; Corry, 1988; Hogan et al., 1998; Cruden, 1998).

7.3.2 Emplacement models for granitic magmas

The actual mechanism of the formation of a pluton in its final resting place is known as emplacement. There are two main types of emplacement models: passive intrusions and forceful intrusions. Passive intrusions indicate that emplacement occurred in a tectonically opened cavity, while forceful intrusions are either squeezed or sheared into place. The main emplacement models include ballooning, passive emplacement in shear zones, and emplacement of tabular granites by roof uplift or floor depression. Each is discussed further below.

Ballooning

Ballooning is defined as the expansion of a pluton due to continuous magma pumping from below. This leads to a deformation history of bulk inhomogenous shortening (Bell, 1981). The overall effect of this is ductile bulk shortening (flattening) along the contacts of the pluton (in both the pluton and the country rocks). Other evidence of ballooning includes a total lack of development of stretching lineation within the foliation planes. This is a good indication of equal stretching on all directions within the YZ plane of the strain ellipsoid. Also, the continuous addition of buoyant material to the core of the inflating head of the pluton results in an inner zone of vertical stretching and an outer zone of shortening. This will result in strong foliation at the contact, which will diminish inward (Bateman, 1985). The foliations within the granite should form closed, concentric trend lines close to the contact. The aureole foliation should be parallel to and continuous with the foliation of the intrusive pluton.

Emplacement in shear zones

Passive emplacement in shear zones occurs when the magma places itself in a cavity created by active tectonism. Most "shear zone" models propose that the space for pluton emplacement is created in tensional or potentially dilational sites in, or adjacent to, faults and shear zones. Examples of such sites are found at releasing bends, at jogs, between step-overs and between bifurcations in transcurrent structures, and in ramp-flat bends in extensional structures. Hutton (1997) suggests that emplacement in shear zones can also occur in compressional settings without the requirement of magma being localized in dilational zones. Hutton (1997) also states that forces due to: buoyancy, confining pressure, volume change resulting from melting, and tectonic differential stresses, all play a part in contractional orogenic settings. These forces can combine to exceed the force due to tectonic compression (Hutton, 1997).

Field evidence for shear zone emplacement comes from a correlation between pluton geometry and external shear zones or faults. Further evidence can be gathered by comparing the relative timing of deformation and crystallization stages in the granites. Finally, examination of the strain types and strain gradients present, as well as structural kinematics, can give the final piece of evidence to support shear zone emplacement.

Tabular granites emplaced by roof uplift or by floor depression

Tabular granites are created when the ascending magma is arrested by one of the mechanisms discussed above and the melt spreads laterally. This will generally either cause roof lifting, floor depression, or a hybrid of the two.

With roof lifting, the magma occupies some sub-horizontal plane of weakness and lifts the overlying country rock. This arching of the country rock is also often referred to as doming. The magmatic intrusion formed in this situation will adopt a tabular, laccolithic shape.

Roof uplift is believed to occur at shallow levels in the crust, usually at less than three kilometers in paleodepth (Dehls, Cruden, and Vigneresse, 1998), although recent work by Benn et al. (1998b; in press) shows that laccolithic intrusions may occur at considerably deeper levels than previously thought. Benn et al. (1998b, in press) state that tectonic forces and the development of shear zones may displace crustal blocks and so create space for granitic intrusions in transpressional settings. Most roof lifting models assume a two-stage process starting with the formation of an initial sill and then vertical displacement. The driving pressure of laccolith creation is caused by the overpressure of magma. Laccoliths are plano-convex in form and roughly circular in plan. Laccoliths, and tabular plutons in general, are usually much wider than they are thick (i.e. a pluton eight kilometers in diameter, will only be 10's of meters thick). As depth increases, lateral expansion of the sill will be favored over roof lifting. Therefore, laccoliths emplaced at depth will be thinner than those emplaced at higher crustal levels (Roman-Berdiel et al., 1995). One important characteristic is a rather flat and concordant basal surface (Roman-Berdiel et al., 1995). Other field observations can include: a preserved horizontal foliation or magmatic layering, elastic, elastic-plastic or ductile bending of the roof rocks (Cruden, 1998), lifting of the roof along oblique reverse shear zones (Benn et al., 1998b, in press), and/or extensional shearing above intrusions (Benn et al., 1998b, in press).

In the case of floor depression, the resulting intrusion will be a lopolith. Lopoliths are proposed to occur at greater depths than laccoliths. Corry (1988) suggests that with increasing depth, laccoliths will slowly become laccolith-lopolith hybrids, which will in turn eventually become lopoliths.

The material pushed downward must somehow be accommodated at depth, therefore it is believed that as the magma is withdrawn from the source region, it provides space for the floor to descend, principally by ductile flow. Field evidence may consist of asymmetric melt-filled structures, similar to those seen in migmatites (Brown, 1994).

Cruden (1998) describes two end-member models of floor depression: 1) the "cantilever model" and 2) the "piston model." In the cantilever model, the floor of the pluton is rotated about a pivot at the edge of the pluton, away from the feeder zone. The cantilever model will result in the base of the pluton looking similar to an inverted cone. Deformation in the underlying rocks will occur by bulk progressive shear and may be expressed as a series of stepped high-angle normal faults, or as low angle shear zones which are sub-parallel to the floor. In the piston model the floor depresses as a whole, with the floor remaining horizontal. The "block" of material moves downward with the aid of faults or shears. The pluton will have vertical sides that correspond to planes of weakness (faults, shear zones, feeder dykes, etc.). Due to the nature of floor depression in the "piston" model, negligible bulk strains are proposed for the underlying crust.

7.3.3 Model for the Prosperous Suite

Davis et al. (1994) propose that two-mica and potassium feldspar granite magmas (ca. 2.60-2.58 Ga), which includes the Prosperous Suite, were generated as a result of lithospheric delamination due to crustal shortening and thickening which led to heating of the crust and partial melting of the Burwash Formation sediments. Based on the rectilinear map pattern of volcanic belts in the Slave Province (Fyson, 1990) and the orientation of the pegmatite dykes coupled with a compressional setting, it is possible to interpret that an extensive fracture system is present in the region. It is proposed that magma ascended as dykes by exploiting this fracture system. Field evidence suggests magma ascent through dykes may be a valid interpretation. Fig. 7-1a shows a pegmatite dyke intersecting the base of the Prosperous Pluton. Once the dyke has penetrated the base its contacts disappear and the area just above the base becomes a mixture of granite and pegmatite. The pegmatite dyke either emanated from the pluton or from a source below (such as a granite body similar to one of the numerous smaller bodies that are part of the Prosperous Suite) and exploited the nearest fracture available, which may have also previously been exploited by ascending magma. The absence of a sharp contact between the pegmatite and granite, as seen in most outcrops that are cross cut by pegmatite dykes, suggests that the

Fig. 7-1: A) Map of the Prosperous Pluton showing the trend of stations where pegmatite was mixed with granite. To the right is a drawing of a pegmatite dyke intersecting the base of the Prosperous Pluton. B) Cartoon E-W cross section of the Prosperous Pluton and the Sparrow Pluton. Position of feeder dyke for the Prosperous Pluton is influenced by the position of the dashed line shown on the map in A. Dyke position for the Sparrow Pluton is arbitrary. C) Gravity model for the Yellowknife area showing the modelled shapes of the Prosperous and Sparrow Plutons. Gravity model from Shepley (2000).

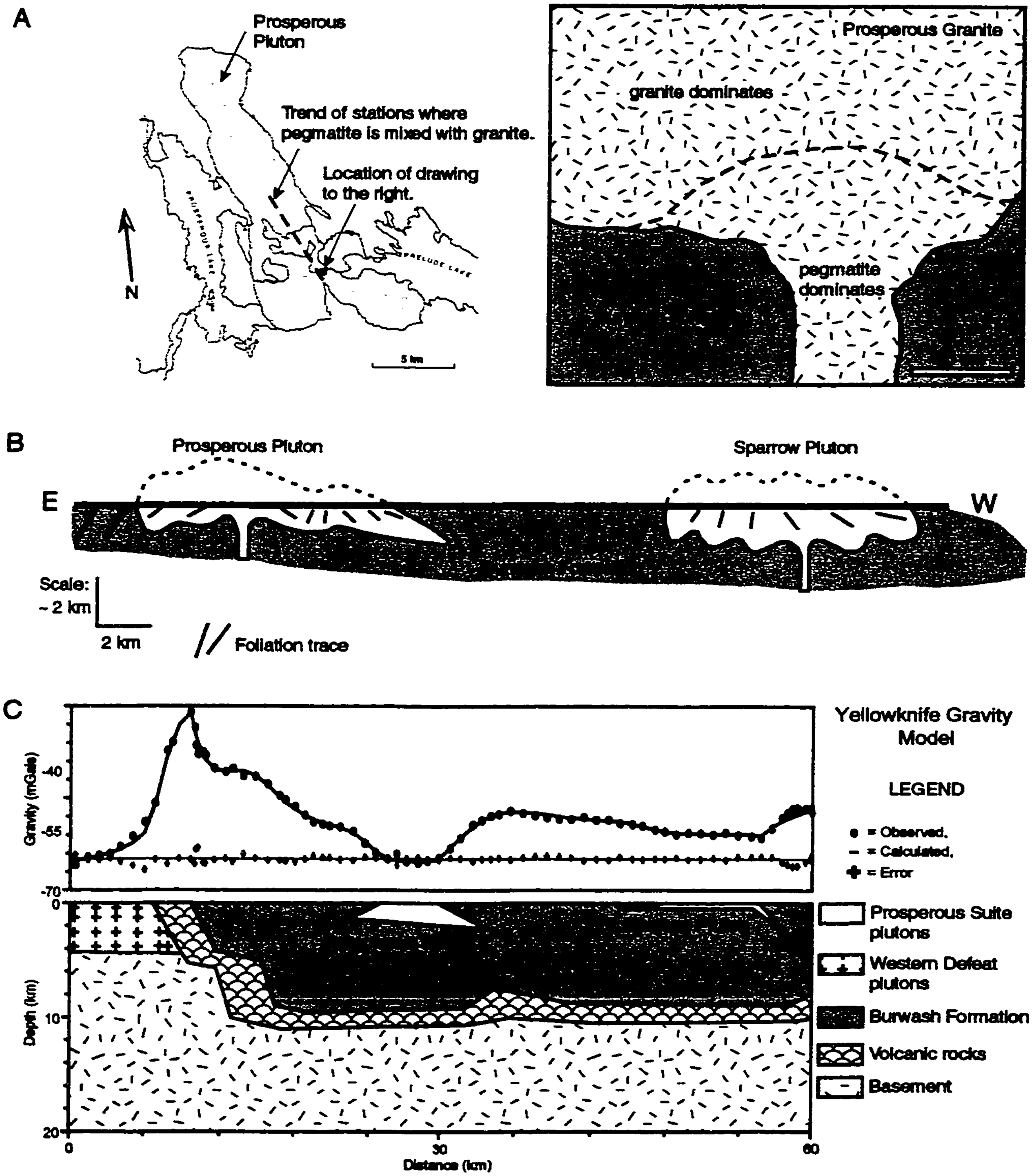

pegmatite was emplaced into magma that had not yet crystallized and was therefore still hot. Proximity to a feeder zone might provide enough heat to keep the granite at the base of the pluton hot enough for this to occur. Magma rose in the crust until it hit a magma trap such as some horizontal strength anisotropy within the crust (Clemens and Mawer, 1992), and then began to pool. Such an anisotropy may correspond to a shear zone, a lithological contact, or the brittle-ductile transition in the crust. It is unknown which mechanism was responsible for arresting the ascent of magma. Metamorphic mineral assemblages suggest that emplacement occurred at depths between 9 and 13 km (3.0-3.5 kbar and 550-600^{0}C; Bethune et al., 1999; see section 2.3 for details).

Kretz et al. (1982) suggested that the Prosperous Suite, prior to emplacement, accumulated as a tabular mass of solid material. The crystallized mass rose plastically to form separate diapiric domes that broke through the Archean volcanics and sediments that were previously deformed. This is an unlikely model since the source of the granites was partial melting of the Burwash Formation sediments. Also, if this model were applicable, the granites should be characterized by intense solid state plastic deformation, concentric foliation patterns, down-dip extension lineations, and by rim synclines in the host rocks around the pluton margins. The present work demonstrates that none of these features are present in the Prosperous Suite, thus the solid-state diapir model must be discarded. Also, rather than an increase in deformation of the granites from the center of the plutons to the margins, as would be the case if ballooning occurred, AMS data shows that deformation was concentrated in the central zones of the plutons. This leaves two possible models: passive emplacement in a shear zone and emplacement by roof uplift and/or floor depression.

Based on the sub-horizontal nature of the pluton contacts and the absence of field evidence of a large scale shear zone surrounding the plutons (although small scale shear zones occur within the plutons; see section 6.1), it is proposed that the Sparrow and Prosperous plutons are laccoliths that were emplaced horizontally during D_2, and then deformed as they crystallized during ongoing D_2 (Fig. 7-1b). Evidence supporting a laccolithic emplacement model includes the following:

1) The exposed floor and roof contacts of the Prosperous Pluton dip shallowly to the east, suggesting a tabular shape. The apparent absence of evidence for a "sagging" floor, suggests that emplacement occurred dominantly by roof uplift rather than depression of the floor. Using simple trigonometry, the outcrop width of the pluton, and the dip of the pluton contact, it is estimated that the pluton is roughly 2 km thick.

2) Small bedding-parallel granite sheets were observed between the Sparrow and Prosperous plutons. The Prosperous Suite may similarly be made up of a series of different sized sheets that were emplaced horizontally and then deformed.

3) Magnetic fabric data for the Prosperous Pluton are compatible with a horizontal foliation that was subsequently folded. This suggests that the pluton was emplaced as a horizontal sheet that was then deformed during D_2.

4) Magmatic layers, defined by variations in mica content, seen in outcrop near the base of the Prosperous Pluton, are parallel to the basal contact of the pluton. This may be the result of a crystallization front parallel to the floor of the pluton through which heat would have been lost, once again suggesting a horizontal geometry, at least locally.

5) Mapping of the susceptibility for the Sparrow Pluton showed zonation that is consistent with folded horizontal layers. The zonation is interpreted to be reflecting the variation in mica and magnetite (which is proposed to be associated with the mica) content in different layers. The magnetite may be due to the alteration of biotite, or it may be present as impurities in the biotite.

6) Gravity modeling of profiles across the Prosperous and Sparrow plutons (Shepley, 2000; Fig. 7-1c), supports the conclusions that the plutons are thin tabular sheets that have been subsequently folded.

Benn et al. (1998b, in press) showed that space may be made for laccolithic intrusions in a transpressional setting by the formation of oblique reverse shear zones, which may or may not be accompanied by extensional shearing above the intrusions. These shear zones allow the upward movement of the overburden. Reverse shear zones were not identified in the field, but it is possible that they have been eroded. Another possibility is that the shear zones are located to the side of the pluton or part of the regional deformation field (Benn et al., 1998b, in press) and so are not solely associated with the plutons. Regardless of origin, the absence of preserved shear zones associated with the plutons does not invalidate the laccolithic model as applied to the Sparrow and Prosperous plutons.

7.4 SUGGESTIONS FOR FURTHER STUDIES

Two areas for further study are suggested below:

1) Although suggestions for the origin of the magnetite in the granites have been proposed, the exact nature of how and when the magnetite formed cannot be determined with the present data set. SEM/TEM analyses could provide information on this subject.

2) Further work might also involve a detailed microstructural analysis of the Burwash Formation inside and outside the cordierite isograd surrounding the Prosperous Suite, involving extensive sampling and mapping of the country rocks. Detailed mapping and sampling of the Burwash Formation (which was beyond the scope of this study) is needed due to the proximity of other plutonic suites. The purpose would be to determine porphyroblast-fabric relationships around various plutons to see if the relative timing of the different plutons in the suite can be determined. By determining the length of time it took for the Prosperous Suite aureole to form and by using U-Pb dates for the different plutons in the suite, further constraints on the absolute timing of D_2 could be obtained.

7.5 CONCLUSIONS

During D_2 compression and crustal thickening, lithospheric delamination led to heating of the crust and the generation of magma through partial melting of the Burwash Formation (Davis et al., 1994). It is proposed that magma then ascended as dykes, exploiting crustal fractures. Based on field and microstructural observation, and magnetic fabric analyses, it is interpreted that the Sparrow and Prosperous plutons were emplaced early during D_2 as a series of thin tabular laccolithic intrusions (Fig. 7-1), which, along with other plutonic suites, enhanced regional metamorphism (M_2; Bethune and Carmichael, 1998). The use of the term laccolith implies that emplacement was localized along some horizontal strength anisotropy within the crust (Clemens and Mawer, 1992). Such an anisotropy may correspond to a shear zone, a lithological contact, or the brittle-ductile transition in the crust. Following emplacement, the granites were deformed into a folded sheet geometry as D_2 continued with a bulk shortening direction of ENE-WSW to NE-SW and extension occurring in a NNW-SSE to NW-SE direction. Once the granites cooled small-scale shear zones localized the continuing deformation. Based on the results of this study and the similarity between the Prosperous and Sparrow plutons, it is proposed that the Prosperous Suite granites are a series of thin laccolithic intrusions emplaced early during D_2.

The results of this study are also important in terms of the larger picture. In regions with complex deformation histories, such as the southern Slave Province, the internal fabrics of syntectonic granite plutons can preserve a record of the strain field associated with synmagmatic tectonics. Also, dates for syntectonic plutons can be used to help constrain the absolute timing of deformation and metamorphism in the Yellowknife Domain.

REFERENCES:

Aranguren, A., Cuevas, J., and Tubia, J. M., 1996. Composite magnetic fabrics from S-C mylonites: Journal of Structural Geology, v. 18, p. 863-869.

Bateman, R., 1985. Aureole deformation by flattening around a diapir during in situ ballooning: the Cannibal Creek Granite: Journal of Geology, v. 93, p. 293-310.

Bell, T.H., 1981. Foliation development - the contribution, geometry, and significance of progressive, bulk, inhomogeneous shortening: Tectonophysics, v. 75, p. 273-296.

Benn, K., 1994. Overprinting of magnetic fabrics in granites by small strains: numerical modelling: Tectonophysics, v. 233, p. 153-162.

Benn, K., Horne, R. J., Kontak, D. J., Pignotta, G., and Evans, N. G., 1997. Syn-Acadian emplacement model for the South Mountain Batholith, Meguma Terrane, Nova Scotia: magnetic fabric and structural analysis: Geological Society of America Bulletin, v. 109, p. 1279-1293.

Benn, K., Ham, N. M., Pignotta, G. S., and Bleeker, W., 1998a. Emplacement and deformation of granites during transpression: magnetic fabrics of the Archean Sparrow pluton, Slave Province, Canada: Journal of Structural Geology, v. 20, p. 1247-1259.

Benn, K., Odonne, F., and de Saint Blanquat, M., 1998b. Pluton emplacement during transpression in brittle crust: new views from analogue experiments: Geology, v. 26, p. 1079-1082.

Benn, K., Odonne, F., Lee, S. K. Y., and Darcovich, K., in press. Analogue scale models of pluton emplacement during transpression in brittle and ductile crust: Transactions of the Royal Society of Edinburgh: Earth Sciences, Hutton IV Special Issue.

Bethune, K. M., and Carmichael, D. M., 1998, Metamorphism along the Slave portion of the SNORCLE transect: Slave-Northern Cordillera Lithospheric Evolution Transect Meeting, Simon Fraser University, Lithoprobe report No. 64, p. 17-24.

Bethune, K. M., Villeneuve, M., and Bleeker, W., 1999. Laser $^{40}Ar/^{39}Ar$ thermochronology of Archean rocks in the Yellowknife Domain, southwestern Slave Province: insights into the cooling history of an Archean granite-greenstone belt: Canadian Journal of Earth Sciences, v. 36, p. 1189-1206.

Bickle, M. J., Nisbet, E. G., and Martin, A., 1994. Archean greenstone belts are not oceanic crust: Journal of Geology, v. 102, p. 121-137.

Bleeker, W., 1996, Thematic structural studies in the Slave Province, Northwest Territories: the Sleepy Dragon Complex: Geological Survey of Canada Current Research 1996-C, p. 37-48.

Bleeker, W., and Beaumont-Smith, C., 1995, Thematic structural studies in the Slave Province: preliminary results and implications for the Yellowknife Domain, Northwest Territories: Geological Survey of Canada Current Research 1995-C, p. 87-96.

Bleeker, W., and Davis, B., 1999a. The 1991-1996 Slave Province NATMAP Project: introduction: Canadian Journal of Earth Sciences, v. 36, p. 1033-1042.

Bleeker, W., and Ketchum, J., 1998a, The Central Slave Basement Complex, its autochthonous cover, decollement, and structural topology: towards a new terrane model for the Slave Province: Slave-Northern Cordillera Lithospheric Evolution Transect Meeting, Simon Fraser University, Lithoprobe report No. 64, p. 31-35.

Bleeker, W., and Ketchum, J., 1998b, Central Slave Basement Complex, Northwest Territories: its autochthonous cover, decollement, and structural topology: Geological Survey of Canada Current Research 1998-C, p. 9-19.

Bleeker, W., Davis, B., and Villeneuve, M., 1997a, The Slave Province: evidence for contrasting crustal domains and a complex, multistage tectonic evolution: Slave-Northern Cordillera Lithospheric Evolution Transect Meeting, University of Calgary, Lithoprobe report No. 56, p. 36-37.

Bleeker, W., Ketchum, J. F., and Davis, 1999a. The Central Slave Basement Complex, part II: age and tectonic significance of high-strain zones along the basement-cover contact: Canadian Journal of Earth Sciences, v. 36, p. 1111-1130.

Bleeker, W., Ketchum, J. F., Jackson, V. A., and Villeneuve, M., 1999b. The Central Slave Basement Complex, part I: its structural topology and autochthonous cover: Canadian Journal of Earth Sciences, v. 36, p. 1083-1109.

Bleeker, W., Villeneuve, M. and Bethune, K. 1997b, Thematic structural studies in the Slave Province, Northwest Territories: contrasting basement/cover relationships on the western and southwestern flanks of the Sleepy Dragon Complex: Geological Survey of Canada Current Research 1996-C, pp.27-37.

Borradaile, G. J., and Henry, B., 1997. Tectonic applications of magnetic susceptibility and its anisotropy: Earth Science Reviews, v. 42, p. 49-93.

Borradaile, G.J., and Werner, T., 1994. Magnetic anisotropy of some phyllosilicates: Tectonophysics, v. 235, p. 223-248.

Bouchez, J. L., 1997, Granite is never isotropic: an introduction to AMS studies of granitic rocks, *in* Bouchez, J. L., and Hutton, D. H. W., and Stephens, W. E., eds., Granite: from segregation of melt to emplacement fabrics: Dordrecht, Kluwer Academic, pp. 95-112.

Bouillin, J. P., Bouchez, J. L., Lespinasse, P., and Pecher, A., 1993. Granite emplacement in an extensional setting: an AMS study of the magmatic structures of Monte Capanne (Elba, Italy): Earth and Planetary Science Letters, v. 118, p. 263-279.

Bouma, A. H., 1962, Sedimentology of some flysch deposits: Amsterdam, Elsevier, 168 p.

Boyle, R. W., 1961, The geology, geochemistry and origin of the gold deposits of the Yellowknife District: Geological Survey of Canada Memoir 310, 193 p.

Brown, M., 1994. The generation, segregation, ascent and emplacement of granite magma: the migmatite-to-crustally-derived granite connection in thickened orogens: Earth-Science Reviews, v. 36, p. 83-130.

Brown, M., and Solar, G. S., 1998. Granite ascent and emplacement during contractional deformation in convergent orogens: Journal of Structural Geology, v. 20, p. 1365-1393.

Brun, J. P., Gapais, D., Cogne, J. P., et al., 1990. The Flamanville granite (northwest France): an unequivocal example of a syntectonically expanding pluton: Geological Journal, v. 25, p. 271-286.

Brun, J.P., and Pons, J., 1981. Strain patterns of pluton emplacement in a crust undergoing non-coaxial deformation, Sierra Morena, southern Spain: Journal of Structural Geology, v. 3, p. 218-229.

Card, K. D., and King, J. E., 1992. The tectonic evolution of the Superior and Slave provinces of the Canadian Shield: introduction: Canadian Journal of Earth Sciences, v. 29, p. 2059-2065.

Carmichael, D. M., 1978. Metamorphic bathozones and bathograds: a measure of the depth of post-metamorphic uplift and erosion on the regional scale: American Journal of Science, v. 278, p. 769-797.

Clarke, D. B., 1992, Granitoid rocks: London, Chapman & Hall, 283 p.

Clemens, J. D., 1998. Observations on the origin and ascent mechanisms of granitic magmas: Journal of the Geological Society of London, v. 155, p. 843-851.

Clemens, J. D., and Mawer, C. K., 1992. Granite magma transport by fracture propagation: Tectonophysics, v. 204, p. 339-360.

Clemens, J. D., Petford, N. and Mawer, C. K., 1997, Ascent mechanisms of granitic magmas: causes and consequences, *in* Holness, M., ed., Deformation-enhanced fluid transport in the earth's crust and mantle. The Mineralogical Society Series, v. 8: London, Chapman & Hall.

Corry, C. E., 1988. Laccoliths: Mechanics of emplacement and growth, Geological Society of America Special Paper 220, Boulder, Colarado, USA, 110 p.

Cruden, A.R., 1998. On the emplacement of tabular granites: Journal of the Geological Society, London, v. 155, p. 853-862.

Davidson, A., 1967, Metamorphism and intrusion in the Benjamin Lake map-area, Northwest Territories [Ph.D. Thesis], Vancouver, University of British Columbia, 204 p.

Davidson, A., 1972, Granite studies in the Slave province, *in* Report of activities, part A: Geological Survey of Canada, Paper 72-1A, p. 109-115.

Davis, W. J., King, J. E., and Fryer, B. J., 1994. Geochemistry and evolution of Lake Archean plutonism and its significance to the tectonic development of the Slave craton: Precambrian Research, v. 67, p. 207-241.

Davis, W. J., and Bleeker, W., 1997, Timing of plutonism and regional deformation in the Yellowknife-Sleepy Dragon area, southern Slave Province: NWT Geoscience Forum, Yellowknife, Program and Abstracts of Talks and Posters, November 26-28, 1997, p.34-36.

Davis, W. J., and Bleeker, W., 1999. Timing of plutonism, deformation and metamorphism in the Yellowknife Domain, Slave Province, Canada: Canadian Journal of Earth Sciences, v. 36, p. 1169-1187.

Dehls, J.F., Cruden, A.R., and Vigneresse, J.-L., 1998: Fracture control of late Archean pluton emplacement in the northern Slave Province, Canada: Journal of Structural Geology, v. 20, p. 1145-1154.

Day, R., Fuller, M., and Schmidt, V. A., 1977. Hysteresis properties of titanomagnetites: grain-size and compositional dependence: Physics of the Earth and Planetary Interiors, v. 13, p. 260-267.

Drury, S. A., 1979. Rare-earth and other trace element data bearing on the origin of Archean granitic rocks from Yellowknife, Northwest Territories: Canadian Journal of Earth Sciences, v. 16, p. 809-815.

Dudás, F. O., Henderson, J. B., and Mortensen, J. K., 1990, U-Pb ages of zircons from the Anton Complex, southern Slave Province, Northwest Territories, *in* Radiogenic age and isotopic studies, Report 3: Geological Survey of Canada, Paper 89-2A, p. 39-44.

Easton, R. M., 1985, The nature and significance of pre-Yellowknife Supergroup rocks in the Point Lake area, Slave Structural Province, Canada, *in* Ayres, L. D., Thurston, P. C., Card, K. D., Weber, W., eds., Evolution of Archean supracrustal sequences: Geological Association of Canada Special Paper 28, p. 153-167.

Emerman, S. H., and Marret, R., 1990. Why dykes?: Geology, v. 18, p. 231-233.

Folinsbee, R. E., Baadsgaard, H., Cumming, G. L., and Green, D. C., 1968, A very ancient island arc, *in* Knopoff, L., Drake, C. L., and Hart, P. J., eds., The crust and upper mantle of the Pacific area: American Geophysical Union Geophysical Monograph 12, p. 441-448.

Fyson, W. K., 1975. Fabrics and deformation of Archean metasedimentary rocks, Ross Lake-Gordon Lake area, Slave Province, Northwest Territories: Canadian Journal of Earth Sciences, v. 12, p. 765-776.

Fyson, W. K., 1980. Fold fabrics and emplacement of an Archean granitoid pluton, Cleft Lake, Northwest Territories: Canadian Journal of Earth Sciences, v. 17, p. 325-332.

Fyson, W. K., 1982. Complex evolution of folds and cleavages in Archean rocks, Yellowknife, N. W. T.: Canadian Journal of Earth Sciences, v. 19, p. 878-893.

Fyson, W. K., 1990. Structural development of angular volcanic belts in the Archean Slave Province: Canadian Journal of Earth Sciences, v. 27, p. 403-413.

Fyson, W. K., and Helmstaedt, H., 1988. Structural patterns and tectonic evolution of supracrustal domains in the Archean Slave Province, Canada: Canadian Journal of Earth Sciences, v. 25, p. 301-315.

Gapais, D, 1989. Shear structures within deformed granites: mechanical and thermal indicators: Geology, v. 17, p. 1144-1147.

Gleizes, G., Nédélec, A., Bouchez, J. L., Autran, A., and Rochette, P., 1993. Magnetic susceptibility of the Mont-Louis Andorra ilmenite-type granite (Pyrenees): a new tool for the petrographic characterization and regional mapping of zoned granite plutons: Journal of Geophysical Research, v. 98, p. 4317-4331.

Green, D. C., and Baadsgaard, 1971. Temporal evolution and petrogenesis of an Archean crustal segment at Yellowknife, N. W. T., Canada: Journal of Petrology, v. 12, p. 117-217.

Green, D. C., Baadsgaard, H., and Cumming, G.L., 1968. Geochronology of the Yellowknife area, Northwest Territories, Canada: Canadian Journal of Earth Sciences, v. 5, p. 725-735.

Ham, N. M., and Benn, K., 1996, Structural analysis of the Sparrow Lake Pluton (Prosperous Suite) in the southern Yellowknife Belt: Department of Indian Affairs and Northern Development, NWT Geology Division, Exploration Overview 1996, Nov. 1996 edition, part 3, p. 17.

Ham, N. M., and Benn, K., 1998, Final report on structural studies of the Archean Prosperous Granites, Slave Province: the Prosperous and Sparrow plutons: Indian and Northern Affairs Canada, NWT Geology Division, Yellowknife, Open File Report EGS 1998-10, 29 p.

Ham, N. M., Benn, K., and Bleeker, W., 1997a, Structural studies of the Prosperous Granite Suite: syn-D2 laccoliths in the southern Yellowknife Domain: NWT Geoscience Forum, Yellowknife, Program and Abstracts of Talks and Posters, November 26-28, 1997, p.48-50.

Ham, N. M., Benn, K., and Bleeker, W., 1998a, The Late-Archean Prosperous Granite Suite: syn-D2 laccoliths in the Yellowknife Domain, Slave Province: Slave-Northern Cordillera Lithospheric Evolution Transect Meeting, Simon Fraser University, Lithoprobe report No. 64, pp. 36.

Ham, N. M., Benn, K., and Bleeker, W., 1998b, Magnetic fabric study of the Archean Prosperous Granite Suite: syn-D2 laccoliths in the Yellowknife Domain, Slave Province, Canada: Geological Association of Canada-Mineralogical Association of Canada Abstract Volume, v. 23, p. A-71.

Ham, N. M., Benn, K., Pignotta, G., and Bleeker, W., 1997b, Magnetic fabrics in the Sparrow Granite Pluton: markers of the Late Archean strain field in the southern Yellowknife Domain, Slave Province, Canada: Slave-Northern Cordillera Lithospheric Evolution Transect Meeting, University of Calgary, Lithoprobe report No. 56, pp. 210.

Ham, N. M., Benn, K., Pignotta, G., and Bleeker, W., 1997c, Magnetic fabrics in the Sparrow Granite Pluton: markers of the Late Archean strain field in the southern Yellowknife Domain, Slave Province, Canada:

Geological Association of Canada-Mineralogical Association of Canada Abstract Volume, v. 22, p. A-61 - A-62.

Heider, R., Sunlop, D. J., and Sugiura, N., 1987. Magnetic properties of hydrothermally recrystallized magnetite crystals: Science, v. 236, p. 1287-1290.

Heider, R., Zitzelsberger, A., and Fabian, K., 1996. Magnetic susceptibility and remanent coercive force in grown magnetite crystals from 0.1μm to 6 mm: Physics of the Earth and Planetary Interiors, v. 93, p. 239-256.

Helmstaedt, H., and Padgham, W. A., 1986. A new look at the stratigraphy of the Yellowknife Supergroup at Yellowknife, N. W. T. -- implications for the age of gold-bearing shear zones and Archean basin evolution: Canadian Journal of Earth Sciences, v. 23, p. 454-475.

Henderson, J. B., 1970. Stratigraphy of the Yellowknife Supergroup, Yellowknife Bay--Prosperous Lake area, District of Mackenzie: Geological Survey of Canada Paper 70-26, 12 p.

Henderson, J. B., 1981, Archean basin evolution in the Slave Province, Canada, *in* Kroner, A., ed., Precambrian plate tectonics: Amsterdam, Elsevier, p. 213-235.

Henderson, J. B. 1985, Geology of the Yellowknife - Hearne Lake area, District of Mackenzie: a segment across an Archean basin: Geological Survey of Canada Memoir 414, 135 p., 1:250,000 map.

Henderson, J. B., van Breemen, O., and Loveridge, W. D. 1987, Some U-Pb zircon ages from Archean basement, supracrustal and intrusive rocks, Yellowknife-Hearne Lake area, District of Mackenzie, *in* Radiogenic age and isotopic studies: Report 1: Geological Survey of Canada Paper 87-2, p. 111-121.

Hoffman, P. F., 1986, Crustal accretion in a 2.7-2.5 Ga granite-greenstone terrane, Slave Province, N. W. T.: a prograding trench-arc system?: Geological Association of Canada-Mineralogical Association of Canada Program with Abstracts, v. 11, pp.82.

Hoffman, P. F., 1989, Precambrian geology and tectonic history of North America, *in* Bally, A. W., and Palmer, A. R., eds., The geology of North America overview: Boulder, Colorado, Geological Society of America, The Geology of North America, v. A, p. 447-512.

Hogan, J. P. and Gilbert, M. C., 1995. The A-type Mount Scott Granite Sheet: importance of crustal magma traps: Journal of Geophysical Research, v. 100, p. 15779-15793.

Hogan, J.P., Price, J.D. and Gilbert, M.C., 1998. Magma traps and driving pressure: consequences for pluton shape and emplacement in an extensional regime: Journal of Structural Geology, v 20, p. 1155-1168.

Housen, , B. A., Richter, C., and van der Pluijm, B. A., 1993. Composite magnetic anisotropy fabrics: experiments, numerical models, and implications for the quantification of rock fabrics: Tectonophysics, v. 220, p. 1-12.

Hrouda, F., and Schulmann, K., 1990. Conversion of the magnetic susceptibility tensor into the orientation tensor in some rocks: Physics of the Earth and Planetary Interiors, v. 63, p. 71-77.

Hutton, D. H. W., 1997, Syntectonic granites and the principle of effective stress: a general solution to the space problem?, *in* Bouchez, J. L., and Hutton, D. H. W., and Stephens, W. E., eds., Granite: from segregation of melt to emplacement fabrics: Dordrecht, Kluwer Academic, pp. 189-197.

Isachsen, C. E., and Bowring, S. A., 1994. Evolution of the Slave craton: Geology, v. 22, p. 917-920.

Isachsen, C. E., and Bowring, S. A., 1997. The Bell Lake group and Anton Complex: a basement-cover sequence beneath the Archean Yellowknife greenstone belt revealed and implicated in greenstone belt formation: Canadian Journal of Earth Sciences, v. 34, p. 169-189.

Jelinek, V., 1978. Statistical processing of anisotropy of magnetic susceptibility measured on groups of specimens: Stud. Geophys. Geod., v. 22, p. 50-62.

Jelinek, V., 1981. Characterization of the magnetic fabric of rocks: Tectonophysics, v. 79, p. 63-67.

Ketchum, J., and Bleeker, W., 1998, U-Pb geochronology of the Sleepy Dragon Complex in the Morose-Patterson Lakes area, southwestern Slave Province, with tectonic implications: Slave-Northern Cordillera

Lithospheric Evolution Transect Meeting, Simon Fraser University, Lithoprobe report No. 64, p. 25-30.

King, J. and Helmstaedt, H., 1997, The Slave Province, North–West Territories, Canada, *in* De Wit, M. J., and Ashwal, L. D., eds., Greenstone belts: Oxford, Clarendon Press, p. 459-479.

King, J. E., Davis, W. J., and Relf, C., 1990, Late Archean tectonomagmatic evolution of the central Slave Province, Canada: International Archaean Symposium, Perth, Extended Abstracts Volume, v. 3, p. 75-76.

Kretz, R., 1964, Examination of intersecting pegmatite dikes and inclusions in dikes near Yellowknife, Canada: 22nd International Geology Congress, India, Sec 6, p. 1-18.

Kretz, R., 1968, Study of pegmatite bodies and enclosing rocks, Yellowknife-Beaulieu Region, District of Mackenzie: Geological Survey of Canada Bulletin 159, 109 p.

Kretz, R., 1970. Variation in composition of muscovite and albite in a pegmatite dike near Yellowknife: Canadian Journal of Earth Sciences, v. 7, p. 1219-1235.

Kretz, R., 1985. Chemical composition of the Sparrow pluton and associated pegmatite dykes: Contributions to the Geology of the NWT, v. 2, p. 1-13.

Kretz, R., Garrett, D., and Garrett, R. G., 1982. Na-K-Li geochemistry of the Prestige pluton in the Slave Province of the Canadian Shield: Canadian Journal of Earth Sciences, v. 19, p. 540-554.

Kretz, R., Hartree, R., and Jones, P., 1989a. Metasomatic crystallization of muscovite in granite and tourmaline in schist related to pegmatite emplacement near Yellowknife, Canada: Contributions to Mineralogy and Petrology, v. 102, p. 191-204.

Kretz, R., Loop, J., and Hartree, R., 1989b. Petrology and Li-Be–B geochemistry of muscovite-biotite granite and associated pegmatite near Yellowknife, Canada: Contributions to Mineralogy and Petrology, v. 102, p. 174-190.

Kusky, T. M., 1989. Accretion of the Archean Slave Province: Geology, v. 17, p. 63-67.

Kusky, T. M., 1990. Evidence for Archean ocean opening and closing in the southern Slave Province: Tectonics, v. 9, p. 1533-1563.

Leblanc, D., Gleizes, G., Roux, L. and Bouchez, J. L., 1996. Variscan dextral transpression in the French Pyrenees: new data from the Pic des Trois-Seigneurs granodiorite and its country rocks: Tectonophysics, v. 261, p. 331-345.

O'Reilly, W., 1984, Rock and mineral magnetism. Glasgow, Blackie and Sons Ltd., 220pp.

Padgham, W. A., 1985, Observation and speculations on supracrustal successions in the Slave Structural Province, *in* Ayres, L. D., Thurston, P. C., Card, K. D., Weber, W., eds., Evolution of Archean supracrustal sequences: Geological Association of Canada Special Paper 28, p. 133-151.

Pavlis, T. L., 1996. Fabric development in syn-tectonic intrusive sheets as a consequence of melt-dominated flow and thermal softening of the crust: Tectonophysics, v. 253, p. 1-31.

Petford, N., 1996. Dykes or diapirs?: Transactions of the Royal Society of Edinburgh: Earth Sciences, v. 87, p. 311-321.

Petford, N., Lister, J. R., and Kerr, R. C., 1994. The ascent of felsic magma in dykes: Lithos, v. 32, p. 161-168.

Pollard, D. D. and Johnson, A. M., 1973. Mechanics of growth of some laccolithic intrusions in the Henry Mountains, Utah; II, Bending and failure of overburden layers and sill formation: Tectonophysics, v. 18, p. 311-354.

Potter, D. K., and Stephenson, A., 1988. Single-domain particles in rocks and magnetic fabric analysis: Geophysical Research Letters, v. 15, p. 1097-1100.

Ramsay, J. G., 1989. Emplacement kinematics of a granite diapir: the Chindamora batholith, Zimbabwe: Journal of Structural Geology, v. 11, p. 191-209.

Rochette, P., 1994. Comment on "Magnetic fabrics, crystallographic preferred orientation, and strain of progressively deformed metamorphosed pelites in the Helvetic zone of the Central Alps (Quartenschiefer Formation)" by Carl Richter, Lothar Ratschbacher, and Wolfgang Frisch: Journal of Geophysical Research, v. 99, p. 21825-21827.

Rochette, P., Jackson, M., and Aubourg, C., 1992. Rock magnetism and the interpretation of anisotropy of magnetic susceptibility: Reviews of Geophysics, v. 30, p. 209-226.

Roman-Berdiel , T., Gapais, D., and Brun, J.P., 1995. Analogue models of laccolith formation: Journal of Structural Geology, v. 17, p. 1337-1346.

Rutter, E. H., 1997, The influence of deformation on the extraction of crustal melts: a consideration of the role of melt-assisted granular flow, *in* Holness, M., ed., Deformation-enhanced fluid transport in the earth's crust and mantle. The Mineralogical Society Series, v. 8: London, Chapman & Hall, p. 82-110.

Schmeling, H., Cruden, A. R., and Marquart, G., 1988. Finite deformation in and around a fluid sphere moving through a viscous medium: implications for diapiric ascent: Tectonophysics, v. 149, p. 17-34.

Shepley, K. A. B., 2000, Regional geophysical modelling and paleo-reconstruction in and around the Southern Slave Structural Province [M. Sc. Thesis]: Ottawa, Ottawa-Carleton Geoscience Centre, University of Ottawa, 130 p.

Spark, R., Benn, K., Bleeker, W., and Roest, W., 1999, Syn-D_2 plutonism in the southern Slave Province: evidence from magnetic fabrics and field mapping: Slave-Northern Cordillera Lithospheric Evolution Transect Meeting, University of Calgary, Lithoprobe report No. 69, p. 42-45.

Streckeisen, A., 1976. To each plutonic rock its proper name: Earth Science Reviews, v. 12, p. 1-33.

Tarling, D. H., and Hrouda, F., 1993, The magnetic anisotropy of rocks: London, Chapman & Hall, 217 p.

Thompson, P. H., 1978, Archean regional metamorphism in the Slave Structural Province--a new perspective on some old rocks, *in* Metamorphism in the Canadian Shield: Geological Survey of Canada Paper 78-10, p. 85-102.

Thompson, P. H., 1989, An empirical model for metamorphic evolution of the Archaean Slave Province and adjacent Thelon Tectonic Zone, northwestern Canadian Shield, *in* Daly, J. S., Cliff, R. A., and Yardley, B. W. D., eds., Evolution of metamorphic belts: Geological Society Special Publication (London) no. 43, p. 245-263.

van Breemen, O., Davis, W. J., and King, J. E., 1992. Temporal distribution of granitoid plutonic rocks in the Archean Slave Province, northwest Canadian Shield: Canadian Journal of Earth Sciences, v. 29, p. 2186-2199.

Waldron, J. W. F. and Bleeker, W., 1997, Late Archean turbidites and their tectonic setting in the southern Slave Province: Slave-Northern Cordillera Lithospheric Evolution Transect Meeting, University of Calgary, Lithoprobe report No. 56, p. 21-24.

Walker, R. G., 1992, Turbidites and submarine fans, *in* Walker, R. G., and James, N. P., eds., Facies models: response to sea level change: St. John's, Newfoundland, Geological Association of Canda, p. 239-263.

Weeterman, J., 1980. The stopping of a rising, liquid-filled crack in the Earth's crust by a freely slipping horizontal joint: Journal of Geophysical Research, v. 85(B2), 967-976.

Weinberg, R. F., 1996. The ascent of felsic magmas: news and views: Transactions of the Royal Society of Edinburgh: Earth Sciences, v. 87, p. 95-103.

APPENDIX I: AMS DATA

This appendix contains all the raw AMS data. Pages 166-177 gives the values of individual specimens for the Sparrow Pluton (sample numbers containing "sp") followed by the Prosperous Pluton (sample numbers containing "pr"). Pages 178-180 give site averages for both plutons. Following this, on pages 181-189, are the stereonets for individual sites. On the stereo nets squares are K1, triangles are K2, and circles are K3. Small symbols are for individual specimens and large symbols are the averages.

Specimen #	Av. Mean K	Normaled Principal Susceptibilities K1	K2	K3	Anisotropy Factors L	F	P	P'	T	q	Principal Directions K1 Azimuth	Plunge	Principal Directions K2 Azimuth	Plunge	Principal Directions K3 Azimuth	Plunge
96sp1a1	15.48	1.0239	1.0009	0.9751	1.023	1.026	1.05	1.05	0.057	0.617	123	21	234	44	16	39
96sp1a2	21.81	1.02	1.0162	0.9838	1.004	1.054	1.058	1.065	0.863	0.071	307	2	216	44	39	46
96sp1b1	17.25	1.0283	1.0026	0.9682	1.027	1.036	1.063	1.063	0.126	0.559	127	34	36	2	303	56
96sp1b2	14.12	1.0177	1.0043	0.9779	1.013	1.027	1.041	1.042	0.327	0.404	126	20	234	39	16	44
96sp1c1	13.39	1.0263	0.998	0.9756	1.028	1.023	1.052	1.052	-0.116	0.774	285	7	190	36	25	53
96sp1c2	13.65	1.203	0.9984	0.9813	1.022	1.017	1.04	1.04	-0.126	0.784	127	26	248	47	20	32
96sp2a1	12.69	1.0297	0.9955	0.9748	1.034	1.021	1.056	1.057	-0.244	0.903	118	6	212	38	20	51
96sp2a2	17.12	1.0206	0.9979	0.9815	1.023	1.017	1.04	1.04	-0.163	0.82	115	9	217	54	19	34
96sp2b1	19.95	1.034	1.0041	0.962	1.03	1.044	1.075	1.075	0.169	0.524	115	10	215	43	16	45
96sp2b2	21.56	1.0432	0.9968	0.98	1.047	1.038	1.087	1.087	-0.117	0.775	116	18	257	67	22	14
96sp2c1	17.21	1.0245	0.9961	0.9794	1.028	1.017	1.046	1.047	-0.258	0.918	111	9	209	40	11	49
96sp2c2	24.1	1.0207	1.0017	0.9776	1.019	1.025	1.044	1.044	0.116	0.567	262	11	56	78	171	5
96sp3a1	101.3	1.1383	1.0094	0.8523	1.128	1.184	1.336	1.337	0.098	0.582	318	1	227	28	50	62
96sp3a2	33.74	1.1965	1.1688	0.6347	1.024	1.842	1.885	2.052	0.901	0.051	351	54	120	25	222	25
96sp3b1	26.55	1.0046	1.0023	0.9931	1.002	1.009	1.012	1.012	0.595	0.225	152	2	244	34	58	55
96sp3b2	38.09	1.0026	1	0.9975	1.003	1.003	1.005	1.005	-0.025	0.689	309	18	207	32	63	52
96sp3c1	34.54	1.0096	1.0022	0.9883	1.007	1.014	1.022	1.022	0.304	0.422	132	0	223	56	42	34
96sp3c2	37.28	1.0051	0.9986	0.9963	1.007	1.002	1.009	1.009	-0.478	1.171	312	19	69	53	211	31
96sp4a1	14.96	1.017	1.0068	0.9762	1.01	1.031	1.042	1.044	0.5	0.286	302	0	212	49	32	41
96sp4a2	28.78	1.0314	1.0165	0.952	1.015	1.068	1.083	1.089	0.625	0.207	162	49	358	40	261	8
96sp4b1	19.46	1.0132	1.0084	0.9784	1.005	1.031	1.036	1.039	0.724	0.148	142	31	247	23	7	50
96sp4b2	26.33	1.0324	1.008	0.9598	1.024	1.05	1.076	1.077	0.33	0.403	132	20	223	3	321	70
96sp4c1	18.2	1.012	1.005	0.983	1.007	1.022	1.03	1.031	0.514	0.277	93	3	189	69	2	21
96sp4c2	25.04	1.012	1.0001	0.9879	1.012	1.012	1.024	1.024	0.016	0.652	131	44	280	42	205	16
96sp5a1	33.33	1.0627	0.9892	0.9481	1.074	1.043	1.121	1.122	-0.283	0.945	319	1	228	45	49	45
96sp5a2	21.03	1.0125	0.9995	0.988	1.013	1.012	1.025	1.025	-0.083	0.724	249	38	131	30	15	37
96sp5b1	42.88	1.0103	0.9987	0.9911	1.012	1.008	1.019	1.02	-0.208	0.866	129	38	320	52	223	5
96sp5b2	42.28	1.0116	0.9988	0.9895	1.013	1.009	1.022	1.022	-0.156	0.813	135	22	311	68	45	2
96sp6a1	20.47	1.0231	1.0034	0.9735	1.02	1.031	1.051	1.051	0.204	0.497	270	12	1	4	110	77
96sp6a2	25.23	1.0179	1.0001	0.982	1.018	1.018	1.037	1.037	0.008	0.659	276	6	17	62	183	27
96sp6b1	28.1	1.0144	0.9937	0.9919	1.021	1.002	1.023	1.025	-0.841	1.705	289	10	197	12	59	74
96sp6b2	31.22	1.0127	1.0006	0.9867	1.012	1.014	1.026	1.026	0.072	0.605	286	26	196	0	105	63
96sp7a1	53.34	1.0501	1.0142	0.9357	1.035	1.084	1.122	1.126	0.372	0.373	112	9	19	22	224	66
96sp7a2	73.14	1.0511	0.9987	0.9502	1.052	1.051	1.106	1.106	-0.038	0.701	113	13	17	25	229	62
96sp7b1	27.64	1.0443	0.9946	0.9612	1.05	1.035	1.086	1.087	-0.197	0.854	118	20	8	44	226	40
96sp7b2	27.74	1.0395	0.9943	0.9662	1.045	1.029	1.076	1.077	-0.233	0.891	118	19	11	39	228	44
96sp8a1	15.87	1.0165	0.9992	0.9851	1.017	1.014	1.031	1.031	-0.083	0.743	175	22	43	59	274	21
96sp8a2	25.82	1.0169	0.9963	0.9868	1.021	1.01	1.031	1.031	-0.372	1.044	143	9	236	16	26	71
96sp8b1	19.7	1.0232	1.0136	0.9632	1.009	1.052	1.062	1.067	0.68	0.174	98	8	190	12	337	75
96sp8b2	27.93	1.0419	0.9891	0.9691	1.053	1.021	1.075	1.076	-0.45	1.137	126	4	34	25	224	65
96sp9a1	34.83	1.0497	0.9847	0.9656	1.066	1.02	1.087	1.091	-0.547	1.261	141	4	237	58	48	32
96sp9a2	15.87	1.0554	0.9843	0.9603	1.072	1.025	1.099	1.103	-0.495	1.194	135	9	27	61	230	27
96sp9b1	90.94	1.052	0.9875	0.9606	1.065	1.028	1.095	1.098	-0.412	1.091	132	2	223	14	33	76
96sp9b2	22.82	1.0426	0.9896	0.9678	1.054	1.022	1.077	1.079	-0.418	1.099	322	3	231	24	58	65
96sp10a1	75.17	1.0428	1.001	0.9562	1.042	1.047	1.091	1.091	0.034	0.637	298	2	204	71	29	19
96sp10a2	54.76	1.0421	0.993	0.9649	1.049	1.029	1.08	1.081	-0.271	0.932	117	5	351	82	208	6
96sp10b1	30.88	1.0394	0.9824	0.9781	1.058	1.004	1.063	1.07	-0.859	1.736	131	4	223	30	34	60
96sp10b2	33.05	1.0429	0.985	0.9721	1.059	1.013	1.073	1.078	-0.636	1.384	122	6	221	55	28	35
96sp11a1	43.45	1.0291	0.9951	0.9758	1.034	1.02	1.055	1.055	-0.277	0.938	135	2	42	52	227	38
96sp11a2	46.28	1.0303	1.0065	0.9632	1.024	1.045	1.07	1.071	0.29	0.432	131	5	252	80	41	6
96sp11b1	52.99	1.0333	0.9946	0.9721	1.039	1.023	1.063	1.064	-0.285	0.925	304	6	38	31	205	58
96sp11b2	87.74	1.0343	0.996	0.9697	1.038	1.027	1.067	1.067	-0.185	0.842	122	4	218	49	29	40
96sp12a1	57.57	1.0381	0.9995	0.9624	1.039	1.039	1.079	1.079	-0.019	0.684	136	11	41	21	252	66
96sp12a2	63.29	1.0388	0.9969	0.9643	1.042	1.034	1.077	1.077	-0.123	0.781	134	12	39	23	251	64
96sp12b1	51.69	1.0262	1.0068	0.987	1.019	1.041	1.061	1.062	0.344	0.393	124	15	26	28	239	58

Specimen #	Av. Mean K	Normaled Principal Susceptibilities			Anisotropy Factors						Principal Directions K1		Principal Directions K2		Principal Directions K3	
		K1	K2	K3	L	F	P	P'	T	q	Azimuth	Plunge	Azimuth	Plunge	Azimuth	Plunge
96sp12b2	40.5	1.0405	1.0036	0.958	1.037	1.05	1.088	1.089	0.127	0.558	325	8	61	37	224	52
96sp13a1	55.69	1.0302	1.0058	0.964	1.024	1.043	1.069	1.07	0.281	0.453	299	2	207	38	32	51
96sp13a2	95.72	1.031	1.0084	0.9607	1.022	1.05	1.073	1.075	0.357	0.383	139	7	236	44	41	45
96sp13b1	46.69	1.0237	1.0146	0.9617	1.009	1.055	1.064	1.07	0.707	0.158	125	6	220	44	29	46
96sp13b2	47.03	1.022	1.0129	0.9651	1.009	1.049	1.059	1.063	0.68	0.174	143	21	250	38	31	45
96sp14a1	36.44	1.0378	0.9937	0.9684	1.044	1.026	1.072	1.072	-0.27	0.931	131	2	221	17	34	73
96sp14a2	39.47	1.0359	0.9919	0.9723	1.044	1.02	1.065	1.067	-0.384	1.058	310	4	219	14	56	76
96sp14b1	23.91	1.036	0.9995	0.9646	1.037	1.036	1.074	1.074	-0.023	0.687	116	3	206	8	7	81
96sp14b2	44.03	1.0366	0.9841	0.9792	1.053	1.005	1.059	1.065	-0.829	1.684	121	4	27	49	215	41
96sp15a1	37.14	1.0389	0.9971	0.9639	1.042	1.034	1.078	1.078	-0.115	0.773	309	2	216	60	40	30
96sp15a2	49.39	1.036	0.9996	0.9644	1.036	1.036	1.074	1.074	-0.017	0.681	316	2	219	72	47	18
96sp15b1	83.46	1.0485	0.9821	0.9694	1.068	1.013	1.082	1.088	-0.678	1.445	303	4	198	76	34	13
96sp15b2	69.31	1.0374	0.9867	0.9759	1.051	1.011	1.063	1.067	-0.648	1.401	121	2	218	75	31	15
96sp16a1	14.64	1.0535	0.9886	0.9579	1.066	1.032	1.1	1.102	-0.359	1.029	138	7	240	60	44	28
96sp16a2	14.09	1.0455	0.9819	0.9726	1.065	1.01	1.075	1.082	-0.746	1.55	133	1	228	76	43	13
96sp16b1	37.33	1.0296	0.9934	0.977	1.036	1.017	1.054	1.055	-0.377	1.05	143	9	265	73	51	14
96sp16b2	28.12	1.0515	0.9769	0.9715	1.076	1.006	1.082	1.092	-0.865	1.747	138	8	39	49	234	40
96sp17a1	15.8	1.048	0.9925	0.9595	1.056	1.034	1.092	1.093	-0.255	0.914	321	5	217	69	53	21
96sp17a2	18.52	1.0561	0.9895	0.9544	1.067	1.037	1.107	1.108	-0.31	0.974	135	1	226	40	45	50
96sp17b1	37.4	1.0392	0.9822	0.9787	1.058	1.004	1.062	1.07	-0.883	1.779	325	5	73	74	234	15
96sp17b2	33.18	1.0512	0.9901	0.9587	1.062	1.033	1.097	1.098	-0.322	0.988	328	0	238	21	58	69
96sp18a1	47.38	1.0332	0.9958	0.971	1.038	1.026	1.064	1.064	-0.203	0.86	299	5	205	33	37	56
96sp18a2	52.33	1.0382	0.991	0.9708	1.048	1.021	1.069	1.071	-0.402	1.079	295	2	204	28	29	62
96sp18b1	42.26	1.0367	0.9963	0.987	1.041	1.03	1.072	1.072	-0.16	0.817	305	2	214	18	40	72
96sp18b2	49.21	1.0389	1.0009	0.9601	1.038	1.042	1.082	1.082	0.035	0.636	298	2	207	29	31	61
96sp19a1	44.51	1.0181	0.992	0.9899	1.026	1.002	1.028	1.032	-0.85	1.721	134	0	224	36	44	54
96sp19a2	44.46	1.0209	0.9938	0.9853	1.027	1.009	1.036	1.038	-0.523	1.229	307	11	147	78	38	4
96sp19b1	33.95	1.02054	1.0001	0.9744	1.025	1.026	1.052	1.052	0.008	0.66	311	6	217	33	51	56
96sp19b2	21.3	1.0178	0.999	0.9833	1.019	1.016	1.035	1.035	-0.088	0.748	124	9	219	28	17	61
96sp20a1	12.77	1.0391	1.0121	0.9488	1.027	1.067	1.095	1.098	0.402	0.352	320	23	93	58	220	21
96sp20a2	9.07	1.0693	0.9969	0.9339	1.073	1.067	1.145	1.145	-0.069	0.729	131	8	357	78	222	8
96sp20b1	25.56	1.0383	0.9954	0.9663	1.043	1.03	1.074	1.075	-0.19	0.847	121	5	21	62	214	28
96sp20b2	22.54	1.0338	1.0038	96.24	1.03	1.043	1.074	1.075	0.16	0.532	306	12	168	74	38	11
96sp21a1	19.65	1.0146	1.0002	0.9853	1.014	1.015	1.03	1.03	0.019	0.65	291	10	191	44	30	44
96sp21a2	9.1	1.032	0.9893	0.9788	1.043	1.011	1.054	1.058	-0.604	1.339	202	77	303	3	34	12
96sp21b1	25.24	1.0235	1.0015	0.975	1.022	1.027	1.05	1.05	0.091	0.588	111	19	224	49	7	35
96sp21b2	35.33	1.0225	1.0097	0.9679	1.013	1.043	1.056	1.059	0.531	0.265	112	4	204	24	12	65
96sp22a1	32.43	1.0419	0.9852	0.9728	1.058	1.013	1.071	1.076	-0.64	1.39	118	5	207	4	334	84
96sp22a2	36.17	1.0273	0.9922	0.9805	1.035	1.012	1.048	1.05	-0.501	1.201	108	9	196	2	298	81
96sp22b1	27.04	1.0395	0.9953	0.9652	1.044	1.031	1.077	1.077	-0.191	0.848	94	8	191	44	356	45
96sp22b2	27.09	1.0223	0.997	0.9807	1.025	1.017	1.042	1.043	-0.217	0.874	97	5	354	69	189	21
96sp23a1	68.99	1.0269	0.9929	0.9802	1.034	1.013	1.048	1.049	-0.458	1.147	115	2	207	42	22	48
96sp23a2	75.38	1.0235	0.9904	0.9862	1.033	1.004	1.038	1.041	-0.775	1.595	122	1	21	86	212	4
96sp23b1	37.69	1.0355	1.0021	0.9624	1.033	1.041	1.076	1.076	0.086	0.592	127	8	222	33	24	56
96sp23b2	44.03	1.0392	0.9932	0.9576	1.046	1.026	1.074	1.075	-0.285	0.946	136	8	232	38	35	51
96sp24a1	17.69	1.0429	1.0074	0.9497	1.035	1.061	1.098	1.099	0.238	0.471	144	7	240	39	45	50
96sp24a2	19	1.0356	1.0048	0.9596	1.031	1.047	1.079	1.08	0.189	0.508	150	13	251	39	45	48
96sp24b1	14.5	1.0138	1.0022	0.984	1.012	1.018	1.03	1.03	0.218	0.486	303	3	197	70	34	11
96sp24b2	22.36	1.0374	0.9972	0.9654	1.04	1.033	1.075	1.075	-0.115	0.773	151	24	251	21	18	57
96sp25a1	46.02	1.0148	0.9956	0.9896	1.019	1.006	1.026	1.027	-0.526	1.233	336	12	246	1	151	78
96sp25a2	43.01	1.017	0.9964	0.9866	1.021	1.1	1.031	1.031	-0.354	1.024	344	13	254	1	162	77
96sp25b1	55.72	1.0161	1.0061	0.9778	1.01	1.029	1.039	1.041	0.477	0.301	149	3	241	35	54	54
96sp25b2	59.58	1.0138	1.0023	0.9839	1.012	1.019	1.03	1.031	0.229	0.477	347	16	238	49	90	36

Specimen #	Av. Mean K	Normaled Principal Susceptibilities K1	K2	K3	Anisotropy Factors L	F	P	P'	T	q	Principal Directions K1 Azimuth	Plunge	Principal Directions K2 Azimuth	Plunge	Principal Directions K3 Azimuth	Plunge
96sp26a1	49.35	1.0508	0.9869	0.9624	1.065	1.025	1.092	1.095	-0.466	1.133	310	3	41	29	214	61
96sp26a2	57.22	1.0478	0.9828	0.9694	1.066	1.014	1.081	1.087	-0.658	1.416	309	0	39	28	218	62
96sp26b1	52.99	1.0474	0.9814	0.9712	1.067	1.01	1.078	1.085	-0.734	1.531	321	8	66	61	227	28
96sp26b2	54.38	1.0469	0.982	0.9721	1.065	1.01	1.076	1.083	-0.732	1.528	321	2	54	46	229	44
96sp27a1	47.02	1.0492	0.9934	0.9574	1.056	1.038	1.096	1.097	-0.216	0.874	138	17	235	22	14	61
96sp27a2	49.12	1.0481	0.989	0.9629	1.06	1.027	1.088	1.09	-0.386	1.061	140	23	237	15	357	62
96sp27b1	58.34	1.0401	0.9988	0.9611	1.041	1.039	1.082	1.082	-0.045	0.707	131	16	228	24	10	60
96sp27b2	65.69	1.032	1.0007	0.9673	1.031	1.035	1.067	1.067	0.033	0.637	131	18	228	20	3	63
96sp28a1	37.25	1.0245	1.0095	0.9661	1.015	1.045	1.06	1.063	0.487	0.294	188	61	293	8	27	27
96sp28a2	41.21	1.0249	1.0031	0.972	1.022	1.032	1.054	1.055	0.175	0.52	212	63	112	5	20	26
96sp28b1	37.66	1.021	1.018	0.961	1.003	1.059	1.062	1.071	0.899	0.052	124	20	238	48	19	35
96sp28b2	47.67	1.028	1.0108	0.9612	1.017	1.052	1.069	1.072	0.487	0.294	132	39	249	30	5	37
96sp29a1	26.03	1.0384	1.013	0.9486	1.025	1.068	1.095	1.098	0.433	0.33	184	11	278	18	64	69
96sp29a2	22.94	1.064	1.0061	0.9575	1.03	1.051	1.082	1.083	0.234	0.474	203	5	293	2	42	84
96sp29b1	21.39	1.0451	0.998	0.9569	1.047	1.043	1.092	1.092	-0.069	0.729	32	5	301	10	148	79
96sp29b2	31.36	1.0439	1.0227	0.9335	1.021	1.096	1.118	1.126	0.615	0.213	19	5	288	8	138	81
96sp30a1	30.56	1.0142	1.0008	0.9851	1.013	1.016	1.03	1.03	0.078	0.599	353	3	253	64	85	26
96sp30a2	49.91	1.011	0.9999	0.9892	1.011	1.011	1.022	1.022	-0.017	0.682	312	41	196	26	84	38
96sp30b1	29.59	1.0131	0.9964	0.9905	1.017	1.006	1.023	1.024	-0.473	1.166	146	13	346	76	237	5
96sp30b2	46.33	1.0111	1.0052	0.9837	1.006	1.022	1.028	1.029	0.57	0.24	325	1	234	52	55	38
96sp31a1	61.07	1.0102	0.9978	0.992	1.012	1.006	1.018	1.019	-0.355	1.025	342	25	110	53	239	26
96sp31a2	68.91	1.0067	1.0009	0.9924	1.006	1.009	1.014	1.015	0.192	0.506	329	7	69	54	235	35
96sp31b1	55.32	1.0128	1.0033	0.9839	1.01	1.02	1.029	1.03	0.339	0.396	348	25	94	31	227	49
96sp31b2	63.47	1.0113	1.0006	0.988	1.011	1.013	1.024	1.024	0.083	0.595	343	19	95	47	238	36
96sp32a1	54.16	1.0217	0.9987	0.9795	1.023	1.02	1.043	1.043	-0.09	0.749	26	26	137	36	269	43
96sp32a2	55.17	1.0254	1.0026	0.9721	1.023	1.031	1.055	1.055	0.145	0.544	32	36	153	36	273	34
96sp32b1	53.04	1.0214	1.0023	0.9763	1.019	1.027	1.046	1.046	0.154	0.536	11	27	257	38	126	39
96sp32b2	61.38	1.0239	1.0025	0.9736	1.021	1.03	1.052	1.052	0.147	0.542	8	21	258	42	118	41
96sp33a1	45.93	1.016	0.9967	0.9873	1.019	1.01	1.029	1.03	-0.343	1.011	171	18	76	17	304	65
96sp33a2	41.96	1.0179	0.9964	0.9857	1.022	1.011	1.033	1.033	-0.336	1.033	173	15	268	18	46	66
96sp33b1	39.52	1.0233	0.9936	0.9831	1.03	1.011	1.041	1.042	-0.478	1.172	339	1	243	83	69	7
96sp33b2	46.11	1.0269	1.0078	0.9653	1.019	1.044	1.064	1.065	0.382	0.365	159	12	302	75	67	9
96sp34a1	50.45	1.0255	1.011	0.9635	1.014	1.049	1.064	1.068	0.531	0.266	350	20	224	58	59	24
96sp34a2	46.79	1.0242	1.0071	0.9687	1.017	1.04	1.057	1.059	0.385	0.363	340	18	230	46	85	38
96sp34b1	46.65	1.018	1.0067	0.9753	1.011	1.032	1.044	1.045	0.473	0.304	150	25	37	40	263	39
96sp34b2	51.18	1.018	1.0031	0.979	1.015	1.025	1.04	1.04	0.238	0.471	149	23	24	54	251	27
96sp35a1	60.54	1.021	1.0098	0.9692	1.011	1.042	1.053	1.056	0.566	0.243	168	17	260	7	13	71
96sp35a2	63.6	1.02	1.014	0.966	1.006	1.05	1.056	1.061	0.78	0.116	180	16	271	2	9	74
96sp35b1	55.69	1.0161	1.005	0.9789	1.011	1.027	1.038	1.039	0.402	0.351	200	21	99	26	323	55
96sp35b2	65.65	1.0137	0.9978	0.9886	1.016	1.009	1.025	1.026	-0.269	0.929	193	17	101	8	348	71
96sp36a1	40.61	1.0216	1.0012	0.9773	1.02	1.024	1.045	1.045	0.078	0.599	134	58	323	32	231	4
96sp36a2	47.75	1.0201	1.0094	0.9705	1.011	1.04	1.051	1.054	0.568	0.242	137	52	337	36	240	10
96sp36b1	37.11	1.0166	0.9992	0.9842	1.017	1.015	1.033	1.033	-0.072	0.732	164	34	17	51	265	17
96sp36b2	33.8	1.0152	1.0028	0.982	1.012	1.021	1.034	1.034	0.251	0.461	148	25	12	57	247	20
96sp37a1	51.96	1.031	1.0056	0.9631	1.025	1.044	1.071	1.071	0.258	0.455	351	12	93	43	249	45
96sp37a2	48.15	1.0299	0.9957	0.9744	1.034	1.022	1.057	1.057	-0.234	0.893	4	33	116	31	239	42
96sp37b1	26.82	1.0224	1.0106	0.9668	1.012	1.046	1.058	1.061	0.582	0.233	152	6	54	51	247	38
96sp37b2	37.34	1.0225	1.0109	0.9666	1.012	1.046	1.058	1.061	0.583	0.233	11	36	133	36	252	34
96sp38a1	42.13	1.0189	1.0019	0.9792	1.017	1.023	1.041	1.041	0.147	0.542	353	12	131	74	261	11
96sp38a2	55.13	1.019	1.001	0.98	1.018	1.021	1.04	1.04	0.074	0.602	175	3	79	68	266	22
96sp38b1	32.85	1.008	1.0049	0.9871	1.003	1.018	1.021	1.023	0.704	0.16	138	15	352	72	231	10
96sp38b2	56.26	1.0132	0.997	0.9898	1.016	1.037	1.024	1.024	-0.381	1.054	320	15	112	74	228	7

Specimen #	Av. Mean K	Normaled Principal Susceptibilities K1	K2	K3	Anisotropy Factors L	F	P	P'	T	q	Principal Directions K1 Azimuth	Plunge	Principal Directions K2 Azimuth	Plunge	Principal Directions K3 Azimuth	Plunge
96sp39a1	31.52	1.0252	1.0177	0.9571	1.007	1.063	1.071	1.078	0.779	0.117	348	46	125	35	232	22
96sp39b1	44.73	1.0168	1.0098	0.9734	1.007	1.037	1.045	1.048	0.88	0.174	145	16	9	68	240	14
96sp39b2	49.96	1.0148	1.0131	0.9721	1.002	1.042	1.044	1.05	0.921	0.04	152	11	35	66	246	21
96sp39c1	32.25	1.0202	1.0021	0.9777	1.018	1.025	1.044	1.044	0.15	0.54	17	29	131	37	259	39
96sp40a1	45.66	1.0467	0.9886	0.9646	1.059	1.025	1.085	1.087	-0.415	1.095	143	10	264	71	51	16
96sp40a2	52.99	1.0485	0.9861	0.9654	1.063	1.021	1.086	1.09	-0.502	1.202	144	9	295	80	54	5
96sp40b1	57.83	1.0379	0.9915	0.9706	1.047	1.021	1.069	1.071	-0.379	1.053	151	11	45	55	249	32
96sp40b2	62.77	1.0393	0.9931	0.9676	1.047	1.026	1.074	1.075	-0.289	0.951	153	14	39	60	250	26
96sp41a1	70.92	1.022	1.0053	0.9727	1.017	1.034	1.051	1.052	0.322	0.408	168	13	258	1	351	77
96sp40a2	61.95	1.023	1.0042	0.9727	1.019	1.032	1.052	1.052	0.252	0.46	171	17	263	4	5	73
96sp41b1	59.47	1.0189	1.0021	0.979	1.017	1.024	1.041	1.041	0.154	0.536	177	14	268	5	16	75
96sp41b2	59.05	1.0275	1.0036	0.9689	1.024	1.036	1.061	1.061	0.182	0.514	186	6	276	2	22	84
96sp42a1	79.18	1.0147	1.0038	0.9815	1.011	1.023	1.034	1.034	0.347	0.39	118	56	15	9	279	33
96sp42a2	66.52	1.0142	1.0059	0.9798	1.008	1.027	1.035	1.037	0.517	0.275	144	35	37	22	281	47
96sp42b1	58.18	1.0168	1.002	0.9812	1.015	1.021	1.036	1.036	0.17	0.524	144	34	27	34	265	38
96sp42b2	60.6	1.0121	1.0073	0.9808	1.005	1.027	1.032	1.035	0.693	0.166	142	34	24	35	262	37
96sp43a1	63.49	1.0077	0.998	0.9943	1.01	1.004	1.013	1.014	-0.448	1.134	38	36	191	51	298	13
96sp43a2	66.5	1.0091	0.9991	0.9917	1.01	1.007	1.018	1.018	-0.147	0.804	59	26	173	40	305	39
96sp43b1	65.78	1.0161	0.9964	0.9875	1.02	1.009	1.029	1.03	-0.376	1.049	61	53	318	10	221	35
96sp43b2	70.08	1.0078	0.9986	0.9936	1.009	1.005	1.014	1.015	-0.299	0.962	49	47	140	2	232	43
96sp44a1	52.21	1.043	0.9921	0.9649	1.051	1.028	1.081	1.082	-0.304	0.968	160	7	67	16	273	72
96sp44a2	52.2	1.0465	0.9927	0.9608	1.054	1.033	1.089	1.09	-0.257	0.916	165	6	72	23	268	66
96sp44b1	53.88	1.0367	0.9976	0.9658	1.039	1.033	1.073	1.074	-0.103	0.762	163	7	70	25	268	64
96sp44b2	73.49	1.0398	0.9976	0.9626	1.042	1.036	1.08	1.08	-0.094	0.752	161	11	68	19	280	68
96sp45a1	62.45	1.0434	0.992	0.9647	1.052	1.028	1.082	1.083	-0.306	0.97	328	1	56	18	233	72
96sp45a2	63.69	1.0399	0.9933	0.9669	1.047	1.027	1.075	1.076	-0.277	0.938	148	2	58	6	251	84
96sp45b1	54.91	1.0409	0.9871	0.972	1.055	1.016	1.071	1.075	-0.581	1.281	327	1	237	19	60	71
96sp45b2	57.2	1.0394	0.9919	0.9686	1.048	1.024	1.073	1.074	-0.341	1.009	149	1	240	12	55	78
96sp46a1	67.91	1.0353	1.092	0.9554	1.026	1.056	1.084	1.086	0.347	0.39	336	14	78	43	232	43
96sp46a2	74.84	1.0383	1.0062	0.9555	1.032	1.053	1.087	1.088	0.224	0.482	336	5	71	42	240	48
96sp46b1	82.48	1.0252	1.0054	0.9593	1.03	1.048	1.079	1.08	0.212	0.491	177	4	84	37	273	53
96sp46b2	80.15	1.0326	1.007	0.9604	1.025	1.049	1.075	1.076	0.291	0.431	180	6	85	42	276	48
96sp47a1	76.48	1.0156	0.9946	0.9899	1.021	1.005	1.026	1.028	-0.632	1.378	171	4	265	38	76	51
96sp47a2	66.93	1.0185	0.9974	0.9841	1.021	1.014	1.035	1.035	-0.226	0.884	347	1	78	58	256	32
96sp47b1	92.8	1.0245	1.0035	0.9721	1.021	1.032	1.054	1.054	0.198	0.502	144	18	235	4	336	72
96sp47b2	71.59	1.0207	0.9918	0.9875	1.029	1.004	1.034	1.037	-0.741	1.542	142	0	232	53	52	37
96sp48a1	33.44	1.0206	1.0081	0.9712	1.012	1.038	1.051	1.053	0.495	0.289	343	19	137	69	250	9
96sp48a2	43.12	1.0174	1.0097	0.9729	1.008	1.038	1.046	1.049	0.652	0.19	160	3	63	70	251	20
96sp48b1	50.28	1.0231	1.0058	0.9711	1.017	1.036	1.054	1.055	0.335	0.399	101	38	5	8	265	51
96sp48b2	70.49	1.0247	1.0076	0.9677	1.017	1.041	1.059	1.061	0.398	0.354	7	6	103	43	270	47
96sp49a1	55.96	1.0409	1.0216	0.9375	1.019	1.09	1.11	1.118	0.627	0.206	32	36	151	33	270	37
96sp49a2	53.89	1.0424	1.02	0.9376	1.022	1.088	1.112	1.118	0.573	0.239	66	47	171	14	273	40
96sp49b1	58.17	1.0418	1.0224	0.9358	1.019	1.093	1.113	1.121	0.634	0.202	63	53	167	11	265	35
96sp49b2	51.41	1.0331	1.0175	0.9494	1.015	1.072	1.088	1.094	0.628	0.205	97	53	359	6	265	36
96sp50a1	58.36	1.0176	0.9977	0.9847	1.02	1.013	1.033	1.034	-0.212	0.869	155	4	65	6	278	83
96sp50a2	53.65	1.0171	0.999	0.9839	1.018	1.015	1.034	1.034	-0.091	0.75	293	17	194	28	50	56
96sp50b1	39.37	1.0187	0.9935	0.9878	1.025	1.006	1.031	1.033	-0.632	1.378	141	10	234	17	20	70
96sp50b2	35.05	1.0274	0.9997	0.9729	1.028	1.028	1.056	1.056	-0.018	0.683	151	17	14	67	246	15
96sp51a1	36.3	1.0304	0.9932	0.9764	1.037	1.017	1.055	1.057	-0.378	1.051	12	20	240	61	109	20
96sp51a2	35.43	1.029	0.9996	0.9714	1.029	1.029	1.059	1.059	-0.018	0.683	15	27	164	59	278	13
96sp51b1	57.56	1.0272	0.9921	0.9807	1.035	1.012	1.047	1.049	-0.507	1.209	4	14	111	50	263	37
96sp51b2	60.24	1.024	0.996	0.9801	1.028	1.016	1.045	1.045	-0.276	0.937	3	16	124	60	266	25
96sp52a1	50.55	1.0173	1.0005	0.9823	1.017	1.019	1.036	1.036	0.04	0.631	189	13	91	31	299	56

Specimen #	Av. Mean K	Normaled Principal Susceptibilities K1	K2	K3	Anisotropy Factors L	F	P	P'	T	q	Principal Directions K1 Azimuth	Plunge	Principal Directions K2 Azimuth	Plunge	Principal Directions K3 Azimuth	Plunge
96sp52a2	49.78	1.021	1.0007	0.9783	1.02	1.023	1.044	1.044	0.047	0.625	196	11	98	31	303	56
96sp52b1	55.29	1.024	0.9999	0.9761	1.024	1.024	1.049	1.049	-0.004	0.67	11	4	105	42	277	48
96sp52b2	47.62	1.0194	1.0024	0.9782	1.017	1.025	1.042	1.042	0.173	0.522	182	1	91	50	273	40
96sp53a1	44.39	1.0508	0.9894	0.9598	1.052	1.031	1.095	1.097	-0.35	1.019	161	6	254	26	59	64
96sp53a2	48.68	1.0571	0.9909	0.952	1.067	1.041	1.11	1.111	-0.259	0.919	158	6	253	35	59	54
96sp53b1	49.35	1.0386	0.9914	0.97	1.048	1.022	1.071	1.072	-0.375	1.048	162	12	259	30	53	57
96sp53b2	49.36	1.0488	0.9859	0.9652	1.064	1.021	1.087	1.09	-0.504	1.205	166	7	261	34	66	55
96sp54a1	47.26	1.0231	1.0015	0.9754	1.022	1.027	1.049	1.049	0.095	0.585	107	71	10	3	279	19
96sp54a2	49.07	1.0114	1.0033	0.9853	1.008	1.016	1.027	1.027	0.376	0.37	137	70	352	16	259	11
96sp54b1	53.81	1.019	1.0106	0.9704	1.008	1.041	1.05	1.054	0.653	0.19	170	58	356	32	265	3
96sp54b2	47.3	1.015	1.0106	0.9744	1.004	1.037	1.042	1.046	0.782	0.115	181	7	72	60	273	19
96sp55a1	64.75	1.0329	0.9865	0.9806	1.047	1.006	1.053	1.059	-0.772	1.591	360	7	145	81	269	5
96sp55a2	47.62	1.0274	0.9991	0.9735	1.028	1.026	1.055	1.055	-0.052	0.713	178	7	71	66	271	22
96sp55b1	57.53	1.0298	1.0008	0.9694	1.029	1.032	1.062	1.062	0.04	0.631	168	2	74	62	259	28
96sp55b2	52.2	1.0297	1.0074	0.9629	1.022	1.046	1.069	1.071	0.33	0.402	167	2	69	77	258	13
96sp56a1	34.72	1.0268	0.9878	0.9853	1.039	1.003	1.042	1.047	-0.88	1.773	164	32	284	38	47	35
96sp56a2	33.59	1.0224	0.9964	0.9812	1.026	1.015	1.042	1.042	-0.263	0.922	161	6	257	49	66	40
96sp56b1	53.56	1.0405	1.0009	0.9587	1.04	1.044	1.085	1.085	0.031	0.639	162	15	260	27	47	59
96sp56b2	53.26	1.0375	0.9973	0.9652	1.04	1.033	1.075	1.075	-0.113	0.771	169	11	264	28	60	60
96sp57a1	54.22	1.0343	0.9962	0.9695	1.038	1.028	1.067	1.067	-0.176	0.833	179	24	25	64	273	10
96sp57a2	52.44	1.0385	0.9931	0.9684	1.046	1.026	1.072	1.073	-0.295	0.958	175	21	333	67	82	8
96sp57b1	63.99	1.0309	0.9894	0.9797	1.042	1.01	1.052	1.055	-0.621	1.363	171	17	321	70	78	9
96sp57b2	56.1	1.0236	0.9947	0.9816	1.029	1.013	1.043	1.044	-0.375	1.048	174	13	320	74	82	9
96sp58a1	49.33	1.0323	1.0046	0.9631	1.028	1.043	1.072	1.02	0.199	0.501	137	49	5	30	259	25
96sp58a2	41.11	1.0313	1.0006	0.9681	1.031	1.034	1.065	1.065	0.03	0.64	156	49	14	34	270	19
96sp58b1	41.33	1.0275	0.9998	0.9726	1.028	1.028	1.056	1.056	-0.009	0.674	158	4	62	56	251	34
96sp58b2	41.13	1.0339	1.0084	0.9577	1.025	1.053	1.08	1.081	0.331	0.402	153	15	38	60	250	26
96sp59a1	74.76	1.028	0.999	0.972	1.03	1.028	1.059	1.059	-0.052	0.714	325	3	56	1	163	86
96sp59a2	71.08	1.029	0.9985	0.9725	1.031	1.027	1.058	1.056	-0.079	0.739	320	5	230	1	125	84
96sp59b1	58.29	1.0299	0.9879	0.9822	1.043	1.006	1.049	1.053	-0.765	1.579	340	9	70	2	174	81
96sp59b2	68.08	1.0247	0.9971	0.9781	1.028	1.019	1.048	1.048	-0.183	0.84	337	9	68	6	169	79
96sp60a1	102.9	1.0327	0.9987	0.9686	1.034	1.031	1.066	1.066	-0.061	0.722	358	5	91	28	258	61
96sp60a2	113.9	1.03	0.9996	0.9704	1.03	1.03	1.061	1.061	-0.021	0.686	353	8	88	34	252	55
96sp60b1	85.03	1.0317	0.9925	0.9758	1.04	1.017	1.057	1.059	-0.403	1.08	357	7	92	36	258	53
96sp60b2	88.25	1.0274	0.9954	0.9771	1.032	1.019	1.051	1.052	-0.274	0.934	354	10	94	45	254	43
96sp61a1	51.59	1.0275	0.9937	0.9789	1.034	1.015	1.05	1.051	-0.392	1.067	165	42	313	44	60	16
96sp61a2	48.96	1.0253	1.0037	0.9711	1.022	1.034	1.056	1.056	0.203	0.498	156	33	315	55	59	10
96sp61b1	53.3	1.0192	1.0057	0.9751	1.013	1.031	1.045	1.046	0.368	0.361	154	31	287	49	48	25
96sp61b2	49.42	1.0237	1.0064	0.9699	1.017	1.038	1.055	1.057	0.359	3.82	154	25	304	62	58	12
96sp62a1	41.98	1.0251	0.9995	0.9754	1.026	1.025	1.051	1.051	-0.031	0.694	132	11	237	52	34	35
96sp62a2	53.97	1.0301	0.9887	0.9812	1.042	1.008	1.05	1.054	-0.693	1.468	139	11	239	42	37	46
96sp62b1	41.07	1.0148	0.9942	0.9909	1.021	1.003	1.024	1.026	-0.723	1.513	160	14	250	0	341	76
96sp62b2	61.03	1.0252	0.9921	0.9827	1.033	1.009	1.043	1.045	-0.562	1.281	140	10	241	44	41	44
96sp63a1	64.93	1.0402	0.9873	0.9725	1.054	1.015	1.07	1.073	-0.562	1.282	337	6	69	15	228	74
96sp63a2	71.45	1.0369	0.9923	0.9708	1.045	1.022	1.068	1.069	-0.352	1.021	339	2	248	24	74	66
96sp63b1	70.89	1.0425	0.9927	0.9648	1.05	1.029	1.081	1.082	-0.28	0.942	149	1	242	61	58	29
96sp63b2	64.46	1.0427	0.9911	0.9662	1.052	1.026	1.079	1.081	-0.347	1.016	329	1	238	39	61	51
96sp64a1	44.49	1.0286	1.009	0.9624	1.019	1.048	1.069	1.071	0.409	0.347	336	2	70	61	245	29
96sp64a2	46.85	1.0295	1.012	0.9585	1.017	1.056	1.074	1.077	0.505	0.282	155	7	53	58	249	31
96sp64b1	54.26	1.0296	0.9979	0.9725	1.032	1.026	1.059	1.059	-0.109	0.767	344	11	87	49	245	38
96sp64b2	57.54	1.0289	1.0001	0.9711	1.029	1.03	1.06	1.06	0.004	0.663	333	3	67	55	240	35
96sp65a1	58.07	1.014	1.0069	0.9791	1.007	1.028	1.036	1.036	0.596	0.225	175	10	82	18	292	70
96sp65a2	55.04	1.0142	1.0042	0.9816	1.01	1.023	1.033	1.034	0.391	0.359	148	18	55	7	304	71

Specimen #	Av. Mean K	Normaled Principal Susceptibilities K1	K2	K3	Anisotropy Factors L	F	P	P'	T	q	Principal Directions K1 Azimuth	Plunge	Principal Directions K2 Azimuth	Plunge	Principal Directions K3 Azimuth	Plunge
96sp65b1	54.08	1.0263	1.0006	0.9731	1.026	1.028	1.055	1.055	0.037	0.635	138	19	229	1	323	71
96sp65b2	50.96	1.0282	0.9927	0.9791	1.036	1.014	1.05	1.052	-0.449	1.135	144	8	52	13	264	75
96sp66a1	23.11	1.0428	0.9938	0.9634	1.049	1.032	1.082	1.083	-0.234	0.892	136	4	241	74	45	15
96sp66a2	36.57	1.0499	0.9901	0.96	1.06	1.031	1.094	1.095	-0.332	0.998	135	3	225	7	21	82
96sp66b1	65.55	1.0461	0.9822	0.9716	1.065	1.011	1.077	1.083	-0.715	1.502	134	5	225	11	21	77
96sp66b2	32.59	1.0493	0.9936	0.9571	1.056	1.038	1.096	1.097	-0.207	0.864	128	11	230	48	29	40
96sp67a1	31.26	1.0568	0.9827	0.9605	1.075	1.023	1.1	1.105	-0.54	1.252	122	6	233	74	30	15
96sp67a2	34.18	1.0474	0.9903	0.9624	1.058	1.029	1.088	1.09	-0.343	1.011	125	3	222	65	34	25
96sp67b1	21.31	1.0465	0.9911	0.9624	1.056	1.03	1.087	1.089	-0.318	0.982	308	1	214	83	38	7
96sp67b2	20.12	1.0564	0.9786	0.9649	1.079	1.014	1.095	1.102	-0.7	1.479	130	6	261	81	39	4
96sp68a1	40.51	1.053	0.9854	0.9616	1.069	1.025	1.095	1.099	-0.479	1.174	146	2	55	8	248	82
96sp68a2	49.35	1.052	0.9849	0.9631	1.068	1.023	1.092	1.096	-0.51	1.213	147	3	55	19	247	71
96sp68b1	23	1.0499	0.9888	0.9613	1.062	1.029	1.092	1.094	-0.38	1.053	150	7	242	18	38	71
96sp68b2	22.68	1.0641	0.9853	0.9506	1.08	1.036	1.119	1.122	-0.39	1.065	143	3	233	2	359	86
97pr1a1	64.77	1.0319	1.0115	0.9566	1.02	1.057	1.079	1.082	0.457	0.314	320	13	224	27	73	60
97pr1a2	67.64	1.0289	1.0077	0.9634	1.021	1.046	1.068	1.07	0.351	0.387	325	10	227	34	69	54
97pr1b1	62.82	1.0355	1.0122	0.9523	1.023	1.063	1.087	1.09	0.439	0.326	326	2	235	36	60	54
97pr1b2	67.65	1.0275	1.0083	0.9642	1.019	1.046	1.066	1.068	0.391	0.359	329	1	238	38	60	52
97pr2a1	60.64	1.0385	0.9987	0.9628	1.04	1.037	1.079	1.079	-0.05	0.712	333	1	243	15	67	75
97pr2a2	63.53	1.0362	0.9978	0.9661	1.038	1.033	1.073	1.073	-0.096	0.755	333	3	242	14	73	76
97pr2b1	57.56	1.0375	1.0051	0.9574	1.032	1.05	1.084	1.084	0.191	0.507	328	3	237	26	65	64
97pr2b2	73.3	1.0396	0.9889	0.9715	1.051	1.018	1.07	1.073	-0.488	1.185	346	14	249	24	103	62
97pr3a1	70.6	1.0331	1.0081	0.9588	1.025	1.052	1.078	1.079	0.329	0.403	334	0	244	39	65	51
97pr3a2	58.47	1.0382	1.0102	0.9516	1.028	1.062	1.091	1.093	0.352	0.387	155	1	245	33	63	57
97pr3b1	71.18	1.0327	1.0077	0.9596	1.025	1.05	1.076	1.078	0.317	0.412	155	0	245	43	64	47
97pr3b2	59.18	1.0363	1.0113	0.9524	1.025	1.062	1.088	1.091	0.404	0.35	330	1	239	36	62	54
97pr4a1	63.72	1.0263	1.0105	0.9632	1.016	1.049	1.066	1.068	0.498	0.267	331	11	238	15	97	71
97pr4a2	68.66	1.0239	1.0109	0.9652	1.013	1.047	1.061	1.064	0.554	0.251	326	11	232	15	91	71
97pr4b1	85.17	1.0295	1.0039	0.9666	1.025	1.039	1.065	1.066	0.187	0.51	346	8	253	18	100	70
97pr4b2	105.1	1.0305	1.0026	0.967	1.028	1.037	1.066	1.066	0.121	0.563	346	13	250	25	102	61
97pr5a1	57.08	1.0375	0.9943	0.9682	1.043	1.027	1.072	1.072	-0.246	0.904	321	6	231	7	90	81
97pr5a2	52.46	1.0384	0.9946	0.9669	1.044	1.029	1.074	1.074	-0.22	0.877	321	8	230	8	96	79
97pr5b1	52.4	1.0311	1.0017	0.9673	1.029	1.036	1.066	1.066	0.078	0.599	325	10	232	11	97	75
97pr5b2	54.58	1.0316	1.011	0.9673	1.03	1.035	1.066	1.067	0.052	0.622	322	11	226	20	80	67
97pr6a1	30.41	1.0026	1.0011	0.9964	1.001	1.005	1.006	1.066	0.518	0.274	238	28	6	50	133	27
97pr6a2	40.72	1.0173	1.0085	0.9742	1.009	1.035	1.044	1.047	0.594	0.226	0	12	223	74	92	11
97pr6b1	15.32	1.0072	0.9985	0.9944	1.009	1.004	1.013	1.013	-0.361	1.031	261	16	81	74	171	0
97pr6b2	14.2	1.0107	0.9999	0.9894	1.011	1.011	1.022	1.022	-0.017	0.681	285	0	194	43	15	47
97pr7a1	41.24	1.06	1.0092	0.9307	1.05	1.084	1.139	1.14	0.214	0.489	323	19	122	70	231	7
97pr7a2	47.06	1.0506	1.001	0.9484	1.05	1.055	1.108	1.108	0.03	0.641	321	18	153	72	52	4
97pr7b1	40.848	1.064	0.9972	0.9388	1.067	1.062	1.133	1.133	-0.066	0.727	321	17	102	68	227	13
97pr7b2	39.43	1.0683	0.9957	0.936	1.073	1.064	1.141	1.141	-0.097	0.756	324	15	99	69	230	14
97pr8a1	60.24	1.0167	1	0.9833	1.017	1.017	1.034	1.034	-0.003	0.67	289	34	23	6	122	55
97pe8a2	53.36	1.009	1.0023	0.9887	1.007	1.014	1.021	1.021	0.338	0.397	264	31	1	11	109	56
97pr8b1	66.53	1.0129	0.9955	0.9916	1.018	1.004	1.022	1.023	-0.636	1.387	96	28	222	48	349	28
97pr8b2	58.63	1.0087	1	0.9912	1.009	1.009	1.018	1.018	0.002	0.665	98	23	0	19	235	60
97pr9a1	55.59	1.0227	1.0037	0.9737	1.019	1.031	1.05	1.051	0.226	0.48	162	18	266	35	51	49
97pr9a2	53.54	1.0234	1.0073	0.9694	1.016	1.039	1.056	1.057	0.403	0.351	169	16	270	34	58	52
97pr9b1	45.81	1.0232	1.0081	0.9687	1.015	1.041	1.056	1.056	0.444	0.323	224	28	321	14	74	58
97pr9b2	59.14	1.0211	1.0071	0.9718	1.014	1.036	1.051	1.052	0.431	0.331	234	28	332	15	87	57
97pr10a1	65.15	1.0192	0.9975	0.9833	1.022	1.014	1.036	1.037	-0.212	0.87	320	21	210	42	69	41

Specimen #	Av. Mean K	Normaled Principal Susceptibilities K1	K2	K3	Anisotropy Factors L	F	P	P'	T	q	Principal Directions K1 Azimuth	Plunge	Principal Directions K2 Azimuth	Plunge	Principal Directions K3 Azimuth	Plunge
97pr10a2	67.65	1.0229	0.9935	0.9837	1.03	1.01	1.04	1.042	-0.5	1.2	320	28	202	43	72	35
97pr10b1	61.29	1.0146	1.002	0.9834	1.013	1.019	1.032	1.032	0.194	0.505	311	31	206	24	85	49
97pr10b2	57.54	1.0169	0.9977	0.9854	1.019	1.012	1.032	1.032	-0.218	0.875	314	22	217	17	93	62
97pr11a1	39.52	1.06787	1.026	0.9187	1.055	1.0102	1.163	1.166	0.252	0.46	145	23	35	40	257	42
97pr11a2	41.71	1.0644	1.0117	0.9239	1.052	1.095	1.152	1.154	0.23	0.461	144	22	35	40	256	42
97pr11b1	38.9	1.0469	1.007	0.9461	1.04	1.064	1.107	1.108	0.208	0.494	320	26	203	43	71	36
97pr11b2	41.02	1.0545	1.01	0.9355	1.044	1.08	1.127	1.129	0.253	0.459	317	24	205	40	69	41
97pr12a1	50.14	1.0671	1.0262	0.9067	1.04	1.132	1.177	1.185	0.489	0.293	332	3	242	4	99	85
97pr12a2	56.25	1.0615	1.0243	0.9141	1.036	1.12	1.161	1.169	0.494	0.29	334	3	244	4	102	85
97pr12b1	52.21	1.0555	1.017	0.9275	1.038	1.096	1.138	1.142	0.399	0.354	332	6	62	4	187	83
97pr12b2	43.43	1.0582	1.0047	0.9371	1.053	1.072	1.129	1.13	0.115	0.568	161	2	71	2	301	87
97pr13a1	23.81	1.0581	1.0052	0.9368	1.053	1.073	1.129	1.13	0.128	0.557	135	0	45	6	227	84
97pr13a2	28.54	1.065	1.0077	0.9274	1.057	1.087	1.148	1.149	0.167	0.526	139	7	48	8	269	79
97pr13b1	30.02	1.0474	1.0006	0.9521	1.047	1.051	1.1	1.1	0.018	0.651	141	2	232	10	39	79
97pr13c1	24.96	1.0515	0.9869	0.9615	1.065	1.026	1.094	1.096	-436	1.12	149	3	240	23	53	66
97pr14a1	39.39	1.0577	1.0122	0.9301	1.045	1.088	1.137	1.14	0.287	0.434	304	12	211	12	79	73
97pr14a2	49.51	1.0605	1.0192	0.9203	1.04	1.107	1.152	1.157	0.411	0.345	299	31	200	15	87	55
97pr14b1	53.25	1.0473	1.0165	0.9362	1.03	1.086	1.119	1.123	0.446	0.322	316	75	196	8	104	13
97pr14b2	43.58	1.0550	1.0186	0.9255	1.037	1.101	1.141	1.146	0.428	0.334	305	64	202	7	108	25
97pr15a1	30.88	1.0278	1.0101	0.9621	1.018	1.05	1.068	1.071	0.461	0.311	314	36	164	50	55	15
97pr15a2	29.11	1.0256	1.0159	0.9585	1.01	1.06	1.07	1.076	0.71	0.156	315	38	156	51	53	10
97pr15b1	12.07	1.0161	1.004	0.9799	1.012	1.025	1.037	1.038	0.331	0.402	330	74	146	16	236	1
97pr15c1	30.76	1.0209	1.003	0.9761	1.018	1.028	1.046	1.046	0.2	0.5	113	26	350	48	220	30
97pr16a1	38.42	1.072	0.9806	0.9474	1.093	1.035	1.132	1.136	-4.66	1.157	160	5	68	30	258	60
97pr16a2	32.39	1.0613	0.9748	0.9638	1.089	1.011	1.101	1.111	-0.774	1.594	323	6	222	59	57	30
97pr16b1	34.84	1.0545	0.9969	0.9487	1.058	1.051	1.112	1.112	-0.089	0.748	318	14	220	30	69	56
97pr16b2	48.55	1.0416	1.0001	0.9584	1.041	1.044	1.087	1.087	0.003	0.664	319	11	224	23	73	64
97pr17a1	29.6	1.02111	1.0043	0.9746	1.017	1.031	1.048	1.048	0.28	0.439	156	24	67	3	330	65
97pr17a2	22.32	1.0278	1.0001	0.9721	1.028	1.029	1.057	1.057	0.003	0.664	159	19	65	11	305	68
97pr17b1	40.24	1.0206	1.0019	0.9975	1.019	1.025	1.044	1.044	0.132	0.554	156	35	266	23	22	46
97pr17b2	33.18	1.0213	1.0031	0.9756	1.018	1.028	1.047	1.047	0.2	0.5	173	42	274	12	17	45
97pr18a1	73.79	1.0118	0.9983	0.9899	1.013	1.008	1.022	1.022	-0.233	0.892	352	0	262	56	82	34
97pr18a2	55.41	1.0193	0.9931	0.9876	1.026	1.006	1.032	1.034	-0.655	1.412	345	1	255	27	76	63
97pr18b1	68.63	1.049	1.0175	0.9336	1.031	1.09	1.124	1.129	0.454	0.316	185	13	93	8	331	75
97pr18b2	65.98	1.0499	1.0172	0.9329	1.032	1.09	1.125	1.13	0.442	0.324	179	11	87	7	325	77
97pr19a1	46.84	1.0247	0.9961	0.9792	1.029	1.017	1.046	1.047	-0.254	0.914	144	17	48	18	275	65
97pr19a2	51.88	1.0262	0.9952	0.9786	1.031	1.017	1.049	1.049	-0.303	0.966	154	17	62	5	316	72
97pr19b1	36.27	1.0324	0.9938	0.9738	1.039	1.02	1.06	1.061	-0.319	0.984	154	27	39	40	268	38
97pr19b2	39.65	1.032	0.9942	0.9738	1.038	1.021	1.06	1.061	-0.301	0.964	155	30	26	47	262	28
97pr20a1	77.6	1.0202	1.01	0.9698	1.01	1.041	1.052	1.055	0.594	0.226	314	18	84	63	217	19
97pr20a2	72.12	1.0193	1.0114	0.9693	1.008	1.043	1.052	1.056	0.686	0.17	325	30	102	52	221	21
97pr20b1	77.52	1.013	1.0107	0.9763	1.002	1.035	1.038	1.042	0.877	0.064	150	6	346	84	241	2
97pr20b2	69.24	1.0208	1.0091	0.97	1.012	1.04	1.052	1.055	0.541	0.26	324	5	211	76	55	13
97pr21a1	36.42	1.0228	0.9962	0.981	1.027	1.016	1.043	1.043	-0.27	0.931	6	29	241	46	114	30
97pr21a2	33.35	1.0294	0.9936	0.977	1.036	1.017	1.054	1.055	-0.369	1.04	7	29	252	38	123	39
97pr21b1	66.73	1.0428	1.0161	0.9411	1.026	1.08	1.108	1.113	0.475	0.302	350	15	252	29	105	57
97pr21b2	77.88	1.0343	1.0169	0.9488	1.017	1.072	1.09	1.096	0.593	0.226	354	12	258	27	106	60
97pr22a1	50.06	1.0344	0.9932	0.9724	1.041	1.021	1.064	1.065	-0.331	0.997	5	13	132	70	272	16
97pr22a2	46.46	1.0362	0.9922	0.9717	1.044	1.021	1.066	1.068	-0.365	1.035	8	8	145	78	277	8
97pr22b1	51.87	1.0182	1.0019	0.9799	1.016	1.022	1.039	1.039	0.151	0.539	330	25	60	1	152	65
97pr22b2	43.92	1.0094	0.9972	0.9933	1.012	1.004	1.016	1.017	-0.511	1.214	11	41	190	49	281	1
97pr23a1	40.36	1.025	1.0037	0.9713	1.021	1.033	1.055	1.056	0.208	0.494	11	16	106	18	242	66
97pr23a2	44.76	1.0252	1.0035	0.9713	1.022	1.033	1.056	1.056	0.195	0.504	19	12	111	9	236	75

Specimen #	Av. Mean K	Normaled Principal Susceptibilities			Anisotropy Factors						Principal Directions K1		Principal Directions K2		Principal Directions K3	
		K1	K2	K3	L	F	P	P'	T	q	Azimuth	Plunge	Azimuth	Plunge	Azimuth	Plunge
97pr23b1	14.89	1.0539	1.0125	0.9335	1.041	1.085	1.129	1.132	0.312	0.416	254	4	163	4	28	84
97pr23b2	13.79	1.0646	1.0059	0.9295	1.058	1.082	1.145	1.146	0.132	0.555	258	5	168	5	30	83
97pr24a1	21.67	1.0077	0.9991	0.9932	1.009	1.006	1.015	1.015	-0.188	0.845	234	5	328	34	137	55
97pr24a2	18.93	1.0092	0.9984	0.9924	1.011	1.006	1.017	1.017	-0.285	0.947	305	35	61	32	181	39
97pr24b1	13.46	1.0191	1.0075	0.9734	1.012	1.035	1.047	1.049	0.49	0.292	295	34	26	0	116	56
97pr24b2	22.19	1.0079	1.0021	0.99	1.006	0.012	1.018	1.018	0.347	0.39	315	34	47	2	140	56
97pr25a1	96.44	1.024	0.9964	0.9796	1.028	1.017	1.045	1.046	-0.243	0.901	167	12	76	1	342	78
97pr25a2	88.63	1.0249	0.9951	0.98	1.03	1.015	1.046	1.047	-0.331	0.997	171	16	77	14	307	69
97pr25b1	94.66	1.0021	0.9997	0.9982	1.002	1.001	1.004	1.004	-0.258	0.918	355	74	252	4	161	15
97pr25b2	82.99	1.0025	0.9992	0.9983	1.003	1.001	1.004	1.004	-0.588	1.317	250	0	159	51	340	39
97pr26a1	21.75	1.0316	1.0102	0.9582	1.021	1.054	1.077	1.079	0.416	0.342	12	14	278	16	140	68
97pr26a2	28.32	1.0207	1.0021	0.9972	1.019	1.025	1.044	1.045	0.145	0.544	353	20	258	12	140	67
97pr26b1	24.01	1.0273	0.9972	0.9755	1.03	1.022	1.053	1.053	-0.164	0.821	354	67	198	21	1.05	9
97pr26b2	28.99	1.0271	1.0097	0.9632	1.017	1.048	1.066	1.069	0.454	0.316	310	80	219	0	129	10
97pr27a1	26.76	1.0046	1.001	0.9943	1.004	1.007	1.01	1.011	0.299	0.425	318	38	52	6	150	51
97pr27a2	135.8	1.0009	1.0005	0.9986	1	1.002	1.002	1.002	0.642	0.197	312	14	219	11	92	72
97pr27b1	46.06	1.0127	0.9968	0.9905	1.016	1.006	1.022	1.023	-0.434	1.118	182	33	355	57	90	4
97pr27b2	47.88	1.0088	0.9976	0.9936	1.011	1.004	1.015	1.016	-0.476	1.169	169	38	25	46	275	19
97pr28a1	2.14	1.2285	1.0156	0.7559	1.21	1.344	1.625	1.632	0.099	0.581	65	30	328	13	217	57
97pr28a2	8.36	1.1218	1.0098	0.8684	1.111	1.163	1.292	1.294	0.116	0.568	216	45	35	45	126	1
97pr28b1	14.71	1.0174	0.9953	0.9873	1.022	1.008	1.031	1.032	-0.47	1.162	58	7	186	78	327	9
97pr28b2	12.71	1.0262	0.9988	0.975	1.027	1.024	1.052	1.053	-0.072	0.732	52	29	201	57	314	14
97pr29a1	10.4	1.0329	1.0076	0.9595	1.025	1.05	1.076	1.078	0.309	0.418	326	31	230	9	125	57
97pr29a2	8.47	1.0305	1.0096	0.9599	1.021	1.052	1.074	1.076	0.407	0.348	33	36	283	26	166	43
97pr29b1	52.75	1.038	1.0084	0.9536	1.029	1.057	1.088	1.09	0.3	0.424	58	44	324	4	230	45
97pr29b2	52.39	1.0333	1.0152	0.9514	1.018	1.067	1.086	1.091	0.558	0.248	67	44	327	11	225	44
97pr30a1	64.7	1.03	1.0025	0.9675	1.027	1.036	1.065	1.065	0.121	0.563	4	30	271	7	169	60
97pr30a2	67.3	1.0296	1.0059	0.9645	1.024	1.043	1.068	1.068	0.27	0.446	4	28	272	4	174	62
97pr30b1	63.77	1.0453	1.0047	0.95	1.04	1.058	1.1	1.101	0.148	0.542	9	26	104	9	212	62
97pr30b2	52.58	1.048	1.0043	0.9477	1.044	1.06	1.106	1.106	0.128	0.557	12	23	102	1	196	67
97pr31a1	45.61	1.0371	1.0049	0.9579	1.032	1.049	1.083	1.083	0.187	0.51	350	22	105	46	243	36
97pr31a2	48.35	1.0387	1.0016	0.9597	1.037	1.044	1.082	1.082	0.061	0.613	354	25	108	41	242	39
97pr31b1	46.07	1.0383	1.0077	0.954	1.03	1.056	1.088	1.09	0.273	0.444	348	18	103	52	246	32
97pr31b2	43.08	1.0378	1.0048	0.9574	1.033	1.049	1.084	1.085	0.178	0.517	350	19	108	52	248	32
97pr32a1	49.07	1.0491	1.0038	0.947	1.045	1.06	1.108	1.0108	0.113	0.57	10	12	101	6	218	77
97pr32a2	56.3	1.051	1.0031	0.9459	1.048	1.06	1.111	1.111	0.089	0.59	8	17	100	6	209	72
97pr32b1	84.08	1.0458	1.0114	0.9428	1.034	1.073	1.109	1.112	0.332	0.401	3	45	99	6	194	44
97pr32b2	80.65	1.0479	1.0093	0.9429	1.038	1.07	1.111	1.113	0.265	0.45	8	45	100	3	193	45
97pr33a1	15.83	1.0235	0.9976	0.9788	1.026	1.019	1.046	1.046	-0.158	0.815	144	1	251	87	53	3
97pr33a2	27.5	1.0142	0.9971	0.9887	1.017	1.008	1.026	1.026	-0.344	1.012	154	3	245	20	57	70
97pr33b1	26.09	1.0192	0.9911	0.9897	1.028	1.001	1.03	1.034	-0.9	1.81	146	5	248	66	54	24
97pr33b2	24.11	1.0167	0.9962	0.9871	1.021	1.009	1.03	1.031	-0.385	1.059	330	4	235	45	64	44
97pr34a1	35.02	1.017	1.0105	0.9724	1.006	1.039	1.046	1.05	0.708	0.158	330	0	238	77	60	13
97pr34a2	50.72	1.0284	1.0033	0.9684	1.025	1.036	1.062	1.062	0.164	0.528	334	3	232	74	65	15
97pr34b1	49.54	1.0226	1.0116	0.9658	1.011	1.047	1.059	1.063	0.612	0.215	163	9	280	70	70	18
97pr34b2	40.21	1.035	1.001	0.964	1.034	1.038	1.074	1.074	0.042	0.63	339	3	244	62	70	28
97pr35a1	39.83	1.014	1.0003	0.9857	1.014	1.015	1.029	1.029	0.031	0.64	306	18	210	18	78	64
97pr35a2	45.29	1.0151	1.0123	0.9726	1.003	1.041	1.044	1.049	0.871	0.067	274	24	178	12	65	63
97pr35b1	43.92	1.0136	1.0058	0.9806	1.008	1.026	1.034	1.035	0.527	0.268	318	23	225	8	117	66
97pr35b2	55.81	1.0189	1.003	0.9781	1.016	1.025	1.042	1.042	0.224	0.481	322	31	211	30	87	44
97pr36a1	26.87	1.0215	1.0101	0.9684	1.011	1.043	1.055	1.056	0.572	0.239	187	30	87	16	334	55
97pr36a2	32.43	1.0126	1.0061	0.9812	1.006	1.025	1.032	1.034	0.588	0.23	148	25	239	3	336	65
97pr36b1	29.06	1.0171	0.9963	0.9866	1.021	1.01	1.031	1.032	-0.366	1.037	153	20	266	46	47	37

Specimen #	Av. Mean K	Normated Principal Susceptibilities K1	K2	K3	Anisotropy Factors L	F	P	P'	T	q	Principal Directions K1 Azimuth	Plunge	Principal Directions K2 Azimuth	Plunge	Principal Directions K3 Azimuth	Plunge
97pr36b2	33.46	1.0127	1.0022	0.9851	1.011	1.017	1.028	1.028	0.237	0.472	122	13	32	2	293	76
97pr37a1	55.82	1.006	0.9991	0.9949	1.007	1.004	1.011	1.011	-0.242	0.901	22	70	146	11	239	16
97pr37a2	51.6	1.0041	1.002	0.9939	1.002	1.008	1.01	1.011	0.591	0.228	348	31	106	38	232	36
97pr37b1	38.49	1.0216	1.0046	0.9738	1.017	1.032	1.049	1.05	0.291	0.431	12	59	129	15	227	26
97pr37b2	45.19	1.0251	0.9909	0.984	1.034	1.007	1.042	1.045	-0.661	1.421	304	47	76	32	184	25
97pr38a1	14	1.015	1.0026	0.9825	1.012	1.02	1.033	1.033	0.238	0.47	246	66	157	0	67	24
97pr38a2	7.28	1.069	1.0006	0.9302	1.068	1.076	1.149	1.149	0.017	0.651	196	74	46	14	316	8
97pr38b1	36.94	1.0124	1.0062	0.9814	1.006	1.025	1.032	1.033	0.602	0.221	190	73	309	8	41	15
97pr38b2	39.5	1.0185	1.0092	0.9724	1.009	1.038	1.047	1.05	0.585	0.225	336	77	187	11	96	7
97pr39a1	29.28	1.03	1.0076	0.9624	1.022	1.047	1.07	1.072	0.337	0.398	142	9	52	1	317	81
97pr39a2	29.95	1.0356	1.0102	0.9542	1.025	1.059	1.085	1.088	0.376	0.37	137	10	230	16	16	71
97pr39b1	65.94	1.0079	0.9991	0.993	1.009	1.006	1.015	1.015	-0.191	0.848	132	16	226	14	354	68
97pr39b2	52.36	1.0089	0.9984	0.9928	1.01	1.006	1.016	1.016	-0.3	0.963	135	6	25	73	226	16
97pr40a1	62.18	1.0183	1.0051	0.9767	1.013	1.029	1.043	1.044	0.365	0.378	190	28	283	6	23	62
97pr40a2	62.25	1.0161	1.027	0.9813	1.013	1.022	1.035	1.036	0.23	0.477	194	31	102	2	9	59
97pr40b1	63.83	1.0257	1.005	0.9694	1.021	1.037	1.058	1.059	0.264	0.451	173	16	268	16	41	67
97pr40b2	64.75	1.223	1.0039	0.9738	1.018	1.031	1.05	1.05	0.243	0.467	170	19	272	8	24	70
97pr41a1	64.81	1.0261	0.9982	0.9757	1.028	1.023	1.052	1.052	-0.106	0.764	158	21	333	69	68	2
97pr41a2	62.99	1.0248	1.0005	0.9746	1.024	1.027	1.052	1.052	0.032	0.639	150	17	6	70	244	11
97pr41b1	63.13	1.0265	1.0024	0.9711	1.024	1.032	1.057	1.057	0.129	0.557	162	19	8	69	255	8
97pr41b2	65.52	1.0282	1.0039	0.9679	1.024	1.037	1.062	1.063	0.194	0.505	157	23	0	65	251	9
97pr42a1	13.29	1.0072	1.0005	0.9923	1.007	1.008	1.015	1.015	0.103	0.578	280	53	126	34	28	13
97pr42a2	26.49	1.0136	0.9967	0.9897	1.017	1.007	1.024	1.025	-0.416	1.096	298	78	150	11	59	6
97pr42b1	24.24	1.0153	1.0122	0.9725	1.003	1.041	1.044	1.049	0.852	0.077	143	42	312	48	48	5
97pr42b2	26.3	1.0215	1.0045	0.974	1.017	1.031	1.049	1.05	0.283	0.437	167	52	306	30	49	21
97pr43a1	39.09	1.0337	0.9946	0.9717	1.039	1.024	1.064	1.065	-0.26	0.92	205	42	341	39	92	24
97pr43a2	41.64	1.0241	1.0023	0.9736	1.022	1.03	1.052	1.052	0.138	0.549	201	51	313	17	55	34
97pr43b1	37.93	1.0309	1.0021	0.967	1.029	1.036	1.066	1.066	0.098	0.582	198	38	305	20	56	46
97pr43b2	42.84	1.0418	1.0123	0.946	1.029	1.07	1.101	1.104	0.384	0.364	194	50	288	4	21	40
97pr44a1	26.72	1.0074	1.0029	0.9897	1.005	1.013	1.018	1.019	0.486	0.295	134	17	12	59	232	25
97pr44a2	30.77	1.0079	1.0016	0.9902	1.006	1.012	1.018	1.018	0.313	0.415	125	49	342	35	238	18
97pr44b1	26.72	1.0076	1.0003	0.9921	1.007	1.008	1.016	1.016	0.066	0.61	140	9	39	51	237	38
97pr44b2	31.35	1.0071	1.0034	0.9895	1.004	1.014	1.018	1.019	0.585	0.231	141	14	27	59	238	27
97pr45a1	30.42	1.0071	1.0051	0.9879	1.002	1.017	1.019	1.021	0.795	0.108	116	51	292	39	23	2
97pr45a2	31.51	1.0114	0.9996	0.989	1.012	1.011	1.023	1.023	-0.054	0.715	190	12	30	77	281	4
97pr45b1	5.61	1.0416	1.0108	0.9475	1.03	1.067	1.099	1.102	0.345	0.392	10	82	136	5	226	7
97pr45b2	12.22	1.018	1.0032	0.9788	1.015	1.025	1.04	1.04	0.247	0.464	111	76	309	14	218	4
97pr46a1	32.64	1.0119	0.9972	0.9909	1.015	1.006	1.021	1.022	-0.405	1.083	165	9	71	25	274	64
97pr46a2	26.91	1.0238	0.9955	0.9806	1.028	1.015	1.044	1.045	-0.31	0.974	156	14	54	41	261	46
97pr46b1	26.44	1.0128	0.9996	0.9874	1.013	1.013	1.026	1.026	-0.2	0.884	355	16	102	45	251	40
97pr46b2	28.09	1.0151	0.9976	0.9873	1.017	1.01	1.028	1.028	-0.258	0.918	154	11	51	51	252	37
97pr47a1	47.69	1.0211	0.9942	0.9847	1.027	1.01	1.037	1.038	-0.475	1.168	133	8	35	43	231	46
97pr47a2	50.45	1.0141	1.0007	0.9852	1.013	1.016	1.029	1.029	0.07	0.605	132	15	32	31	243	55
97pr47b1	35.45	1.0139	1.0016	0.9845	1.012	1.017	1.03	1.03	0.163	0.529	131	13	29	42	234	45
97pr47b2	37.14	1.018	1.0021	0.98	1.016	1.023	1.039	1.039	0.162	0.53	143	4	52	24	242	66
97pr48a1	38.42	1.0339	0.9909	0.9752	1.043	1.016	1.06	1.062	-0.463	1.154	326	18	221	40	74	44
97pr48a2	58.04	1.0314	0.9946	0.974	1.037	1.021	1.059	1.06	-0.282	0.943	323	3	55	29	228	60
97pr48b1	39.65	1.0255	1.0128	0.9617	1.012	1.053	1.066	1.071	0.603	0.22	332	11	77	54	234	34
97pr48b2	45.31	1.0261	1.0124	0.9615	1.014	1.053	1.067	1.071	0.575	0.238	128	14	25	41	233	46
97pr49a1	44.79	1.0547	0.9891	0.9562	1.066	1.034	1.103	1.105	-0.332	0.998	338	8	69	11	213	76
97pr49a2	42.87	1.0505	0.9901	0.9595	1.061	1.032	1.095	1.096	-0.328	0.994	338	12	69	8	193	76
97pr49b1	43.62	1.0474	1.0049	0.9477	1.042	1.06	1.105	1.106	0.148	0.541	324	6	57	21	220	68
97pr49b2	46.17	1.0407	1.0321	0.9272	1.008	1.113	1.122	1.137	0.847	0.079	16	26	112	12	224	61

Specimen #	Av. Mean K	Normaled Principal Susceptibilities K1	K2	K3	Anisotropy Factors L	F	P	P'	T	q	Principal Directions K1 Azimuth	Plunge	Principal Directions K2 Azimuth	Plunge	Principal Directions K3 Azimuth	Plunge
97pr50a1	53.17	1.0651	1.0517	0.8832	1.013	1.191	1.206	1.233	0.853	0.076	10	47	149	35	255	21
97pr50a2	45.53	1.0601	1.0292	0.9106	1.03	1.13	1.164	1.175	0.586	0.231	162	4	68	47	256	42
97pr50b1	49.28	1.0617	1.0476	0.8907	1.014	1.176	1.192	1.216	0.835	0.086	358	8	107	68	265	21
97pr50b2	53.28	1.0595	1.047	0.8935	1.012	1.172	1.186	1.21	0.849	0.079	180	0	90	58	270	32
97pr51a1	39.78	1.0457	1.0154	0.9389	1.03	1.081	1.114	1.118	0.432	0.331	150	13	300	75	58	7
97pr51a2	54.64	1.0554	0.9923	0.9523	1.064	1.042	1.108	1.109	-0.223	0.881	151	12	343	78	241	2
97pr51b1	49.4	1.0555	1.0291	0.9155	1.026	1.124	1.153	1.164	0.623	0.208	141	21	285	64	46	14
97pr51b2	51.5	1.057	1.0272	0.9158	1.029	1.122	1.154	1.164	0.578	0.236	135	14	294	75	44	5
97pr52a1	36.16	1.048	1.0368	0.9152	1.011	1.133	1.145	1.163	0.831	0.088	172	40	287	27	40	38
97pr52a2	24.94	1.037	1.0294	0.9337	1.007	1.103	1.111	1.124	0.853	0.076	316	7	215	58	50	31
97pr52b1	46.4	1.0689	1.0123	0.9188	1.056	1.102	1.163	1.166	0.245	0.465	325	3	224	74	55	15
97pr52b2	46.3	1.0694	0.9935	0.9372	1.076	1.06	1.141	1.141	-0.148	0.805	327	3	229	73	58	17
97pr53a1	30.86	1.0031	0.9997	0.9972	1.003	1.022	1.006	1.006	-0.163	0.82	109	16	214	41	3	45
97pr53b1	5	1.0609	1.0012	0.938	1.06	1.067	1.131	1.131	0.028	0.642	137	18	14	50	236	25
97pr53b2	36.12	1.0354	0.9905	0.9741	1.045	1.017	1.063	1.065	-0.464	1.155	328	45	179	41	75	16
97pr53c1	46.04	1.0056	1.0026	0.9918	1.003	1.011	1.014	1.015	0.564	0.245	79	50	312	27	207	27
97pr54a1	26.61	1.04	1.0094	0.9507	1.03	1.062	1.094	1.096	0.315	0.414	319	1	51	68	229	22
97pr54b1	39.65	1.0429	1.0289	0.9282	1.014	1.108	1.124	1.136	0.756	0.13	335	21	91	49	230	33
97pr54b2	48.44	1.0445	1.0232	0.9323	1.021	1.097	1.12	1.129	0.62	0.21	328	17	79	48	225	37
97pr54c1	32.56	1.0281	1.0068	0.9651	1.021	1.043	1.065	1.067	0.323	0.407	142	9	8	78	233	9
97pr55a1	42.65	1.0564	1.0066	0.9369	1.049	1.075	1.128	1.128	0.17	0.524	147	2	55	35	240	55
97pr55a2	43.75	1.0541	1.0072	0.9387	1.047	1.073	1.123	1.124	0.168	0.509	323	0	53	33	232	57
97pr55b1	44.2	1.0454	1.0057	0.949	1.039	1.06	1.102	1.102	0.177	0.518	127	9	32	28	234	60
97pr55b2	53.28	1.045	1.0064	0.9484	1.039	1.061	1.102	1.103	0.197	0.502	137	4	45	25	236	64
97pr56a1	55.51	1.0639	1.0091	0.927	1.054	1.088	0.148	1.149	0.198	0.501	188	20	279	2	15	69
97pr56a2	59.11	1.07	1.0067	0.9233	1.063	1.09	1.159	1.16	0.136	0.551	188	12	280	6	36	76
97pr56b1	49.27	1.0672	1.0019	0.9309	1.065	1.076	1.146	1.147	0.042	0.63	5	24	99	10	209	64
97pr56b2	55.78	1.0679	1.003	0.9291	1.065	1.079	1.149	1.15	0.064	0.611	7	25	106	20	230	57
97pr57a1	24.32	1.0113	1.0021	0.9866	1.009	1.016	1.025	1.025	0.253	0.46	93	36	230	45	345	23
97pr57b1	40.27	1.0077	1.0022	0.9902	1.006	1.012	1.018	1.018	0.37	0.374	200	62	51	24	315	13
97pr57b2	26.35	1.0113	1.0001	0.9887	1.011	1.012	1.023	1.023	0.009	0.659	115	59	208	2	299	31
97pr57c1	30.82	1.0063	0.9997	0.994	1.007	1.006	1.012	1.012	-0.075	0.735	351	59	241	11	145	28
97pr58a1	45.52	1.0482	1.0252	0.9266	1.022	1.106	1.131	1.141	0.622	0.209	141	18	49	8	295	71
97pr58a2	40.17	1.0628	1.0357	0.9015	1.026	1.149	1.179	1.194	0.664	0.183	131	21	37	8	287	67
97pr58b1	36.66	1.0639	1.032	0.9041	1.031	1.142	1.177	1.189	0.601	0.222	141	19	46	15	281	65
97pr58b2	38.11	1.0658	1.0318	0.9024	1.033	1.143	1.181	1.193	0.585	0.232	139	16	45	15	274	67
97pr59a1	76.85	1.0298	1.0239	0.9463	1.006	1.082	1.088	1.099	0.861	0.072	158	58	311	29	48	12
97pr59a2	76.74	1.0287	1.0167	0.9546	1.012	1.065	1.078	1.084	0.674	0.177	206	67	314	7	47	22
97pr59b1	73.61	1.0279	1.022	0.9501	1.006	1.076	1.082	1.092	0.847	0.08	164	46	300	35	48	24
97pr59b2	74.14	1.024	1.0212	0.9549	1.003	1.069	1.072	1.082	0.92	0.041	153	45	293	37	40	21
97pr60a1	47.3	1.093	1.0689	0.8381	1.023	1.275	1.304	1.343	0.811	0.099	141	24	33	34	259	46
97pr60a2	53.24	1.0828	1.0673	0.8499	1.015	1.256	1.274	1.312	0.867	0.069	151	17	46	40	259	45
97pr60b1	51.6	1.0821	1.0701	0.8478	1.011	1.262	1.276	1.317	0.898	0.052	146	15	44	36	255	49
97pr60b2	53.28	1.0828	1.07	0.8472	1.012	1.263	1.278	1.319	0.891	0.056	153	11	54	40	255	48
97pr61a1	43.34	1.0582	0.9791	0.9627	1.081	1.017	1.099	1.106	-0.658	1.415	130	2	227	74	40	15
97pr61a2	44.07	1.0561	0.9849	0.9589	1.072	1.027	1.101	1.105	-0.466	1.157	130	2	229	76	40	14
97pr61b1	42.24	1.0628	0.9757	0.9614	1.089	1.015	1.106	1.114	-0.717	1.505	127	6	249	79	36	9
97pr61b2	47.78	1.0569	0.9901	0.953	1.067	1.039	1.109	1.11	-0.285	0.947	128	2	22	81	218	6
97pr62a1	43.92	1.0618	0.9905	0.9478	1.072	1.045	1.12	1.121	-0.251	0.91	326	20	222	32	83	51
97pr62a2	53.32	1.0601	0.9876	0.9523	0.1073	1.037	1.113	1.115	-0.344	1.012	325	18	227	24	88	59
97pr62b1	51.58	1.0615	0.9858	0.9528	1.077	1.035	1.114	1.117	-0.393	1.069	328	19	231	21	97	61
97pr62b2	44.15	1.0624	0.9909	0.9467	1.072	1.047	1.122	1.123	-0.236	0.895	327	17	229	24	89	60

Specimen #	Av. Mean K	Normalized Principal Susceptibilities K1	K2	K3	Anisotropy Factors L	F	P	P'	T	q	Principal Directions K1 Azimuth	Plunge	Principal Directions K2 Azimuth	Plunge	Principal Directions K3 Azimuth	Plunge
97pr63a1	61.11	1.0784	1.0372	0.8844	1.04	1.173	1.219	1.234	0.575	0.238	307	3	215	31	41	58
97pr63a2	58.91	1.0788	1.0365	0.8847	1.041	1.172	1.219	1.234	0.564	0.244	308	3	216	33	42	57
97pr63b1	57.83	1.077	1.0414	0.8817	1.034	1.181	1.221	1.239	0.635	0.201	304	2	212	29	38	61
97pr63b2	59.77	1.0794	1.0403	0.8803	1.038	1.182	1.226	1.243	0.608	0.218	299	6	206	29	40	60
97pr64a1	52.92	1.0498	0.9946	0.9556	1.055	1.041	1.099	1.099	-0.172	0.829	324	11	130	79	234	3
97pr64a2	55.44	1.0531	0.9854	0.9614	1.069	1.025	1.095	1.099	-0.477	1.17	320	14	88	63	233	23
97pr64b1	51.75	1.0566	0.9887	0.9547	1.069	1.036	1.107	1.108	-0.332	0.999	321	20	212	42	70	41
97pr64b2	54.12	1.0557	0.9806	0.9637	1.077	1.018	1.096	1.102	-0.632	1.370	318	20	211	39	69	44
97pr65a1	67.56	1.0387	1.0065	0.9548	1.032	1.054	1.088	1.089	0.231	476	163	26	73	1	341	64
97pr65a2	74	1.0402	1.0042	0.9556	1.036	1.051	1.089	1.089	0.147	0.542	164	24	254	1	347	66
97pr65b1	65.66	1.038	1.004	0.958	1.034	1.048	1.083	1.084	0.140	0.541	158	23	67	3	331	66
97pr65b2	60.75	1.0409	1.0049	0.9542	1.036	1.053	1.091	1.091	0.171	0.523	155	27	247	3	343	63
97pr66a1	38.11	1.0477	1.0384	0.9139	1.009	1.136	1.146	1.165	0.86	0.072	127	10	24	53	225	35
97pr66a2	36.14	1.504	1.0377	0.9119	1.012	1.138	1.152	1.17	0.816	0.096	120	13	13	52	219	35
97pr66b1	45.42	1.0444	1.0351	0.9205	1.009	1.124	1.135	1.151	0.849	0.078	126	29	359	48	233	28
97pr66b2	42.97	1.0520	1.0437	0.9034	1.009	1.155	1.165	1.188	0.877	0.063	326	8	69	59	232	30
97pr67a1	43.37	1.0451	1.0253	0.9296	1.019	1.103	1.124	1.134	0.658	0.187	141	14	37	44	244	42
97pr67a2	40.89	1.0428	1.0295	0.9277	1.013	1.11	1.124	1.137	0.77	0.122	138	19	29	43	245	41
97pr67b1	39.75	1.0447	1.0179	0.9374	1.026	1.086	1.114	1.12	0.501	0.285	135	20	35	25	258	57
97pr67b2	47.65	1.0446	1.0151	0.9403	1.029	1.08	1.111	1.115	0.434	0.33	133	19	33	27	254	56
97pr68a1	38.69	1.0527	1.0309	0.9164	1.021	1.125	1.149	1.161	0.68	0.174	81	29	343	13	231	58
97pr68a2	39.9	1.0426	1.0293	0.9281	1.013	1.109	1.123	1.136	0.767	0.123	97	22	357	23	227	57
97pr68b1	48.68	1.0547	1.0411	0.9043	1.013	1.151	1.166	1.186	0.819	0.095	72	23	338	8	231	65
97pr68b2	44.79	1.0578	1.0358	0.9064	1.021	1.143	1.167	1.182	0.71	0.157	95	29	354	20	233	54
97pr69a1	49.48	1.061	1.0279	0.9111	1.032	1.128	1.164	1.174	0.558	0.248	324	7	57	21	217	68
97pr69a2	50.81	1.0578	1.028	0.9142	1.029	1.124	1.157	1.167	0.585	0.232	319	1	50	23	227	67
97pr69b1	50.52	1.0568	1.034	0.9092	1.022	1.137	1.162	1.177	0.691	0.168	326	13	61	21	207	65
97pr69b2	51.35	1.063	1.0382	0.8988	1.024	1.155	1.183	1.199	0.698	0.163	325	7	58	22	218	68
97pr70a1	48.6	1.0644	1.0238	0.9118	1.04	1.123	1.167	1.175	0.467	0.307	319	10	51	12	191	74
97pr70a2	45.74	1.068	1.0259	0.9061	1.041	1.132	1.179	1.187	0.48	0.299	317	11	49	12	185	74
97pr70b1	44.39	1.0515	1.0354	0.913	1.016	1.134	1.152	1.168	0.767	0.124	315	12	49	15	189	71
97pr70b2	52.74	1.0517	1.0328	0.9155	1.018	1.128	1.149	1.163	0.723	0.149	317	9	49	14	195	73
97pr71a1	59.07	1.0266	1.0021	0.9713	1.024	1.032	1.057	1.057	0.114	0.569	343	12	243	39	87	48
97pr71a2	60.96	1.0239	1.0013	0.9748	1.023	1.027	1.05	1.05	0.078	0.599	348	12	241	54	86	34
97pr71b1	54.38	1.003	1.0012	0.9957	1.002	1.005	1.007	1.008	0.502	0.284	172	55	335	34	70	8
97pr71b2	60.65	1.0183	1.0001	0.9825	1.018	1.019	1.037	1.037	0.011	0.657	152	2	59	55	243	35
97pr72a1	81.79	1.0194	0.9915	0.9891	1.028	1.002	1.031	1.034	-0.844	1.71	143	3	44	71	233	19
97pr72a2	86.45	1.0277	0.9936	0.9786	1.034	1.015	1.05	1.051	-0.388	1.063	151	5	241	2	351	85
97pr72b1	80.25	1.0219	0.9898	0.9883	1.032	1.001	1.034	1.039	-0.912	1.831	145	10	321	80	54	1
97pr72b2	84.04	1.0281	0.9903	0.9816	1.038	1.009	1.047	1.05	-0.623	1.365	145	8	51	32	248	57
97pr73a1	31.65	1.0449	1.0092	0.948	1.035	1.067	1.105	1.106	0.278	0.44	337	9	199	79	68	7
97pr73a2	37.61	1.052	1.0139	0.9341	1.038	1.085	1.126	1.129	0.354	0.385	335	10	180	79	66	5
97pr73b1	35.02	1.0337	1.0095	0.9567	1.024	1.055	1.081	1.083	0.371	0.373	144	1	50	76	234	14
97pr73b2	38.1	1.038	1.0109	95.1	1.027	1.063	1.091	1.094	0.376	0.37	334	9	114	78	243	7
97pr74a1	54.48	1.0251	1.0085	0.9664	1.016	1.044	1.061	1.063	0.434	0.33	338	0	248	1	69	89
97pr74a2	49.2	1.0218	1.0026	0.9753	1.019	1.028	1.048	1.048	0.184	0.513	334	4	65	6	210	82
97pr74b1	37.79	1.0319	1.0061	0.962	1.026	1.046	1.073	1.074	0.26	0.454	171	2	261	8	69	82
97pr74b2	42.67	1.0388	1.0036	0.9576	1.035	1.048	1.085	1.085	0.133	0.553	174	8	83	7	312	79
97pr75a1	50.11	1.0423	1.0114	0.9463	1.03	1.069	1.101	1.104	0.357	0.383	181	12	88	11	316	74
97pr75a2	46.39	1.0397	1.0078	0.9525	1.032	1.058	1.092	1.093	0.267	0.449	174	17	81	7	330	71
97pr75b1	37.01	1.0438	0.9936	0.9624	1.05	1.033	1.085	1.085	-0.23	0.886	185	9	95	3	347	81
97pr75b2	40.45	1.0427	0.9892	0.9682	1.054	1.022	1.077	1.079	-0.436	1.12	183	7	275	17	71	72
97pr76a1	54.23	1.0542	0.9865	0.9593	1.069	1.028	1.099	1.102	-0.427	1.109	349	1	80	30	256	60

Specimen #	Av. Mean K	Normaled Principal Susceptibilities K1	K2	K3	Anisotropy Factors L	F	P	P'	T	q	Principal Directions K1 Azimuth	Plunge	Principal Directions K2 Azimuth	Plunge	Principal Directions K3 Azimuth	Plunge
97pr76a2	55.04	1.0498	0 9939	0.9562	1.056	1.039	1.098	1.099	-0.196	0 853	167	2	76	34	259	56
97pr76b1	60.58	1.0548	0 9966	0.9486	1.058	1.051	1.112	1.112	-0.096	0.755	168	5	77	14	279	75
97pr76b2	60.67	1.0491	1.0002	0.9508	1.049	1.052	1.103	1.103	0.005	0.663	168	7	76	13	283	75
97pr77a1	57.83	1.038	1.0143	0.9477	1.023	1.07	1.095	1.099	0.476	0.302	209	7	118	15	322	74
97pr77a2	58.7	1.0381	1.0189	0.943	1.019	1.081	1.101	1.107	0.598	0.224	210	6	118	14	323	75
97pr77b1	48.63	1.0565	1.0201	0.9234	1.036	1.105	1.144	1.15	0.452	0.317	198	1	108	24	292	66
97pr77b2	51.18	1.0508	1.015	0.9342	1.035	1.087	1.125	1.128	0.387	0.362	195	4	103	27	292	63
97pr78a1	63.39	1.0619	1.0065	0.9316	1.055	1.08	1.14	1.141	0.149	0 541	168	5	77	13	277	76
97pr78a2	59.1	1 0579	1 0033	0.9388	1.054	1.069	1.127	1.127	0.082	0 595	170	3	79	15	272	74
97pr78b1	66.74	1.0629	1 0059	0.9312	1.057	1.08	1.141	1.142	0.134	0.552	338	5	66	8	217	81
97pr78b2	60.42	1.0641	1.0035	0.9323	1.06	1.076	1.141	1.142	0.08	0.598	337	4	68	12	227	77
97pr79a1	53.24	1.0539	1.0085	0.9376	1.045	1.076	1.124	1.125	0.219	0.485	326	31	58	4	155	59
97pr79a2	59.9	1.0524	1.0157	0.9319	1.036	1.09	1.129	1.133	0.392	0.359	329	32	66	11	171	55
97pr79b1	58.12	1.0471	1.017	0.9359	1.03	1.097	1.119	1.124	0.459	0 313	335	46	240	5	145	44
97pr79b2	55.35	1.049	1.0116	0.9394	1.037	1.077	1.117	1.119	3.18	0 411	334	47	241	3	148	43
97pr80a1	51.52	1.0438	1.0241	0.9322	1.019	1.099	1.12	1.129	0.647	0.194	309	24	40	2	135	66
97pr80a2	58.61	1 0405	1.016	0.9435	1.024	1.077	1.103	1.107	0.494	0 29	323	24	233	1	140	66
97pr80b1	50.64	1.0451	1.0263	0.9286	1.018	1.105	1.125	1.136	0.677	0.175	323	24	53	0	144	66
97pr80b2	45.33	1.0444	1.0263	0.9293	1.018	1.104	1.124	1.134	0.684	0.171	321	25	230	2	136	65
97pr81a1	55.28	1.0511	0 9954	0.9534	1.056	1.044	1.102	1.103	-0.141	0.798	316	4	47	14	208	76
97pr81a2	63.87	1.041	1.002	0.9569	1.039	1.047	1.088	1.088	0.073	0.603	321	9	54	23	211	66
97pr81b1	42	1.0606	1.008	0.9314	1.052	1.082	1.139	1.14	0.186	0.511	318	6	49	15	207	74
97pr81b2	51.92	1.053	1.0089	0.9381	1.044	1.076	1.123	1.124	0.232	0.475	320	6	51	15	207	74

Site	Kavg	K1	K2	K3	L	F	P	P'	T	q	K1		K2		K3	
											Azimuth	plunge	Azimuth	plunge	Azimuth	plunge
96sp1	15.95	1.02	1.0022	0.9778	1.018	1.025	1.043	1.043	0.159	0.533	128	18	231	37	15	47
96sp2	18.77	1.0262	0.9974	0.9764	1.029	1.021	1.051	1.051	-0.159	0.816	111	8	212	55	15	34
96sp3	45.25	1.0559	1.004	0.9401	1.052	1.068	1.123	1.123	0.104	0.577	316	5	58	67	223	22
96sp4	22.13	1.0151	0.9969	0.988	1.018	1.009	1.028	1.028	-0.314	1.008	145	32	254	27	15	46
96sp5	35.38	1.0194	0.9983	0.9823	1.021	1.016	1.038	1.038	-0.14	0.797	136	5	232	54	42	35
96sp6	26.26	1.0163	0.9968	0.9869	1.02	1.01	1.03	1.03	-0.328	0.994	280	14	13	14	146	70
96sp7	45.47	1.0455	0.9992	0.9953	1.046	1.046	1.094	1.094	-0.028	0.692	116	14	17	30	228	57
96sp8	22.33	1.0198	0.9997	0.9806	1.02	1.019	1.04	1.04	-0.026	0.69	136	11	46	1	311	79
96sp9	41.12	1.0491	0.979	0.9718	1.072	1.007	1.8	1.086	-0.813	1.658	137	3	229	29	42	61
96sp10	48.47	1.0411	0.9887	0.9702	1.053	1.019	1.073	1.076	-0.479	1.174	122	4	225	74	31	16
96sp11	57.62	1.031	0.9894	0.9796	1.042	1.01	1.052	1.056	-0.62	1.361	128	1	297	89	38	0
96sp12	53.26	1.0344	1.0021	0.9635	1.032	1.04	1.074	1.074	0.089	0.59	136	7	41	30	238	59
96sp13	61.29	1.0258	1.011	0.9632	1.015	1.05	1.065	1.068	0.528	0.267	130	6	225	43	34	47
96sp14	35.78	1.0359	0.9917	0.9725	1.045	1.02	1.065	1.067	-0.394	1.07	125	1	215	10	28	80
96sp15	59.83	1.0394	0.9911	0.9694	1.049	1.022	1.072	1.074	-0.379	1.053	307	2	212	68	38	22
96sp16	23.55	1.0447	0.9841	0.9712	1.062	1.013	1.076	1.081	-0.648	1.401	138	6	243	69	45	20
96sp17	28.23	1.048	0.9853	0.9667	1.064	1.019	1.084	1.088	-0.541	1.254	322	2	230	44	54	46
96sp18	47.8	1.0366	0.9958	0.9676	1.041	1.029	1.071	1.072	-0.182	0.838	299	3	208	27	34	63
96sp19	35.97	1.0198	0.9951	0.9851	1.025	1.01	1.035	1.036	-0.425	1.107	309	2	217	38	42	52
96sp20	17.49	1.0427	1.0015	0.9958	1.041	1.048	1.091	1.091	0.052	0.621	309	1	42	78	219	12
96sp21	22.33	1.0118	1.0062	0.982	1.006	1.025	1.03	1.032	0.622	0.209	118	15	227	50	17	36
96sp22	30.68	1.0315	0.9878	0.9807	1.044	1.007	1.052	1.056	-0.722	1.512	103	7	197	25	385	64
96sp23	56.52	1.0304	0.9946	0.9751	1.036	1.02	1.057	1.056	-0.295	0.958	125	5	220	37	28	52
96sp24	18.39	1.0306	1.0022	0.9672	1.028	1.036	1.066	1.066	0.103	0.578	145	13	246	39	40	48
96sp25	51.08	1.0144	0.9986	0.9871	1.016	1.012	1.028	1.028	-0.156	0.813	338	8	243	31	82	57
96sp26	53.6	1.047	0.9832	0.9697	1.065	1.014	1.08	1.085	-0.85	1.404	315	3	48	36	221	54
96sp27	55.04	1.042	0.9957	0.9623	1.047	1.035	1.083	1.083	-0.162	0.819	136	19	233	20	7	62
96sp28	40.95	1.022	1.0119	0.9661	1.01	1.047	1.058	1.062	0.641	0.197	171	56	260	13	17	31
96sp29	25.43	1.0382	1.0104	0.9514	1.027	1.062	1.091	1.093	0.36	0.381	201	2	292	8	98	82
96sp30	38.1	1.0096	1.0014	0.989	1.008	1.012	1.021	1.021	0.2	0.5	334	6	234	59	68	31
96sp31	62.19	1.0101	1.0006	0.9894	1.009	1.011	1.021	1.021	0.083	0.595	342	21	92	43	233	40
96sp32	55.94	1.0221	0.9906	0.9873	1.032	1.003	1.035	1.039	-0.809	1.651	18	24	214	65	111	6
96sp33	43.35	1.0202	0.995	0.9848	1.025	1.01	1.036	1.037	-0.423	1.105	163	11	287	71	70	16
96sp34	48.77	1.0184	0.9992	0.9824	1.019	1.017	1.037	1.037	-0.07	0.731	348	4	227	82	79	7
96sp35	61.37	1.0171	1.0062	0.9787	1.011	1.03	1.041	1.043	0.46	0.312	189	19	97	4	354	71
96sp36	39.82	1.017	1.0032	0.9798	1.014	1.024	1.038	1.038	0.255	0.458	144	45	345	43	244	11
96sp37	41.07	1.0244	1.0075	0.9681	1.017	1.041	1.058	1.06	0.4	0.353	357	22	109	43	248	39
96sp38	45.59	1.012	1.0014	0.9866	1.011	1.015	1.026	1.026	0.184	0.529	343	6	95	75	251	14
96sp39	39.62	1.0158	1.012	0.9722	1.004	1.041	1.045	1.05	0.823	0.092	349	32	123	48	242	24
96sp40	54.81	1.0426	0.9868	0.9706	1.057	1.017	1.074	1.078	-0.551	1.266	148	11	10	75	240	10
96sp41	62.86	1.0223	1.004	0.9737	1.018	1.031	1.05	1.051	0.247	0.464	177	12	267	2	4	78
96sp42	66.12	1.0139	1.0048	0.9813	1.009	1.024	1.033	1.034	0.444	0.323	138	40	24	26	271	39
96sp43	66.46	1.0094	0.9967	0.9939	1.013	1.003	1.016	1.017	-0.637	1.385	55	44	158	13	260	43
96sp44	57.94	1.0414	0.995	0.9637	1.047	1.032	1.081	1.081	-0.195	0.852	162	8	69	21	271	67
96sp45	59.56	1.0408	0.9898	0.9694	1.052	1.021	1.074	1.076	-0.43	1.112	147	0	57	1	243	89
96sp46	76.35	1.0312	1.007	0.9618	1.024	1.047	1.072	1.073	0.304	0.422	346	2	78	40	253	50
96sp47	76.95	1.0178	0.9947	0.9875	1.023	1.007	1.031	1.032	-0.529	1.237	155	8	65	5	305	80
96sp48	49.33	1.0163	1.0083	0.9754	1.008	1.034	1.042	1.044	0.61	0.216	163	5	65	55	257	34
96sp49	54.86	1.0379	1.0217	0.9404	1.016	1.097	1.104	1.112	0.687	0.181	61	50	168	14	268	37
96sp50	46.61	1.0177	0.9923	0.9901	1.026	1.002	1.028	1.031	-0.843	1.709	146	7	241	34	46	55
96sp51	47.38	1.0272	0.9934	0.9795	1.034	1.014	1.049	1.05	-0.419	1.099	9	19	152	66	274	14
96sp52	50.19	1.0196	1.0006	0.9798	1.019	1.021	1.041	1.041	0.047	0.626	189	5	94	39	285	50
96sp53	47.95	1.0485	0.9895	0.982	1.06	1.029	1.09	1.092	-0.366	1.037	162	8	256	31	59	58
96sp54	49.36	1.0155	1.0071	0.9774	1.008	1.03	1.039	1.041	0.582	0.246	144	68	4	17	270	13
96sp55	55.53	1.0291	0.9984	0.9725	1.031	1.027	1.058	1.058	-0.086	0.745	353	0	85	71	263	19
96sp56	43.75	1.0305	0.9955	0.974	1.035	1.022	1.058	1.058	-0.239	0.897	165	15	265	32	53	54
96sp57	56.63	1.0316	0.9929	0.9755	1.039	1.018	1.057	1.059	-0.379	1.052	175	19	350	70	85	2
96sp58	43.23	1.0268	1.0065	0.9667	1.02	1.041	1.062	1.063	0.323	0.407	151	30	18	49	257	24
96sp59	68.55	1.0274	0.9962	0.9764	1.031	1.02	1.052	1.053	-0.223	0.881	331	6	61	2	166	83
96sp60	97.52	1.0303	0.9963	0.9734	1.034	1.024	1.059	1.059	-0.195	0.852	355	7	91	35	255	54
96sp61	50.82	1.0235	1.0023	0.9742	1.021	1.029	1.051	1.051	0.138	0.55	158	35	306	51	57	16
96sp62	49.51	1.0231	0.9936	0.9833	1.03	1.01	1.04	1.042	-0.483	1.179	140	12	242	43	38	44
96sp63	67.93	1.0401	0.9872	0.9727	1.054	1.015	1.069	1.073	-0.57	1.292	333	2	242	36	65	54
96sp64	50.78	1.0286	1.005	0.9664	1.024	1.04	1.064	1.065	0.241	0.468	338	4	73	57	245	32
96sp65	54.54	1.0198	1.0015	0.9787	1.018	1.023	1.042	1.042	0.109	0.573	145	15	53	7	299	73

Site	Kavg	K1	K2	K3	L	F	P	P'	T	q	K1 Azimuth	K1 plunge	K2 Azimuth	K2 plunge	K3 Azimuth	K3 plunge
96sp66	39.96	1.0465	0.9845	0.969	1.063	1.016	1.08	1.085	-0.599	1.332	133	6	228	41	36	48
96sp67	26.72	1.0513	0.9854	0.9633	1.067	1.023	1.091	1.095	-0.498	1.197	126	5	234	76	35	14
96sp68	33.89	1.0545	0.9848	0.9607	1.071	1.025	1.098	1.101	-0.485	1.181	146	4	56	0	325	86
97pr1	65.72	1.0307	1.0099	0.9595	1.021	1.053	1.074	1.077	0.416	0.342	325	7	230	34	65	55
97pr2	63.76	1.0367	0.9976	0.9657	1.039	1.033	1.073	1.074	-0.102	0.761	335	5	244	19	78	70
97pr3	64.86	1.035	1.0091	0.9559	1.026	1.056	1.083	1.085	0.346	0.391	333	0	243	37	63	53
97pr4	80.66	1.027	1.0072	0.9658	1.02	1.043	1.063	1.065	0.355	0.385	340	11	246	18	99	69
97pr5	54.13	1.0345	0.9977	0.9678	1.037	1.031	1.069	1.069	-0.103	0.761	322	9	230	12	88	75
97pr6	25.16	1.0029	1.0013	0.9959	1.002	1.005	1.007	1.007	0.546	0.256	218	43	339	29	90	33
97pr7	42.14	1.0606	1	0.9394	1.061	1.065	1.129	1.129	0	0.667	322	17	116	71	230	8
97pr8	59.69	1.0066	0.9991	0.9943	1.008	1.005	1.012	1.013	-0.22	0.877	277	13	12	22	159	64
97pr9	53.52	1.018	1.01	0.972	1.008	1.039	1.047	1.051	0.656	0.188	194	24	295	23	64	56
97pr10	62.91	1.0182	0.9973	0.9845	1.021	1.013	1.034	1.035	-0.243	0.902	318	25	211	32	79	48
97pr11	40.29	1.0479	0.9857	0.9663	1.063	1.02	1.084	1.088	-0.525	1.232	153	4	48	74	245	15
97pr12	50.51	1.0601	1.0178	0.9221	1.041	1.104	1.15	1.154	0.388	0.361	335	3	245	2	125	87
97pr13	26.83	1.0548	0.9985	0.9467	1.056	1.055	1.114	1.114	-0.042	0.704	142	3	52	0	316	87
97pr14	46.43	1.0341	1.0168	0.9491	1.017	1.071	1.09	1.095	0.595	0.226	307	43	202	15	97	42
97pr15	25.71	1.0173	1.0095	0.9731	1.008	1.037	1.045	1.049	0.648	0.193	318	30	145	60	50	3
97pr16	38.05	1.0539	0.9846	0.9615	1.07	1.024	1.096	1.1	-0.5	1.2	328	4	236	25	67	65
97pr17	31.34	1.0216	1.0001	0.9784	1.021	1.022	1.044	1.044	0.005	0.662	158	29	253	9	358	60
97pr18	65.95	1.0316	1.0049	0.9635	1.027	1.043	1.071	1.071	0.217	0.487	177	10	86	4	335	79
97pr19	43.67	1.0281	0.9928	0.9791	1.036	1.014	1.05	1.052	-0.442	1.128	153	23	48	32	272	49
97pr20	74.12	1.0176	1.0077	0.9747	1.01	1.034	1.044	1.046	0.541	0.259	321	19	116	69	228	8
97pr21	53.6	1.0305	1.0052	0.9644	1.025	1.042	1.069	1.069	0.234	0.474	358	18	257	31	114	53
97pr22	48.08	1.0224	0.9914	0.9862	1.031	1.005	1.037	1.04	-0.713	1.497	5	16	170	73	273	4
97pr23	28.45	1.0323	1.0131	0.9546	1.019	1.061	1.081	1.085	0.506	0.282	66	1	336	0	231	89
97pr24	19.06	1.0091	1.0029	0.988	1.006	1.015	1.021	1.022	0.413	0.344	295	33	30	7	131	56
97pr25	90.68	1.0115	0.9983	0.9902	1.013	1.008	1.002	1.002	-0.237	0.896	170	14	78	7	321	74
97pr26	25.77	1.0175	1.0021	0.9804	1.015	1.022	1.038	1.038	0.171	0.523	9	32	249	39	124	35
97pr27	64.13	1.0043	0.9991	0.9966	1.005	1.003	1.008	1.008	-0.349	1.018	161	26	335	61	65	11
97pr28	9.48	1.0671	0.9688	0.9641	1.101	1.005	1.107	1.121	-0.908	1.825	53	28	165	36	295	42
97pr29	31	1.025	1.0077	0.9674	1.017	1.042	1.06	1.061	0.4	0.353	19	39	110	1	201	51
97pr30	62.09	1.038	1.0035	0.9585	1.034	1.047	1.083	1.083	0.133	0.553	9	26	99	0	190	64
97pr31	45.78	1.0379	1.0047	0.9574	1.033	1.049	1.084	1.085	0.176	0.519	351	21	106	48	245	34
97pr32	67.53	1.0409	1.0069	0.9522	1.034	1.057	1.093	1.094	0.233	0.474	8	30	101	4	198	60
97pr33	23.38	1.0182	0.9937	0.9881	1.025	1.006	1.03	1.032	-0.631	1.377	147	1	240	64	57	26
97pr34	43.87	1.0254	1.0064	0.9682	1.019	1.039	1.059	1.06	0.336	0.398	336	1	242	71	67	19
97pr35	46.23	1.0143	1.005	0.9807	1.009	1.025	1.034	1.035	0.446	0.322	312	22	214	19	86	60
97pr36	30.46	1.0139	1.0035	0.9825	1.01	1.021	1.032	1.033	0.338	0.397	152	25	244	3	340	64
97pr37	47.77	1.0116	0.9998	0.9886	1.012	1.011	1.023	1.023	-0.023	0.687	339	54	114	27	215	22
97pr38	24.43	1.0277	0.9929	0.9794	1.035	1.014	1.049	1.051	-0.44	1.125	207	74	21	16	111	2
97pr39	44.38	1.0205	1.002	0.9776	1.018	1.025	1.044	1.044	0.138	0.549	137	10	229	9	359	77
97pr40	63.25	1.0199	1.0044	0.9758	1.015	1.029	1.045	1.046	0.298	0.426	182	23	276	9	26	65
97pr41	64.11	1.0261	1.0011	0.9728	1.025	1.029	1.055	1.055	0.063	0.612	157	20	359	69	250	7
97pr42	22.59	1.0118	1.0053	0.983	1.006	1.023	1.029	1.031	0.549	0.254	196	76	316	7	48	12
97pr43	40.38	1.032	0.9985	0.9695	1.034	1.03	1.064	1.064	-0.073	0.733	201	46	304	12	46	41
97pr44	28.89	1.007	1.0025	0.9906	1.004	1.012	1.017	1.017	0.449	0.319	135	21	11	56	236	26
97pr45	19.94	1.0162	1.0035	0.9803	1.013	1.024	1.037	1.037	0.292	0.43	85	84	317	4	227	5
97pr46	28.52	1.0149	0.9981	0.9869	1.017	1.011	1.028	1.029	-0.202	0.859	160	7	62	45	257	44
97pr47	42.68	1.0166	0.9994	0.984	1.017	1.016	1.033	1.033	-0.053	0.714	135	9	39	34	238	55
97pr48	45.36	1.0279	0.9991	0.9731	1.029	1.027	1.056	1.056	-0.051	0.713	327	7	64	47	230	43
97pr49	44.36	1.0468	1.0046	0.9485	1.042	1.059	1.104	1.104	0.142	0.546	335	10	69	20	220	67
97pr50	50.32	1.0579	1.0427	0.8994	1.015	1.159	1.176	1.197	0.807	0.101	354	4	92	62	262	28
97pr51	48.83	1.0517	1.0151	0.9332	1.036	1.088	1.127	1.131	0.383	0.365	143	15	294	73	51	8
97pr52	38.45	1.053	1.068	0.9302	1.036	1.093	1.132	1.136	0.41	0.346	144	3	240	62	52	27
97pr53	29.51	1.0169	1.0043	0.9788	1.013	1.026	1.039	1.04	0.336	0.398	323	5	68	72	232	17
97pr54	36.82	1.0377	1.0159	0.9463	1.021	1.074	1.097	1.101	0.523	0.271	323	7	65	60	229	29
97pr55	45.98	1.0493	1.0071	0.9435	1.042	1.067	1.112	1.113	0.202	0.499	139	4	47	31	236	59
97pr56	54.92	1.0508	1.0019	0.9473	1.049	1.058	1.109	1.109	0.054	0.62	2	3	92	6	241	84
97pr57	30.44	1.0062	1.001	0.9928	1.005	1.008	1.014	1.014	0.217	0.487	98	63	229	18	325	19
97pr58	40.12	1.0599	1.031	0.9091	1.028	1.134	1.166	1.178	0.617	0.212	138	19	44	12	283	68
97pr59	75.34	1.0268	1.0211	0.9521	1.006	1.072	1.078	1.088	0.846	0.08	173	59	307	23	46	19
97pr60	51.36	1.0847	1.0692	0.8461	1.014	1.264	1.282	1.322	0.87	0.067	147	18	43	37	257	47

Site	Kavg	K1	K2	K3	L	F	P	P'	T	q	K1 Azimuth	K1 plunge	K2 Azimuth	K2 plunge	K3 Azimuth	K3 plunge
97pr61	44.36	1.0584	0.9817	0.9599	1.078	1.023	1.103	1.108	-0.556	1.274	129	3	253	84	39	5
97pr62	48.24	1.0614	0.9884	0.9502	1.074	1.04	1.117	1.119	-0.312	0.976	327	19	227	26	88	58
97pr63	59.41	1.0782	1.0389	0.8829	1.038	1.177	1.221	1.237	0.597	0.224	304	3	212	31	40	59
97pr64	53.56	1.0531	0.9816	0.9653	1.073	1.017	1.091	1.097	-0.627	1.371	324	17	187	68	58	14
97pr65	66.99	1.0393	1.0049	0.9558	1.034	1.051	1.087	1.088	0.176	0.519	160	25	250	0	341	65
97pr66	40.66	1.0471	1.0392	0.9137	1.008	1.137	1.146	1.166	0.881	0.062	131	10	26	56	227	32
97pr67	42.92	1.0441	1.0202	0.9357	1.023	1.09	1.116	1.123	0.558	0.248	137	19	33	36	249	48
97pr68	43.02	1.0509	1.0345	0.9146	1.016	1.131	1.149	1.164	0.759	0.128	88	26	349	16	231	59
97pr69	50.54	1.0591	1.0321	0.9087	1.026	1.136	1.165	1.178	0.641	0.197	323	7	56	22	217	66
97pr70	47.87	1.0588	1.0295	0.9117	1.029	1.129	1.161	1.172	0.601	0.222	317	11	50	13	190	73
97pr71	58.77	1.0171	0.9966	0.9863	1.021	1.01	1.031	1.032	-0.335	1.002	343	10	238	55	79	33
97pr72	78.14	1.0241	0.9901	0.9858	1.034	1.004	1.039	1.043	-0.773	1.592	146	6	54	14	260	75
97pr73	35.6	1.0415	1.0095	0.949	1.032	1.064	1.097	1.099	0.308	0.419	334	9	144	81	243	1
97pr74	46.04	1.0285	1.0054	0.9662	1.023	1.041	1.065	1.065	0.258	0.456	167	2	257	0	345	88
97pr75	43.49	1.0416	0.9997	0.9587	1.042	1.043	1.086	1.086	-0.01	0.675	182	11	91	6	332	77
97pr76	57.63	1.0517	0.9932	0.955	1.059	1.04	1.101	1.102	-0.21	0.867	168	3	77	21	266	69
97pr77	54.09	1.0451	1.0164	0.9385	1.028	1.083	1.114	1.118	0.462	0.311	200	4	109	20	302	70
97pr78	62.41	1.06	1.0052	0.9348	1.055	1.075	1.134	1.134	0.124	0.561	343	0	73	11	251	79
97pr79	56.65	1.0487	1.0124	0.9389	1.036	1.078	1.117	1.12	0.338	0.397	332	39	63	1	154	51
97pr80	51.53	1.0433	1.0233	0.9335	1.02	1.096	1.118	1.126	0.636	0.2	319	24	220	0	139	66
97pr81	53.27	1.0514	1.0035	0.9452	1.048	1.062	1.112	1.113	0.098	0.583	318	6	50	16	208	73

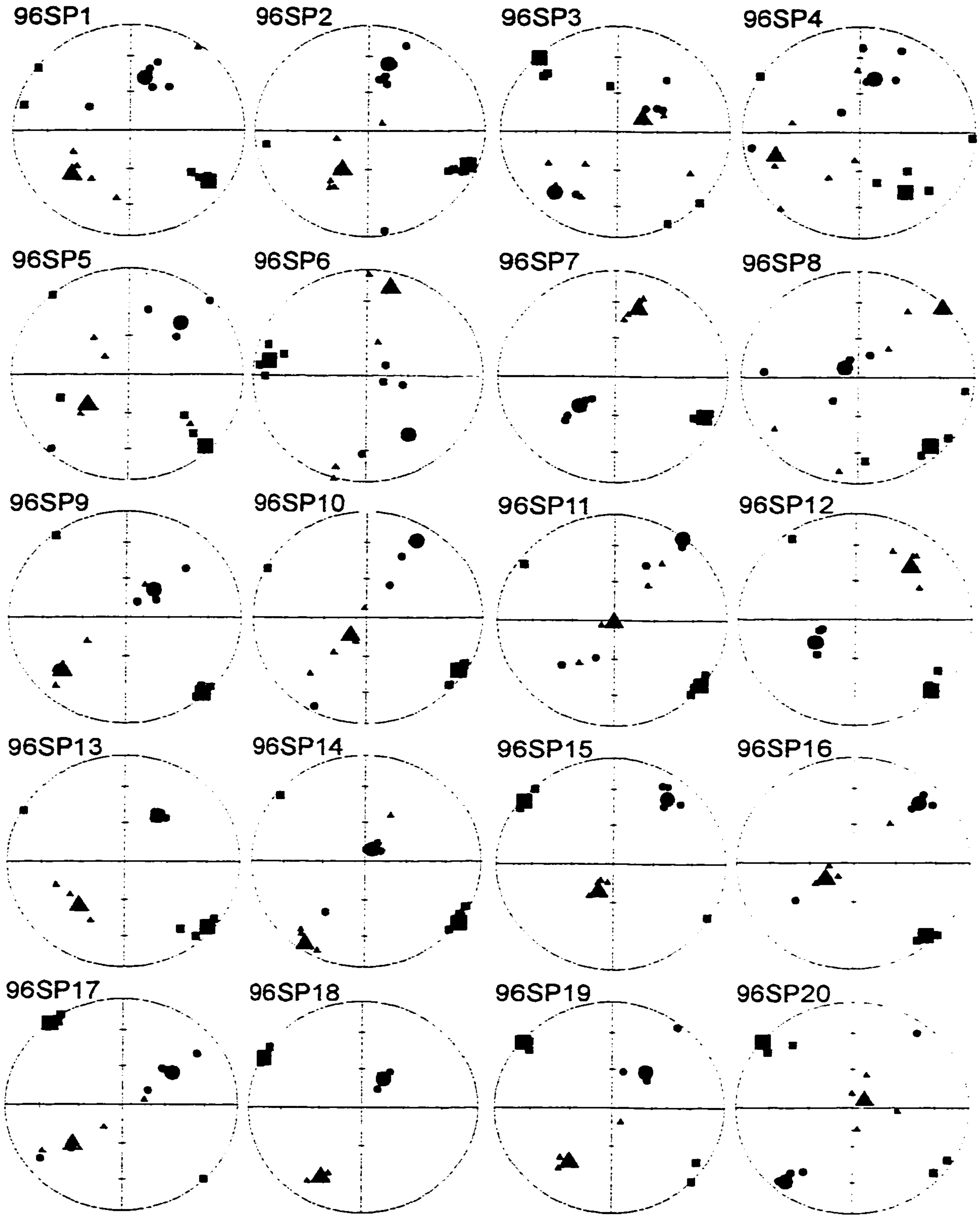
96SP1
96SP2
96SP3
96SP4
96SP5
96SP6
96SP7
96SP8
96SP9
96SP10
96SP11
96SP12
96SP13
96SP14
96SP15
96SP16
96SP17
96SP18
96SP19
96SP20

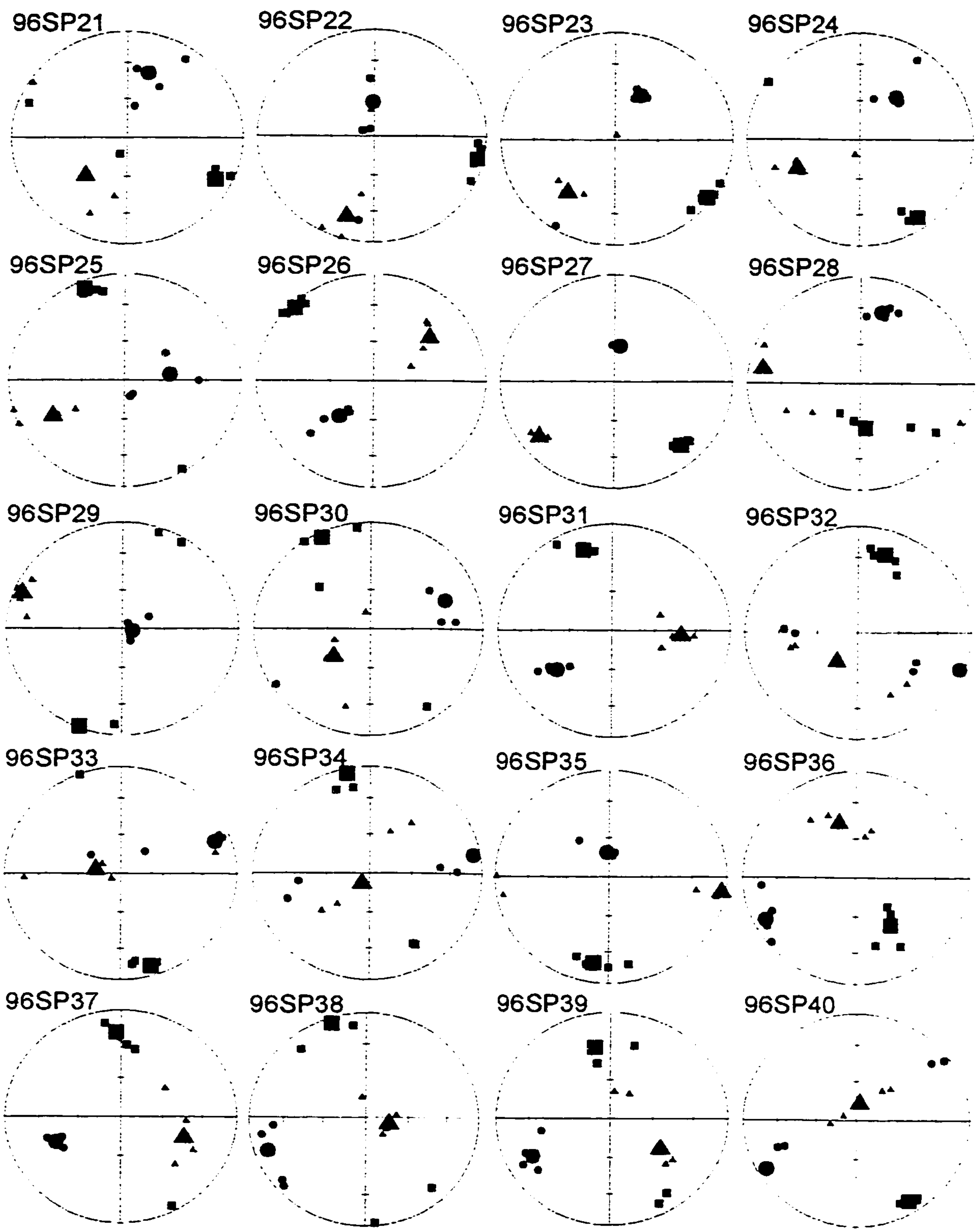
96SP21
96SP22
96SP23
96SP24
96SP25
96SP26
96SP27
96SP28
96SP29
96SP30
96SP31
96SP32
96SP33
96SP34
96SP35
96SP36
96SP37
96SP38
96SP39
96SP40

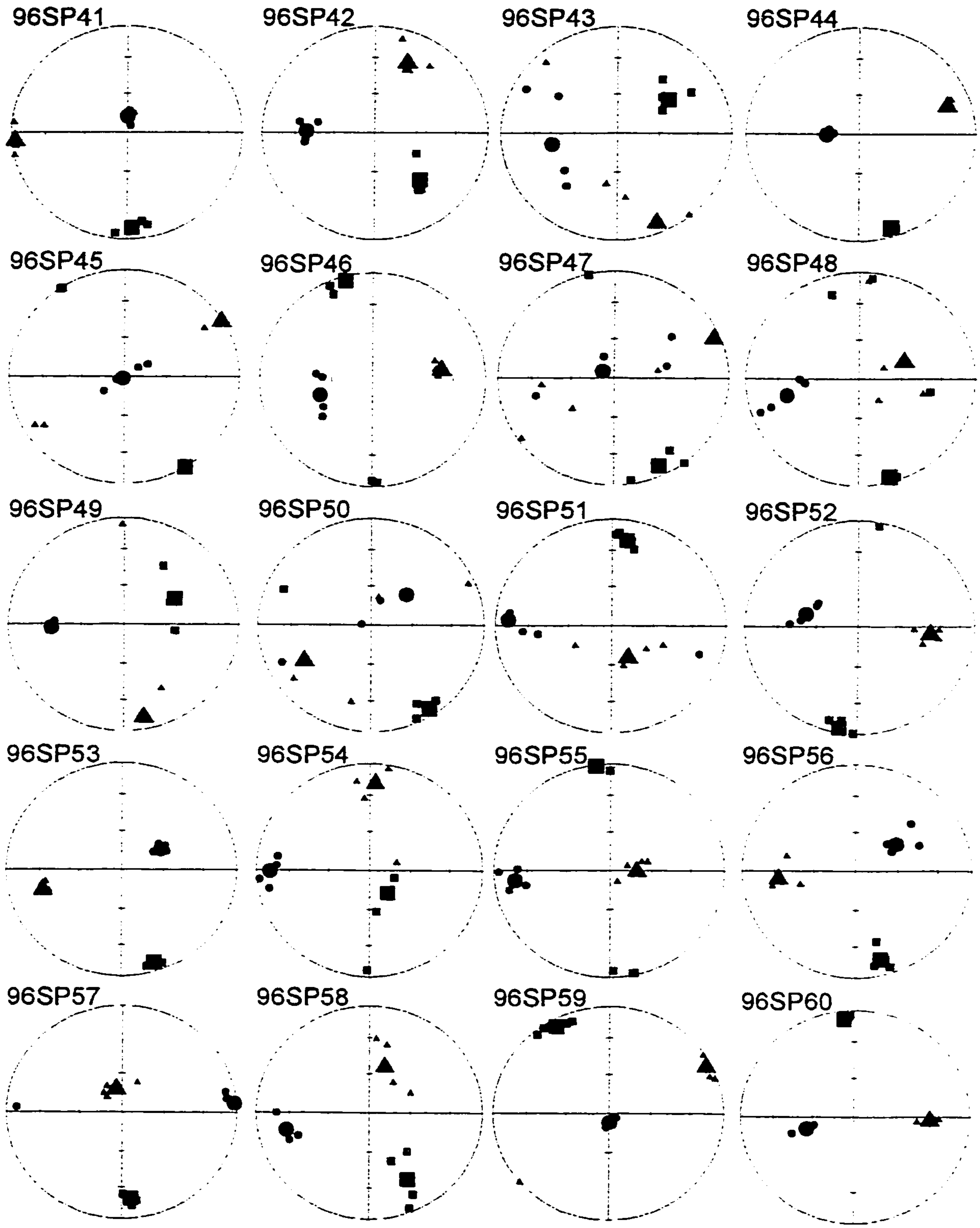
96SP41
96SP42
96SP43
96SP44
96SP45
96SP46
96SP47
96SP48
96SP49
96SP50
96SP51
96SP52
96SP53
96SP54
96SP55
96SP56
96SP57
96SP58
96SP59
96SP60

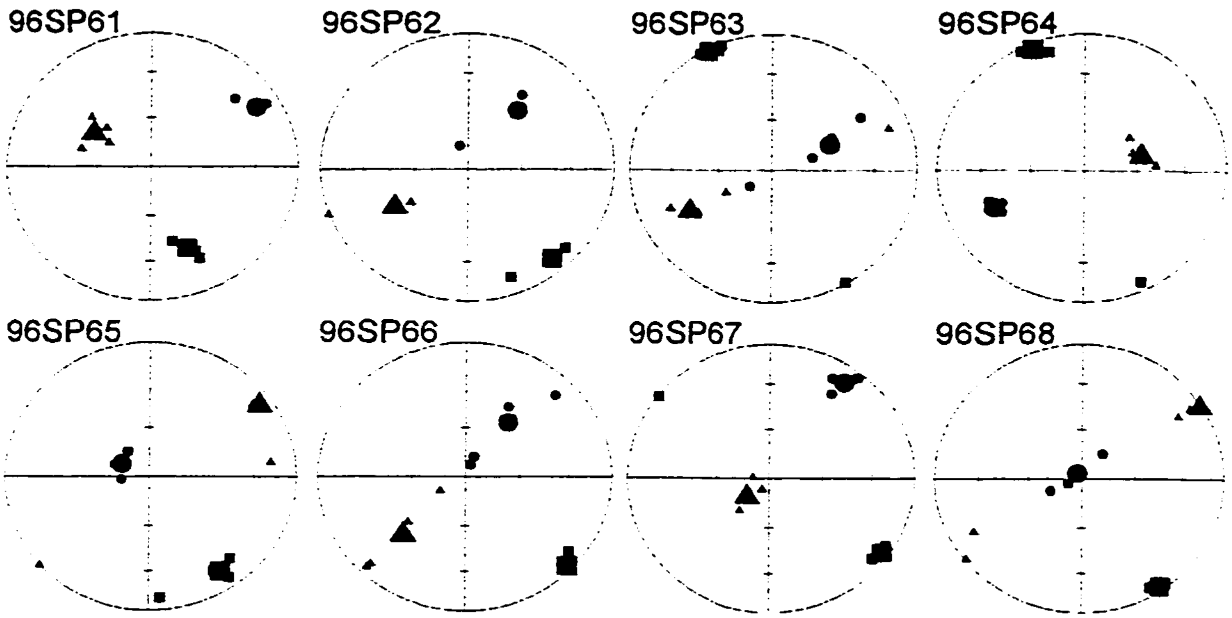
96SP61
96SP62
96SP63
96SP64
96SP65
96SP66
96SP67
96SP68

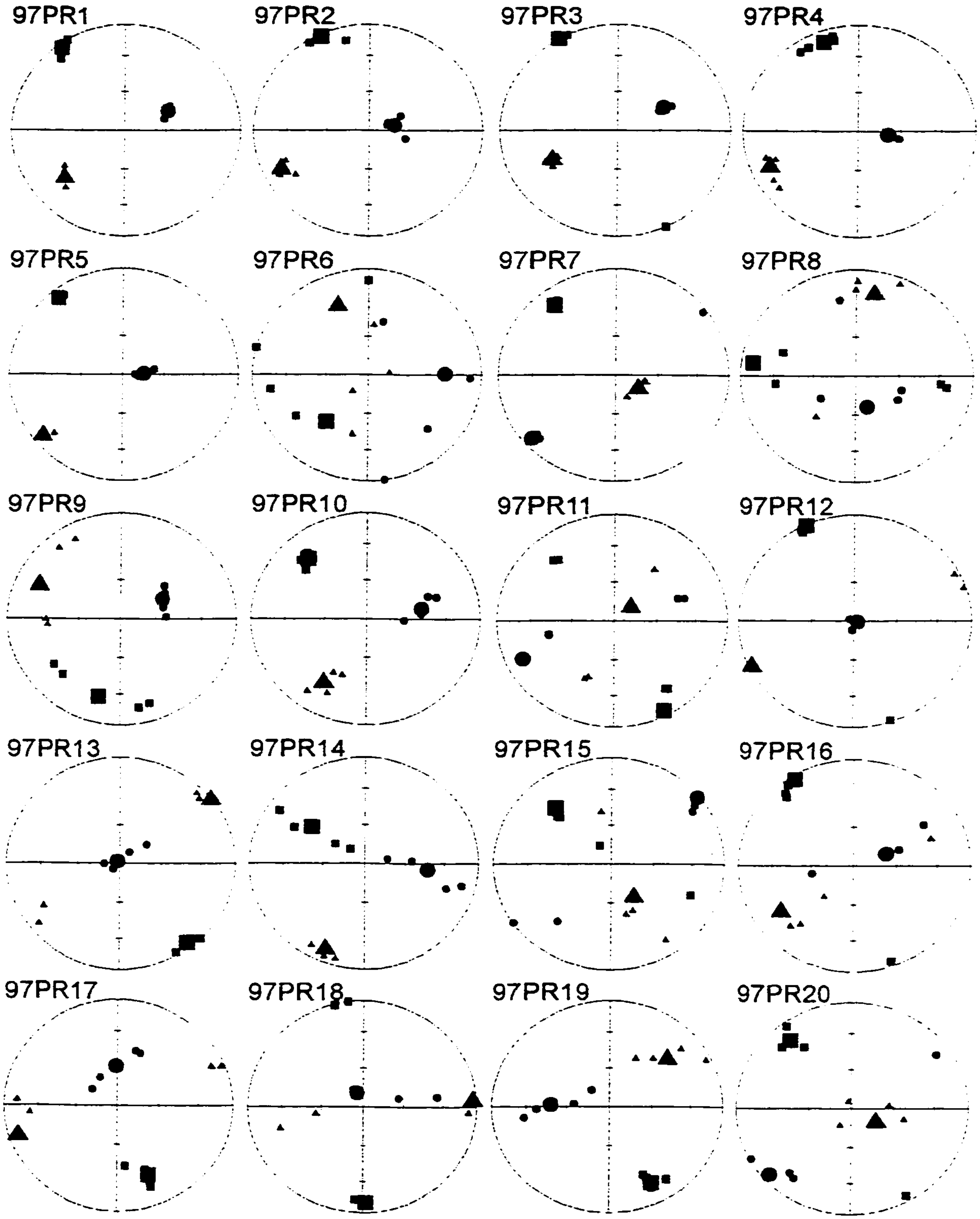
97PR1
97PR2
97PR3
97PR4
97PR5
97PR6
97PR7
97PR8
97PR9
97PR10
97PR11
97PR12
97PR13
97PR14
97PR15
97PR16
97PR17
97PR18
97PR19
97PR20

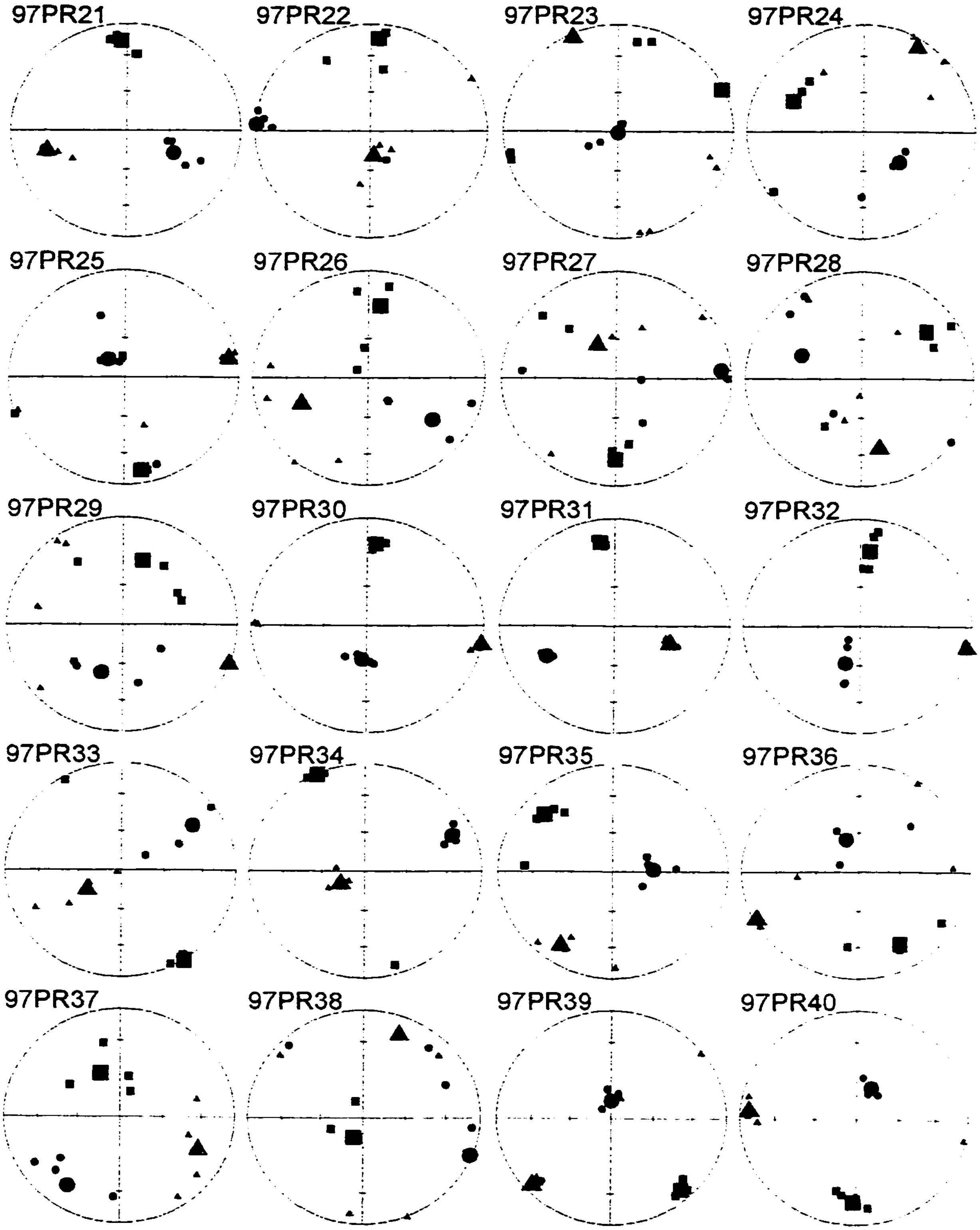
97PR21
97PR22
97PR23
97PR24
97PR25
97PR26
97PR27
97PR28
97PR29
97PR30
97PR31
97PR32
97PR33
97PR34
97PR35
97PR36
97PR37
97PR38
97PR39
97PR40

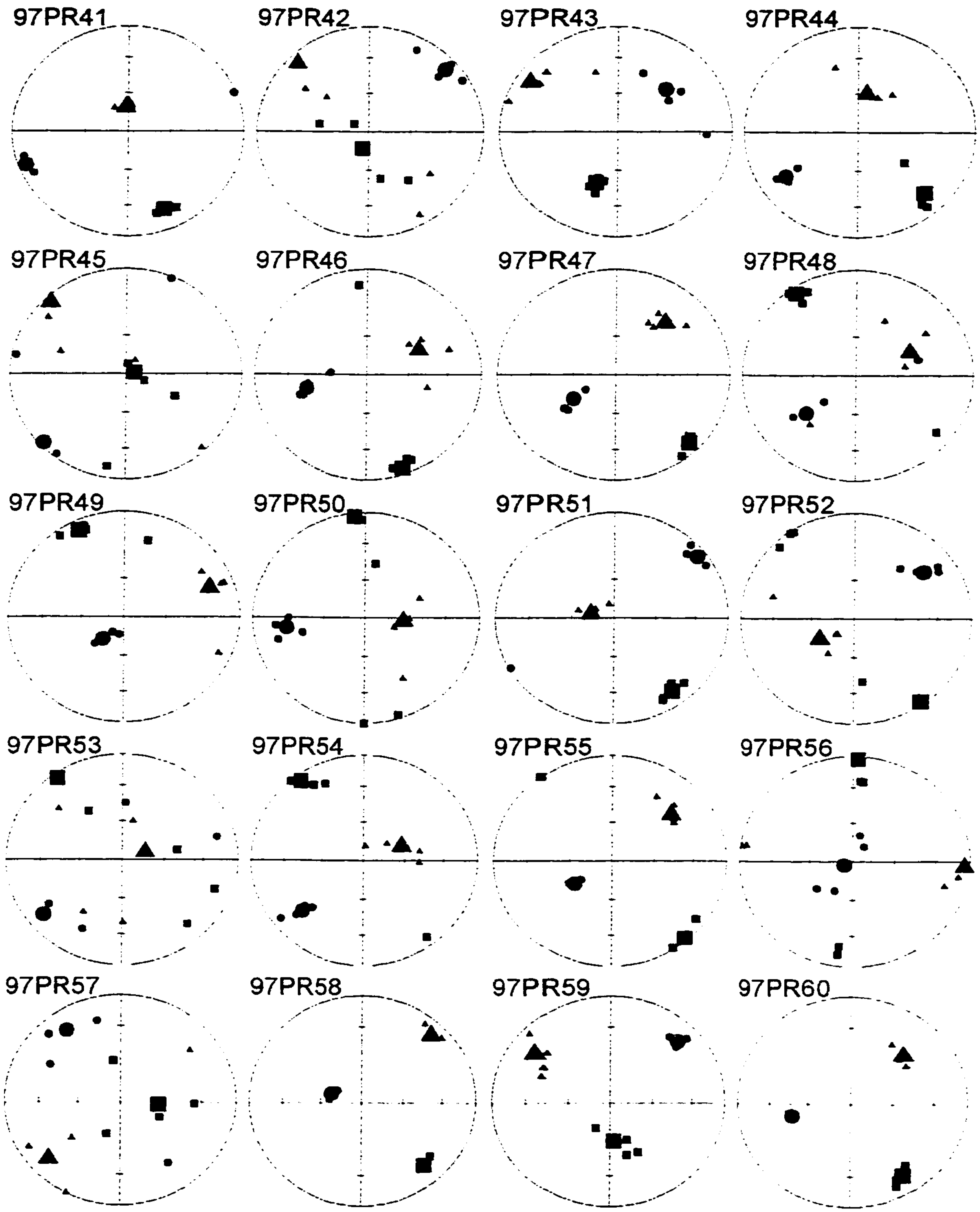
97PR41
97PR42
97PR43
97PR44
97PR45
97PR46
97PR47
97PR48
97PR49
97PR50
97PR51
97PR52
97PR53
97PR54
97PR55
97PR56
97PR57
97PR58
97PR59
97PR60

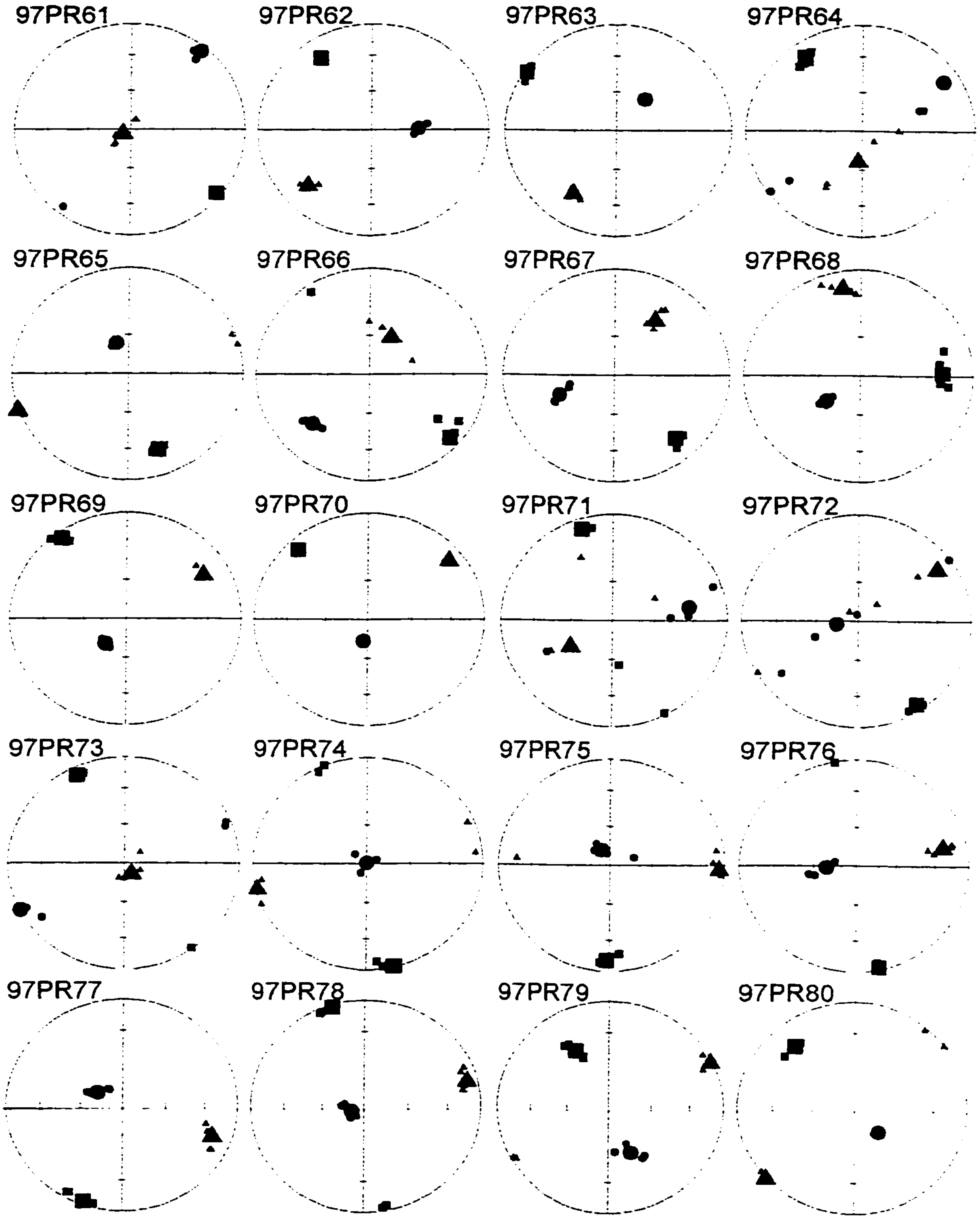
97PR61
97PR62
97PR63
97PR64
97PR65
97PR66
97PR67
97PR68
97PR69
97PR70
97PR71
97PR72
97PR73
97PR74
97PR75
97PR76
97PR77
97PR78
97PR79
97PR80

97PR81

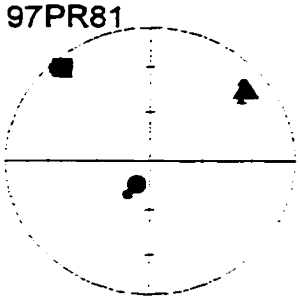

APPENDIX II: STATION LOCATIONS

Page 191 is a map of the Sparrow station locations. All station numbers contain a 96-NL- prefix. Page 192 is a map of the Prosperous Pluton. Sample numbers for the Prosperous Pluton contain the 97-NL- prefix. Pages 193-202 consist of a table that lists all station numbers and corresponding: drill site numbers, drill core orientations, hand sample numbers, hand sample orientations and thin section orientations. For the thin sections, sections are numbered with the drill core number (for the AMS granite samples) or the hand sample number (for the hand samples). Orientations of thin sections marked "A" are given in strike and dip. The strike corresponds to the arrow direction and the dip direction is 90^0 counterclockwise from the given strike direction. All other attitudes are in the Right Hand Rule (RHR) unless a direction is given with the dip or as stated above.

SPARROW PLUTON STATION LOCATION MAP

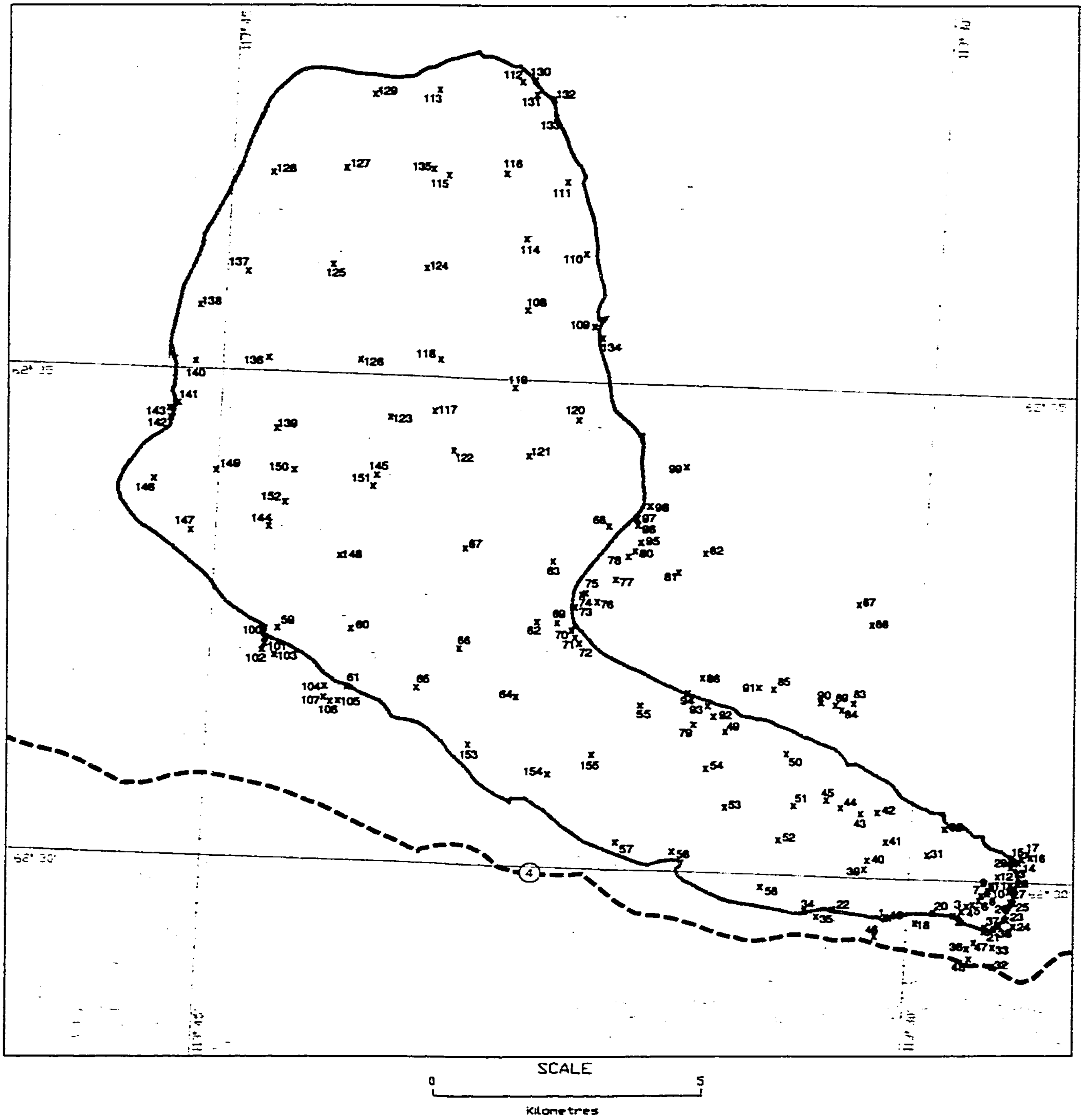

PROSPEROUS PLUTON STATION LOCATION MAP

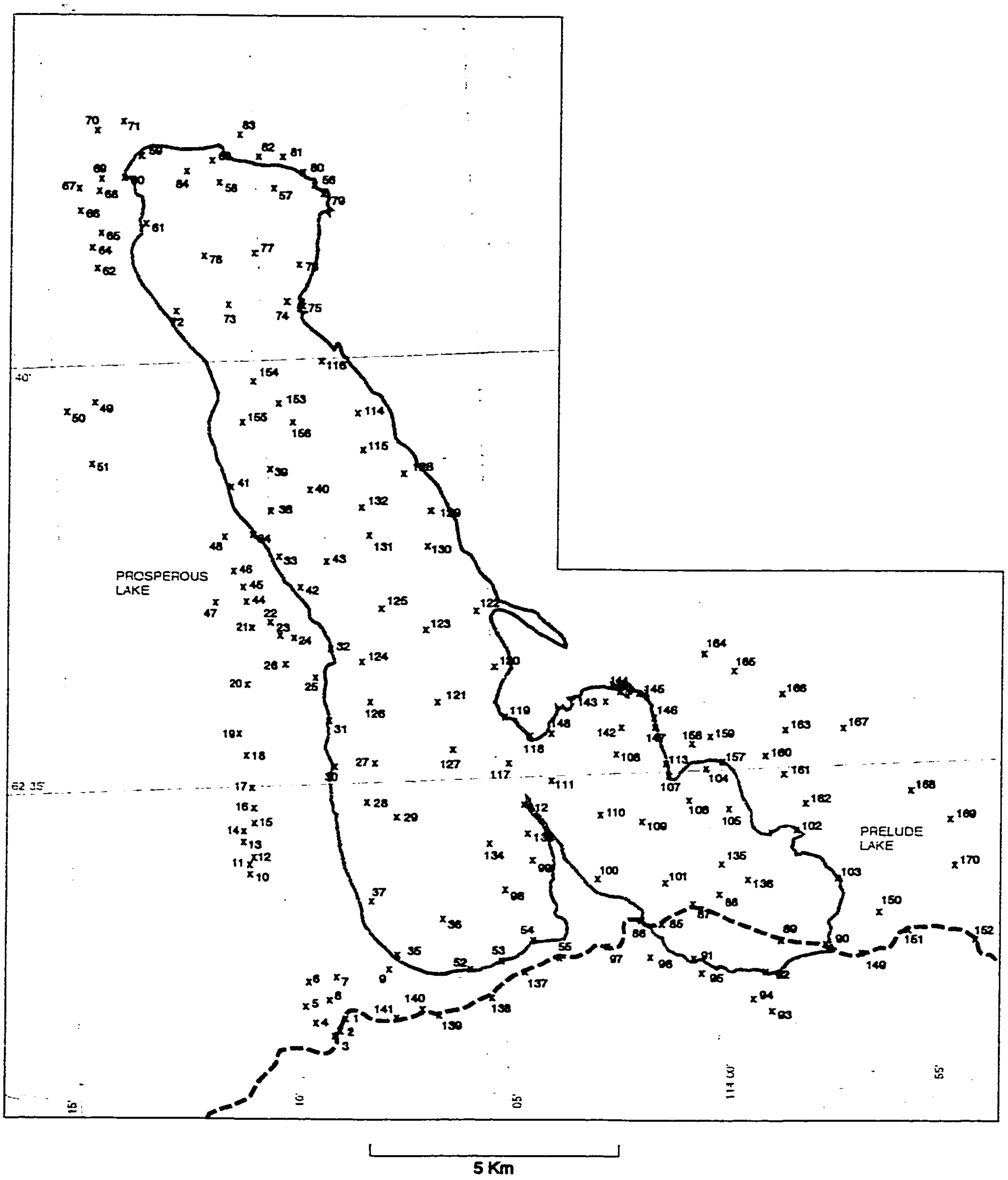

OUTCROP #	DRILL CORES Drill Station	Thin section	Drill Cores	Core Orientation	HAND SAMPLES Hand Sample	Sample Orientation	THIN SECTIONS ORIENTATIONS A: strike/dip	B: strike/dip	B: arrow trend/plunge
96-NL-001									
96-NL-002									
96-NL-003									
96-NL-004									
96-NL-005									
96-NL-006									
96-NL-007									
96-NL-008									
96-NL-009									
96-NL-010									
96-NL-011									
96-NL-012									
96-NL-013									
96-NL-014									
96-NL-015									
96-NL-016									
96-NL-017					96-N-1	356 / 44 NE	356/46	266/90	086/44
96-NL-018					96-N-7	102 / 66 S	102/24	192/90	192/66
96-NL-019	96-SP-1	Yes	A	329 / 84					
			B	007 / 83					
			C	130 / 80					
96-NL-020	96-SP-2	Yes	A	156 / 86.5					
			B	000 / 90					
			C	142 / 85					
96-NL-021	96-SP-3	Yes	A	067 / 87					
			B	088 / 79					
			C	198 / 82					
96-NL-022	96-SP-4	Yes	A	018 / 83					
			B	014 / 82.5					
			C	118 / 86					
96-NL-023									
96-NL-024									
96-NL-025									
96-NL-026	96-SP-5	Yes	A	131 / 88					
			B	344 / 81					
96-NL-027									
96-NL-028									
96-NL-029	96-SP-6	Yes	A	314 / 85					
			B	162 / 87					
96-NL-030	96-SP-7	Yes	A	317 / 86					
			B	168 / 86					
96-NL-031	96-SP-8	Yes	A	132 / 88					
			B	218 / 88					
96-NL-032					96-N-2	072 / 32 NW	B: 285/02	A:206/90	A: 206/88
96-NL-033					96-N-3	105 / 76 SW			
96-NL-034									
96-NL-035									
96-NL-036									
96-NL-037					96-N-4	135 / 66 SW	135/24	045/90	225/66
96-NL-038					96-N-5	065 / 54 SE	65/36	335/90	155/54
					96-N-6a	000 / 00	000/90	270/90	090/00

OUTCROP #	DRILL CORES				HAND SAMPLES		THIN SECTIONS ORIENTATIONS		
	Drill Station	Thin section	Drill Cores	Core Orientation	Hand Sample	Sample Orientation	A: strike/dip	B: strike/dip	B: arrow trend/plunge
96-NL-039	96-SP-9	Yes	A	207 / 87.5	96-N-6b	010 / 90			
			B	234 / 89					
96-NL-040									
96-NL-041									
96-NL-042									
96-NL-043	96-SP-10	Yes	A	000 / 90					
			B	000 / 90					
96-NL-044									
96-NL-045	96-SP-11	Yes	A	000 / 90					
			B	124 / 89					
96-NL-046									
96-NL-047									
96-NL-048									
96-NL-049	96-SP-12	Yes	A	000 / 90					
			B	207 / 88					
96-NL-050	96-SP-13	Yes	A	121 / 89.5					
			B	327 / 89					
96-NL-051	96-SP-14	Yes	A	099 / 87					
			B	152 / 88.5					
96-NL-052	96-SP-15	Yes	A	310 / 86					
			B	029 / 86.5					
96-NL-053	96-SP-16	Yes	A	306 / 86					
			B	224 / 88.5					
96-NL-054	96-SP-17	Yes	A	346 / 87					
			B	308 / 85.5					
96-NL-055	96-SP-18	Yes	A	047 / 88					
			B	003 / 87					
96-NL-056	96-SP-19	Yes	A	226 / 87.6					
			B	061 / 89					
96-NL-057	96-SP-20	Yes	A	000 / 90					
			B	220 / 88					
96-NL-058									
96-NL-059	96-SP-21	Yes	A	115 / 88					
			B	145 / 89					
96-NL-060	96-SP-22	Yes	A	186 / 85.5	96-N-8	084 / 82 NW	264/08	354/90	354/82
			B	300 / 88.5					
96-NL-061	96-SP-23	Yes	A	266 / 87					
			B	246 / 88					
96-NL-062	96-SP-24	Yes	A	017 / 89					
			B	000 / 90					
96-NL-063	96-SP-25	Yes	A	006 / 87					
			B	221 / 89					
96-NL-064	96-SP-26	Yes	A	202 / 89					
			B	341 / 89.5					
96-NL-065	96-SP-27	Yes	A	349 / 86.5					
			B	080 / 88					
96-NL-066	96-SP-28	Yes	A	025 / 89					
			B	015 / 85					
96-NL-067	96-SP-29	Yes	A	299 / 88					
			B	344 / 88					
96-NL-068	96-SP-30	Yes	A	253 / 89					

OUTCROP #	DRILL CORES Drill Station	Thin section	Drill Cores	Core Orientation	HAND SAMPLES Hand Sample	Sample Orientation	THIN SECTIONS ORIENTATIONS A: strike/dip	B: strike/dip	B: arrow trend/plunge
			B	324 / 89					
96-NL-069					96-N-9	220 / 85	220/05	130/90	310/85
96-NL-070									
96-NL-071									
96-NL-072					96-N-10a	205 / 85	205/05	295/90	295/85
					96-N-10b	000 / 20			
96-NL-073									
96-NL-074									
96-NL-075					96-N-11	350 / 75	350/15	260/90	080/75
96-NL-076									
96-NL-077									
96-NL-078									
96-NL-079									
96-NL-080									
96-NL-081									
96-NL-082					96-N-12		thin section not oriented		
96-NL-083									
96-NL-084					96-N-13	022 / 18 E	022/72	292/90	112/18
96-NL-085									
96-NL-086									
96-NL-087									
96-NL-088									
96-NL-089									
96-NL-090									
96-NL-091									
96-NL-092									
96-NL-093									
96-NL-094					96-N-14	126 / 85	126/05	036/90	216/85
96-NL-095					96-N-15	185 / 65	185/25	095/90	275/65
96-NL-096					96-N-16	345 / 55	345/35	255/90	075/55
96-NL-097									
96-NL-098									
96-NL-099									
96-NL-100					96-N-17	120 / 63	120/27	030/90	210/63
96-NL-101					96-N-18	100 / 78			
96-NL-102									
96-NL-103									
96-NL-104					96-N-19	080 / 67			
96-NL-105					96-N-20	135 / 82	135/08	045/90	225/82
96-NL-106					96-N-21	328 / 76	328/14	238/90	058/76
96-NL-107					96-N-22	320 / 86			
96-NL-108	96-SP-31	Yes	A	304 / 86					
			B	000 / 90					
96-NL-109	96-SP-32	Yes	A	000 / 90					
			B	000 / 90					
96-NL-110	96-SP-33	Yes	A	230 / 87					
			B	014 / 88.5					
96-NL-111	96-SP-34	Yes	A	275 / 89					
			B	000 / 90					
96-NL-112	96-SP-35	Yes	A	000 / 90					

OUTCROP #	DRILL CORES Drill Station	Thin section	Drill Cores	Core Orientation	HAND SAMPLES Hand Sample	Sample Orientation	THIN SECTIONS ORIENTATIONS A: strike/dip	B: strike/dip	B: arrow trend/plunge
			B	140 / 89					
96-NL-113	96-SP-36	Yes	A	167 / 86					
			B	230 / 86					
96-NL-114	96-SP-37	Yes	A	170 / 88.5					
			B	314 / 86.5					
96-NL-115	96-SP-38	Yes	A	060 / 89					
			B	179 / 88					
96-NL-116	96-SP-39	Yes	A	000 / 90					
			B	000 / 90					
			C	220 / 89.5					
96-NL-117	96-SP-40	Yes	A	257 / 87					
			B	204 / 87.5					
96-NL-118	96-SP-41	Yes	A	064 / 88.5					
			B	298 / 89.5					
96-NL-119	96-SP-42	Yes	A	262 / 89					
			B	328 / 88					
96-NL-120	96-SP-43	Yes	A	329 / 87					
			B	097 / 88					
96-NL-121	96-SP-44	Yes	A	249 / 85					
			B	088 / 84					
96-NL-122	96-SP-45	Yes	A	036 / 87					
			B	040 / 87					
96-NL-123	96-SP-46	Yes	A	122 / 88					
			B	316 / 88.5					
96-NL-124	96-SP-47	Yes	A	227 / 89					
			B	000 / 90					
96-NL-125	96-SP-48	Yes	A	111 / 86.5					
			B	141 / 88					
96-NL-126	96-SP-49	Yes	A	066 / 88.5					
			B	154 / 87					
96-NL-127	96-SP-50	Yes	A	145 / 87					
			B	027 / 85					
96-NL-128	96-SP-51	Yes	A	197 / 86.5					
			B	262 / 86.5					
96-NL-129	96-SP-52	Yes	A	135 / 87					
			B	117 / 82					
96-NL-130					96-N-23	011 / 90	011/00	281/90	101/90
96-NL-131									
96-NL-132									
96-NL-133									
96-NL-134									
96-NL-135									
96-NL-136	96-SP-53	Yes	A	240 / 87					
			B	258 / 87.5					
96-NL-137	96-SP-54	Yes	A	158 / 86					
			B	256 / 86					
96-NL-138	96-SP-55	Yes	A	150 / 88					
			B	150 / 89					
96-NL-139	96-SP-56	Yes	A	202 / 85					
			B	169 / 86.5					
96-NL-140	96-SP-57	Yes	A	226 / 86.5					
			B	270 / 88					

OUTCROP #	DRILL CORES				HAND SAMPLES		THIN SECTIONS ORIENTATIONS		
	Drill Station	Thin section	Drill Cores	Core Orientation	Hand Sample	Sample Orientation	A: strike/dip	B: strike/dip	B: arrow trend/plunge
96-NL-141	96-SP-58	Yes	A	041 / 85					
			B	347 / 87					
96-NL-142									
96-NL-143					96-N-24	183 / 65			
96-NL-144	96-SP-59	Yes	A	237 / 86.5					
			B	260 / 89					
96-NL-145	96-SP-60	Yes	A	042 / 83					
			B	034 / 85					
96-NL-146	96-SP-61	Yes	A	060 / 89.5					
			B	160 / 87					
96-NL-147	96-SP-62	Yes	A	045 / 85					
			B	065 / 85.5					
96-NL-148	96-SP-63	Yes	A	091 / 84.5					
			B	070 / 86					
96-NL-149	96-SP-64	Yes	A	238 / 86.5					
			B	259 / 85					
96-NL-150	96-SP-65	Yes	A	287 / 87					
			B	309 / 89					
96-NL-151									
96-NL-152									
96-NL-153	96-SP-66	Yes	A	215 / 89					
			B	233 / 88					
96-NL-154	96-SP-67	Yes	A	045 / 86.5					
			B	086 / 87					
96-NL-155	96-SP-68	Yes	A	218 / 84					
			B	263 / 83.5					
97-NL-001					97-N-1	134 / 73	134/17	044/90	224/73
97-NL-002									
97-NL-003									
97-NL-004									
97-NL-005									
97-NL-006									
97-NL-007					97-N-2	138 / 52			
97-NL-008									
97-NL-009									
97-NL-010									
97-NL-011									
97-NL-012									
97-NL-013					97-N-3	315 / 88 NE	315/02	225/90	045/88
97-NL-014									
97-NL-015									
97-NL-016									
97-NL-017									
97-NL-018									
97-NL-019									
97-NL-020									
97-NL-021					97-N-4	350 / 80 SW			
97-NL-022					97-N-5	135 / 90			
97-NL-023					97-N-6	248 / 73 NW			

OUTCROP #	DRILL CORES				HAND SAMPLES		THIN SECTIONS ORIENTATIONS		
	Drill Station	Thin section	Drill Cores	Core Orientation	Hand Sample	Sample Orientation	A: strike/dip	B: strike/dip	B: arrow trend/plunge
97-NL-024					97-N-7	300 / 79 NE			
97-NL-025					97-N-8	173 / 68 SW			
97-NL-026									
97-NL-027	97-PR-1	Yes	A	234 / 88.5					
			B	114 / 83					
97-NL-028	97-PR-2		A	250 / 84					
			B	296 / 86					
97-NL-029	97-PR-3		A	125 / 83					
97-NL-030	97-PR-4		A	229 / 87					
			B	061 / 87					
97-NL-031	97-PR-5		A	337 / 89					
			B	306 / 85					
97-NL-032	97-PR-6		A	110 / 86					
			B	044 / 83.5					
97-NL-033	97-PR-7		A	060 / 87					
			B	328 / 88					
97-NL-034					97-N-9	140 / 82			
97-NL-035	97-PR-8		A	009 / 86					
			B	283 / 88					
97-NL-036	97-PR-9		A	232 / 86					
			B	064 / 89					
97-NL-037	97-PR-10		A	316 / 83.5					
			B	348 / 87					
97-NL-038	97-PR-11	Yes	A	211 / 83					
			B	125 / 83					
97-NL-039	97-PR-12		A	162 / 83					
			B	204 / 85					
97-NL-040	97-PR-13		A	300 / 83					
			B	076 / 87					
			C	320 / 84					
97-NL-041	97-PR-14		A	000 / 90					
			B	060 / 88					
97-NL-042	97-PR-15	Yes	A	018 / 87					
			B	335 / 88					
			C	021 / 86					
97-NL-043	97-PR-16		A	273 / 82					
			B	048 / 85					
97-NL-044									
97-NL-045									
97-NL-046									
97-NL-047									
97-NL-048					97-N-10	352 / 55 W			
97-NL-049									
97-NL-050									
97-NL-051									
97-NL-052	97-PR-17		A	031 / 86.5					
			B	302 / 87					
97-NL-053	97-PR-18		A	000 / 90					
			B	003 / 86					
97-NL-054	97-PR-19		A	314 / 83					
			B	182 / 82.5					
97-NL-055					97-N-11	100 / 08 S	100/82	010/90	190/08

OUTCROP #	DRILL CORES				HAND SAMPLES		THIN SECTIONS ORIENTATIONS		
	Drill Station	Thin section	Drill Cores	Core Orientation	Hand Sample	Sample Orientation	A: strike/dip	B: strike/dip	B: arrow trend/plunge
97-NL-056	97-PR-20		A	172 / 85					
			B	146 / 86					
97-NL-057	97-PR-21		A	324 / 88					
			B	133 / 87					
97-NL-058	97-PR-22		A	284 / 89					
			B	058 / 89.5					
97-NL-059	97-PR-23		A	312 / 87					
			B	306 / 89					
97-NL-060	97-PR-24		A	022 / 87					
			B	206 / 85					
97-NL-061	97-PR-25	Yes	A	093 / 87					
			B	275 / 89.5					
97-NL-062									
97-NL-063	97-PR-26		A	100 / 88					
			B	070 / 85					
97-NL-064					97-N-12	164 / 68 W			
97-NL-065									
97-NL-066									
97-NL-067									
97-NL-068									
97-NL-069									
97-NL-070									
97-NL-071									
97-NL-072	97-PR-27		A	330 / 86.5					
			B	070 / 86					
97-NL-073	97-PR-28	Yes	A	107 / 88					
			B	045 / 86					
97-NL-074	97-PR-29		A	183 / 88.5					
			B	343 / 86.5					
97-NL-075									
97-NL-076	97-PR-30	Yes	A	350 / 89					
			B	209 / 89					
97-NL-077	97-PR-31		A	073 / 88					
			B	283 / 87					
97-NL-078	97-PR-32		A	336 / 85					
			B	289 / 87					
97-NL-079					97-N-13a	302 / 25			
97-NL-080									
97-NL-081									
97-NL-082					97-N-14	261 / 25 NW	261/65	171/90	351/25
97-NL-083									
97-NL-084									
97-NL-085	97-PR-33		A	256 / 89.5					
			B	068 / 86					
97-NL-086					97-N-15	294 / 82 N	294/08	204/90	024/82
					97-N-16	180 / 74 W			
					97-N-17	154 / 06 S	154/06	064/90	244/06
					97-N-33	184 / 84 W	184/06	094/90	274/84
97-NL-087	97-PR-34		A	306 / 88.5					
			B	010 / 88					
97-NL-088	97-PR-35		A	006 / 85					
			B	329 / 84					

OUTCROP #	DRILL CORES				HAND SAMPLES		THIN SECTIONS ORIENTATIONS		
	Drill Station	Thin section	Drill Cores	Core Orientation	Hand Sample	Sample Orientation	A: strike/dip	B: strike/dip	B: arrow trend/plunge
97-NL-089	97-PR-36		A	000 / 90					
			B	190 / 88					
97-NL-090	97-PR-37		A	000 / 90					
			B	020 / 87					
97-NL-091	97-PR-38		A	235 / 87					
			B	322 / 83					
97-NL-092	97-PR-39		A	296 / 87.5					
			B	225 / 87					
97-NL-093									
97-NL-094									
97-NL-095									
97-NL-096									
97-NL-097									
97-NL-098	97-PR-40		A	126 / 87					
			B	116 / 88					
97-NL-099	97-PR-41		A	273 / 86					
			B	334 / 89					
97-NL-100	97-PR-42		A	328 / 85					
			B	330 / 86.5					
97-NL-101	97-PR-43		A	091 / 88					
			B	046 / 86					
97-NL-102	97-PR-44		A	191 / 80					
			B	214 / 84					
97-NL-103	97-PR-45		A	170 / 85					
			B	062 / 85					
97-NL-104	97-PR-46		A	121 / 88					
			B	159 / 87					
97-NL-105	97-PR-47		A	158 / 87					
			B	105 / 87.5					
97-NL-106	97-PR-48		A	295 / 88					
			B	232 / 86					
97-NL-107									
					97-N-18	260 / 88	260/02	170/90	350/88
					97-N-19	341 / 48	341/42	251/90	071/48
					97-N-20	358 / 70	358/20	268/90	088/70
					97-N-21	010 / 60			
97-NL-108	97-PR-49		A	236 / 78					
			B	052 / 76					
97-NL-109	97-PR-50		A	150 / 86					
			B	106 / 85					
97-NL-110	97-PR-51		A	213 / 89					
			B	211 / 85.5					
97-NL-111	97-PR-52		A	329 / 89					
			B	117 / 87					
97-NL-112	97-PR-53		A	265 / 86					
			B	245 / 86					
			C	000 / 90					
97-NL-113									
97-NL-114	97-PR-54		A	028 / 87					
			B	120 / 88					
			C	239 / 84					
97-NL-115	97-PR-55		A	332 / 88					
			B	124 / 88					

OUTCROP #	DRILL CORES				HAND SAMPLES		THIN SECTIONS ORIENTATIONS		
	Drill Station	Thin section	Drill Cores	Core Orientation	Hand Sample	Sample Orientation	A: strike/dip	B: strike/dip	B: arrow trend/plunge
97-NL-116	97-PR-56		A	225 / 85					
			B	118 / 87.5					
97-NL-117	97-PR-57	Yes	A	273 / 84.5					
			B	309 / 83					
			C	282 / 82					
97-NL-118									
97-NL-119									
97-NL-120	97-PR-58		A	058 / 86.5					
			B	085 / 84					
97-NL-121	97-PR-59		A	125 / 88					
			B	190 / 88					
97-NL-122	97-PR-60	Yes	A	252 / 86.5					
			B	324 / 85					
97-NL-123	97-PR-61		A	005 / 86.5					
			B	237 / 84					
97-NL-124	97-PR-62		A	223 / 86					
			B	291 / 85					
97-NL-125	97-PR-63		A	055 / 89					
			B	295 / 85					
97-NL-126	97-PR-64		A	327 / 87					
			B	174 / 89					
97-NL-127	97-PR-65		A	248 / 86					
			B	140 / 87					
97-NL-128	97-PR-66		A	064 / 88.5					
			B	149 / 88					
97-NL-129	97-PR-67	Yes	A	140 / 85					
			B	097 / 86					
97-NL-130	97-PR-68		A	194 / 85					
			B	145 / 88					
97-NL-131	97-PR-69		A	031 / 88.5					
			B	278 / 89.5					
97-NL-132	97-PR-70		A	230 / 88					
			B	169 / 88.5					
97-NL-133	97-PR-71		A	080 / 89					
			B	190 / 81					
97-NL-134	97-PR-72		A	140 / 86					
			B	165 / 84					
97-NL-135	97-PR-73		A	245 / 86					
			B	267 / 86					
97-NL-136	97-PR-74		A	222 / 84					
			B	210 / 87					
97-NL-137					97-N-22	102 / 31 SW			
97-NL-138					97-N-23	000 / 00			
97-NL-139					97-N-24	113 / 41			
97-NL-140					97-N-25	114 / 59 SW	114/31	024/90	204/59
97-NL-141					97-N-26	125 / 50 SW	125/40	035/90	215/50
97-NL-142	97-PR-75		A	204 / 88					
			B	254 / 80					
97-NL-143	97-PR-76		A	092 / 86					
			B	300 / 86					
97-NL-144					97-N-26A	298 / 75 E			
97-NL-145					97-N-27	112 / 84 S	112/06	022/90	202/84

OUTCROP #	DRILL CORES				HAND SAMPLES		THIN SECTIONS ORIENTATIONS		
	Drill Station	Thin section	Drill Cores	Core Orientation	Hand Sample	Sample Orientation	A: strike/dip	B: strike/dip	B: arrow trend/plunge
					97-N-28	337 / 40 NE	337/50	247/90	067/40
97-NL-146					97-N-29	352 / 25 E			
97-NL-147					97-N-30	161 / 05	161/85	071/90	251/05
					97-N-31	321 / 44 NE	321/46	231/90	051/44
					97-N-32	360 / 65 E	360/25	270/90	090/65
97-NL-148	97-PR-77		A	151 / 84					
			B	265 / 88					
97-NL-149					97-N-34	106 / 87 SW			
97-NL-150					97-N-35	326 / 51 NE			
97-NL-151					97-N-36	020 / 80 E			
97-NL-152					97-N-37	326 / 80 NE			
97-NL-153	97-PR-78		A	325 / 88					
			B	239 / 83					
97-NL-154	97-PR-79	Yes	A	146 / 88					
			B	329 / 85					
97-NL-155	97-PR-80		A	164 / 87					
			B	094 / 87					
97-NL-156	97-PR-81		A	340 / 89					
			B	138 / 88					
97-NL-157					97-N-38	310 / 68 NE			
97-NL-158					97-N-39	329 / 20 E			
					97-N-40	295 / 52 NE			
97-NL-159					97-N-41	097 / 70 W			
97-NL-160					97-N-42	307 / 53 NE	307/37	217/90	037/53
97-NL-161					97-N-43	150 / 60 SW	150/30	060/90	240/60
97-NL-162					97-N-44	324 / 53 NE			
97-NL-163					97-N-45	314 / 56 NE	314/34	224/90	044/56
97-NL-164					97-N-46	320 / 55 NE			
97-NL-165					97-N-47	303 / 52	303/38	213/90	033/52
97-NL-166					97-N-48	316 / 65 NE			
97-NL-167					97-N-49	305 / 60 NE	305/30	215/90	035/60
97-NL-168					97-N-50	303 / 78 NE			
97-NL-169					97-N-51	302 / 78 NE			
97-NL-170					97-N-52	298 / 70			

APPENDIX III: STEREONETS FOR BEST FIT GREAT CIRCLE AND FOLD AXIS (MAGNETIC FOLIATIONS)

SPARROW PLUTON: NORTHERN REGION (MAGNETIC FOLIATION)

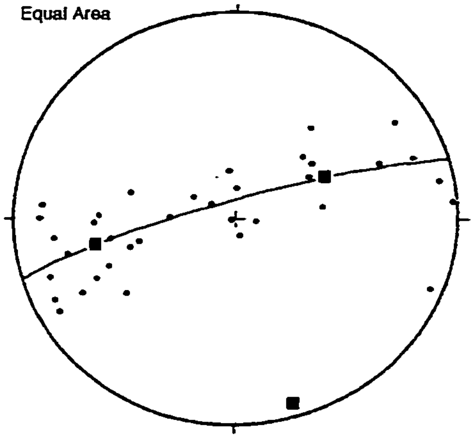

Eigenvalue		Eigenvector Trend	Plunge
1.	0.5728	258.6	36.2
2.	0.3892	63.4	52.9
3.	0.0380	163.2	7.3

95 % Elliptical Confidence Cones:

Axis 1: Max = 43.3°, Min = 6.0°

Axis 3: Max = 7.6°, Min = 5.5°

Best Fit Great Circle: 253/83 N

Fold Axis (Trend/Plunge): 163/07

SPARROW PLUTON: SOUTHERN REGION (MAGNETIC FOLIATION)

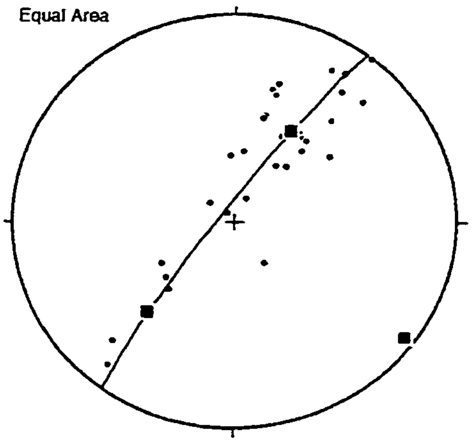

Eigenvalue		Eigenvector Trend	Plunge
1.	0.7081	30.3	48.2
2.	0.2694	221.0	41.3
3.	0.0225	126.3	5.3

95 % Elliptical Confidence Cones:

Axis 1: Max = 18.1°, Min = 4.8°

Axis 3: Max = 6.9°, Min = 4.7°

Best Fit Great Circle: 216/85 W

Fold Axis (Trend/Plunge): 126/05

PROSPEROUS PLUTON (MAGNETIC FOLIATION)

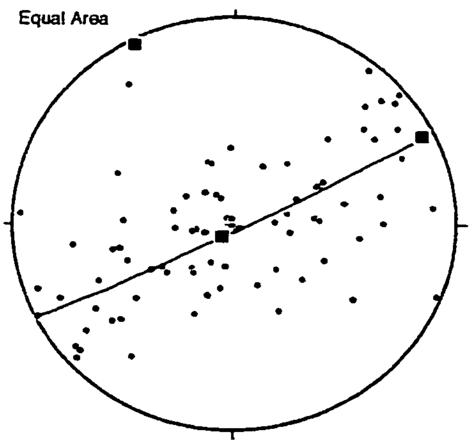

Eigenvalue		Eigenvector Trend	Plunge
1.	0.5393	219.4	83.5
2.	0.3707	63.3	5.9
3.	0.0900	333.0	2.6

95 % Elliptical Confidence Cones:

Axis 1: Max = 29.3°, Min = 6.7°

Axis 3: Max = 8.9°, Min = 6.7°

Best Fit Great Circle: 63/87 S

Fold Axis (Trend/Plunge): 333/03